TR3021S

STELLINGEN

behorende bij het proefschrift

Countercurrent sorption equipment using transported open sorbent material

A.M. Diederen

1. Voor een aantal voor tegenstrooms-sorptie belangrijke eigenschappen kunnen de reeds voorhanden zijnde relaties voor gepakte vezelbedden ook toegepast worden op opencellige schuimen door het schuim een equivalente vezeldiameter toe te kennen (dit proefschrift).

2. Vacuüm stoomstrippen als scheidingstechniek voor de verwijdering van opgeloste vluchtige organische componenten uit water is ten onrechte niet aangemerkt *als Best Available Technology* door het *United States Environmental Protection Agency* (dit proefschrift).

3. Bij het vergelijken van het ruimtebeslag van kolomprocessen zijn de onderlinge verhoudingen van kolomvolumina van geringe praktische betekenis daar de grootte van het benodigde vloeroppervlak van de complete systemen meestal maatgevend is voor de beoordeling van het ruimtebeslag (dit proefschrift).

4. Van diverse publikaties op het gebied van kostenevaluatie van processen kan de betrouwbaarheid drastisch worden verbeterd door het verdisconteren van een Lang-faktor of installatie-faktor op de aanschafprijs van de betreffende apparatuur (dit proefschrift).

5. Liever één afdichting in de hand, dan tien "tegen stoom bestand".

6. In het licht van de zakelijke successen van makelaars en autohandelaren, heeft het spreekwoord "eerlijk duurt het langst" betrekking op het maken van winst.

7. De langste files staan in de computer.

8. Een hongerstaker is net zo overtuigend als een overvaller die zichzelf onder schot houdt.

9. Burgerlijkheid kan worden gekenschetst als het lid worden van de Postcodeloterij, niet om de goede doelen te steunen en zelfs niet in de eerste plaats om de hoofdprijs te winnen, maar om te voorkomen dat alleen de buren rijker worden als de straatprijs valt.

10. Na cafeïnevrije koffie en alcoholvrij bier is de tijd rijp voor accijnsvrije benzine.

Countercurrent sorption equipment using transported open sorbent material

Countercurrent sorption equipment using transported open sorbent material

PROEFSCHRIFT

ter verkrijging van de graad van doctor
aan de Technische Universiteit Delft,
op gezag van de Rector Magnificus Prof.dr.ir. J. Blaauwendraad,
in het openbaar te verdedigen ten overstaan van een commissie,
door het College van Dekanen aangewezen,
op dinsdag 28 oktober 1997 te 10.30 uur
door

André Marcel DIEDEREN

werktuigkundig ingenieur
geboren te Den Haag

Dit proefschrift is goedgekeurd door de promotoren:

Prof.dr.ir. A.W. Veenman
Prof.dr.ir. J. de Graauw

Samenstelling promotiecommissie:

Rector Magnificus, voorzitter	
Prof.dr.ir. A.W. Veenman,	Technische Universiteit Delft, promotor
Prof.dr.ir. J. de Graauw,	Technische Universiteit Delft, promotor
Prof.dr.ir. C.J. Asselbergs,	Universiteit Twente
Prof.dr.ir. M.P.C. Weijnen,	Technische Universiteit Delft
Prof.dr.ir. A.A.H. Drinkenburg,	Technische Universiteit Eindhoven
Prof.dr.ir. R.M. Voncken,	Rijksuniversiteit Groningen
Dr.ir. A.M. Trommelen,	Unilever Research Laboratorium, Vlaardingen

Published and distributed by:

Delft University Press
Mekelweg 4
2628 CD Delft
The Netherlands
Telephone: +31 15 2783254
fax: +31 15 2781661
E-mail: DUP@DUP.TUDelft.NL

ISBN 90-407-1527-0 / CIP

Printed in The Netherlands

Samenvatting

Tegenstrooms sorptie apparatuur met getransporteerd open sorbens materiaal

In theorie kan het volume van apparatuur voor tegenstrooms sorptie aanmerkelijk worden verkleind door gebruik te maken van mechanisch getransporteerde gepakte bedden bestaande uit sorbensmateriaal met hoge bedporositeit en kleine deeltjesafmetingen. Aan zowel de eis ten aanzien van hoge bedporositeit als de eis ten aanzien van kleine deeltjesafmetingen kan worden voldaan door open materialen toe te passen: dit zijn hoog-poreuze materialen met kleine afmetingen van de samenstellende deeltjes die op een of andere wijze onderling verbonden zijn, zoals vezelmaterialen, nonwovens en opencellige schuimen. Het doel van dit onderzoek is de realisatie van een pilot unit om de technische haalbaarheid aan te tonen van continu tegenstrooms sorptie apparatuur met gebruikmaking van mechanisch transport van gepakte bedden bestaande uit open sorbensmaterialen. Vervolgens zullen de mogelijkheden van deze nieuwe scheidingstechniek worden onderzocht.
In het beginstadium van dit project is verwijdering van lage concentraties VOCs (Vluchtige Organische Componenten) uit grote waterdebieten gekozen als modelsysteem voor stofoverdracht, experimenten en haalbaarheidsstudies. Voor dit scheidingsprobleem blijkt siliconenrubber een van de meest geschikte sorbensmaterialen te zijn: siliconenrubber heeft een hoge sorptiecapacitiet voor VOCs, een lage sorptiecapaciteit voor water, een relatief hoge diffusiecoëfficiënt voor dit scheidingsprobleem, is bestand tegen stoom (van belang voor regeneratie met stoom) en beschikbaar zowel in de vorm van vezels als opencellig schuim.
Om de benodigde apparaat afmetingen te kunnen bepalen die nodig zijn om met deze nieuwe scheidingstechniek een bepaalde verwijderingsgraad te kunnen realiseren voor een gegeven scheidingsprobleem, moeten eerst een aantal gegevens en eigenschappen bekend zijn. Daartoe zijn eerst de maximaal toelaatbare vloeistofsnelheid, de drukval, de dispersie en de stofoverdrachtseigenschappen bepaald in gepakte bedden van vezel- en schuimmaterialen. Vervolgens is een pilot unit ontwikkeld om tegenstrooms stofoverdrachtsexperimenten te kunnen uitvoeren en om de werking van een dergelijk apparaat te bestuderen. Met de opgedane kennis is een ontwerpstudie verricht naar een verbeterde versie van de pilot unit, opgeschaald voor industriële toepassing. Tenslotte is dit verbeterde en opgeschaalde ontwerp in een technisch-economische evaluatie vergeleken met alle concurrerende technieken voor de verwijdering van VOCs uit grote waterdebieten.

Om de maximaal toelaatbare vloeistofsnelheid te kunnen voorspellen waarbij het gepakte bed nog net niet wordt samengedrukt, moet eerst de compressibiliteit van het sorbens materiaal bekend zijn. Daartoe zijn eerst de compressibiliteit van zowel willekeurig verdeelde vezelmassa's als opencellige schuimen bepaald met behulp van een speciaal hiertoe ontwikkelde compressiebank. Hoewel elastomere open materialen onder eenzijdige compressie in feite transversaal isotroop materiaalgedrag vertonen, kan de compressibiliteit van hoog poreuze open materialen benaderd worden door uit te gaan van isotroop materiaalgedrag. Niet-lineair viscoëlastisch gedrag kan dan verrekend worden door de elasticiteitsmodulus voor lineair elastisch gedrag te vermenigvuldigen

met een factor die spanningsrelaxatie verdisconteerd en een factor die niet-lineariteit verdisconteerd.
Vervolgens is een 1-dimensionaal model geformuleerd dat de toelaatbare vloeistofsnelheid in een gepakt bed van compressibel open materiaal voorspelt waarbij het gepakte bed net niet wordt samengedrukt en de hoge bedporositeit gehandhaafd blijft. In tegenstelling tot reeds bestaande modellen wordt in dit model de ondersteuning van het gepakte bed door wrijving met de wand in rekening gebracht; deze wandwrijving kan een belangrijke bijdrage leveren in het behoud van de hoge porositeit tijdens doorstroming van het gepakte bed. Het model kan gebruikt worden voor ontwerpdoeleinden om de toelaatbare vloeistofsnelheid in gepakte bedden van open materialen te schatten voor verschillende bedporositeiten, zeefplaat-configuraties en kolom-afmetingen. Een aantal doorstromingsproeven met verschillende vezel- en schuimmaterialen heeft de geldigheid van dit model voor de toegepaste vezelbedden aangetoond. Voor de gebruikte schuimbedden waren de voorspelde toelaatbare snelheden echter zowel te laag als te hoog. Het model is wel geschikt om de orde van grootte van de toelaatbare vloeistofsnelheid in gepakte schuimbedden te schatten ten behoeve van de ontwerpstudie later in dit onderzoek.

De drukval en axiale dispersie in gepakte bedden van vezels en opencellige schuimen zijn experimenteel bepaald. De resultaten zijn vergeleken met theoretische en empirische voorspellingen uit de literatuur. De theoretische voorspellingen voor de drukval van vezelbedden kunnen ook worden toegepast voor opencellige schuimen door gebruik te maken van een equivalente vezeldiameter voor het schuim. De axiale dispersie in gepakte bedden van deze open materialen wordt beschreven door het axially dispersed plug flow model. In het algemeen is de overeenkomst tussen de voorspellingen en de experimentele resultaten voor drukval en dispersie slecht en kunnen deze voorspellingen hooguit de orde van grootte aangeven. Daarom is het ten behoeve van voldoende nauwkeurigheid noodzakelijk om voor gepakte bedden van slappe polymere vezels (zoals siliconenrubber vezels) of opencellige schuimen (zoals polyurethaanschuim en siliconenrubber schuim) de drukval en dispersie experimenteel te bepalen.
De verschillen tussen de theoretische en empirische voorspellingen uit de literatuur en de experimentele resultaten worden hoofdzakelijk veroorzaakt door verschillen in structuur van de gepakte bedden. Als gevolg van deze verschillen in gepakt bed structuur vertonen bedden van siliconenrubber vezels en -schuim tevens een aanzienlijk hogere drukval en axiale dispersie dan bedden van kristallijne vezels en gereticuleerd polyurethaanschuim. Het siliconenrubber schuim heeft namelijk een structuur waarin alleen de dunne gedeelten van de celmembranen verwijderd zijn, terwijl gereticuleerd polyurethaanschuim hoofdzakelijk uit celribben bestaat.

Een model ter beschrijving van tegenstrooms stofoverdracht van één component, inclusief axiale dispersie in de vloeistof- of gasfase (regeneratie), wordt gegeven door Miyauchi en Vermeulen. Dit stofoverdrachtsmodel wordt gebruikt om de scheidende werking te beschrijven van de pilot unit en het hieruit opgeschaalde en verbeterde ontwerp. Het model maakt gebruik van een aantal stofoverdrachtseigenschappen die ofwel geschat ofwel experimenteel bepaald moeten worden voor ieder afzonderlijk scheidingsprobleem.

De stofoverdrachtscoëfficiënt in de vloeistoffase kan worden geschat met behulp van een empirische relatie die is gebaseerd op verschillende stofoverdrachtscorrelaties uit de literatuur voor de vloeistoffase. Deze empirische relatie zal ook voor de gasvormige regeneratiefase worden gebruikt. De stofoverdrachtscoëfficiënt in de sorbensfase kan worden geschat aan de hand van het Sherwood getal, dat geschat wordt op 8 voor vezelachtige polymere sorbentia, maar kan ook experimenteel worden bepaald door het fitten van doorbraakcurven van vastbed experimenten. De verdelingscoëfficiënt voor sorbens / water kan worden bepaald door middel van een eenvoudige evenwichtsproef of door het fitten van doorbraakcurven van vastbed experimenten. De laatste methode blijkt betrouwbaarder en verdient daarom de voorkeur. De verdelingscoëfficiënt voor stoom / sorbens (regeneratiesectie) wordt berekend door vermenigvuldiging van de verdelingscoëfficiënten voor stoom / water en water / sorbens, beiden bij 100°C.

De pilot unit maakt gebruik van een gepakt bed dat zich bevindt in de annulusvormige ruimte tussen een langzaam roterende behuizing (in de vorm van een lege kabelhaspel) en een statische cilinder. Het sorbens is bevestigd aan en wordt getransporteerd door de roterende behuizing. De in- en uitlaatpoorten voor de procesmedia (voedingswater en stoom voor regeneratie) zijn op de statische cilinder aangebracht. In de annulusvormige ruimte waarin het sorbens zich bevindt zijn loodrecht op de stromingsrichting van water en stoom op regelmatige afstanden klepplaten aangebracht. Deze klepplaten verdelen het sorbens in een aantal gelijke bedsegmenten en zijn voorzien van terugslagkleppen die de procesmedia alleen in de richting tegengesteld aan de transportrichting van het sorbens laten passeren. Op deze manier wordt tegenstroom bewerkstelligd. Er is een internationale octrooiaanvraag voor dit apparaat ingediend (licentieverlening is mogelijk).
Dit concept, dat gebruik maakt van een gesegmenteerd annulusvormig sorbens, blijkt goed te functioneren. Echter, de levensduur van het apparaat, met name van de gepakte bedden plus afdekkend filterdoek en van de afdichtingen, dient nog geverifieerd te worden. Met de pilot unit zijn een aantal tegenstrooms stofoverdrachtsexperimenten uitgevoerd met siliconenrubber vezels en gereticuleerd polyurethaanschuim. De verwijderingsgraad is niet zo hoog als voorzien als gevolg van kortsluitstroming veroorzaakt door te hoge compressibiliteit van de gepakte bedden (siliconenrubber vezels) en als gevolg van krimp van het sorbens materiaal veroorzaakt door regeneratie met stoom (polyurethaanschuim). Ondanks de verschillen in voorspelde en gemeten verwijderingsgraad lijkt het stofoverdrachtsmodel geschikt om de verwijderingsgraad te voorspellen bij afwezigheid van kortsluitstroming of krimp. Met verse polyurethaanschuim bedden (geen krimp) lijkt een verwijderingsgraad van 95% haalbaar. Met geschikt sorbens materiaal (bijvoorbeeld siliconenrubber schuim) en met een opgeschaald en verbeterd ontwerp zal naar verwachting een verwijderingsgraad van 99% kunnen worden gerealiseerd.

De pilot unit kan worden opgeschaald voor de behandeling van afvalwater op industriële schaal. De gekozen toepassing is de verwijdering van in water opgelost tolueen bij een concentratie van 100 wt.ppm, een debiet van 10 m^3 water per uur en een verwijderingsgraad van 99%. Het opgeschaalde en verbeterde ontwerp is gebaseerd op absorptie van VOCs uit water in opencellig siliconenrubber schuim, in het Engels afgekort tot CFA (Countercurrent Foam Absorption). Verbeteringen in het ontwerp

hebben met name betrekking op de afdichting tussen de roterende trommel en de statische cilinder en de verbeterde montage / demontage procedure voor de trommel. De annulusvormige kolom is zowel in radiale als in axiale richting opgeschaald, resulterend in een hoger en veel breder gepakt bed in vergelijking met de pilot unit.
Er is verondersteld dat het siliconenrubber schuim bij afname van grotere hoeveelheden leverbaar zal zijn met een enigszins verbeterde structuur in vergelijking met de voor de experimenten ontvangen monsters, zodat de drukval en dispersie lager zullen zijn. De toelaatbare vloeistofsnelheid door de gepakte bedden wordt geschat op 1 cm/s, niet alleen om compressie van het bed te voorkomen maar ook om de drukval en dispersie te beperken.
Berekeningen aan de gekromde sorptie sectie met verrekening van de invloed van concentratieverschillen over de diameter van de bedsegmenten en het vereffenen van deze concentratieverschillen door menging ter plaatse van de klepplaten laten zien, dat de benodigde totale bedlengte ongeveer 25% groter is dan je op basis van rechte bedsegmenten met vloeistofsnelheden en stroomlijnlengtes behorende bij de gemiddelde beddiameter zou verwachten. Voor de regeneratiesectie is het verschil tussen de "gekromde" berekening en de "rechte" benadering, welke gebaseerd is op de gemiddelde diameter, minimaal.
In vergelijking met actief kool adsorptie kan het benodigde kolomvolume met een factor 7 verminderd worden als CFA (tegenstrooms schuim absorptie) wordt toegepast. Echter, dit voordeel in benodigd kolomvolume valt weg zodra het benodigde vloeroppervlak van de complete systemen in beschouwing wordt genomen. De compactheid van de tegenstrooms sorptie kolom zal toenemen als opencellig siliconenrubber schuim beschikbaar komt met gunstiger structuureigenschappen met betrekking tot drukval, compressibiliteit en dispersie, zodat een hogere toelaatbare vloeistofsnelheid in de kolom mogelijk wordt (nu beperkt tot circa 1 cm/s).

De economische haalbaarheid van CFA is onderzocht door middel van een technisch-economische evaluatie, gebaseerd op de toepassing van opencellig siliconenrubber schuim en gebaseerd op het opgeschaalde en verbeterde apparaatontwerp. Bij waterdebieten van 10 of 100 m^3 per uur, een voedingsconcentratie van 100 wt.ppm tolueen en een verwijderingsgraad van 99% liggen de schattingen voor kosten en afmetingen van het CFA-systeem binnen de grenzen van de andere in aanmerking komende technieken, echter CFA onderscheidt zich noch qua kosten noch qua afmetingen van de andere scheidingstechnieken. De economische haalbaarheid van CFA voor VOC-verwijdering uit afvalwater zal afhangen van specifieke omstandigheden voor de betreffende toepassing.
CFA kan economisch aantrekkelijker worden gemaakt door de toelaatbare vloeistofsnelheid te verhogen en de investeringskosten van het scheidingsapparaat te verlagen. Verder zal CFA economisch aantrekkelijker zijn voor hogere concentraties en lagere debieten. Voor een debiet van 10 m^3 per uur zal CFA concurrerend zijn met de andere technieken voor de genoemde toepassing als de toelaatbare vloeistofsnelheid verhoogd kan worden naar 2 cm/s (siliconenrubber schuim met verbeterde celstructuur, geoptimaliseerd voor CFA toepassing) en als de kosten per kilogram scheidingsapparaat afnemen tot ongeveer 150 NLG/kg (ruimere bewerkingstoleranties).
Economisch meer aantrekkelijke toepassingen voor tegenstrooms sorptie apparatuur kunnen mogelijk gevonden worden in:

- verwijdering van VOCs uit lucht
- drogen van oplosmiddelen door toepassing van hydrofiel absorptiemateriaal
- extractie van zware metalen uit afvalwater door toepassing van ionenwisselaars
- winning van eiwitten door middel van hoog-selectieve sorbentia

Dit onderzoek heeft aangetoond dat continu tegenstrooms sorptie apparatuur met mechanisch getransporteerde gepakte bedden technisch realiseerbaar is. De beoogde reductie in apparaatvolume ten opzichte van traditionele scheidingstechnieken is nog niet gerealiseerd als gevolg van beperkingen van de toelaatbare vloeistofsnelheid voor beschikbare open sorbens materialen die goede stofoverdrachtseigenschappen en bestendigheid tegen stoom dienen te combineren met lage compressibiliteit, lage drukval en lage dispersie. De economische haalbaarheid van het proces wordt op dit moment eveneens beperkt door de toelaatbare vloeistofsnelheid, maar CFA bied goede perspectieven voor kleine debieten ($10m^3$ per uur) met op maat gemaakt sorbens materiaal (betere celstructuur) en een verder ontwikkeld (minder duur) apparaat.

A.M. Diederen, 1997.

Summary

Countercurrent sorption equipment using transported open sorbent material

In theory, equipment size for countercurrent sorption processes can be reduced considerably by applying mechanical transport of packed beds with high void fraction and small particle size. The combined requirement of high packed bed porosity and small particle size results in the application of open materials: highly porous materials with small solid dimensions and with some kind of interconnection such as fiber materials, nonwovens and open-cell foams. The objective of this research is the realisation of a pilot unit proving the technical feasibility of continuous countercurrent sorption equipment using mechanical transport of a packed bed consisting of open sorbent material. Next, the potential of this new separation technique will be investigated.
In an early stage of the project the removal of low concentrations of VOCs (volatile organic compounds) from large flows of water has been chosen as a model system for mass transfer modelling, experiments and feasibility studies. For this separation problem, silicone rubber has been identified as the choice sorbent material, combining a high capacity for VOC sorption and a low capacity for water sorption, a relatively large diffusion coefficient, steam resistance (regeneration) and availability both as fibers and open-cell foam.
In order to evaluate the equipment specifications for a desired separation performance to be achieved by this new separation technique, a number of key parameters have to be known. First, the allowable liquid velocity, the pressure drop, the dispersion and the mass transfer properties in packed beds of fiber and foam materials have been established. Next, a pilot unit has been constructed to conduct countercurrent mass transfer experiments and to investigate its functioning. Based on the experience acquired with the pilot unit, a design study for scaled up and improved equipment has been conducted. Finally, a techno-economic evaluation based on this design for industrial-scale waste water treatment has been made, comparing the new technique to all competing techniques.

In order to determine the maximum allowable water velocity before compression of the packed bed occurs, first the compressibility of the sorbent material had to be established. The compressibility of both random orientated fiber masses and open-cell foams have been determined using a special compression bench. Although elastomeric open materials subject to uni-axial pressure actually exhibit transversal isotropic material behaviour, the compressibility of a highly porous open material can be approximated by assuming isotropic material behaviour. Non-linear viscoelastic behaviour has been accounted for by factorisation of the linear elastic Young's modulus with a stress-relaxation factor and a non-linearity function.
Next, a 1-dimensional model has been derived which can predict the maximum allowable liquid velocity through a packed bed of compressible open material for which the bed remains uncompressed and for which its high porosity is maintained. In contrast to existing models, this model includes the support of the bed by wall friction, which can contribute considerably to the preservation of the bed porosity. The model can be

used for design purposes to estimate the allowable liquid velocity in packed beds of open material for different bed porosities, sieve plate configurations and column dimensions. A number of flow tests with different fiber and foam materials has demonstrated the validity of this model for the applied packed fiber beds. For the applied packed foam beds the predicted allowable velocities however were both too low and too high. Nevertheless, the model can be used for an order of magnitude estimation of the maximum allowable liquid velocity through the packed foam bed for the design established later in this research.

Pressure drop and axial dispersion in both packed fiber beds and open-cell foam beds have been investigated by experiment. Comparisons have been made between theoretical and empirical predictions from literature and experimental results. The theoretical predictions for pressure drop in fiber materials can be used for open-cell foam materials as well, by using an equivalent fiber diameter for the foam. The axial dispersion of a packed bed of open material is described by the axially dispersed plug flow model. Generally, the agreement between the predictions and the experimental results is poor and the predictions will only serve as order of magnitude estimates. As a consequence, experimental determination of both the pressure drop and the axial dispersion coefficient of packed beds of slack polymeric fibers (like silicone rubber fibers) or open-cell foam beds (like polyurethane foam and cellular silicone) is inevitable to obtain an accuracy better than an order of magnitude.
The deviations between theoretical and empirical predictions from literature and experimental results are mainly caused by differences in packed bed structure. Also, due to these differences in packed bed structure, the beds consisting of silicone rubber material (both fibers and foam) show considerably higher pressure drop and axial dispersion than the beds consisting of crystalline fibers and reticulated polyurethane foam. The cellular silicone (silicone rubber foam) has a structure in which only the thin parts of the cell membranes were removed, whereas in reticulated polyurethane foam only the cell struts were left

A model describing countercurrent mass transfer of a single component, including axial dispersion in the liquid (or gaseous) phase, is given by Miyauchi and Vermeulen. This model is used to evaluate the separation efficiency of the pilot unit and the scaled-up and improved design based on the pilot unit. The model uses a number of mass transfer properties which will have to be estimated or determined by experiment for each specific separation problem.
The liquid side mass transfer coefficient can be estimated using an empirical relation representing the various mass transfer correlations for the liquid phase found in literature. For the gaseous regenerant phase the same empirical relation will be used. The sorbent side mass transfer coefficient can be estimated from the Sherwood number, which is assumed to have a value of 8 for fiberlike polymeric sorbents, but can also be experimentally determined by fitting outlet concentration profiles of fixed bed experiments. The sorbent / water distribution coefficient can be determined either by simple batch equilibrium tests or by fitting outlet concentration profiles of fixed bed experiments. The latter method appears to be more reliable and is therefore preferred. The steam / sorbent distribution coefficient for the regeneration section is calculated by

multiplying the steam / water and water / sorbent distribution coefficients, both at 100°C.

The pilot unit uses a packed bed located in the annular space between a slowly rotating housing, shaped like a spool, and a static cylinder. The sorbent bed is attached to and transported by the rotating housing. The inlet and outlet ports for the process media (feed water and steam for regeneration) are placed on the static cylinder. Perpendicular to the direction of fluid (water or steam) flow a number of check valve plates are placed at equal distances throughout the annulus, dividing the annular sorbent into similar bed segments. These plates are provided with check valves (non-return valves) which allow fluids only to pass the plates in the direction opposite to the direction of sorbent transport, so countercurrent operation is achieved. An international patent application for this apparatus has been filed (licensing is possible).
The concept of the countercurrent annular sorption column has been demonstrated to function correctly. However, a sufficient service life, particularly of the sorbent material (plus covering screens) and the seals, has yet to be verified. A number of countercurrent mass transfer experiments have been conducted with the pilot unit using silicone rubber fibers and reticulated polyurethane foam. The removal efficiency is not as high as expected due to by-pass flows caused by too large compressibility (silicone rubber fibers) or shrinkage of the sorbent due to steam regeneration (polyurethane foam). Despite the observed differences in removal efficiencies between model and experiments, the model seems to be suitable to predict the removal efficiency for packed sorbent beds in the absence of by-pass flows or shrinkage. With fresh polyurethane foam beds (no shrinkage), removal efficiencies of 95% seem to be feasible. With suitable sorbent material (for instance cellular silicone) and with a scaled-up and improved design, a removal efficiency of 99% is expected to be feasible.

The pilot unit can be scaled-up for industrial-scale waste water treatment. The chosen target application is to remove dissolved toluene from water at flow rate of 10 m^3/h, a concentration of 100 wt.ppm and a removal efficiency of 99%. The scaled-up and improved design is based on absorption of VOCs from water into cellular silicone, called "countercurrent foam absorption", abbreviated by "CFA". Improvements of the design particularly refer to the sealing between the rotating drum and the static cylinder and the improved assembly / disassembly procedure for the drum. Scaling-up has taken place in both radial and axial direction, resulting in a higher and much wider packed bed compared with the pilot unit.
The cellular silicone has been assumed to be available with a slightly improved cellular structure compared with the samples received for experiments, so that pressure drop and dispersion will be lower. The maximum allowable liquid velocity through the packed foam bed is estimated at 1 cm/s, not only to prevent compression of the bed, but also to restrict pressure drop and dispersion.
Calculations of the curved sorption section taking into account concentration differences along the diameter of the bed segments and balancing of these concentration differences by mixing between the segments, show an increase of the total required packed bed length of approximately 25% compared to the calculated required packed bed length for straight bed segments with velocities and lengths applying for the mean diameter. For

the regeneration section, the difference between the "curved" calculation and the "straight" approximation based on the mean diameter is minimal.
The required column volume can be decreased by a factor 7 when applying countercurrent foam absorption instead of granular activated carbon adsorption, however this profit in column size falls into the background when the footprints of the complete systems are considered. The compactness of the countercurrent sorption column will increase as cellular silicone with more favourable structural properties regarding pressure drop, compressibility and dispersion will be available, allowing a higher mean liquid velocity in the column (now restricted at approximately 1 cm/s).

Based on the scaled-up and improved design applying cellular silicone to remove dissolved toluene from water (countercurrent foam absorption or CFA), a techno-economic evaluation has been made to asses its economic potential. At waste water flow rates of 10 m^3/h or 100 m^3/h, a feed concentration of 100 wt.ppm toluene and a removal efficiency of 99%, cost and size estimates for CFA lie within the margins set by the other applicable techniques, but CFA stands out neither on cost nor on space requirements. The economic attractiveness of CFA for VOC-removal from waste water will depend on site-specific conditions.
CFA can become more attractive if the allowable water velocity in the packed bed increases and the manufacturing cost of the main equipment decreases. A higher water velocity will require sorbent material with an improved cellular structure. Also, CFA will be more competitive for higher concentrations and smaller flow rates. For a flow rate of 10 m^3/h, CFA will be competitive with the other techniques for the regarding application assuming a water velocity of approximately 2 cm/s (cellular silicone optimised for CFA application) and assuming a cost per kilogram of main equipment of approximately 150 NLG/kg (increased manufacturing tolerances).
Economically more attractive applications for countercurrent sorption equipment may be found in other applications (yet to be investigated):

- removal of VOCs from air
- dewatering of solvents using hydrophilic absorption material
- heavy metal extraction from waste water using ion-exchange material
- protein recovery and antibiotics recovery from dedicated streams using highly selective sorption materials

This research has demonstrated the technical feasibility of continuous countercurrent sorption equipment using mechanical transport of the sorbent bed. The intended reduction in equipment size relative to traditional techniques has not been achieved yet due to limitations of the allowable liquid velocity for available open sorbent materials which have to combine good mass transfer properties and steam resistance with low compressibility, low pressure drop and small dispersion. The economic feasibility of the process is limited at present by the allowable liquid velocity as well, but CFA offers good perspectives for smaller flow rates (10 m^3/h) with optimised sorbent material and further developed equipment.

A.M. Diederen, 1997.

Table of contents

Appendices:

1

Introduction

In September 1990 the project "Compact separation equipment using countercurrent fiber sorption" started at the Laboratory for Process Equipment of Delft University of Technology. The project was aimed at achieving equipment size reduction for countercurrent sorption processes by mechanical transport of a highly porous packed fiber bed. During the first years, Gerard van Zee proved the feasibility of the countercurrent fiber sorption process, which in theory could result in a space efficiency improvement by one order of magnitude [1]. The next aim was to develop a small scale pilot unit to prove the feasibility of the required equipment as well. At this point, the author of this thesis joined the project and focussed on equipment related subjects.

Van Zee discussed the theoretical advantages of applying packed beds with high void fraction and small particle size. The combined requirement of high packed bed porosity and small particle size results in the application of open materials in our new equipment. In this thesis, open materials is used as a generic term for highly porous materials with small solid dimensions and with some kind of interconnection. Examples are fiber materials, nonwovens and open-cell foams. Van Zee also showed that the small scale pilot unit to be developed had to operate continuous, truly countercurrent and by mechanical transport of the sorbent to fully utilize the theoretical advantages of applying these open materials.

In an early stage of the project the removal of low concentrations of VOCs (volatile organic compounds) from large flows of water was chosen as a model system for mass transfer modelling, experiments and feasibility studies. For this separation problem, elastomers were identified as suitable sorption materials, since these materials have high capacity for VOC sorption and low capacity for water sorption. In this thesis, sorption (be it adsorption, absorption or both) refers to the transfer of a soluble component from a liquid phase into a solid phase called the sorbent. The reverse process is called regeneration, desorption or stripping.

The objective of the research treated in this thesis is the realisation of a pilot unit proving the technical feasibility of continuous countercurrent sorption equipment using mechanical transport of the sorbent bed. Next, the potential of this new separation technique will be investigated.

In order to evaluate the equipment specifications for a desired separation performance to be achieved by this new separation technique, first a number of key parameters have to

be known. Chapters 2, 3 and 4 present the theoretical background, measuring methods and estimated or experimentally established values for allowable liquid velocity, pressure drop, dispersion and mass transfer properties in packed beds of fiber or foam materials. Together with the experience acquired from the mass transfer experiments with the pilot unit, treated in Chapter 5, this information was used in a design study for a scaled up and improved version of the pilot unit. This design study, presented in Chapter 6, is the basis for a techno-economic evaluation presented in Chapter 7 for industrial-scale waste water treatment, comparing the new technique to all competing techniques.

[1] Zee, G. van, *Counter current sorption using fiber sorbents (Ph.D.-thesis)*, Delft University Press, 1996, ISBN 90-407-1328-6

2

Compressibility and allowable liquid velocity for open sorbent materials

2.1 Introduction

The most suitable sorbent material to be used in our separation equipment for VOC-removal from water is an open elastomeric material with a high porosity, for instance elastomers shaped as a random orientated mass of fibers or as an open-cell foam. Due to the open structure of such highly porous materials and the high compressibility or low stiffness of the elastomeric base material, packed fiber or foam beds of these materials have a relatively high compressibility as well and hence can sustain only limited water velocities. The packed bed can be supported by sieve plates or can be assisted by friction with the encasing walls to increase the allowable water velocity before compression of the packed sorbent bed occurs. Since our ultimate goal is to establish compact separation equipment which requires a relatively high water velocity (order of magnitude cm/s), we want to establish the relation between the compressibility of the involved open material and the allowable water velocity, which will also depend on the flow resistance of the open material and the wall-friction.
First, we have to establish the compressibility (the inverse stiffness) of open materials. Section 2.2 discusses the compressibility of open materials on the basis of its stiffness properties. It appears that an exact description of the stiffness properties of open materials is too complex for our purpose. Instead, the open material is treated as a simple continuous material using factorisation to account for non-linearity and time-dependent behaviour.
Next, on the basis of the compressibility of the open material (section 2.2) and the compressional stress exerted on the packed bed due to its flow resistance (Chapter 3 section 3.2), a model is derived, including the frictional resistance between packed bed and enclosing walls, to predict the allowable water velocity before compression of the packed bed occurs. This model is compared with experiments. The model and the validating experiments are discussed in section 2.3.
This chapter is concluded in section 2.4.

2.2 Compressibility of open sorbent materials

2.2.1 Introduction

To characterise the stiffness properties (inverse compressibility) of a highly porous open material it is treated as a continuous medium. In general an open material has different properties in different directions once it is subject to compression. This so-called anisotropic material behaviour is formally described in §2.2.2. Because the selected elastomeric materials to be used as a sorbent show non-linear and time-dependent behaviour, the formal description becomes too complex for our purpose of deriving an approximate estimation of the allowable water velocity through the material before compression occurs. For this reason, a simple approximation was chosen by characterising the stiffness properties assuming linear elastic isotropic material behaviour, factorised for non-linearity and time-dependent behaviour.

Paragraph 2.2.3 is concerned with the compression tests, conducted with a two-step compression bench which was constructed to determine the stiffness properties of a number of open materials.
In an early stage of this research, when the choice for the sorbent material was not yet focused on elastomers, a number of polymeric fiber materials were tested. Although applied as a sorbent material in the pilot unit (Chapter 5), silicone rubber fibers were not used in compression tests due to insufficient stiffness of this material. Later on, besides polyurethane foam, cellular silicone (silicone rubber foam) was tested which is the intended sorbent material for our new separation equipment.
The compression bench measures the pressures in mutually perpendicular directions simultaneously so besides Young's modulus also Poisson's ratio can be determined. The contained material can be compressed in two different directions in order to determine the stiffness properties according to the formal description as well. In this way we will be able to compare these results to the ones for the isotropic approximation. This comparison will be made in §2.2.4, which discusses the results from §2.2.3.

2.2.2 Model

Formal description
A random orientated and uniformly packed open material (fibers or foam) shows isotropic material behaviour. This means that the material properties are independent of direction. When a sample of this material is subject to uni-axial pressure, the open material gets a preferential orientation in the direction of the pressure (see figure 2.1). This causes differences in the material properties in the three mutually perpendicular directions (anisotropic material behaviour).

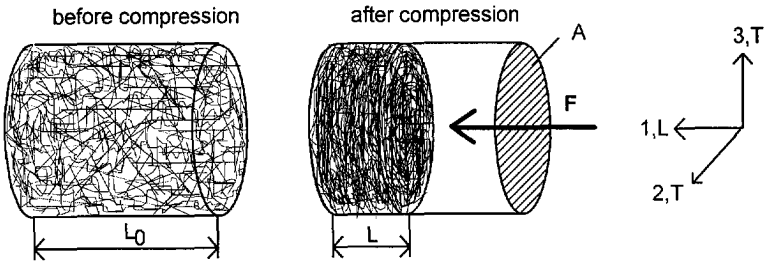

Figure 2.1: Orientation of an open material subject to uni-axial pressure

Uni-axial compression of open material leads to a special case of anisotropic material behaviour, since the material shows different behaviour in only two of the three principal directions. This is called transversal isotropic material behaviour. The material behaviour in longitudinal direction, the direction in which the pressure is applied (index 1 or L), is different from the material behaviour in the directions perpendicular to the applied pressure (indices 2 and 3 or T).

When we consider the open material as a continuous phase, we can characterise its stiffness properties for compression with the according Young's moduli (E) and Poisson's ratio's (ν) for transversal isotropic material behaviour. For linear elastic transversal isotropic material behaviour where stress (σ) is proportional to strain (e), the relations between stress and strain for the three principal directions are as follows (for the complete 6 x 6 stiffness matrices, see Appendix A.1):

$$\begin{bmatrix} e_1 \\ e_2 \\ e_3 \end{bmatrix} = \begin{bmatrix} \frac{1}{E_L} & \frac{-\nu_{TL}}{E_T} & \frac{-\nu_{TL}}{E_T} \\ \frac{-\nu_{TL}}{E_T} & \frac{1}{E_T} & \frac{-\nu_{TT}}{E_T} \\ \frac{-\nu_{TL}}{E_T} & \frac{-\nu_{TT}}{E_T} & \frac{1}{E_T} \end{bmatrix} \cdot \begin{bmatrix} \sigma_1 \\ \sigma_2 \\ \sigma_3 \end{bmatrix} \qquad e_1 = \frac{L_0 - L}{L_0} \quad \sigma_1 = \frac{F}{A} \qquad (2.1)$$

(see figure 2.1)

$$\begin{bmatrix} \sigma_1 \\ \sigma_2 \\ \sigma_3 \end{bmatrix} = \begin{bmatrix} E_L \cdot E_T \cdot \frac{(\nu_{TT}-1)}{(E_T \cdot \nu_{TT} - E_T + 2 \cdot \nu_{TL}^2 \cdot E_L)} & -E_L \cdot E_T \cdot \frac{\nu_{TL}}{(E_T \cdot \nu_{TT} - E_T + 2 \cdot \nu_{TL}^2 \cdot E_L)} & -E_L \cdot E_T \cdot \frac{\nu_{TL}}{(E_T \cdot \nu_{TT} - E_T + 2 \cdot \nu_{TL}^2 \cdot E_L)} \\ -E_L \cdot E_T \cdot \frac{\nu_{TL}}{(E_T \cdot \nu_{TT} - E_T + 2 \cdot \nu_{TL}^2 \cdot E_L)} & E_T \cdot \frac{(-E_T + \nu_{TL}^2 \cdot E_L)}{(1+\nu_{TT})(E_T \cdot \nu_{TT} - E_T + 2 \cdot \nu_{TL}^2 \cdot E_L)} & -E_T \cdot \frac{(-E_T + \nu_{TL}^2 \cdot E_L)}{(1+\nu_{TT})(E_T \cdot \nu_{TT} - E_T + 2 \cdot \nu_{TL}^2 \cdot E_L)} \\ -E_L \cdot E_T \cdot \frac{\nu_{TL}}{(E_T \cdot \nu_{TT} - E_T + 2 \cdot \nu_{TL}^2 \cdot E_L)} & -E_T \cdot \frac{(-E_T + \nu_{TL}^2 \cdot E_L)}{(1+\nu_{TT})(E_T \cdot \nu_{TT} - E_T + 2 \cdot \nu_{TL}^2 \cdot E_L)} & E_T \cdot \frac{(-E_T + \nu_{TL}^2 \cdot E_L)}{(1+\nu_{TT})(E_T \cdot \nu_{TT} - E_T + 2 \cdot \nu_{TL}^2 \cdot E_L)} \end{bmatrix} \cdot \begin{bmatrix} e_1 \\ e_2 \\ e_3 \end{bmatrix}$$

(2.2)

e: strain [-]
σ: stress [N/m²]

E_L:	Young's modulus in longitudinal direction	[N/m²]
E_T:	Young's modulus in transversal direction	[N/m²]
ν_{TL}:	transversal-longitudinal Poisson's ratio	[-]
ν_{TT}:	transversal Poisson's ratio	[-]

The four parameters (E_L, E_T, ν_{TL} and ν_{TT}) characterising the stiffness matrix for linear elastic transversal isotropic material behaviour for compression can be determined by conducting a two-step compression test, resulting in four equations. First, the open material is compressed in longitudinal direction ($e_2 = e_3 = 0$) and the resulting pressures σ_1 and σ_2 or σ_3 are measured. Next, while e_1 is fixed, the material is compressed in transversal direction, for instance direction 2 ($e_1 = e_3 = 0$), and the resulting pressures σ_2 and σ_3 are measured.

Longitudinal compression:

$$\sigma_1 = E_L E_T \frac{(\nu_{TT} - 1)}{(E_T \nu_{TT} - E_T + 2\nu_{TL}^2 E_L)} \cdot e_1 \tag{2.3}$$

$$\sigma_2 = \sigma_3 = -E_L E_T \frac{\nu_{TL}}{(E_T \nu_{TT} - E_T + 2\nu_{TL}^2 E_L)} \cdot e_1 \tag{2.4}$$

Subsequent transversal compression:

$$\sigma_2 = E_T \frac{(-E_T + \nu_{TL}^2 E_L)}{(1 + \nu_{TT})(E_T \nu_{TT} - E_T + 2\nu_{TL}^2 E_L)} \cdot e_2 \tag{2.5}$$

$$\sigma_3 = -E_T \frac{(E_T \nu_{TT} + \nu_{TL}^2 E_L)}{(1 + \nu_{TT})(E_T \nu_{TT} - E_T + 2\nu_{TL}^2 E_L)} \cdot e_2 \tag{2.6}$$

Polymeric materials show viscoelastic material behaviour. Polymeric open materials should therefore be described by viscoelastic transversal isotropic material behaviour showing time-dependency and non-linearity with respect to strain. In such a formal description, at least E_L and E_T are both time-dependent and functions of e_1 and e_2. Characterisation of a polymeric open material using the formal description requires extreme efforts in proportion to the purpose of preliminary assessment of material behaviour or quick parameter variation studies. A simpler approximation for these purposes can be made using linear elastic isotropic material behaviour factorised for time effects and non-linearity. The formal description can be useful as an estimate of the stiffness matrix of a contained precompressed packed bed around a specific strain (see the example in §2.2.4).

Approximation

The formal description can be approximated using factorisation of linear elastic isotropic material behaviour. For linear isotropic material behaviour, the relations

between stress and strain for the three principal directions are as follows (for the complete 6 x 6 stiffness matrices, see Appendix A.1):

$$\begin{bmatrix} e_1 \\ e_2 \\ e_3 \end{bmatrix} = \frac{1}{E} \cdot \begin{bmatrix} 1 & -\nu & -\nu \\ -\nu & 1 & -\nu \\ -\nu & -\nu & 1 \end{bmatrix} \cdot \begin{bmatrix} \sigma_1 \\ \sigma_2 \\ \sigma_3 \end{bmatrix} \tag{2.7}$$

$$\begin{bmatrix} \sigma_1 \\ \sigma_2 \\ \sigma_3 \end{bmatrix} = \frac{E}{(1+\nu)\cdot(1-2\cdot\nu)} \cdot \begin{bmatrix} 1-\nu & \nu & \nu \\ \nu & 1-\nu & \nu \\ \nu & \nu & 1-\nu \end{bmatrix} \cdot \begin{bmatrix} e_1 \\ e_2 \\ e_3 \end{bmatrix} \tag{2.8}$$

For uni-axial compression of a contained open material where $e_2 = e_3 = 0$ (see figure 2.1), Young's modulus E can be established by measuring σ_1 and e_1:

$$E = \frac{\sigma_1}{e_1} \cdot \frac{(1+\nu)\cdot(1-2\nu)}{1-\nu} \tag{2.9}$$

Poisson's ratio ν can be established by measuring σ_2 or σ_3 (see figure 2.1):

$$\nu = \frac{1}{1+\frac{\sigma_1}{\sigma_2}} = \frac{1}{1+\frac{\sigma_1}{\sigma_3}} \tag{2.10}$$

For uni-axial compression of an open material between two flat plates where $\sigma_2 = \sigma_3 = 0$, E can be established without knowing ν:

$$E = \frac{\sigma_1}{e_1} \tag{2.11}$$

Assuming that the time-dependence of viscoelastic polymeric open material is defined by its stress relaxation behaviour, E can be factorised for time dependence by multiplication with a stress-relaxation factor "s" ($s \leq 1$) for a certain time, for instance sufficiently long time for stress relaxation to have reached an arbitrary limit. For non-linearity with regard to strain, E can be factorised by multiplication with a strain function $f(e_1)$ which is equal to 1 for small strains. So, E can be written in the form of:

$$E(e_1) = s \cdot f(e_1) \cdot E \tag{2.12}$$

The stress relaxation factor "s" can be chosen according to published experimental data or own experiments. For the strain function $f(e_1)$ some empirical, semi-empirical and structural models are available. First, a structural model for a random orientated fiber mass will be discussed. Next, several models for low density open-cell foams are treated. This has to result in values or relations for "s" and $f(e_1)$ so that equation (2.12)

can be used as an approximate expression for the stiffness parameter E (Young's modulus) of the open material.

Structural model for a random orientated fiber mass

Van Wyk [1] derived an expression for the relation between uni-axial pressure and the volume of a contained and random orientated fiber mass during compression:

$$P = \frac{c \cdot Y \cdot m^3}{\rho^3}\left(\frac{1}{V^3} - \frac{1}{V_0^3}\right) \tag{2.13}$$

P:	pressure applied in one direction	[N/m²]
c:	constant	[-]
Y:	Young's modulus of a single fiber	[N/m²]
m:	mass of the contained fibers	[kg]
ρ:	specific density of a single fiber	[kg/m³]
V:	volume of the fiber mass	[m³]
V_0:	V at P = 0	[m³]

Equation (2.13) can be rewritten to derive the relation between pressure and porosity:

$$\varepsilon = 1 - \frac{m}{\rho \cdot V} \quad \rightarrow \quad P = c \cdot Y \cdot [(1-\varepsilon)^3 - (1-\varepsilon_0)^3] \tag{2.14}$$

ε:	porosity of the fiber mass	[-]
ε_0:	ε at P = 0	[-]

For strain e_1, equation (2.14) can be rewritten as follows:

$$e_1 = \frac{V_0 - V}{V_0} = \frac{\varepsilon_0 - \varepsilon}{1-\varepsilon} \rightarrow \quad \sigma_1 = c \cdot Y \cdot (1-\varepsilon_0)^3 \cdot \left[\left(\frac{1}{1-e_1}\right)^3 - 1\right] \tag{2.15}$$

As a result, for a contained random fiber mass equation (2.12) can be rewritten using equations (2.9) and (2.15):

$$E(e_1) = s \cdot \frac{1}{e_1} \cdot \left[\left(\frac{1}{1-e_1}\right)^3 - 1\right] \cdot c \cdot Y \cdot (1-\varepsilon_0)^3 \cdot \frac{(1+\nu)\cdot(1-2\nu)}{1-\nu} \tag{2.16}$$

There are no data available on the relaxation factor "s" for a fiber mass. "s" will be incorporated in the experimentally determined function $E(e_1)$ according to equation (2.16). As with PUR foam (see "models for low density open-cell foams" later in this paragraph), $E(e_1)$ in water can be estimated by multiplying $E(e_1)$ in air with a factor of 2/3 (used in section 2.3). An estimate for "s" in air is 0.5 as with PUR foam.

For Poisson's ratio ν a theoretical prediction like equation (2.13) is not available. However, Komori and Itoh [2] and Carnaby and Pan [3] predict a decreasing ν with increasing strain (at larger strains). Both theories predict that $\nu > 0.5$ is possible.

Figure 2.2 shows a typical curve according to equation (2.16).

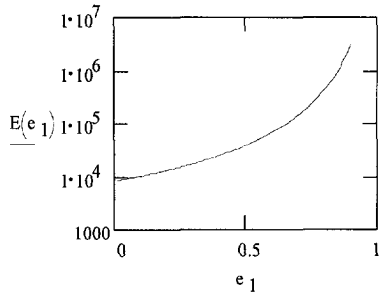

Figure 2.2: Curve according to equation (2.16)

Discussion

Van Wyk's relation is based on a structural model assuming that resistance to compression originates from bending of the fibers. The fiber mass is regarded as a system of bending rods, which are the elements of a fiber between adjacent contacts with other fibers. Possible twisting, slip and extension of the fibers are ignored. It is assumed that the fiber elements are orientated at random, that the mass of fibers is uniformly packed and that frictional forces are negligible.

One of the most important aspects of the theory is the derivation of the mean length of the bending rods. The fiber diameter is included in the expression for this mean length, but is cancelled in the final relation between pressure and volume of the sample [1]. So in theory, the compressibility of a fiber mass is independent of the fiber diameter.

Constant "c" is, among others, dependent on the fiber arrangement. According to Van Wyk, a typical value of "c" is 0.01. One of the major restrictions of Van Wyk's model is the unfamiliarity with this constant. As a result, predictions based on the properties of a single fiber are not possible. Although some investigations account for the turtuosity of the fibers (lower stiffness with larger turtuosity according to [4]), "c" still has to be determined for each separate fiber mass.

Another major restriction is the loss of random orientation during uni-axial compression. According to [5], several investigations demonstrate a linear relation between the mean length between the fiber contact points and the volume of the sample during uni-axial compression, in accordance with Van Wyk. For this reason, equations (2.13) through (2.16) remain valid, but with changing "c" as a result of changing fiber orientation.

A third restriction of Van Wyk's theory is the neglect of slip of the fibers. Because a large part of the fiberslip is irreversible, a "fresh" sample has to be compressed several times before the results are reproducible. Dunlop [6] suspects that the ability of the fibers to slide over one another during compression attributes to the spread in "c". This would imply that the fiber arrangement and alignment would be a strong factor in determining the stiffness of a fiber mass during compression. The influence of fiberslip on the stiffness of a fiber mass is still a subject of research.

Although several aspects of Van Wyk's theory have been refined over the years and the model has been extended at some points [4,7], by lack of better theoretical models this basic model of Van Wyk is still the most solid founded approach available.

Models for low density open-cell foams

Figure 2.3 [8] shows typical stress-strain curves for compression of flexible foams. Foam A is an open cell latex rubber foam with a wide distribution in the size of the cell elements. Foam B is a non-reticulated PUR foam with irregular cell dimensions and some cell membranes. Foams C and D are reticulated PUR foams with uniform cell size and many cell membranes. As can be seen in figure 2.3, the shape of the curve is strongly dependent on the cell structure. Three areas can be distinguished. First, the stress is proportional to the strain up to approximately 3% compression. Next, the stress to strain ratio rapidly decreases due to bending of the cell rods and buckling of the cell elements. Here the curve reaches a plateau region. Finally, the slope of the curve rapidly increases due to collapse of the cell structure. Foams A and B do not have a clear plateau region due to the cell size distribution, which causes a broad area for transition of elastic deformation of the cells into plastic deformation. The rate-dependence of the stress-strain curves is relatively small for many elastomeric foams [9].

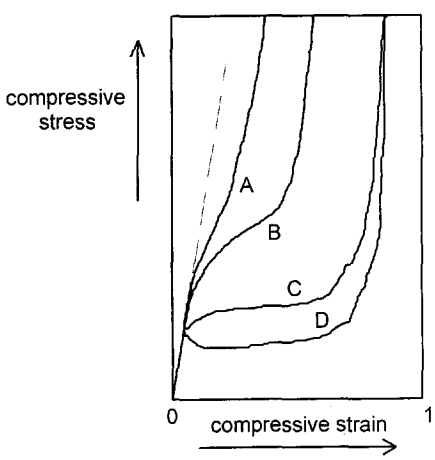

Figure 2.3: Stress-strain diagrams for several types of flexible foam

The stress-strain proportionality factor can be decomposed in an elastic foam modulus E_F and a strain function $f(e_1)$ accounting for the deformation of the cell structure as a function of the strain:

$$\sigma_1 = E_F \cdot f(e_1) \cdot e_1 \tag{2.17}$$

This factorisation was first proposed by Rusch [8]. The structural theory by Gent and Thomas [10,11] for strains larger than the linear part of the stress-strain curve gives a somewhat comparable relation between stress and strain for low density foams with the factor $f(e_1) \cdot e_1$ replaced by $f^*(e_1) \cdot (1-\varepsilon)/3$.
The shape of $f(e_1)$ is mainly determined by the cell geometry. Density and cell size influence the shape of the strain function only insignificantly. E_F depends on the density of the foam. Experiments conducted by Rusch demonstrated that the strain function is independent of rate and temperature and that these parameters are only affecting E_F.

Rusch found an empirical equation that predicts the elastic foam modulus E_F from the modulus E_P of the polymer material and the uncompressed porosity ε_0 satisfactorily as long as the voids in the foam are approximately spherical [12]:

$$E_F = E_P \cdot \frac{(1-\varepsilon_0) \cdot [2 + 7(1-\varepsilon_0) + 3(1-\varepsilon_0)^2]}{12} \tag{2.18}$$

The relation between E_F/E_P and $(1-\varepsilon_0)$ has an initial slope of 1/6, similar to the prediction according to the structural theory by Gent and Thomas for low density foams [10,11] for $\nu=0.25$ and ε close to 1.

When an isotropic foam with approximately spherical voids is subjected to uni-axial compression, the foam will become anisotropic. Young's modulus $E_{F,T}$ for compression in transversal direction, perpendicular to the applied pressure, will be greater than $E_{F,L}$ in longitudinal direction, the direction in which pressure is applied. Huber and Gibson derived a relation between $E_{F,T}$ and $E_{F,L}$ as a function of the shape-anisotropy ratio R, in which R is defined as the mean cell size in transversal direction divided by the mean cell size in longitudinal direction [13]:

$$\frac{E_{F,T}}{E_{F,L}} = \frac{2 \cdot R^2}{1 + \frac{1}{R^3}} \tag{2.19}$$

For R-values between 1 and 1.6, $E_{F,T}/E_{F,L}$ increases from 1 to approximately 4. Many foams are already anisotropic in supplied conditions. It is therefore important to take notice of the orientation of the foam relative to the direction of pressure because of the possibly large influence on E_F.

The strain function $f(e_1)$ from equation (2.17) can be described by the analytic expression proposed by Rusch [14]:

$$f(e_1) = a \cdot e_1^{-p} + b \cdot e_1^{q} \tag{2.20}$$

The log $f(e_1)$-log(e_1) curve can be approximated by two straight lines as indicated in figure 2.4:

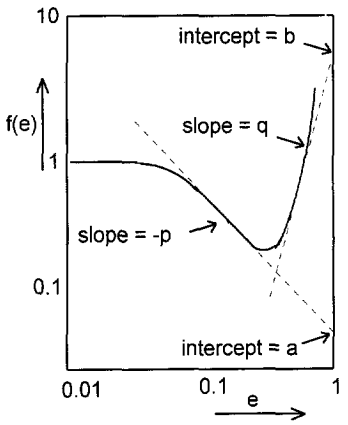

Figure 2.4: Strain function $f(e_1)$ according to equation (2.20)

As a result, equation (2.12) when describing Young's modulus for compression for low-density open-cell foams can be written according to equation (2.21):

$$E(e_1) = s \cdot (a \cdot e_1^{-p} + b \cdot e_1^{q}) \cdot E_P \cdot \frac{(1-\varepsilon_0)[2 + 7(1-\varepsilon_0) + 3(1-\varepsilon_0)^2]}{12} \tag{2.21}$$

Since one very often obtains a set of straight parallel lines when the logarithm of the stress relaxation modulus is plotted against the logarithm of time for different compressive strains [9], it is indeed allowed for open-cell foams to take time-dependence into account by a separate relaxation factor "s" as proposed by equations (2.12) and (2.21). For PUR-foam, Beavers et. al. [15] observed that the final (the fully relaxed) pressure required to compress the foam to a certain strain in water is 2/3 of the final value in air. A possible explanation is the lubricating effect of the water. This means that for PUR foam for which $E(e_1)$ according to equation (2.21) is determined in air for an arbitrary relaxation time (see §2.2.3), $E(e_1)$ in water can be estimated by multiplying $E(e_1)$ in air with a factor of 2/3 (used in section 2.3). Beavers et. al. [15] established a value for "s" of approximately 0.5 in air.

Figure 2.5 shows a typical curve according to equation (2.21):

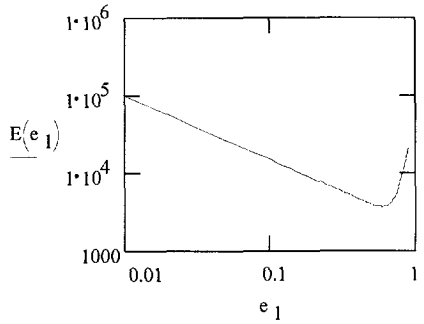

Figure 2.5: Curve according to equation (2.21)

Note that equation (2.21) is actually valid from a certain strain e_1 (order of magnitude 0.1 or smaller, but larger than zero), because for very small strains E is approximately constant. Accordingly, figure 2.5 will show a horizontal straight line for very small strains.

2.2.3 Experiments

Equipment
To conduct a two-step compression test for materials with high porosity and high compressibility (low stiffness), a special compression bench was constructed (see figure 2.6). The compression bench is equipped with PC-control and a data-acquisition system.

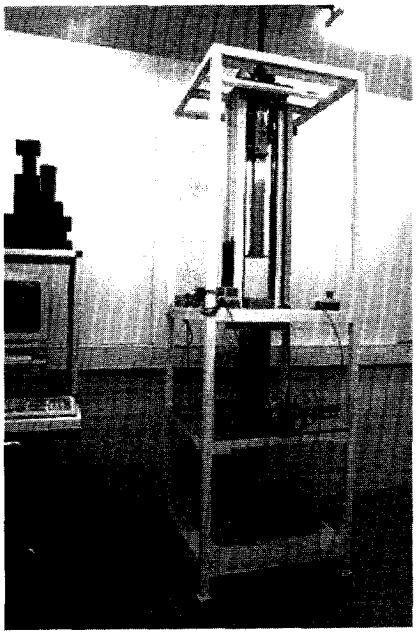

Figure 2.6: Two-step compression bench

To be able to characterise a range of porosities, the compression bench is designed for compression of materials with an initial porosity as high as 0.98 to a compressed porosity of 0.8 or higher. We chose to compress the material in an encasing tube by means of a stamp (see figure 2.7), so the porosity or strain of the compressed material can be determined accurately from the known volume of the enclosed material. The tube has a square cross-section (100 x 100 mm^2) for deformation and pressure measurement in mutually perpendicular directions. Fixing the height of the first compression step to 50 mm gives a required tube height of 500 mm for the chosen porosity range. The total height of the compression bench is 2.2 m. The chosen dimensions of the tube are a compromise between minimising wall-effects and wall-friction on the one hand (large enclosed volume is preferred) and minimising the required amount of sample material on the other hand (small enclosed volume is preferred). The second or horizontal compression step perpendicular to the first or vertical compression step (at a fixed height of 50 mm) takes place by moving a second stamp inside the tube, see figures 2.7 and 2.8.

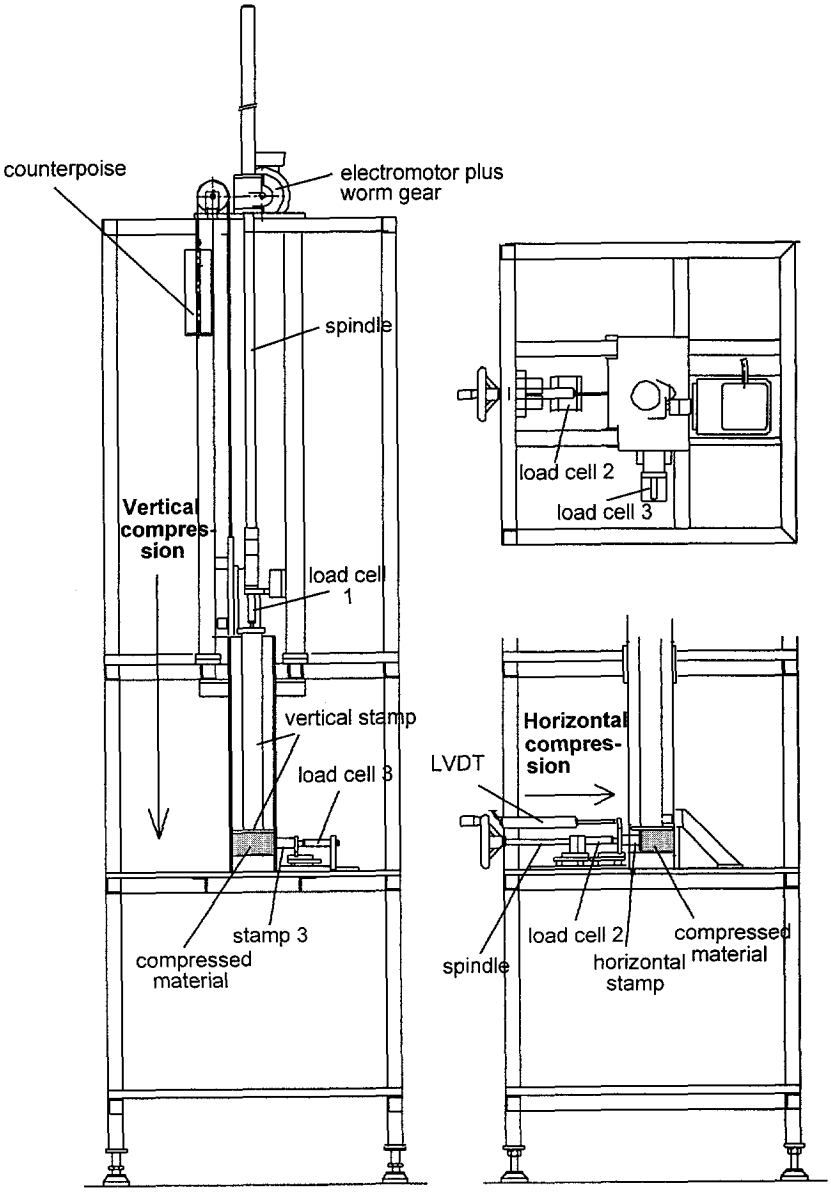

Figure 2.7: Outline view of the two-step compression bench

The vertical compression takes place by a selfbraking spindle (i.e. the spindle has a small lead) driven by an electromotor with frequency control plus worm gear, see figure 2.7. The maximum translational speed of the first compression step is 15 mm/s. The spindle exerts a downward force onto the vertical stamp through load cell 1. To prevent

the weight of the vertical stamp to be exerted on the compressed material, a counterpoise balances the weight of this vertical stamp. The load cell measures the force exerted on the material enclosed in the tube. The pressure σ_1 is found from this force and the surface area of the vertical stamp. The strain e_1 is simply calculated using the left part of equation (2.15) where V is fixed ($5 \cdot 10^5$ mm^3) and V_0 is either known or derived from the left part of equation (2.14) using the mass of the contained material and a known solid material density and initial porosity.
The horizontal compression (see also figures 2.8 and 2.9) is achieved by a selfbraking spindle driven by a handwheel. Just like the vertical compression, the stamp is loaded by the spindle through a load cell (load cell 2), which measures the exerted force on the enclosed material from which the pressure σ_2 is derived. During this second compression step, the surface area of the vertical stamp exposed to the compressed material diminishes proportionally and the calculation of σ_1 has to be adapted accordingly. The strain e_2 of the horizontal compression step is calculated from the displacement of the horizontal stamp into the tube measured by an LVDT (Linear Variable Displacement Transducer) connected to the horizontal stamp. The maximal horizontal displacement inside the tube is 25 mm.
The pressure σ_3 in the direction perpendicular to the vertical and horizontal compression is measured by load cell 3 plus stamp 3.

To reduce shear stresses due to friction between the highly porous material and the walls of the encasing tube, the inner faces of the tube are coated with teflon. The faces of the stamps which are in contact with the compressed material are coated with teflon as well. A gap of approximately 1 mm between the stamps and the tube (vertical stamp) or the involved openings in the tube (horizontal stamp and stamp 3) is provided to prevent jamming or large friction of the stamps by loose fibers or pieces of foam between stamp and tube.

For the measurement of the three mutually perpendicular pressures σ_1, σ_2 and σ_3, the accompanying stamps are mounted on slides with low and constant frictional resistance and small clearance. For the first (vertical) and second (horizontal) compression step the load cells are mounted on slides as well to ensure perfect alignment with the accompanying stamps during the translation of the compression steps (see figures 2.8 and 2.9 for the second compression step). Load cell 3 is supported directly by the frame. For an isotropic material, the pressures σ_2 and σ_3 will be equal during the first compression step. During the second compression step, at a fixed vertical compression, the pressures σ_2 and σ_3 will differ from each other.

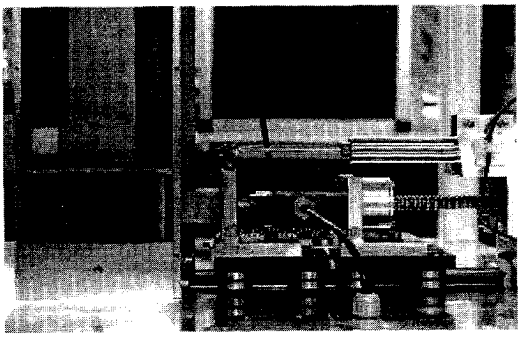

Figure 2.8: Second (horizontal) compression step at a fixed height after the first (vertical) compression step

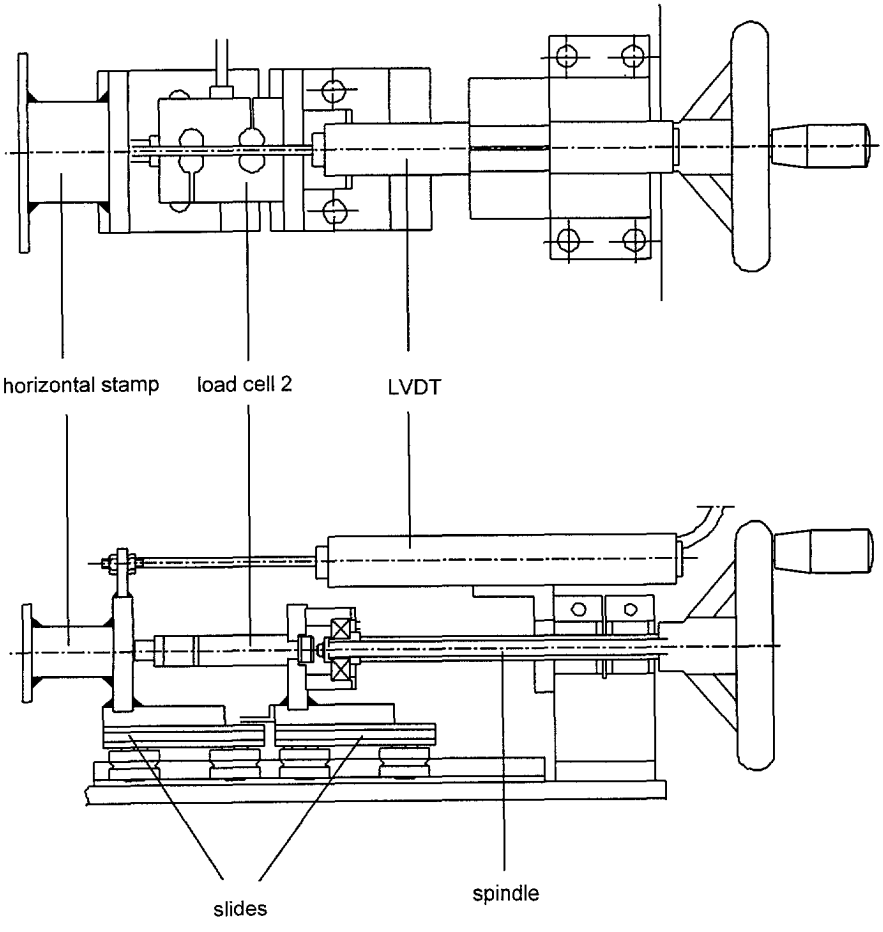

Figure 2.9: Details of the horizontal compression step equipment

The range and the accuracy of the load cells are chosen in such a way that both slack and relatively stiff open materials can be examined with the compression bench. Load cell 1 has a range of 1,000 N and an accuracy of 0.01%. Load cells 2 and 3 have a range of 500 N and an accuracy of 0.01%. This means that the pressure can be determined with a maximum accuracy of 10 Pa.
The accuracy of positioning the vertical stamp to the fixed height (50 mm) after the first compression step is 0.1 mm. This is achieved by closed loop control. The accuracy of the LVDT is 0.125 mm. This means that for final porosities near 0.8 the calculated porosity of the compressed material after the first or second compression step has an accuracy of about 0.0005. For higher final porosities the accuracy is better than 0.0005.

Experiments with fiber material
As discussed in §2.2.2, the formal description of the stiffness of open materials can be approximated using factorisation of linear elastic isotropic material behaviour. For fibers, this approximation results in equation (2.16). To determine the stiffness parameters we need to derive the relation between pressure and porosity in one direction (see equation 2.14) and the relation between the involved stress and the stress in a perpendicular direction (see equation 2.10). This means that for this approximation the vertical compression step is sufficient.
To establish the stiffness parameters for linear elastic isotropic material behaviour, the following procedure applies. First, the vertical compression step is conducted without sample material to be compressed in order to "zero" the load cells. Next, the vertical compression step is conducted a number of times in succession to get reproducible results. A number of 10 cycles appears to be sufficient for the applied sample materials. Because the polymeric sample material shows time-dependent behaviour (stress relaxation), for each cycle the pressures are measured for a certain amount of time after reaching the fixed height of the compression cycle. To limit the duration of the experiments and the number of samples for the data-acquisition system, a relaxation time of one minute has been chosen. So, the final pressures one minute after reaching the fixed height of the 10th cycle are used to determine the stiffness parameters of the fiber material. These 10 cycles result in one single point of the curve according to equation (2.14) representing the relation between σ_1 and ε and results in a value of Poisson's ratio according to equation (2.10) using the relation between σ_1 and σ_2 or σ_3. For the tested fiber materials, the final pressures of the 10th cycle are 20 to 35% lower than the final pressures of the 1st cycle.
To establish another point of the curve according to equation (2.14) and to establish Poisson's ratio at a different strain level, a different amount of sample material has to be compressed (again 10 cycles).

Two fiber materials were tested, PP (polypropylene) and PET (polyethylene tereftalate). Young's modulus Y of a single PP fiber is approximately $1.35 \cdot 10^9$ N/m^2. For PET, Y is approximately $2.95 \cdot 10^9$ N/m^2. The experimental results were fitted with an approximation of equation (2.14), neglecting the term containing the unloaded porosity ε_0 ($\varepsilon_0 \approx 0.965$ for PP and $\varepsilon_0 \approx 0.98$ for PET):

$$\sigma_1 = c \cdot Y \cdot (1-\varepsilon)^3 \qquad (2.22)$$

Figures 2.10 and 2.11 show the results for the final pressure in vertical direction (the direction of compression) for the 1st cycle and the 10th cycle:

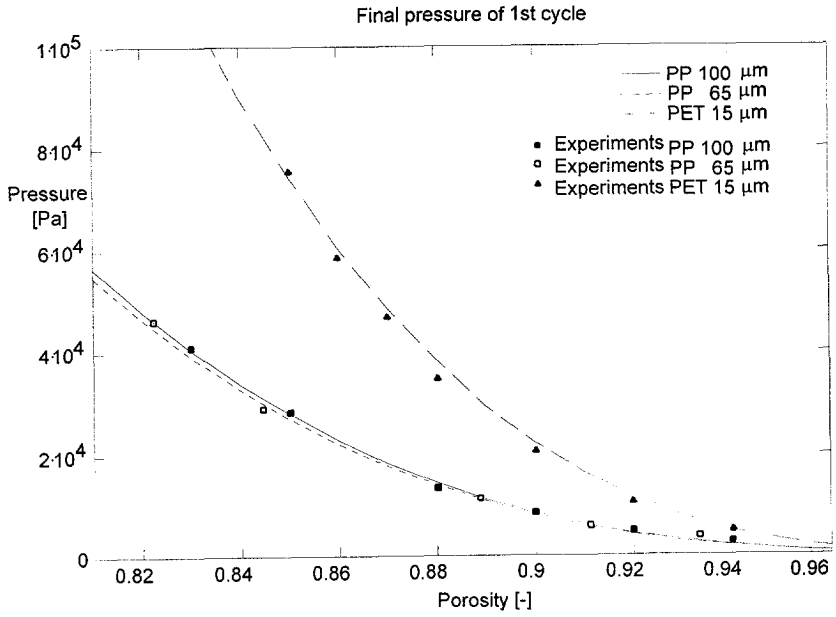

Figure 2.10: Final pressure versus porosity for the 1st cycle

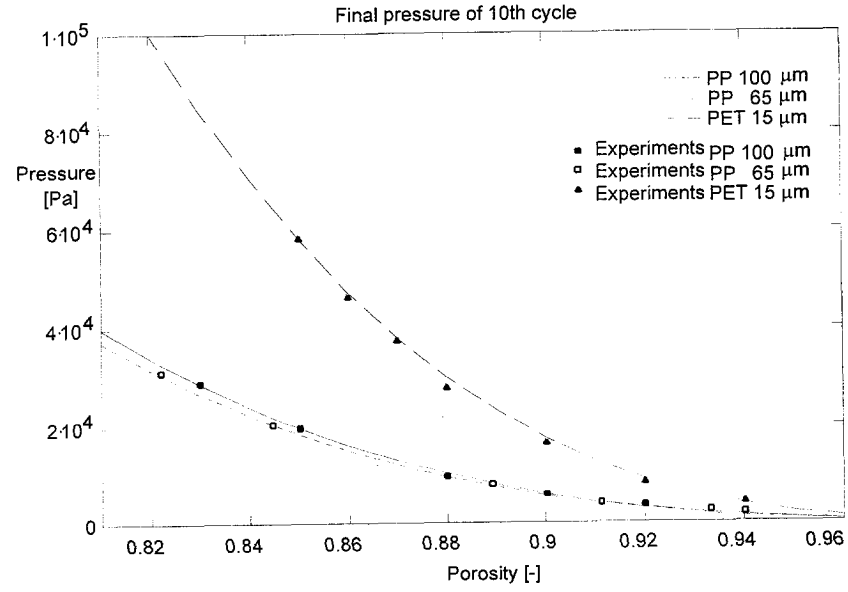

Figure 2.11: Final pressure versus porosity for the 10th cycle

The ratio between σ_1 and σ_2 or σ_3 is approximately constant per sample material for different strains (and hence independent of the strain) and has been used to determine Poisson's ratio ν according to equation (2.10):

$$\nu = \frac{1}{1+\frac{\sigma_1}{\sigma_2}} = \frac{1}{1+\frac{\sigma_1}{\sigma_3}} \tag{2.10}$$

The results for fiber materials are as follows:

Table 2.1: stiffness parameters for fiber materials

fiber material	fiber diameter [μm]	c [-]	ν [-]
PP	100	$4.30 \cdot 10^{-3}$	0.31
PP	65	$4.01 \cdot 10^{-3}$	0.34
PET	15	$5.83 \cdot 10^{-3}$	0.30

The values of "c" and ν according to table 2.1 can now be used in equation (2.16) to express the stiffness of the packed fiber bed as a function of compressive strain. Note that the stress relaxation factor "s" in equation (2.16) is already incorporated in the final pressure of the 10th cycle and hence in the experimentally established parameter "c". Young's modulus E (in N/m^2) for the used PP and PET fiber materials according to equation (2.16) as a function of strain can be depicted as follows:

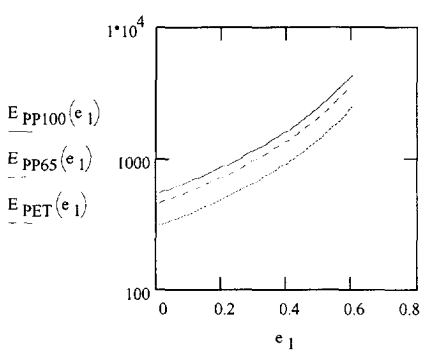

Figure 2.12: Young's modulus of fiber materials as a function of strain

These results are valid in air. For the application of fiber materials in water, E can be estimated by multiplying E in air with a factor of 2/3 as with PUR foam (see §2.2.2).

Summarising, the compressibility of fiber materials (in air) can be characterised as follows:

Table 2.2: experimental results for fiber materials

fiber material	fiber diameter [μm]	$E(e_l)$ [N/m^2]	ν [-]
PP	100	$\frac{1.8 \cdot 10^2}{e_l} \cdot [(\frac{1}{1-e_l})^3 - 1]$	0.31
PP	65	$\frac{1.51 \cdot 10^2}{e_l} \cdot [(\frac{1}{1-e_l})^3 - 1]$	0.34
PET	15	$\frac{1.02 \cdot 10^2}{e_l} \cdot [(\frac{1}{1-e_l})^3 - 1]$	0.30

Experiments with foam materials

Similar to the situation for the fiber materials, the formal description of the stiffness of low-density open-cell foam can be approximated by factorisation of linear elastic isotropic material behaviour. As with the fiber material, we only have to conduct the vertical compression step and we use the final pressures (one minute relaxation) of the 10th cycle.

Two foam materials were tested, PUR (polyurethane) with a mean pore diameter (empty space based) of 294 μm and cellular silicone with a mean pore diameter of about 700 μm. The maximum applied strains e_l agree with a minimum packed bed porosity of 0.8, since the desired porosity range for sorbent materials for our application is 0.8 or higher. For PUR foam the uncompressed porosity of 0.972 was decreased to 0.8 at $e_l = 0.86$, for cellular silicone the uncompressed porosity of 0.87 was decreased to 0.8 at $e_l = 0.35$.

The PUR foam was supplied by Recticel, Belgium (type BPS 90), the cellular silicone was supplied by Dow Corning, Germany (type DC8157).

PUR foam

Table 2.3 gives the results for PUR foam. The linear fit through zero and the first three points (up to and including $\sigma_l = 4026$) gives an elastic foam modulus E_F according to equation (2.17) of 40703 N/m^2 (see also figure 2.13). The strain function $f(e_l)$ accounting for non-linearity between pressure and strain has been calculated according to this same equation. Using equation (2.18), the apparent modulus of the polymeric material E_P is $7.9 \cdot 10^6$ N/m^2, which lies within the range of $E_P = 10^6$ to $2 \cdot 10^7$ N/m^2 for elastomers.

Table 2.3: results for PUR foam

height of unloaded PUR foam [mm]	e_l [-]	σ_l [N/m^2]	$f(e_l)$ [-]
52	0.038	2102	1
54	0.074	3203	1
56	0.107	4026	1
60	0.167	4158	0.612
70	0.286	4065	0.349
80	0.375	4090	0.268
100	0.5	4541	0.223
150	0.667	6019	0.222
200	0.75	9357	0.307
250	0.8	15100	0.464
300	0.833	23100	0.681

Figure 2.13 gives the relation between pressure σ_l and strain e_l:

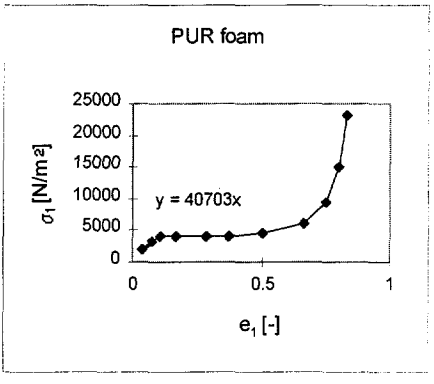

Figure 2.13: Stress versus strain for PUR foam

The strain function $f(e_l)$ can be described by equation (2.20) for $e_l \geq 0.107$:

$$f(e_l) = a \cdot e_l^{-p} + b \cdot e_l^{q} \qquad (e_l \geq 0.107) \qquad (2.20)$$

For PUR, the following parameters apply:

$$a = 0.1, \qquad p = 1.03, \qquad b = 4.07, \qquad q = 10.93.$$

Note that the stress relaxation factor "s" is already incorporated in the final pressure of the 10th cycle and hence in the experimentally established elastic foam modulus. Young's modulus E (in N/m^2) for the used PUR foam material according to equation (2.21) as a function of strain can be depicted as follows (E is assumed to be constant for $e_l < 0.107$):

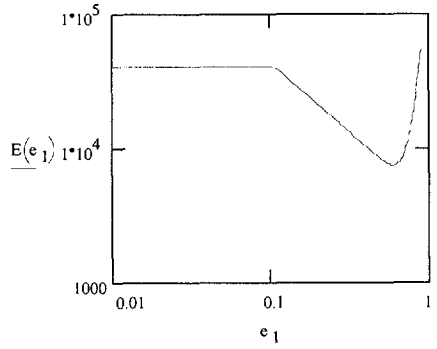

Figure 2.14: Young's modulus of PUR foam as a function of strain

These results for PUR foam are valid in air. For the application of PUR foam in water, E in water is 2/3 of E in air according to Beavers et. al. [15] (see §2.2.2).

PUR appears to have a Poisson's ratio (for compression) of zero. During compression of the foam in vertical direction, no significant pressure differences are measured by neither load cell 2 nor load cell 3.

Summarising, the compressibility of PUR foam (in air) can be characterised as follows:

$\nu = 0$

$e_l < 0.107$: $E = 4.07 \cdot 10^4$ N/m^2

$e_l \geq 0.107$: $E(e_l) = 4.07 \cdot 10^4 \cdot (0.1 \cdot e_l^{-1.03} + 4.07 \cdot e_l^{10.93})$ N/m^2 (2.23)

Cellular silicone

Table 2.4 gives the results for cellular silicone which, as PUR foam, has been approximated by factorisation of linear elastic isotropic material behaviour. Although the structural properties of the cellular silicone are quite different from the highly porous PUR foam, we will try to describe the silicone rubber foam with the formulas applicable to PUR foam. The linear fit through zero and the first point ($\sigma_l = 4354$) gives an elastic foam modulus E_F according to equation (2.17) of 59644 N/m^2. The strain function $f(e_l)$ accounting for non-linearity between pressure and strain has been calculated according to this same equation. Using equation (2.18), the apparent modulus of the polymeric material, E_P, is $1.9 \cdot 10^6$ N/m^2, which lies within the range of $E_P = 1 \cdot 10^6$ to $2 \cdot 10^7$ N/m^2 for elastomers.

Table 2.4: results for cellular silicone

mass of enclosed cellular silicone [kg]	e_1 [-]	σ_1 [N/m^2]	$f(e_1)$ [-]
0.0722	0.073	4354	1
0.075	0.107	4743	0.743
0.0816	0.18	6633	0.618
0.0892	0.25	7430	0.498
0.0953	0.297	8764	0.495
0.1032	0.351	8727	0.417
0.1112	0.398	10620	0.447

Figure 2.15 gives the relation between pressure σ_1 and strain e_1:

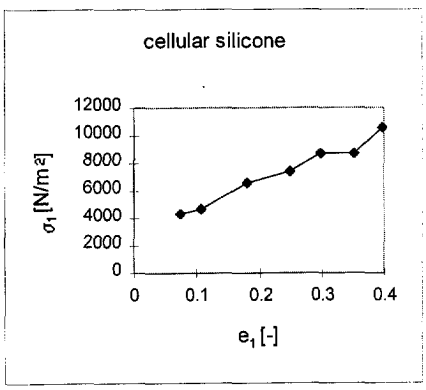

Figure 2.15: Stress versus strain for cellular silicone

Again, the strain function $f(e_1)$ can be described by equation (2.20). For cellular silicone, the following parameters apply:

$$a = 0.233, \quad p = 0.533, \quad b = 565.2, \quad q = 207.9 \quad (e_1 \geq 0.065).$$

We assume that E is approximately constant for $e_1 < 0.065$ (and not $e_1 < 0.073$ according to table 2.4, because the strain function with the fitted parameters equals unity at $e_1 = 0.065$ and hence $E = E_F$ at $e_1 = 0.065$ according to equation 2.21). Parameter q is so high, that the second term in equation (2.20) can be neglected, and the strain function turns into a power function.

Note that the stress relaxation factor "s" is already incorporated in the final pressure of the 10th cycle and hence in the experimentally established elastic foam modulus. Young's modulus E (in N/m^2) for the used silicone rubber foam material according to equation (2.21) as a function of strain can be depicted as follows (E is assumed to be constant for $e_1 < 0.065$):

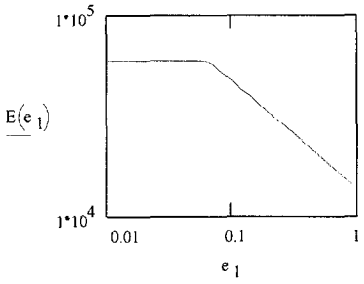

Figure 2.16: Young's modulus of cellular silicone as a function of strain

It should be noted that figure 2.16 has been extrapolated beyond the experimental range ($e_1 < 0.4$). It should also be noted that the results are valid in air. For application of the foam in water, E can be estimated by multiplying E in air with a factor of 2/3 as with PUR foam.

In contrast with PUR foam, cellular silicone does have a Poisson's ratio (for compression) larger than zero. Figure 2.17 gives Poisson's ratio for cellular silicone, determined by the ratio between the final stresses σ_1 and σ_3 (10th cycle) according to equation (2.10), together with a rough approximation by a straight line:

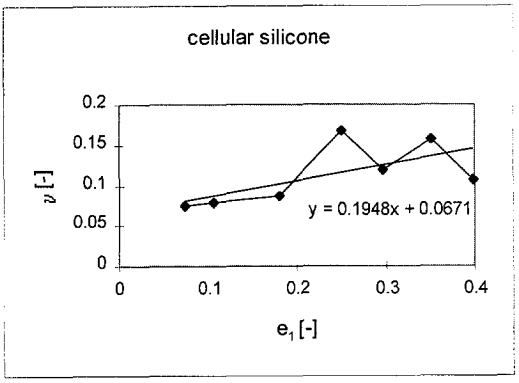

Figure 2.17: Poisson's ratio for cellular silicone according to equation (2.10)

Summarising, the compressibility of cellular silicone (in air) can be characterised as follows:

$$\nu = 0.195 \cdot e_1 + 0.067$$

$e_1 < 0.065$: $\quad E = 5.96 \cdot 10^4$ N/m^2

$e_1 \geq 0.065$: $\quad E(e_1) = 5.96 \cdot 10^4 \cdot (0.233 \cdot e_1^{-0.533})$ N/m^2 $\qquad$ (2.24)

Because cellular silicone does have a Poisson's ratio larger than zero, an attempt was made to characterise the stiffness of the cellular silicone by the formal description given

in §2.2.2. For this purpose, after each 10th cycle including one minute relaxation at the fixed height of the vertical compression step, a single horizontal compression step was carried out including a relaxation time of one minute at the end of this second compression step. Using equations (2.3) through (2.6), the concerning parameters which are valid around strain e_1 of the fixed vertical compression can be determined. Figures 2.18 through 2.21 give these parameters as a function of e_1. E_L can be approximated by a power function, a rough approximation of the other parameters is given by straight lines (equations given in the figures).

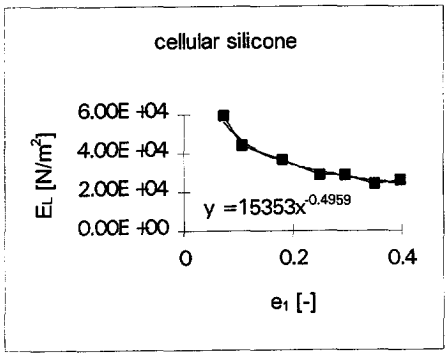

Figure 2.18: E_L as a function of e_1

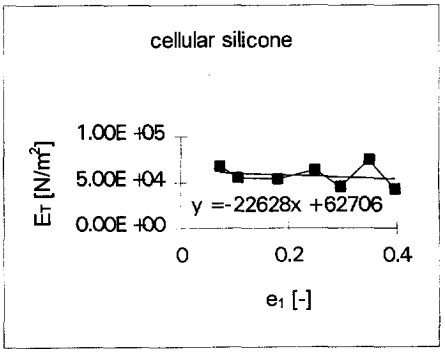

Figure 2.19: E_T as a function of e_1

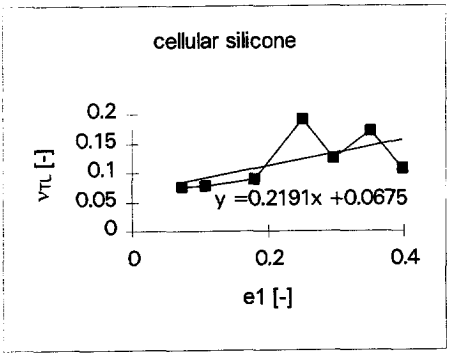

Figure 2.20: ν_{TL} as a function of e_1

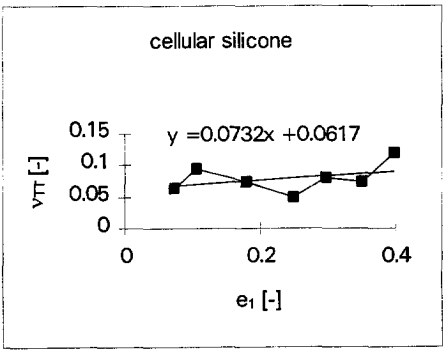

Figure 2.21: ν_{TT} as a function of e_1

As should be expected, the power function describing E_L as a function of e_1 is nearly the same function as Young's modulus E according to the approximation by factorisation of linear elastic isotropic material behaviour:

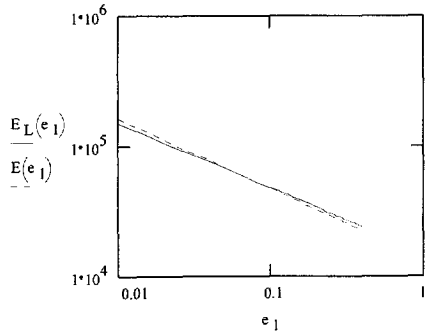

Figure 2.22: E_L (formal description) versus E (isotropic approximation)

These stiffness properties according to the formal description (figures 2.18 through 2.21) will be used to compare the formal description with the isotropic approximation (see §2.2.4).

2.2.4 Discussion

Formal description versus isotropic approximation

In order to assess the validity of the isotropic approximation, a comparison will be made between this approximate description and the formal description for cellular silicone, the only open material for which experimental results for both descriptions are available. This comparison will be made on the basis of a packed bed segment of the separation equipment, see figure 2.23:

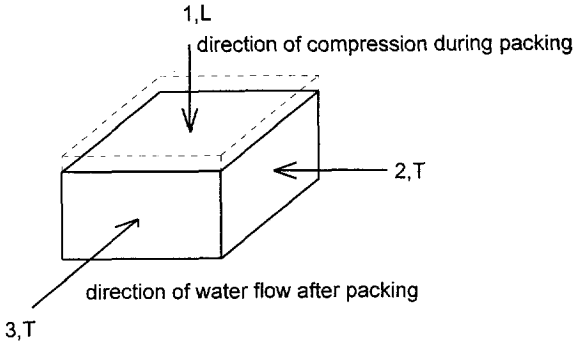

Figure 2.23: Packed bed segment of the separation equipment

Suppose the unpacked block of cellular silicone is 1/9 higher than the packed height within the segment, then the resulting strain in direction 1 in figure 2.23 will be 10% (see the left part of equation 2.15). According to the formal description, the stresses σ_1, σ_2 and σ_3 are given by equations (2.3) through (2.6). Using the experimentally

determined stiffness properties E_L, E_T, ν_{TL} and ν_{TT} from §2.2.3 valid at $e_1 = 0.1$ and with E_L and E_T factorised with s = 2/3 for water, the resulting stresses for $e_1 = 0.1$ are:

$\sigma_1 = 3250\ N/m^2$
$\sigma_2 = \sigma_3 = 312\ N/m^2$.

The stresses σ_1 and σ_2 can be used to estimate the static frictional resistance between the foam and the encasing walls, possibly enlarging the allowable water velocity before the foam is being compressed due to its flow resistance. The stress σ_3 can be seen as a precompression of the packed bed, allowing for a higher pressure exerted on the bed in the direction of flow (direction 3) before compression of the packed bed in this direction occurs.

Using the experimentally determined stiffness properties E and ν according to the isotropic approximation from §2.2.3 (and note that E is nearly the same as E_L, as it should be) and with E factorised with s = 2/3 for water, the resulting stresses for $e_1 = 0.1$ according to the isotropic approximation are:

$\sigma_1 = 3211\ N/m^2$
$\sigma_2 = \sigma_3 = 304\ N/m^2$.

These "isotropic" results are nearly the same as the results according to the formal description for the involved material and strain level. Note however that according to the formal description the transversal Young's modulus E_T is significantly larger than the longitudinal Young's modulus E_L or the isotropic E (see §2.2.3). This is especially true for larger strain levels. As a result, the material stiffness counteracting the pressure exerted on the bed due to the water flow resistance of the packed bed is higher than would be expected on the basis of the isotropic Young's modulus E. This can be a valid reason to pursue the more strenuous experimental determination of the stiffness parameters according to the formal description for a more profound research on these topics or for actual application of a certain open sorbent material in a tangible real-scale separation unit. With such formal description, the pressure in the direction of water flow needed to compress the packed bed (at $e_1 = 0.1$) to a strain e_3 without support of the packed bed by wall-friction is not equal to:

$$\sigma_3 = 304 + \frac{E \cdot (1-\nu)}{(1+\nu)\cdot(1-2\cdot\nu)} \cdot e_3 \quad [N/m^2] \tag{2.25}$$

according to the isotropic approximation (equation 2.8), but follows from the formal description according to equation (2.2):

$$\sigma_3 = 312 + E_T \cdot \frac{(-E_T + \nu_{TL}^{\,2} \cdot E_L)}{[(1+\nu_{TT})\cdot(E_T \cdot \nu_{TT} - E_T + 2\cdot\nu_{TL}^{\,2}\cdot E_L)]} \cdot e_3 \quad [N/m^2] \tag{2.26}$$

For $e_3 = 0.01$, σ_3 according to the isotropic approximation (equation 2.25) would be 625 N/m^2, according to the formal description (equation 2.26) σ_3 would be 720 N/m^2.

In practice, depending on the dimensions of the bed segment, compression of the sorbent material by its flow resistance is not only resisted by the precompression during packing of the bed but also by friction with the encasing walls. Due to the pressure exerted on the bed material in the direction of water flow caused by the flow resistance of the packed bed, the stresses acting on these encasing walls (σ_1 and σ_2 in fig. 2.23) will increase (for materials with a Poisson's ratio $\nu>0$) and so will the frictional resistance against compression of the bed in direction 3.

Reliability of the experimental results

The model (either the formal description or the isotropic approximation) assumes the absence of shear stresses during compression of the enclosed sample material in the compression bench, caused for instance by friction with encasing walls. It is obvious that the occurrence of shear stresses in our test equipment with a moving stamp in an encasing tube can not be avoided. The alternative would be to conduct the compression step between two flat plates without encasing walls. With this alternative method however it is difficult to determine the volume and hence the porosity or strain of the compressed sample material. It was estimated that for the high porosities we work with, a small error in the established compressed porosity or strain has a larger influence on the accuracy than the presence of relatively small shear stresses. For this reason we have chosen to use an encasing tube with teflonised walls and stamps, with a fixed compressed volume.

The influence on the accuracy of possible shear stresses will be small compared to the possible effect on the results of stress relaxation after reaching the fixed compressed volume after the vertical compression step. The relaxation time has arbitrarily been chosen at one minute, but the fully relaxed stress levels will only be reached after a considerably longer period of time. Moreover, the stress relaxation in water will be different from the stress relaxation in air. It has been assumed that the stress relaxation in water results in a decrease in Young's modulus with a factor of 2/3 relative to Young's modulus in air, as was established with PUR foam by Beavers et. al. [15]. As has been remarked before, a more profound research on this topic or an actual application of a certain open sorbent material in a tangible real-scale separation unit can give rise to a more strenuous experimental determination of time-dependent behaviour. The same remark applies for temperature effects on the stiffness properties, which have been neglected so far.

Experimental results for fibers

The experimental results for PP fibers with two different diameters are almost the same, see figure 2.11. This corresponds with Van Wyk's theory which assumes that the compressibility of a fiber mass is independent of the fiber diameter (see §2.2.2).

A difficulty in establishing Young's modulus E for a random orientated fiber mass is the presence of the term containing the unloaded porosity ε_0 in equation (2.16):

$$E(e_1)= s\cdot\frac{1}{e_1}\cdot\left[\left(\frac{1}{1-e_1}\right)^3-1\right]\cdot c\cdot Y\cdot(1-\varepsilon_0)^3\cdot\frac{(1+\nu)\cdot(1-2\nu)}{1-\nu} \qquad (2.16)$$

For highly porous materials like fiber masses, it is difficult to accurately establish ε_0. A high accuracy is required however, since a small error in ε_0 causes a large error in E according to equation 2.16.

Another source of inaccuracy in the results for fiber materials is the lack of reproducibility of the structure of the fiber mass, since the tube of the compression bench is filled by adding small stacks of fiber material until the desired quantity has been reached. This problem does not occur with PUR foam, which has a regular and fixed structure and from which blocks of the desired volume are cut.

Experimental results for foam materials

PUR foam apparently has a Poisson's ratio equal to zero. This means that in the example according to figure 2.23 the stresses σ_1 and σ_2 will only depend on the precompression of the sorbent material during packing of the bed segment and that these stresses will not be increased by an additional stress σ_3 due to the flow resistance of the packed bed. Note however that because of the precompression of the bed in direction 1 (see figure 2.23), Young's modulus in direction 2 will be higher than in direction 1, according to Huber and Gibson [13] possibly as much as a factor 4 (see §2.2.2). This is beneficial for the resistance of the packed bed against compression by the water flow.

Cellular silicone was described with the formulas applicable to PUR foam (see §2.2.3). However, the involved equation (equation 2.21) does not account for Poisson's ratio for cellular silicone, given by figure 2.17. In fact, in equation (2.21) the following term accounting for Poisson's ratio according to equation (2.9) should be included:

$$\frac{(1+\nu)\cdot(1-2\cdot\nu)}{1-\nu} \tag{2.27}$$

However, since this term is almost equal to 1 for cellular silicone in the range of interest ($0 < e_1 \leq 0.35$), the absence of the term according to equation (2.27) in equation (2.21) is allowable for cellular silicone. For PUR foam, with $\nu \approx 0$, the term of equation (2.27) is equal to unity.

Young's modulus for cellular silicone is possibly underestimated, as the linear part of the relation between stress and strain is determined by a linear fit through zero and only one experimentally determined point (see §2.2.3). For future research or dedicated determination of the stiffness properties of a real-application sorbent material, a number of experiments in the low strain range ($e_1 \leq 0.05$) should be conducted.

The spread in the results for cellular silicone is rather large. A possible explanation for this spread is the occurrence of disturbances due to friction between the silicone material and the encasing walls of the tube of the compression bench which is relatively high compared to the friction of the used fiber materials and PUR foam.

2.2.5 Conclusions

For an approximate estimation of the stiffness properties of a highly porous open material, bearing in mind that the ultimate goal is to give an estimate of the allowable water velocity before compression of the packed bed occurs (section 2.3), the open material can be adequately described assuming linear elastic isotropic material behaviour. For future research or dedicated determination of the stiffness properties of a real-application sorbent material, it can be considered to use the more strenuous experimental determination of the stiffness parameters according to the formal description which assumes transversal isotropic material behaviour. The stiffness in the direction of water flow of a packed sorbent bed precompressed in another (perpendicular) direction is larger than in the direction of precompression. This results in higher allowable pressures in the direction of water flow and thus a higher allowable water velocity before compression of the packed bed occurs.

Both the isotropic approximation and the formal description are factorised for non-linearity and viscoelastic behaviour. For one minute relaxation in air, the following results were found using the isotropic approximation:

Fiber materials:

fiber material	fiber diameter [μm]	$E(e_1)$ [N/m^2]	ν [-]
PP	100	$\frac{1.8\cdot 10^2}{e_1}\cdot[(\frac{1}{1-e_1})^3-1]$	0.31
PP	65	$\frac{1.51\cdot 10^2}{e_1}\cdot[(\frac{1}{1-e_1})^3-1]$	0.34
PET	15	$\frac{1.02\cdot 10^2}{e_1}\cdot[(\frac{1}{1-e_1})^3-1]$	0.30

Foam materials:

PUR foam: $\nu = 0$

$e_1 < 0.107$: $E = 4.07\cdot 10^4$ N/m^2

$e_1 \geq 0.107$: $E(e_1) = 4.07\cdot 10^4 \cdot (0.1\cdot e_1^{-1.03} + 4.07\cdot e_1^{10.93})$ N/m^2

Cellular silicone: $\nu = 0.195\cdot e_1 + 0.067$

$e_1 < 0.065$: $E = 5.96\cdot 10^4$ N/m^2

$e_1 \geq 0.065$: $E(e_1) = 5.96\cdot 10^4 \cdot (0.233\cdot e_1^{-0.533})$ N/m^2

Young's moduli for application in water can be estimated by multiplying the above expressions for E and $E(e_1)$, valid in air, with a factor of 2/3.

2.3 Allowable liquid velocity for open sorbent materials

2.3.1 Introduction

In this section a 1-dimensional model is presented to predict the maximum allowable liquid velocity through a packed bed of open material for which the bed remains uncompressed and for which its high porosity is maintained. In contrast to existing models ([15] through [20]), the presented model includes the support of the packed bed by friction between packed bed and enclosing wall. Furthermore, the pressure drop relations, compressibility relations and friction coefficients between packed bed and enclosing wall, constituting the model, were all determined separately by experiment. Hence, the model could be compared directly with flow tests, without debatable parameter adjustments afterwards.

In §2.3.2 the model incorporating pressure drop, compressibility and wall friction is derived. In §2.3.3 the model predictions are compared with flow tests. The results are discussed in §2.3.4.

2.3.2 Model

For an incompressible packed bed subject to liquid flow with constant superficial flow velocity "u", the mechanical pressure P exerted on the packed bed material in the direction of liquid flow is proportional to the bed length already crossed by the flow, see figure 2.24. This mechanical pressure originates from the flow resistance of the bed (decreasing liquid pressure P_L, see figure 2.24). The compressive force acting on the bed is supported by the sieve plate at the bottom of the tube.

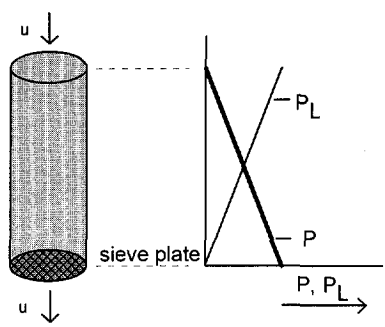

Figure 2.24: Mechanical pressure exerted on an incompressible packed bed subject to liquid flow

For a compressible packed bed the mechanical pressure caused by the flow resistance of the bed will compress the underlying bed material and cause both the bed length and the

porosity to decrease. As a result, the flow resistance of the bed will increase in the direction of flow, causing further compression of the bed, see figure 2.25:

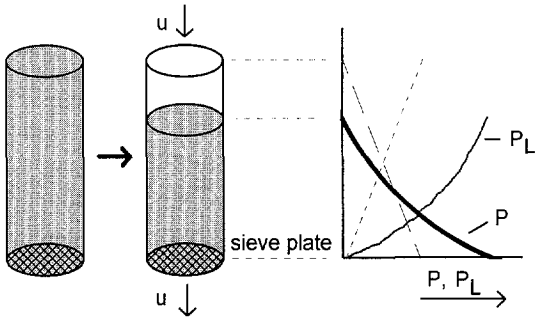

Figure 2.25: Mechanical pressure exerted on a compressible packed bed subject to liquid flow

For a compressible packed bed without precompression (precompression is stiffening the packed bed by applying a lower bed porosity) and without wall-friction (friction between the packed bed and the enclosing walls), the pressure P acting on a bed segment follows directly from the relations for pressure drop $S(\varepsilon)$ and compressibility $\varepsilon(P)$, both as a function of porosity ε, see figure 2.26. The reason for this is that for small enough segments the porosity is approximately constant. The pressure drop relation $S(\varepsilon)$ has to include a correction for the decrease in length of the segment, which is also a function of porosity.

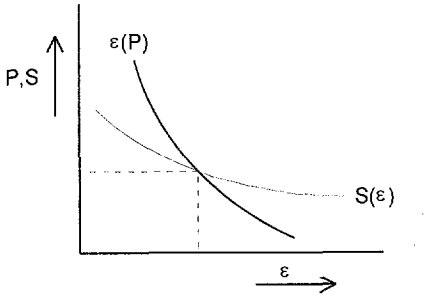

Figure 2.26: For each slice of bed material, the compressibility balances the pressure drop

P as a function of bed length already crossed by the flow can be formulated as follows:

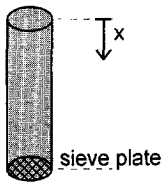

$$P(x) = \int_0^x S(\varepsilon(P(x)))\,dx \tag{2.28}$$

Figure 2.27: Definition of co-ordinate x

in which "x" is a fixed co-ordinate describing the position of the bed segment relative to the uncompressed bed, see figure 2.27.

The resistance to compression can be increased by precompression of the packed bed. This is achieved by decreasing the porosity of the packed bed by adding more material into the bed. As a result, the compressibility has a threshold value, below which value no compression of the bed takes place. The precompression is obtained by forcing the uncompressed material (porosity ε_0) into the tube, thus straining (compressing) the material in the direction of liquid flow (subscript 1). For a certain strain e_1, the resulting porosity ε_1 of the precompressed packed bed follows from equation (2.15) already treated in section 2.2:

$$e_1 = \frac{\varepsilon_0 - \varepsilon_1}{1 - \varepsilon_1} \tag{2.15}$$

P(x) now becomes:

$$P(x) = \int_0^x S[(\varepsilon(P(x)) \le \varepsilon_1) \cdot \varepsilon(P(x)) + (\varepsilon(P(x)) > \varepsilon_1) \cdot \varepsilon_1]\,dx \tag{2.29}$$

resulting in a higher allowable liquid velocity before a decrease in bed length and bed porosity occurs.

When we also include wall friction, both the precompressive stress and the pressure originating from the flow resistance cause a frictional resistance along the enclosing wall, thus decreasing the pressure P on the next bed segments. As a result, the allowable liquid velocity will be higher.
The precompressive stress σ_1 and the pressure P(x) originating from the flow resistance cause a pressure normal to the enclosing wall. σ_1 follows from the compressibility relation and strain e_1, and is assumed to be constant throughout the packed bed. The pressure σ_N normal to the enclosing wall is related to the pressure in the direction of the flow, by Poisson's ratio ν:

$$\sigma_N = \frac{\nu}{1 - \nu} \cdot (\sigma_1 + P) \tag{2.30}$$

Equation (2.30) is valid for linear elastic material behaviour (see equation 2.10). For materials showing a porosity dependent Poisson's ratio, e.g. cellular silicone, equation (2.30) becomes:

$$\sigma_N = \frac{\nu(\varepsilon(P))}{1-\nu(\varepsilon(P))} \cdot (\sigma_1 + P) \tag{2.31}$$

The normal force F_N acting on a bed segment in the direction perpendicular to the direction of liquid flow is the product of normal stress according to equation (2.31) and the wall surface area A. For a segment with original length dx, the wall surface area A of a segment subject to liquid flow is equal to:

$$A = \pi \cdot D \cdot dx \cdot \frac{1-\varepsilon_1}{1-\varepsilon(P)} \tag{2.32}$$

in which D is the column diameter. The factor containing the porosity accounts for the decrease in length of the bed segment.

For materials showing a proportional relation between frictional force F_W (here in the direction opposite to the direction of liquid flow) and normal force F_N, the pressure P(x) acting on the material in the direction of liquid flow is decreased by an amount of $W = F_W/A_C = \mu \cdot F_N/A_C$, A_C being the cross-sectional area of the tube and μ being the friction coefficient between packed bed and tube wall (see Appendix A.2).

Now, P(x) is defined as follows:

$$P(x) = \int_0^x [S[\varepsilon(P(x)) \le \varepsilon_1) \cdot \varepsilon(P(x)) + (\varepsilon(P(x)) > \varepsilon_1) \cdot \varepsilon_1] - W(P(x))]dx \tag{2.33}$$

with

$$W(P) = \frac{4}{D} \cdot \mu \cdot \frac{\nu(\varepsilon(P))}{1-\nu(\varepsilon(P))} \cdot [\sigma_1 + (P \ge 0) \cdot P] \cdot \frac{1-\varepsilon_1}{1-\varepsilon(P)} \tag{2.34}$$

For PUR foam, compressibility tests showed a zero Poisson's ratio (section 2.2). This means that the precompression and the flow resistance of the PUR foam is not accompanied by contraction perpendicular to the central axis of the tube. The only effect of precompressing the PUR foam is creating a threshold value and for pressures below this value no compression of the bed takes place. In contrast, for materials with a Poisson's ratio larger than zero the precompression in addition creates a frictional resistance between bed and tube wall.

Because of the complexity of the functions $S(\varepsilon)$ and $\varepsilon(P)$ for some materials (e.g. silicone rubber), equation (2.33) has to be solved numerically by stepwise calculation and summation. This approach will now be illustrated by calculating the allowable liquid velocity for a packed bed of cellular silicone.

According to Chapter 3 section 3.2, the pressure drop relation for cellular silicone can be described by equation (2.35) with a value of C_1 equal to $3.88 \cdot 10^3$ for Dow Corning cellular silicone with a packed bed porosity of 0.83:

$$S(\varepsilon) = C_1 \cdot \frac{\eta \cdot u \cdot (1-\varepsilon)^2}{\varepsilon^3 \cdot d_{eq}^2} \cdot L(\varepsilon) \tag{2.35}$$

S:	pressure drop	[N/m^2]
ε:	packed bed porosity	[-]
C_1:	structural parameter (see Chapter 3)	[-]
η:	dynamic viscosity	[N·s/m^2]
u:	superficial flow velocity	[m/s]
d_{eq}:	equivalent fiber diameter (equation 3.9)	[m]
L:	packed bed length	[m]

For a bed of length L segmented into "i" segments, $L(\varepsilon)$ is given by equation (2.36):

$$L(\varepsilon) = \frac{L}{i} \cdot \frac{1-\varepsilon_1}{1-\varepsilon} \tag{2.36}$$

According to section 2.2 of this chapter, the compressibility relation for Dow Corning cellular silicone can be described by equations (2.37) and (2.15), assuming that the value of the stress relaxation factor in water is 2/3 of this factor in air as with PUR foam (see section 2.2):

$$\sigma_1(e_1) = E(e_1) \cdot e_1 = (e_1 < 0.065) \cdot 3.97 \cdot 10^4 \cdot e_1 + (e_1 \geq 0.065) \cdot 9.26 \cdot 10^3 \cdot e_1^{0.467} \tag{2.37}$$

$$\text{with } e_1 = \frac{\varepsilon_0 - \varepsilon_1}{1-\varepsilon_1} \tag{2.15}$$

The uncompressed porosity ε_0 is equal to 0.87 and the bed is precompressed to ε_1 = 0.83, so the precompressive stress σ_1 is $4.71 \cdot 10^3$ N/m^2.

Since the model needs the compressibility relation in the form of $\varepsilon = \varepsilon(P)$, equation (2.37) has to be inverted over two piecewise continuous ranges of strain. This has been solved using curve fitting software, resulting in equation (2.38):

$$\varepsilon(P) = (P \geq 4764.5) \cdot \left[\begin{array}{l} (P \leq 6057) \cdot (0.87 - 1.602 \cdot 10^{-8} \cdot P^2 + 4.594 \cdot 10^{-10} \cdot P^{2.5} + \ldots \\ -3.663 \cdot 10^{-12} \cdot P^3) + (P > 6057) \cdot 0.78 \end{array} \right] + (P < 4764.5) \cdot \varepsilon_1 \tag{2.38}$$

Equation (2.38) is only valid for pressures smaller than 6057 N/m^2 because equation (2.37) is only valid for strains up to 0.4.

For friction between wet cellular silicone and perspex, the friction coefficient μ has been experimentally established at 0.65 (see Appendix A.2). This value of μ can be used for the validating flow tests in a perspex tube, discussed in §2.3.3.

Now, the mechanical pressure P exerted on the packed bed material in the direction of liquid flow can be calculated using equation (2.39):

$$P_j \sum_{f=1}^{j} \left(S\left(\varepsilon\left(P_f\right)\right) - W\left(P_f\right)\right) \tag{2.39}$$

$S(\varepsilon)$ is given by equations (2.35) and (2.36) and $\varepsilon(P)$ is given by equation (2.38). $W(P)$ is given by equation (2.40):

$$W(P) = \frac{4}{D} \cdot \mu \cdot \frac{\nu(\varepsilon(P))}{1-\nu(\varepsilon(P))} \cdot \left[\sigma_1 + (P \geq 0) \cdot P\right] \cdot L(\varepsilon(P)) \tag{2.40}$$

with Poisson's ratio given by equation (2.41):

$$\nu(e_1) = 0.195 \cdot e_1 + 0.067 \tag{2.41}$$

The current bed length Z as a function of bed segment number is given by equation (2.42). The compressed total bed length is given by Z_1.

$$Z_j \sum_{f=j}^{i} L\left(\varepsilon\left(P_f\right)\right) \tag{2.42}$$

By calculating Z_1 as a function of the superficial flow velocity "u", the maximum allowable u_{max} can be determined for which Z_1 remains equal to L. The calculated u_{max} can be verified by flow tests, which will be discussed in the next paragraph.

2.3.3 Validating flow tests

The maximum allowable superficial flow velocity u_{max} has been experimentally determined for a number of fiber and foam materials. The compressibility relations and pressure drop relations for these materials are treated in section 2.2 and in Chapter 3 section 3.2. The friction coefficients between the wet fiber or foam beds and perspex from which the test tube is made, are treated in Appendix A.2.

Table 2.5 gives an overview of the applied open materials. For fibers, the fiber diameter "d" and for foam the equivalent fiber diameter d_{eq} (see Chapter 3 equation 3.9) is given to be used for the pressure drop relation.

Table 2.5: applied materials

material	supplier	uncompressed porosity ε_0 [-]	"d" or d_{eq} (foam) [m]
PP-100	Polyost, Belgium	0.965	$d = 100 \cdot 10^{-6}$
PP-65	"	0.965	$d = 65 \cdot 10^{-6}$
PET	"	0.98	$d = 15 \cdot 10^{-6}$
PUR foam	Recticel, Belgium	0.972	$d_{eq} = 8.5 \cdot 10^{-6}$
cellular silicone	Dow Corning, Germany	0.87	$d_{eq} = 104.6 \cdot 10^{-6}$

The validating flow tests were conducted using the same tube as was used for the pressure drop measurements (Chapter 3 section 3.2), see figure 2.28. The tube is made of perspex and provided with scale markers on the outside, so that a small compression of the packed bed can be detected. The tube, which has an internal diameter of 0.06 m, is filled with fibers or foam by consecutively inserting and gently pressing equal quantities of fibers or equal cylindrical foam plugs into the tube with a piston. The maximum bed length is 0.77 m. The flow velocity is derived from the mass flow rate of the water leaving at the top.

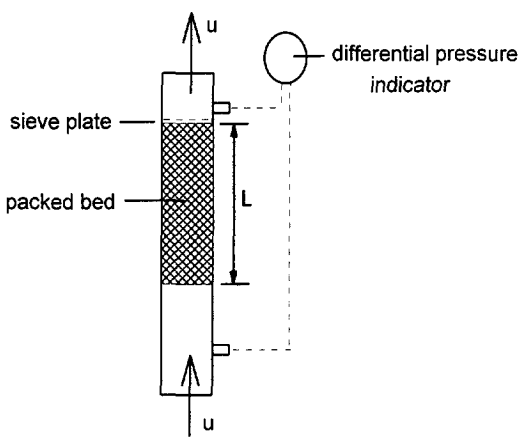

Figure 2.28: Test tube

For PP-100 fibers, the tube was filled to a length L of 73.5 cm and a precompressed porosity ε_1 of 0.9. Figure 2.29 gives the bed length L as a function of the superficial flow velocity "u". According to the experiment, u_{max} is approximately 11.5 cm/s. The bed length as a function of velocity, predicted by the model according to §2.3.2 (see Appendix A.3), is given in figure 2.29 as a continuous line. The predicted value of u_{max} is approximately 12 cm/s which is in agreement with the experiment.

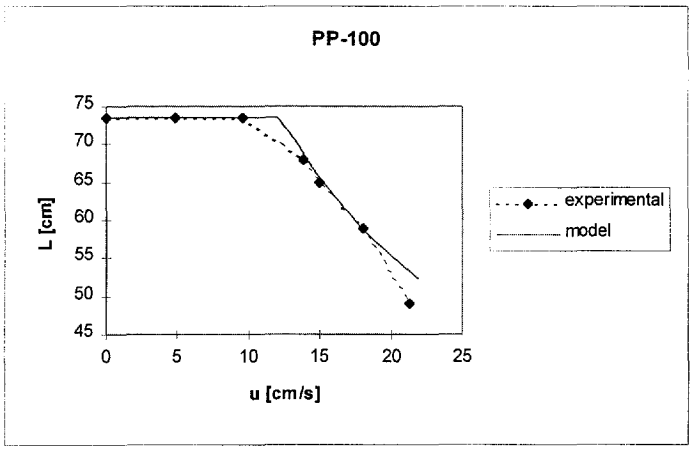

Figure 2.29: Measured and predicted bed length as a function of the superficial flow velocity for PP-100 fibers

For PP-65 fibers, the tube was filled to a length L of 56 cm and a precompressed porosity ε_1 of 0.9. The bed length as a function of velocity, both measured and predicted by the model according to §2.3.2 (see Appendix A.3), is given in figure 2.30. According to the experiment, u_{max} is approximately 7.5 cm/s. The predicted value of u_{max} is approximately 7 cm/s, which is in agreement with the experiment.

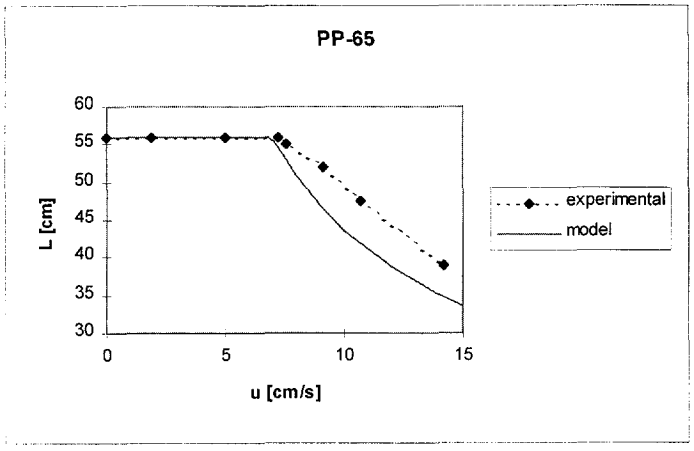

Figure 2.30: Measured and predicted bed length as a function of the superficial flow velocity for PP-65 fibers

For PET fibers, the tube was filled to a length L of 37.5 cm and a precompressed porosity ε_1 of 0.9. The bed length as a function of velocity, both measured and predicted by the model according to §2.3.2 (see Appendix A.3), is given in figure 2.31. According

to the experiment, u_{max} is less than 1.8 cm/s. The predicted value of u_{max} is approximately 1.2 cm/s, which is in agreement with the experiment.

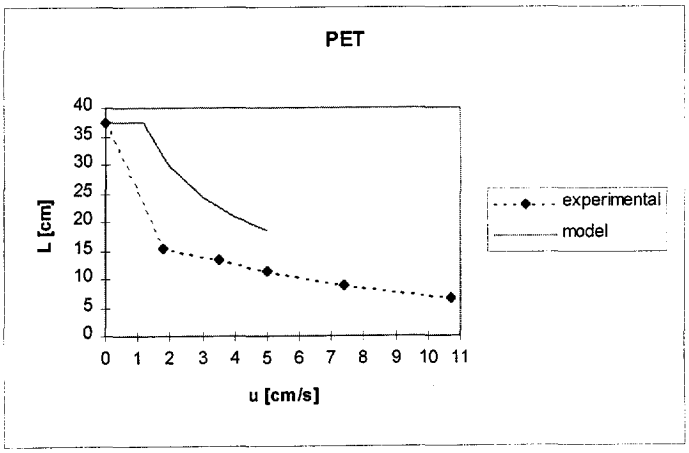

Figure 2.31: Measured and predicted bed length as a function of the superficial flow velocity for PET fibers

Two validating flow tests with PUR foam were conducted. According to the first experiment. with a length L of 27 cm and a precompressed porosity ε_l of 0.957, u_{max} is approximately 4.8 cm/s. u_{max} is predicted at approximately 1.8 cm/s, which is considerably less than u_{max} according to the experiment. The bed length as a function of velocity, both measured and predicted by the model according to §2.3.2 (see Appendix A.3), is given in figures 2.32.

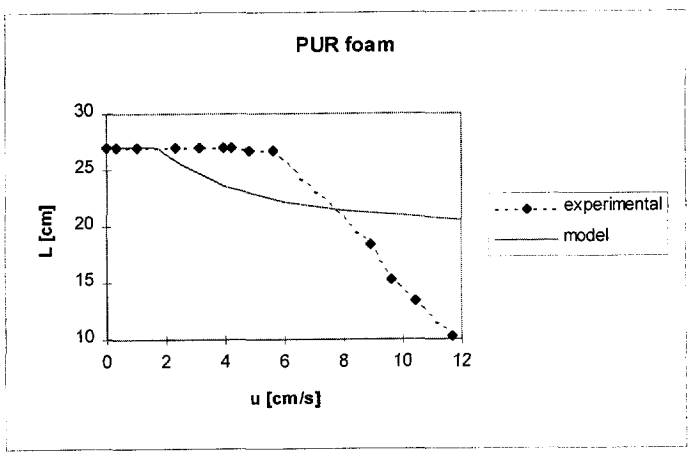

Figure 2.32: Measured and predicted bed length as a function of the superficial flow velocity for PUR foam (first experiment)

The second experiment with PUR foam was conducted with a length of 34.5 cm and a precompressed porosity of 0.941 According to the experiment, u_{max} is approximately 3 cm/s, whereas the model overestimates u_{max} at 4.3 cm/s. Apparently, the model can both overestimate and underestimate u_{max} for PUR foam.

The validating flow test with cellular silicone was conducted with a length L of 13.5 cm and a precompressed porosity ε_1 of 0.83. According to the experiment, u_{max} is 0.87 cm/s, see figure 2.33. At this point, the foam bed is compressed about 1 to 2 mm. Between 0.87 cm/s and 1.16 cm/s, the bed length is further reduced, but in contrast to the experiments with PUR foam or fibers, the compressed bed does not remain continuous: somewhere in the middle of the bed a void is shaped between two of the cylindrical plugs of foam material. For this reason, the two experimental values at the right in figure 2.33 are only estimates because they do not apply to a bed consisting of segments lying against each other. According to the model (see Appendix A.3), u_{max} for cellular silicone is predicted at 0.46 cm/s, which is considerably less than u_{max} according to the experiment.

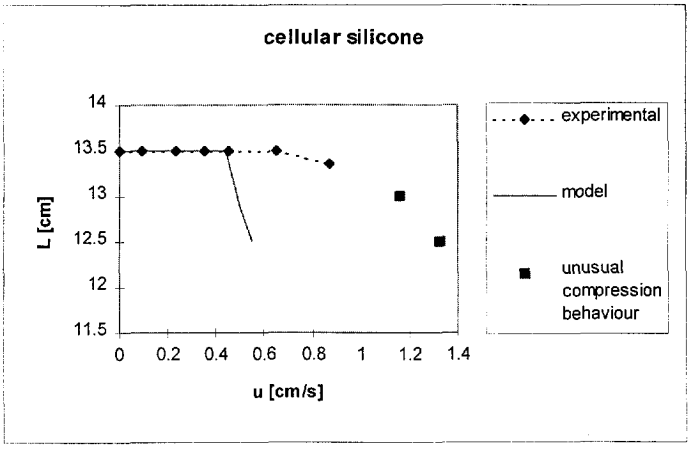

Figure 2.33: Measured and predicted bed length as a function of the superficial flow velocity for cellular silicone

2.3.4 Discussion

For the applied packed foam beds, the model does not predict u_{max} correctly and for PUR foam the model appears to both underestimate and overestimate u_{max}. The reason for this is yet unknown, since all parameters used in the model were determined separately by experiment.

As can be seen from figures 2.29 through 2.31, the model predicts u_{max}, the velocity marking the transition from uncompressed to compressed bed length, correctly for the applied packed fiber beds. The model is based on measured pressure drop relations, compressibility relations and friction coefficients for the applied materials. The only

assumption made in these material dependent data is the difference in stress relaxation between water and air, since all compressibility relations were determined in air (section 2.2). For all fiber (and foam) materials tested, it is assumed that the ratio between the stress relaxation in water and in air is equal to 2/3, which value was experimentally determined for PUR foam by Beavers et. al. [15]. Apparently, this assumption is valid for the applied fiber materials as well, since the maximum allowable velocity u_{max} predicted by the model agrees with the validating flow tests whereas u_{max} is approximately inversely proportional to the compressibility of the packed bed material which means that a relatively large error in compressibility would cause a relatively large error in the predicted u_{max}.
The model is not only sensitive for variations in compressibility, but also for variations in precompressive stress and friction coefficient, thus underlining the good agreement between flow test results and model predictions for the applied packed fiber beds.

Although the model is only intended to predict the transition velocity from which the packed bed starts to be compressed, it is useful to investigate if the model is also valid beyond this transition point.
The model is valid for velocities in the laminar flow regime for which the pressure drop relations were established and for porosities within the range for which the compressibility relations were established. As a result, the reliability of the model gradually decreases for velocities beyond the laminar flow regime and for compressed bed lengths small enough for the bed segments near the sieve plate to cross the valid porosity range. For higher velocities and for advanced compression of the bed the model is therefore increasingly inaccurate. Accordingly, the continuous lines in figures 2.29 through 2.31 representing the model predictions do not correspond with the experiments for higher velocities and smaller bed lengths, except for PP-100 fibers. For velocities increasing beyond the laminar flow regime, the pressure drop will be gradually underestimated resulting in predicted bed lengths which are too high. For bed compressions where the bed segments near the sieve plate cross the minimum porosity for which the compression relation is valid, the compressibility of the material is overestimated, resulting in predicted bed lengths which are too low. Since both effects have opposite effects and since the laminar flow regime and the valid porosity range differ from test to test, the right hand side of the model curves in figures 2.29 through 2.31 can be both higher and lower than the experimental results. For this reason, the model is increasingly unreliable beyond the transition point and the observed agreement between model and experiment for PP-100 fibers has to be regarded as a coincidence. For foam materials, the model is even more unreliable beyond the transition point, because the structural parameter C_1 accounting for the pressure drop is only valid for the initial packed bed porosity.

The presented model is a 1-dimensional model and for this reason restricted to applications with small cross-sectional areas. In this model, bed material initially packed within a small shell perpendicular to the direction of flow is assumed to remain orientated within such a shell after compression of the packed bed. For large tube diameters however, the compression in the direction of the flow will be larger near the centre of the tube and smaller near the tube wall where bed material is restrained by wall friction.

With the model presented in this section, it can be studied how to preserve the high porosity of open materials for application in packed beds subject to liquid flow. Given a certain material and certain bed dimensions, it can be estimated at which porosity the packed bed remains uncompressed for a required u_{max} or which u_{max} can be allowed for a required bed porosity. The effect of sieve plates to support the bed and maintain the required porosity can be investigated by changing the bed length L in the model. Similarly, the effect of enclosing walls can be investigated by changing the ratio between surface area of the enclosing wall and cross-sectional area (restricted to smaller cross-sectional areas).

2.4 Conclusions

A 1-dimensional model has been discussed which predicts the maximum allowable liquid velocity through a packed bed of open material for which the bed remains uncompressed and for which its high porosity is maintained. In contrast to existing models, this model includes the support of the bed by wall friction, which can contribute considerably to the preservation of the bed porosity. The model can be used for design purposes to estimate the allowable liquid velocity in packed beds of open material for different bed porosities, sieve plate configurations and column dimensions.
In order to estimate the compressibility of open sorbent materials required to use this model, these materials were described by linear elastic isotropic material behaviour, factorised for non-linearity and viscoelastic behaviour. The stiffness properties for both random orientated fiber masses and open-cell foams were determined using a special compression bench.
A number of flow tests with different fiber and foam materials demonstrated the validity of this model for the applied packed fiber beds. For the applied packed foam beds the predicted allowable velocities were both too low and too high. The reason for this is yet unknown.

References

[1] Van Wyk, C.M., *Note on the compressibility of wool*, J.Text.Inst., **37** (1946), pp. T285-T292

[2] Komori, T. and Itoh, M., *A new approach to the theory of the compression of fiber assemblies*, Textile Res.J., **61** (1991), pp. 420-428

[3] Carnaby, G.A. and Pan, A., *Theory of the compression hysteresis of fibrous assemblies*, Textile Res.J., **59** (1989), pp. 275-284

[4] Komori, T., Itoh, M., *A model analysis of the compressibility of fiber assemblies*, Textile Res.J., **62** (1992), pp. 567-574

[5] Komori, T., Makishima, K., *Numbers of fiber-to-fiber contacts in general fiber assemblies*, Textile Res.J., **47** (1977), pp. 13-17

[6] Dunlop, J.I., *On the compression characteristics of fibre masses*, J.Text.Inst., **74** (1983), pp. 92-97

[7] Lee, D.H., Carnaby, G.A., Tandon, S.K., *Compressional energy of the random fiber assembly*, Textile Res.J., **62** (1992), pp. 258-265

[8] Rusch, K.C., *Load-compression behavior of flexible foams*, J.Appl.Polym.Sci., **13** (1969), 2297-2311

[9] Meinecke, E.A., Clark, R.C., *Mechanical properties of polymeric foams*, Technomic Publishing, Westport, 1973

[10] Gent, A.N., Thomas, A.G., *The deformation of foamed elastic materials*, J.Appl.Polym.Sci., **1** (1959), 107-113

[11] Gent, A.N., Thomas, A.G., *Mechanics of foamed elastic materials*, Rubber Chem. and Tech., **36** (1963), 597-610

[12] Rusch, K.C., *Load-compression behavior of brittle foams*, J.Appl.Polym.Sci., **14** (1970), 1263-1276

[13] Huber, A.T., Gibson, L.J., *Anisotropy of foams*, J.Mat.Sci., **23** (1988), pp. 3031-3040

[14] Rusch, K.C., *Energy-absorbing characteristics of foamed polymers*, J.Appl.Polym.Sci., **14** (1970), 1433-1447

[15] Beavers, G.S., Wittenberg, K., Sparrow, E.M., *Fluid flow through a class of highly-deformable porous media part II: experiments with water*, Trans.ASME, **103** (1981), pp. 440-444

[16] Zhu, S., Pelton, R.H., Collver, K., *Mechanistic modelling of fluid permeation through compressible fiber beds*, Chem. Eng. Sci.., **50** (1995), pp. 3557-3572

[17] Jönsson, K.A.-S., Jönsson, B.T.L., *Fluid flow in compressible porous media: I: steady-state conditions*, AIChE J., **38** (1992), pp. 1340-1348

[18] Parker, K.H., Mehta, R.V., Caro, C.G., *Steady flow in porous, elastically deformable materials*, Trans. ASME, 1987, pp. 794-800

[19] Beavers, G.S., Hajji, A., Sparrow, E.M., *Fluid flow through a class of highly-deformable porous media Part I: experiments with air*, Trans. ASME, 1981, pp. 432-439

[20] Beavers, G.S., Wilson, T.A., Masha, B.A., *Flow through a deformable porous material*, Trans. ASME, 1975, pp. 598-602

3

Hydrodynamics of open sorbent materials

3.1 Introduction

For design and operation of countercurrent sorption equipment, information on the pressure drop and other flow phenomena is required. Both the pressure drop and the axial dispersion are key parameters in the design of the separation equipment. The pressure drop is a key parameter because of limitations of the allowable water velocity due to the compressibility of open sorbent materials (see Chapter 2). Besides, the pressure drop of the packed bed contributes considerably to the required driving torque of the separation equipment (see Chapter 6) which is limited for constructional reasons. A lower pressure drop means a higher allowable water velocity and hence a higher space efficiency. The axial dispersion is a key parameter as well because the dispersive transport of matter is relatively high in open sorbent materials. As a consequence, axial dispersion has considerable influence on the required total packed bed length for a given removal efficiency and hence on the space efficiency.

Section 3.2 is concerned with the pressure drop of packed beds of open materials. A review of theoretical and empirical relations from literature is given and a comparison is made with experimental results obtained with our laboratory test equipment. In section 3.3 the axial dispersion in packed beds of open materials is studied, using the axially dispersed plug flow model. A number of theoretical and empirical relations from literature are given and experimental results obtained with our laboratory test equipment are compared with these relations. Finally, conclusions are given in section 3.4.

3.2 Pressure drop

3.2.1 Introduction

In order to estimate the expected pressure drop for fluid flow through packed beds of open sorbent material for design purposes, we need a model relating the various parameters involved. For this purpose, in §3.2.2 a semi-empirical relation is formulated which is applicable both to fiber materials with random orientation and open-cell foam

materials (equation 3.6). In addition, other relations from literature are given. In §3.2.3 the results for pressure drop measurements (with water) for a number of open materials used in this research are given. In §3.2.4 these results are compared with the applicable relations from §3.2.2. Finally, §3.2.5 summarises the conclusions for pressure drop for water flow through packed beds of open materials.

3.2.2 Model

According to Darcy's one-dimensional empirical law [1], the pressure drop for fluid flow through rigid homogeneous porous media is proportional to the superficial flow velocity:

$$\frac{|\Delta P|}{L} = \frac{1}{K} \cdot \eta \cdot u \qquad (3.1)$$

ΔP:	pressure drop over length L	$[N/m^2]$
L:	length	$[m]$
K:	permeability coefficient	$[m^2]$
η:	dynamic viscosity of the fluid	$[N \cdot s/m^2]$
u:	superficial flow velocity (relative to fixed co-ordinates)	[m/s]

Darcy's law does not account for effects of inertia and therefore is valid only for low flow velocities ("laminar flow regime", "streamline flow" or "low-Reynolds-number flow"); resistance to flow is assumed to arise mainly from viscous drag. The parameter K depends only on the properties of the porous material.

Kozeny [2,3] derived a general expression for K in terms of porosity and specific surface area, using the analogy between streamline flow through a tube and streamline flow through the pores in a bed of particles ("hydraulic radius theory" or "tube bundle theory"). He assumed the free space in the bed to consist of a series of tortuous cylindrical channels. For streamline flow conditions, it was derived:

$$K = \frac{1}{k} \cdot \frac{\varepsilon^3}{S^2 \cdot (1-\varepsilon)^2} \qquad (3.2)$$

k:	Kozeny's constant	[-]
ε:	bed porosity (void fraction)	[-]
S:	specific surface area of the particles	$[m^2/m^3]$

Kozeny's constant "k", a dimensionless proportionality factor, is dependent on the porosity, particle shape, particle size distribution and other structural factors.

For turbulent flow, when resistance to flow arises also from the energy loss in turbulent eddies and the energy loss at the sudden changes in the cross-section of the channels,

Ergun [4] derived an additional semi-empirical relation between pressure drop and superficial flow velocity:

$$\frac{\Delta P}{L} \div \frac{1-\varepsilon}{\varepsilon^3} \cdot \rho \cdot u^2 \cdot S \qquad (3.3)$$

ρ: density of fluid [kg/m^3]

So the pressure drop relation, consisting of a laminar and a turbulent contribution with dimensionless proportionality factors c_1 and c_2, can be written as follows :

$$\frac{\Delta P}{L} = c_1 \cdot \eta \cdot u \cdot \frac{(1-\varepsilon)^2}{\varepsilon^3} \cdot S^2 + c_2 \cdot \rho \cdot u^2 \cdot \frac{1-\varepsilon}{\varepsilon^3} \cdot S \qquad (3.4)$$

For long fibers with diameter "d" the specific surface area S relative to the volume of the fibers is:

$$S = \frac{4}{d} \qquad (3.5)$$

For open materials, the pressure drop over packed beds can be described by equation (3.4) using S according to equation (3.5):

$$\frac{\Delta P}{L} = C_1 \cdot \frac{\eta \cdot u \cdot (1-\varepsilon)^2}{\varepsilon^3 \cdot d^2} + C_2 \cdot \frac{\rho \cdot u^2 \cdot (1-\varepsilon)}{\varepsilon^3 \cdot d} \qquad (3.6)$$

C_1: structural parameter for viscous term [-]
C_2: structural parameter for inertia term [-]

The countercurrent separation equipment with open sorbent material as discussed here will be applied only in the laminar flow regime (the water velocity has an order of magnitude of 1 cm/s), so for water flow we only need to know parameter C_1. Parameter C_2 may be of interest for applications on gases.

For fibers, "d" in equation (3.6) is the fiber diameter. Foam can be represented by a bundle of cylindrical tortuous pores of diameter d_p, where d_p is the equivalent pore space diameter. For foam, an equivalent fiber diameter d_{eq} can be derived from d_p and the porosity ε of the foam, thus assuming the foam to be equivalent to a fiber mass consisting of fibers with diameter d_{eq}.
This equivalent fiber diameter d_{eq} is derived as follows. According to [5], for open-cell foams with no cell membranes, the specific surface area a_s of the foam bed is given by :

$$a_s = \frac{4 \cdot \varepsilon}{d_p} \qquad (3.7)$$

d_p: equivalent pore space diameter [m]

a_s for a fiber bed is given by:

$$a_s = \frac{4}{d} \cdot (1 - \varepsilon) \tag{3.8}$$

The equivalent fiber diameter for a foam follows from the combination of equations (3.7) and (3.8) :

$$d_{eq} = \frac{1 - \varepsilon_0}{\varepsilon_0} \cdot d_p \tag{3.9}$$

d_{eq}:	uncompressed equivalent fiber diameter	[m]
ε_0:	initial porosity (supplied / uncompressed condition)	[-]
d_p:	mean pore diameter (empty space based) at $\varepsilon = \varepsilon_0$	[m]

So for open-cell foam, "d" in equation (3.6) is replaced by d_{eq}.

The equivalent pore space diameter d_p is defined by equation (3.7). It is convenient to use the uncompressed mean pore diameter (empty space based) for d_p because this size is often given by the supplier of the foam or can easily be established using a microscope. An alternative is to use the mean cell size (including the struts of the foam cells). The difference between using the mean pore diameter or an alternative pore dimension like the mean cell size, will be incorporated in the proportionality factors C_1 and C_2. Therefore it should always be mentioned what real pore dimension has been used to establish d_{eq} according to equation (3.9).

An important advantage of equation (3.6) is that only structural parameters in terms of porosity and particle size (fiber diameter or mean pore diameter) are required, which are available or can be easily determined. Structural parameters that are difficult to quantify, like tortuosity of the channels or particle size distribution, are incorporated in the structural parameters C_1 and C_2.

The Reynolds number is defined as the fluid density times the interstitial flow velocity times the hydraulic mean diameter, divided by the dynamic viscosity. The hydraulic mean diameter is equal to four times the cross-sectional area divided by the wetted perimeter [6]:

$$Re = \frac{\rho \cdot \frac{u}{\varepsilon} \cdot \frac{4 \cdot \varepsilon}{a_s}}{\eta} \tag{3.10}$$

For fibers, combination of equations (3.10) and (3.8) yields:

$$Re = \frac{\rho \cdot u \cdot d}{(1 - \varepsilon) \cdot \eta} \qquad \left(= \frac{\rho \cdot \frac{u}{\varepsilon} \cdot \frac{\varepsilon \cdot d}{1 - \varepsilon}}{\eta}\right) \tag{3.11}$$

This Reynolds number refers to flow through cylindrical channels with a diameter equal to $\varepsilon \cdot d/(1-\varepsilon)$. For fibers, "d" is the fiber diameter and for open-cell foam "d" is replaced by the equivalent fiber diameter d_{eq} according to equation (3.9).

Approximately, for $Re < 8$ flow is dominated by viscous forces and for $8 < Re < 400$ the turbulent flow regime initiates [7].

Because some confusion can exist whether Re is based on the hydraulic mean diameter according to equation (3.10) or based on ¼ of the hydraulic mean diameter like some other authors do (e.g. [7] in §4.2.3), leading to a Reynolds number 4 times as small, it should always be indicated which of these two definitions is used.

Happel derived expressions for the permeability of arrays of cylinders using a unit-cell approach [8]. For flow parallel to an array of cylinders, the result can be written as:

$$C_1 = 16 \cdot \frac{\varepsilon^3}{1-\varepsilon} \cdot \frac{1}{[-\ln(1-\varepsilon) - 1.5 + 2 \cdot (1-\varepsilon) - \frac{(1-\varepsilon)^2}{2}]} \tag{3.12}$$

For flow perpendicular to an array of cylinders Happel derived:

$$C_1 = 32 \cdot \frac{\varepsilon^3}{1-\varepsilon} \cdot \frac{1}{-\ln(1-\varepsilon) + \frac{(1-\varepsilon)^2 - 1}{(1-\varepsilon)^2 + 1}} \tag{3.13}$$

For random orientation of cylinders, values for C_1 are obtained by taking one-third of those for parallel flow plus two-thirds of those for perpendicular flow [9]:

$$C_1 = \frac{16}{3} \cdot \frac{\varepsilon^3}{1-\varepsilon} \cdot \frac{1}{[-\ln(1-\varepsilon) - 1.5 + 2 \cdot (1-\varepsilon) - \frac{(1-\varepsilon)^2}{2}]} + \frac{64}{3} \cdot \frac{\varepsilon^3}{1-\varepsilon} \cdot \frac{1}{-\ln(1-\varepsilon) + \frac{(1-\varepsilon)^2 - 1}{(1-\varepsilon)^2 + 1}} \tag{3.14}$$

Jackson and James made an estimate of the permeability based on a cubical lattice model (three-dimensional array of rods with random orientation), using Happel's relations for the individual resistances of the rods. A revised prediction using Drummond and Tahir's more accurate equations instead of Happel's equations, yields the following expression for C_1 [10]:

$$C_1 = \frac{80}{3} \cdot \frac{\varepsilon^3}{1-\varepsilon} \cdot \frac{1}{-\ln(1-\varepsilon) - 0.931} \tag{3.15}$$

Davies [11] presented an empirical correlation which fit a considerable quantity of experimental data for beds of fibers used for air filters over a range of $\varepsilon = 0.7$ to 0.994. Expressed in the form of equation (3.6), Davies' empirical correlation corresponds with:

$$C_1 = \frac{64 \cdot \varepsilon^3}{(1-\varepsilon)^{0.5}} \cdot [1 + 56 \cdot (1-\varepsilon)^3] \tag{3.16}$$

For foamlike porous materials of very high porosity, metallic foam with $0.97 < \varepsilon < 0.98$, Du Plessis et. al. [12] derived a theoretical prediction, including an inertia term, which can be translated into equation (3.6) for open materials as follows:

$$C_1 = \frac{9 \cdot X^2 \cdot (3-X)^2 \cdot (X-1)}{\varepsilon^2} \tag{3.17}$$

$$C_2 = \frac{X^2 \cdot (3-X) \cdot (X-1)}{2 \cdot \varepsilon} \tag{3.18}$$

$$\frac{1}{X} = \frac{3}{4 \cdot \varepsilon} + \frac{(9 - 8 \cdot \varepsilon)^{0.5}}{2 \cdot \varepsilon} \cdot \cos\left(\frac{4 \cdot \pi}{3} + \frac{1}{3} \cdot \cos^{-1}\left(\frac{8 \cdot \varepsilon^2 - 36 \cdot \varepsilon + 27}{(9 - 8 \cdot \varepsilon)^{1.5}}\right)\right) \tag{3.19}$$

Gent and Rusch [13] experimentally established that for a range of reticulated (cell membranes removed) polyurethane foam with $0.97 < \varepsilon < 0.98$ and rubber foam prepared from latex with $0.82 < \varepsilon < 0.91$ (also without cell membranes) the structural parameter C_1 in equation (3.6) is constant and equal to:

$$C_1 = 90.9 \tag{3.20}$$

Liu et. al. [14] established a semi-empirical relation including tortuosity and curvature ratio as well as wall-effects. This model is not treated here, because structural parameters accounting for tortuosity or curvature ratio most likely are unknown. It is obvious that it is much easier to establish the pressure drop directly by experiment than retrieving the required structural parameters by other experiments or measurements.

The wall-effect, the phenomenon that the particles will not pack as closely in the region near the wall as in the centre of the bed, can be estimated separately using a correction factor f_w according to Coulson et. al. [7]:

$$f_w = \left(1 + \frac{S_{cont}}{2 \cdot S}\right)^2 \tag{3.21}$$

S_{cont} is the surface of the container per unit volume of the bed. The laminar term of equation (3.6) has to be divided by the correction factor f_w. For the open materials and column diameters used in this research, the wall-effects are negligibly small.

Summarising, we now have three relations for fibers with random orientation (equations 3.14 through 3.16) and two relations for open-cell foam (equations 3.17 through 3.19

and equation 3.20) at our disposal to compare with our own experimental results expressed in the form of equation (3.6) (see §3.2.3).

3.2.3 Experiments

Fibers

Three kind of fibers were used: PET (polyethylene tereftalate) fibers with a diameter of 15 μm and PP (polypropylene) fibers with diameters of 50 μm and 100 μm. The fibers were supplied in a more or less random orientation. The PET fibers were manufactured by Akzo Nobel (The Netherlands), the PP fibers by Polyost (Belgium).

A PVC tube with an internal diameter of 3.4 cm is filled with these fibers by consecutively inserting and gently pressing equal quantities of the fibers into the tube with a piston until the desired bed length is reached. The piston rod has scale markers to ensure equal lengths of the fiber bed segments and thus constant porosity across the packed bed. The fiber bed extends from the right-hand side of pressure indicator P1 to the left-hand side of pressure indicator P2 where a sieve plate supports the bed (see figure 3.1). The distance between P1 and P2 is 85 cm. The superficial flow velocity is derived from the mass flow rate of the effluent.

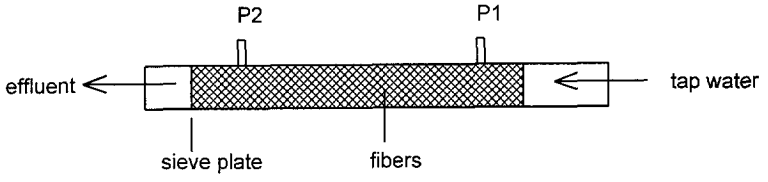

Figure 3.1: Pressure drop measurement equipment used for fiber beds

Table 3.1 gives the results for pressure drop measurements of PET and PP fibers. For each fiber diameter, for two different bed porosities a series of measurements was done. Parameter C_1 was established based on measurements with velocities for which the pressure drop is proportional to the mass flow rate. The Reynolds number (according to equation 3.11) is the maximum value for the concerning material in the proportionality range.

Table 3.1: pressure drop measurements of fiber beds

material	Re (max)	bed porosity	C_1 (equation 3.6)
PET 15 μm	4	0.881	140.9
		0.808	102.2
PP 50 μm	9	0.890	107.9
		0.804	117.4
PP 100 μm	43	0.881	142.9
		0.850	107.9

Experiments were also made with PDMS (Poly Di Methyl Siloxane) silicone rubber fibers (diameter 200 μm), but no reliable pressure drop data are available due to

insufficient stiffness of these fibers. At high bed porosities (0.9 and higher) the high compressibility of the PDMS fiber bed causes an almost immediate collapse of the packed bed with water flow. For relatively low bed porosities (<0.8) steady state conditions can be established, but are not reproducible due to large inhomogenuities in the slack fiber material. The order of magnitude of C_1 for 200 μm PDMS fibers with a porosity around 0.75 is 10^3.

Foam

Three kinds of foam were investigated: silicone rubber foam (mainly consisting of PDMS) from two different manufacturers and reticulated PUR (polyurethane) foam.

The PUR foam was supplied by Recticel, Belgium. The foam has a supplied porosity of 0.972 and a mean pore diameter of 294 μm (determined by microscope), so the equivalent fiber diameter according to equation (3.9) is 8.5 μm A series of measurements was conducted with packed bed porosities ranging from 0.923 to 0.963. A perspex tube with an internal diameter of 6 cm is filled with foam by consecutively inserting and gently pressing 5 cm high cylindrical plugs with a diameter larger than 6 cm into the tube with a piston. The bed is supported by a sieve plate at the end at which the water leaves the tube. The packed bed porosity can be changed using larger plug diameters. Visual inspection ensures equal packed plug heights. The tube is mounted vertically to ensure that the upward water flow will purge all air from the foam. The pressure drop is determined using a differential pressure measurement PI at a single position, so the static pressure of the water column between P1 and P2 (see figure 3.2) is not incorporated. The maximum bed length is 0.77 m. The superficial flow velocity is derived from the mass flow rate of the effluent.

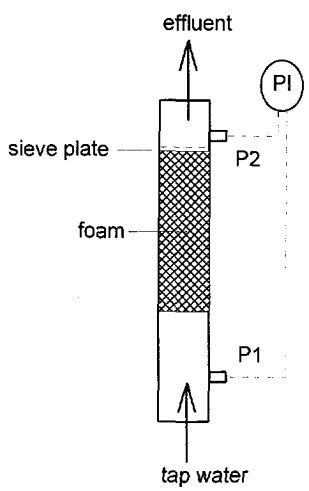

Figure 3.2: Pressure drop measurement of PUR foam

PDMS foam as manufactured by AlliedSignal (USA), M9777 cellular silicone, has a porosity of 0.77 and a mean pore diameter of 675 μm in supplied condition, resulting in an equivalent fiber diameter of 201.6 μm. From the thin sample slabs received, small cylindrical plugs were made. With these plugs a glass tube with an internal diameter of 16.6 mm was filled, the packed bed length is approximately 0.3 m. The test equipment resembles that of figure 3.2, except for the pressure measurement which is done only at P1 (P2 ≈ 1 bar).

Another PDMS foam is manufactured by Dow Corning (Germany). This foam, Dow Corning 8157 silicone foam, has a porosity of 0.87 and a mean pore diameter of approximately 700 μm, resulting in an equivalent fiber diameter of 104.6 μm. It was provided in large enough quantities to use the test equipment from figure 3.2. From the relatively thin slabs received, large cylindrical plugs were made. The 6 cm diameter perspex tube was filled to a bed length of approximately 14 cm (bed porosity 0.83). For comparison, additional tests were made using the glass tube which was used for the AlliedSignal foam. The packed bed porosity in the glass tube was 0.8.

Table 3.2 gives the results for pressure drop measurements of PUR and PDMS foam. For each foam a series of measurements was conducted. Parameter C_1 was established based on measurements with velocities for which the pressure drop is proportional to the mass flow rate. The Reynolds number (according to equation 3.11) is the maximum value for the concerning foam in the proportionality range. The mean pore diameter (empty space based) was used for the equivalent pore space diameter d_p needed to calculate the equivalent fiber diameter d_{eq} according to equation (3.9) which was used in equation (3.6) to establish parameter C_1.

Table 3.2: pressure drop measurements of PUR and PDMS foam

foam	Re (max)	bed porosity	C_1 (equation 3.6)
PUR	6.9	0.963	35.7
		0.957	29.6
		0.955	26.9
		0.941	27.0
		0.923	20.4
PDMS (Dow Corning)	6.6	0.83	$3.88 \cdot 10^3$
		0.8	$2.71 \cdot 10^3$
PDMS (AlliedSignal)	2.1	0.6	$1.58 \cdot 10^3$

3.2.4 Discussion

Fibers

In figure 3.3 the results for fibers are compared with the three relations for fibers with random orientation: Happel (equation 3.14), Jackson and James (equation 3.15) and Davies (equation 3.16).

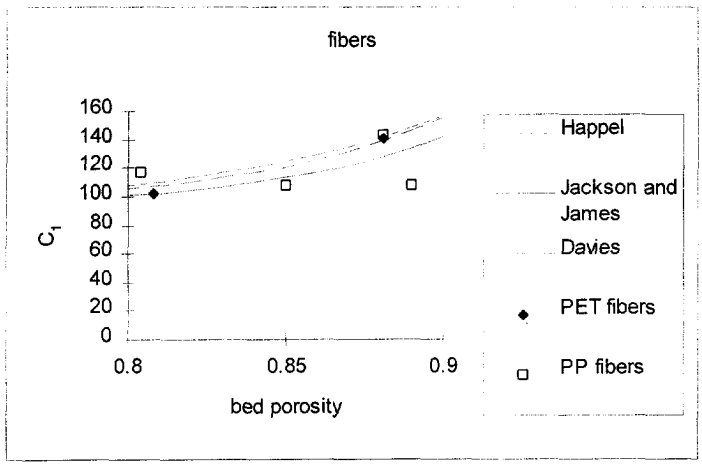

Figure 3.3: Comparison of pressure drop measurements of fiber beds with predictive relations

Figure 3.3 shows the similarity of the predictions according to the different models: C_1-values according to Davies are within 3% deviation of Happel's equation in this porosity range, the values according to Jackson and James are within 10% deviation of Happel's equation.
The results for PET fibers agree with these predictions. The results for PP fibers however show larger deviations from predicted values. This is probably caused by inhomogenuities in the packed fiber bed due to variations in fiber arrangement already present in the supplied fiber material and also caused by the method of packing. PP fibers were supplied as tufts of fibers which had to be arranged manually into a more random and more homogeneous fiber mass. PET fiber beds did not have the kind of inhomogenuities PP fiber beds have, due to the fact that the PET fibers were supplied as a nonwoven.

Foam

In table 3.3 the results for foam (C_1) are compared with the two relations for open-cell foam: Du Plessis et. al. (from equations 3.17 and 3.19) and Gent and Rusch (equation 3.20). The predicted values for cellular silicone (Dow Corning and AlliedSignal) are shown between brackets because these foams deviate too much from the conditions for which the predictions are valid.

Table 3.3: comparison of pressure drop measurements of foam with predictive relations

foam	bed porosity	C_1	Du Plessis et. al.	Gent and Rusch (empirical)
PUR	0.963	35.7	10.6	90.9
	0.957	29.6	11.8	"
	0.955	26.9	12.1	"
	0.941	27.0	14.6	"
	0.923	20.4	17.8	"
Dow Corning cellular silicone	0.83	$3.88 \cdot 10^3$	(34.6)	(")
	0.8	$2.71 \cdot 10^3$	(40.7)	(")
AlliedSignal cellular silicone	0.6	$1.58 \cdot 10^3$	(96.9)	(")

According to Du Plessis et. al., the C_1 values for PUR foam should be smaller and should increase with decreasing ε. On the other hand, according to Gent and Rusch C_1 should be larger and constant with decreasing ε. An explanation for the differences in magnitude between measurements and predictions can not be given, but perhaps this is not essential since the predictions differ largely among themselves. It should be noted however that Gent and Rusch comment that according to their simple theoretical model consisting of an array of circular tubes with a diameter equal to the mean cell size, the value in equation (3.20) should be in theory 40% of this value, resulting in a theoretical C_1 value of about 36 instead of 90.9 [13]. The difference in tendency of C_1 varying with ε between the measured C_1 values and the C_1 values according to Du Plessis et. al. can be explained by the fact that the predictive relation assumes a rigid regular foam structure whereas the PUR foam will be deformed by compressing the cylindrical samples into the test tube, resulting in deformed cell shapes.
In contrast to the predicted C_1 values, the measured C_1 values are based on the mean pore diameter instead of the mean cell size, but this alone can not explain the observed differences between measured and predicted C_1 values for PUR foam.

The measured values for C_1 for cellular silicone are one to two orders of magnitude larger than predicted by Du Plessis et. al. and Gent and Rusch. These large differences are caused by the difference in structure between cellular silicone and reticulated foam for which the predictions are valid: the cellular silicone has a structure in which only the thin parts of the cell membranes were removed, whereas in reticulated foam only the cell struts were left. Moreover, the spread in pore diameter is much larger with cellular silicone than with PUR foam and part of the cell membranes are not removed at all.
As with PUR foam, the C_1 value for cellular silicone decreases with bed porosity. Again this may be explained by deformation of the cells.
Based on the result for the AlliedSignal foam, a value of C_1 of around 10^3 seems to be a reasonable estimate for dedicated batches of cellular silicone with an improved foam structure (in particular larger parts of the cell membranes removed) for higher permeability .

3.2.5 Conclusions

The pressure drop for fluid flow through packed beds of open materials can be estimated using a semi-empirical relation (equation 3.6). This relation is applicable both to fiber materials with random orientation and open-cell foam materials by using an equivalent fiber diameter for foam. Various relations can be used to estimate the structural parameter C_1 to be applied in equation (3.6).

For fiber materials with random orientation, Happel, Jackson and James and Davies give estimates for C_1 as a function of bed porosity. These relations give quite similar results. Values for C_1 determined by the experiments on PET and PP fibers do agree (PET) or agree reasonably well (PP) with these predictions. Deviations from the models and spread in experimental results are mainly caused by differences in the bed structure. The PET fibers show better agreement between model and experiments than the PP fibers, due to their more homogeneous bed structure (the PET fibers were supplied as a nonwoven).

For open-cell foam, Du Plessis et. al. give an estimation for C_1 as a function of bed porosity (equations 3.17 and 3.19) and Gent and Rusch have found a constant value for C_1 (equation 3.20). For PUR foam, these relations do not give accurate estimates, but the order of magnitude is in agreement with the experimental results. For cellular silicone these relations are not applicable because the foam structure is not as open as for reticulated foam for which the models are valid.
In contrast to the situation for crystalline fiber materials like PET and PP where the pressure drop can be estimated reasonably well, for open-cell foam available relations can only give order of magnitude values for C_1 for PUR foam. For cellular silicone it is always necessary to conduct experiments to establish reliable data. A value of C_1 of 10^3 can be used as an order of magnitude estimate for cellular silicone.

3.3 Axial dispersion

3.3.1 Introduction

Axial (or longitudinal) dispersion is a term for the overall effect of turbulence, velocity gradients and molecular diffusion in the continuous phase (i.e. water or steam) on the concentration distribution of a component to be transferred to or from the sorbent phase. Partly due to the lowering of concentration driving force and partly due to the transport of the transferring component induced by longitudinal dispersion resulting in accumulation or depletion effects, the separation effectiveness will be diminished. This effect is particularly undesirable when a high degree of removal or purification has to be achieved.

Molecular diffusion as a cause for axial dispersion is only dominant at low velocities. Microscale channelling, the appearance of preferential flow paths due to structural irregularities of the packed bed of open material, will greatly increase axial dispersion

and will be the dominant mechanism causing axial dispersion for all commonly applied continuous phase velocities in packed beds of open materials.

3.3.2 Model

Deviations from plug flow in packed beds are represented adequately by the axially dispersed plug flow model for which it is assumed that dispersive transport of mass is superimposed on convective transport, the rate being proportional to the concentration gradient. This model uses only one parameter to characterise mixing in the continuous phase: the axial dispersion coefficient D_{ax} [m^2/s].

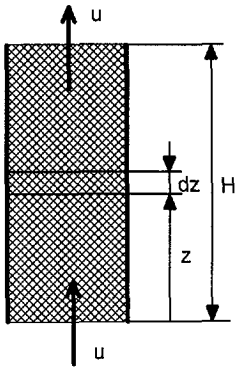

Fig. 3.4: Column with packed bed

Under the following assumptions, we can derive the mass balance for a non-sorbing component in order to describe a tracer pulse response experiment (§3.3.3):

- constant bed porosity
- fluid flow velocity uniformly distributed over the entire cross-section
- radial dispersion negligible in comparison with axial dispersion
- no wall effects

Mass balance over column segment z, z + dz (see figure 3.4):

$$-u\cdot\frac{\partial C}{dz}+\varepsilon\cdot D_{ax}\cdot\frac{\partial^2 C}{\partial z^2}=\varepsilon\cdot\frac{\partial C}{\partial t} \qquad (3.22)$$

u	superficial flow velocity relative to fixed co-ordinates	[m/s]
C	tracer concentration	[kg/m^3]
ε	bed porosity	[-]
D_{ax}	axial dispersion coefficient	[m^2/s]
t	time	[s]

For boundary conditions applying to an open-open pulse response experiment, equation (3.22) can be solved using a convolution integral with the transfer function TR(t) containing the parameter D_{ax} [16].

The normalised input signal (signal 1 in figure 3.6) is represented by I(t) and the normalised output signal (signal 2 in figure 3.6) by C(t). Then C(t) can be predicted from I(t) using a convolution integral with the normalised transfer function TR(t) accounting for the axial dispersion, resulting in M(t):

$$M(t) = \int_0^t I(p) \cdot TR(t-p) \cdot dp \tag{3.23}$$

with

$$TR(t) = \sqrt{\left(\frac{Pe \cdot \tau^3}{4 \cdot \pi \cdot t^3}\right)} \cdot \exp\left\{\frac{-Pe}{4 \cdot t/\tau}\left(1-\frac{t}{\tau}\right)^2\right\} \tag{3.24}$$

$$Pe = \frac{u \cdot H}{\varepsilon \cdot D_{ax}} \tag{3.25}$$

The dimensionless Péclet number "Pe" represents the ratio between convective and dispersive mass transfer. "τ" is the holding time which, for open-open boundaries, is not necessarily equal to the average residence time of the tracer fluid.
Pe and τ are obtained using the minimisation of the goal function Δ as a best fit criterion:

$$\Delta = \sum_0^t \{C(t) - M(t)\}^2 \tag{3.26}$$

Finally, D_{ax} follows from Pe (equation 3.25).

Koch and Brady [17] theoretically derived the following relation for D_{ax} for fluid flow through isotropic packed fiber beds in case of a non-sorbing component:

$$\frac{D_{ax}}{u} = \frac{\frac{171}{3200} \cdot \pi^3 \cdot a^2}{\sqrt{k} \cdot \varepsilon \cdot (1-\varepsilon)} + \frac{4.862 \cdot (1-\varepsilon)^2 \cdot a^3}{k \cdot \varepsilon} \cdot \left[\ln\left(\frac{u \cdot a}{\varepsilon \cdot D}\right)\right]^2 \tag{3.27}$$

a:	fiber radius	[m]
k:	permeability of the packed fiber bed	[m^2]
D:	diffusion coefficient of the tracer in the fluid	[m^2/s]

The permeability "k" for packed fiber beds (for both water and gas flow) can be estimated using the relation from Jackson and James [10], which has been verified to

adequately describe the permeability of the fiber-filled test tube from §3.3.3 (see also §3.2.3):

$$k = \frac{3 \cdot a^2}{20 \cdot (1-\varepsilon)} \cdot (-\ln(1-\varepsilon) - 0.931) \tag{3.28}$$

Combining (3.27) and (3.28) yields the following expression for D_{ax} according to Koch and Brady:

$$\frac{D_{ax}}{u} = \frac{\frac{171}{1600} \cdot \sqrt{\frac{5}{3}} \cdot \pi^3 \cdot a}{\varepsilon \cdot \sqrt{(1-\varepsilon) \cdot (-\ln(1-\varepsilon) - 0.931}} + \frac{32.413 \cdot (1-\varepsilon)^3 \cdot a}{\varepsilon \cdot [-\ln(1-\varepsilon) - 0.931]} \cdot \left[\ln\left(\frac{u \cdot a}{\varepsilon \cdot D}\right)\right]^2 \tag{3.29}$$

Van Zee [19] established an empirical relation for D_{ax} for water flow through PP (polypropylene) and PET (polyethylene tereftalate) fiber beds with fiber diameters of 15 μm (PET) and 50μm and 100 μm (PP), with porosities ranging from 0.82 to 0.94 and with velocities ranging from approximately 10^{-2} to approximately 10^{-1} m/s:

$$\frac{D_{ax}}{u} = \frac{1.2 \cdot 10^{-4}}{\varepsilon \cdot (1-\varepsilon)^{1.3}} \tag{3.30}$$

Montillet et. al. [5] established axial dispersion coefficients for liquid flow through reticulated nickel foams. For nickel foams with an average porosity of 0.977 and velocities smaller than 10^{-2} m/s, they found the following relation for D_{ax}:

$$\frac{D_{ax}}{u} = 10^{-3} \qquad (\varepsilon = 0.977) \tag{3.31}$$

3.3.3 Experiments

Figure 3.5 shows the experimental test equipment used to determine the axial dispersion coefficient D_{ax} for foam materials according to equation (3.25) from tracer pulse response experiments. A so called open-open pulse response system was chosen to eliminate end effects. The test tube is mounted vertically to ensure that the upward water flow (tap water) will purge all air from the porous bed. The tube is made from perspex, so it can be verified that the packed foam bed is not being compressed due to the water flow.

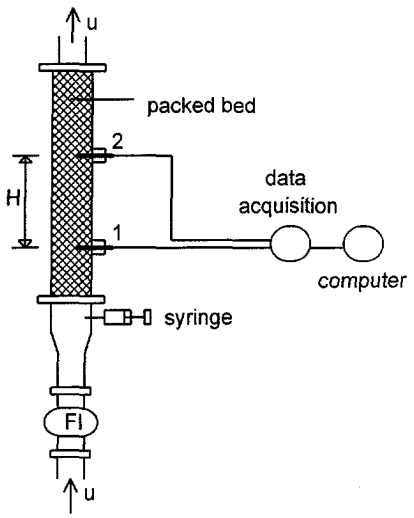

Figure 3.5: Tracer pulse response equipment (open-open type)

Prior to the experiments with foam material, axial dispersion coefficients for fiber materials were determined with the old version of the test equipment using a horizontal PVC tube instead of a vertical perspex tube.

The tracer fluid consists of a 10 wt.% solution of potassium chloride in tap water. The tracer fluid is injected in a short time-interval by means of a hypodermic syringe (see figure 3.5) containing approximately 10 cc. The amount of tracer fluid passing through the packed bed is measured by two conductivity detectors (1 and 2). These detectors are positioned more than 150 mm from the ends of the packed bed. The distance H between the two detection points for the vertically mounted perspex tube according to figure 3.5 is either 180 or 385 mm, the internal tube diameter is 60 mm (for the horizontally mounted PVC tube the distance H is 800 mm and the internal tube diameter is 34 mm). The tap water flow is approximately determined with flow indicator FI and accurately determined by weighing the effluent as a function of time. The pressure drop of the packed bed is monitored (not shown in figure 3.5) to ensure that the water velocity remains in the laminar flow regime.

Figure 3.6 shows a typical result (polyurethane foam with a bed porosity $\varepsilon = 0.934$ and a superficial water velocity $u = 4.86$ cm/s):

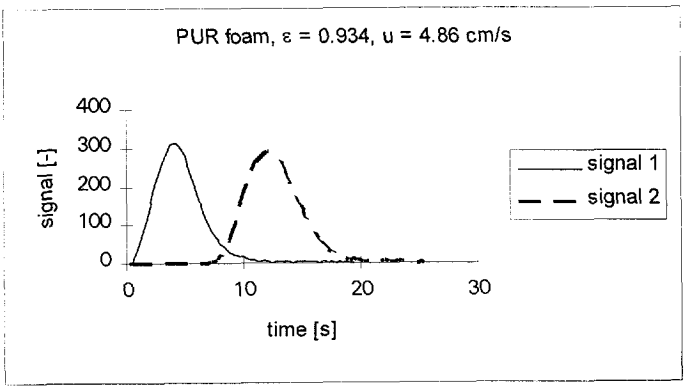

Figure 3.6: Example of measured detection curves

Fibers

Three kinds of fibers were used: PP (polypropylene) fibers with diameters of 32 μm and 43 μm, a different batch of PP fibers with a diameter of 100 μm and PDMS (Poly Di Methyl Siloxane, a silicone rubber) fibers with a diameter of 200 μm. The PP fibers were manufactured by Polyost (Belgium). The fiber materials consisting of either 32 μm or 43 μm fibers have a similar structure. The PDMS fibers were prepared at the Laboratory for Process Equipment by melt spinning [18].

All fibers were tested with the PVC tube, except for the PP fibers with 100 μm diameter which were tested with the vertically mounted perspex tube. In this way the results for the 100 μm PP fibers can be compared with the results obtained by Van Zee [19], who determined the axial dispersion coefficient for the same 100 μm PP fibers with the horizontally mounted PVC tube.

The PVC tube is filled with fibers by consecutively inserting and gently pressing equal quantities of the fibers into the tube with a piston until the desired bed length is reached. The piston rod has scale markers to ensure equal lengths of the fiber bed segments and thus constant porosity across the packed bed. The vertical perspex tube is provided with scale markers on the outside for the same purpose.

For 100 μm PP fibers figure 3.7 gives the axial dispersion coefficient divided by the superficial water velocity, D_{ax}/u, as a function of the superficial water velocity. The packed bed porosity is 0.939. The velocity ranges from 0.4 to 6.2 cm/s. The average value for D_{ax}/u is approximately $3.5 \cdot 10^{-3}$:

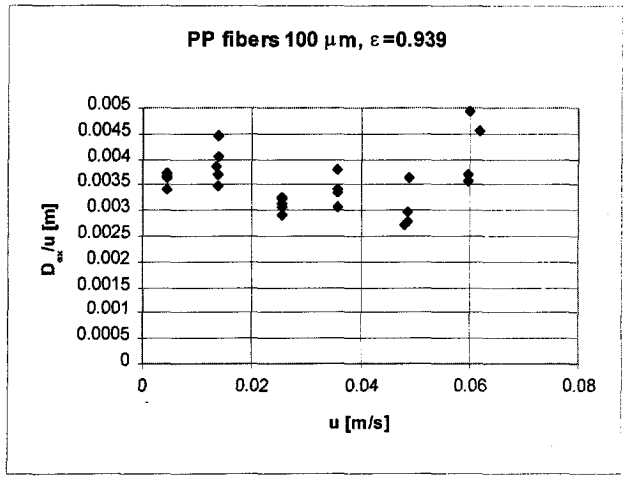

Figure 3.7: Results for 100 μm PP fibers (ε = 0.939)

Figure 3.8 gives D_{ax}/u for 43 μm PP fibers with a packed bed porosity of 0.81 and water velocities of 2.5 to 2.6 cm/s. The average value for D_{ax}/u is approximately $5 \cdot 10^{-3}$:

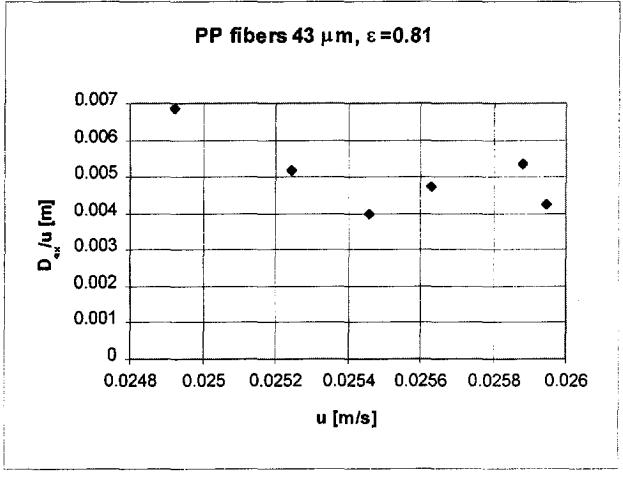

Figure 3.8: Results for 43 μm PP fibers (ε = 0.81)

Figure 3.9 gives D_{ax}/u for 32 μm PP fibers with a packed bed porosity of 0.88 and water velocities of 1.6 to 2 cm/s. The average value for D_{ax}/u is approximately $1 \cdot 10^{-2}$:

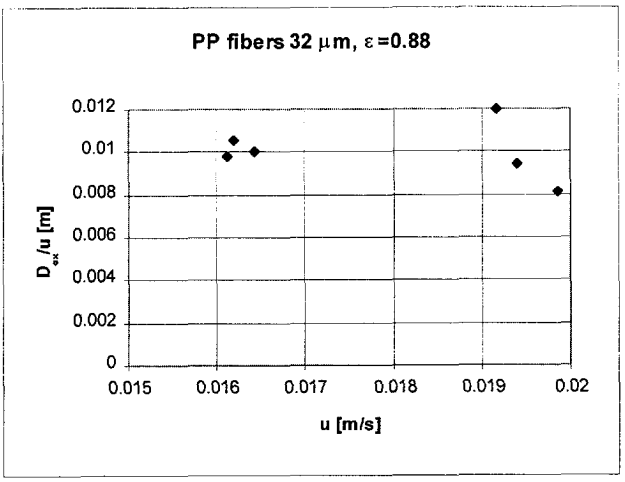

Figure 3.9: Results for 32 μm PP fibers (ε = 0.88)

The PDMS fibers have been tested with two packed bed porosities. Figure 3.10 gives D_{ax}/u for ε = 0.78 and water velocities of 1.9 to 2 cm/s. The average value for D_{ax}/u is approximately $4.7 \cdot 10^{-2}$:

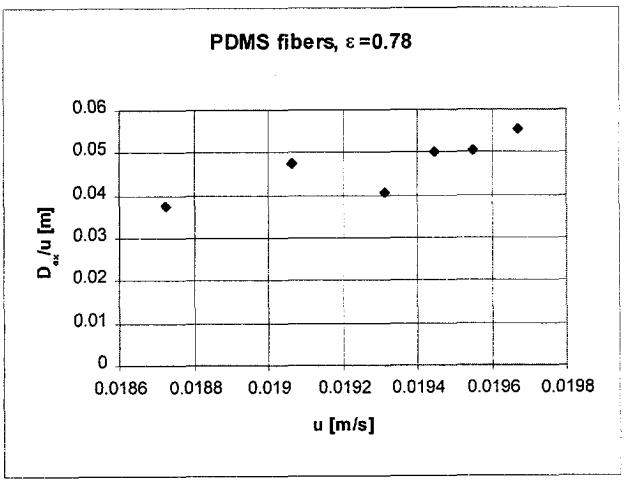

Figure 3.10: Results for 200 μm PDMS fibers (ε = 0.78)

Figure 3.11 gives D_{ax}/u for PDMS fibers with ε = 0.72 and water velocities of 2 to 2.2 cm/s. The average value for D_{ax}/u is approximately $2.8 \cdot 10^{-2}$:

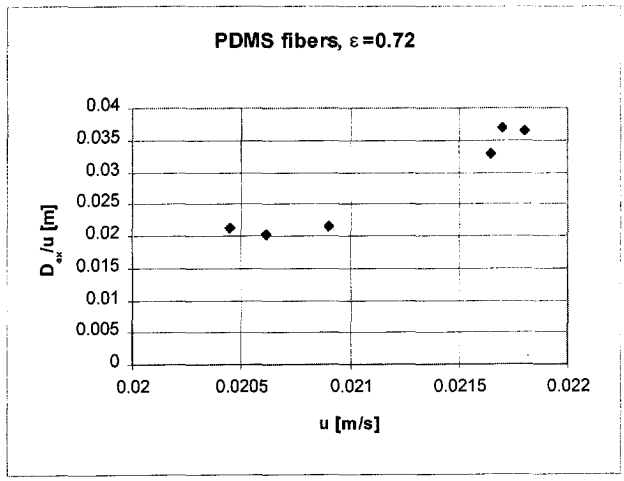

Figure 3.11: Results for 200 μm PDMS fibers (ε = 0.72)

All measurements were conducted in the laminar flow regime.
The measurements with the 32 μm and 43 μm PP-fibers and the ε = 0.72 PDMS fibers were conducted also using a different depth of the second conductivity detector in the packed bed. Only with the ε = 0.72 PDMS fiber experiments a distinct effect of these two different second detector depths was observed: the left three points in figure 3.11 were established with a larger depth (second conductivity detector closer to the centre of the tube) as opposed to the right three points in figure 3.11 which were established with the "normal" depth (both conductivity detectors at the same depth).

Foam materials

Two kinds of foam were investigated: Dow Corning 8157 cellular silicone (mainly consisting of PDMS) manufactured by Dow Corning, Germany, and PUR foam manufactured by Recticel, Belgium. The PUR foam has a mean pore diameter of 294 μm (determined by microscope) and a porosity of 0.972. The silicone rubber foam has a mean pore diameter of approximately 700 μm and a porosity of 0.87. The spread in pore diameter is much larger with cellular silicone than with PUR foam. Also, the cellular silicone has a structure in which only the thin parts of the cell membranes were removed, whereas in reticulated foam only the cell struts were left. Part of the cell membranes of the cellular silicone are not removed at all. Therefore, the cell structure of cellular silicone is much more coarse than with PUR foam.

The vertically mounted perspex tube according to figure 3.5 was used for the experiments, with H = 385 mm for PUR foam and H = 180 mm for cellular silicone. The tube with its internal diameter of 6 cm is filled with PUR foam by consecutively inserting and gently pressing 5 cm high cylindrical plugs with a diameter larger than 6 cm into the tube with a piston. The bed is supported at the top by a sieve plate. The packed bed porosity can be altered by changing the plug diameter. Visual inspection

ensures equal packed plug heights. For cellular silicone the same procedure applies, except that the cylindrical plugs are only 1 cm high.

The PUR foam was tested with two packed bed porosities. For $\varepsilon = 0.934$, figure 3.12 gives the axial dispersion coefficient divided by the superficial water velocity, D_{ax}/u, as a function of the superficial water velocity. The velocity ranges from 0.4 to 4.9 cm/s. The average value for D_{ax}/u is approximately $3.4 \cdot 10^{-3}$:

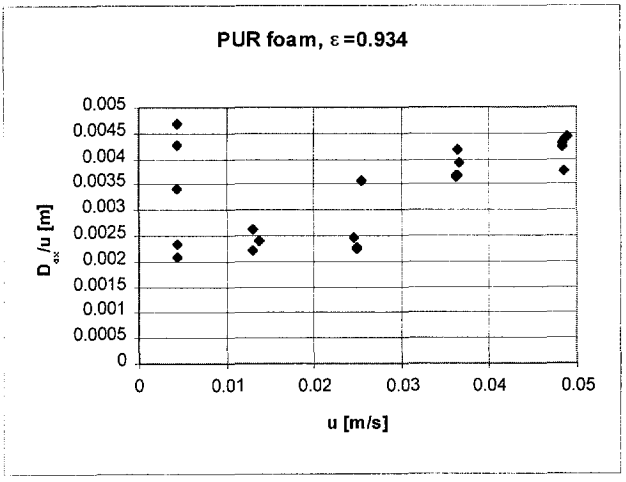

Figure 3.12: Results for PUR foam with $\varepsilon = 0.934$

Figure 3.13 gives D_{ax}/u for PUR foam with $\varepsilon = 0.901$ and water velocities of 0.5 to 4.5 cm/s. The average value for D_{ax}/u is approximately $2.7 \cdot 10^{-3}$:

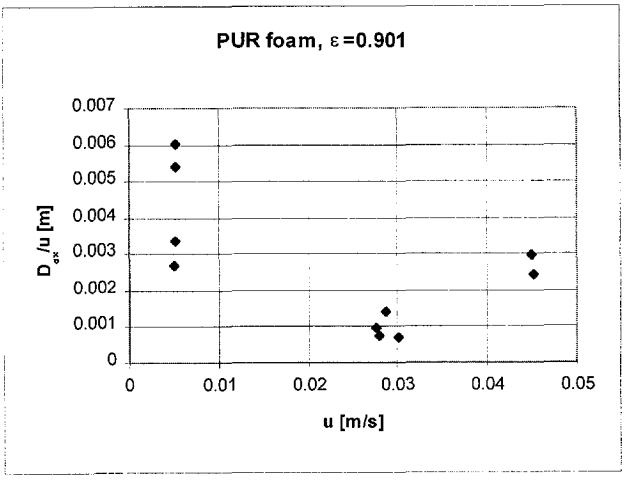

Figure 3.13: Results for PUR foam with $\varepsilon = 0.901$

Figure 3.14 gives D_{ax}/u for cellular silicone with a packed bed porosity of 0.83 and water velocities of 0.6 to 1.05 cm/s. The average value for D_{ax}/u is approximately $5 \cdot 10^{-2}$:

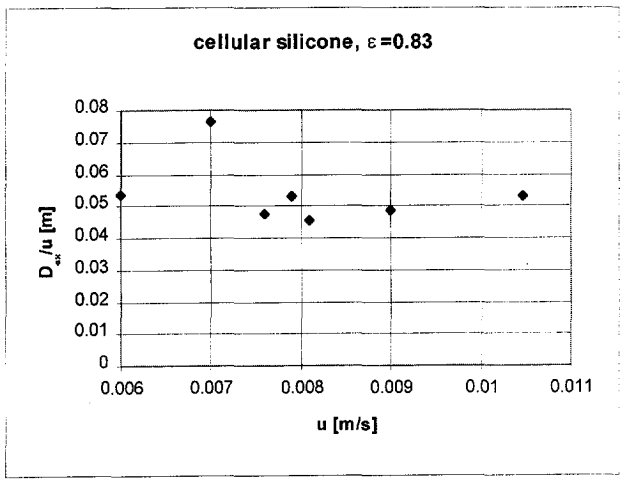

Figure 3.14: Results for cellular silicone with $\varepsilon = 0.83$

3.3.4 Discussion

The results for fibers (see figures 3.7 through 3.11) show considerable spread, so they should be used for comparison with the other experimentally determined values rather than considering them as absolute values.
It was investigated if a wall-effect does occur, i.e. whether the fiber bed is not packed as closely in the region near the wall as near the centre of the tube and hence the quotient D_{ax}/u will be higher near the wall. This effect was indeed observed for PDMS fibers with a bed porosity of $\varepsilon = 0.72$, according to figure 3.11. The experiments with the 43 μm and 32 μm PP fibers did not show wall-effects.

Figure 3.15 shows the results for fiber materials as a function of the bed packing density for mutual comparison as well as comparison with the theoretical relation according to Koch and Brady (equation 3.29) and the empirical relation according to Van Zee (3.30):

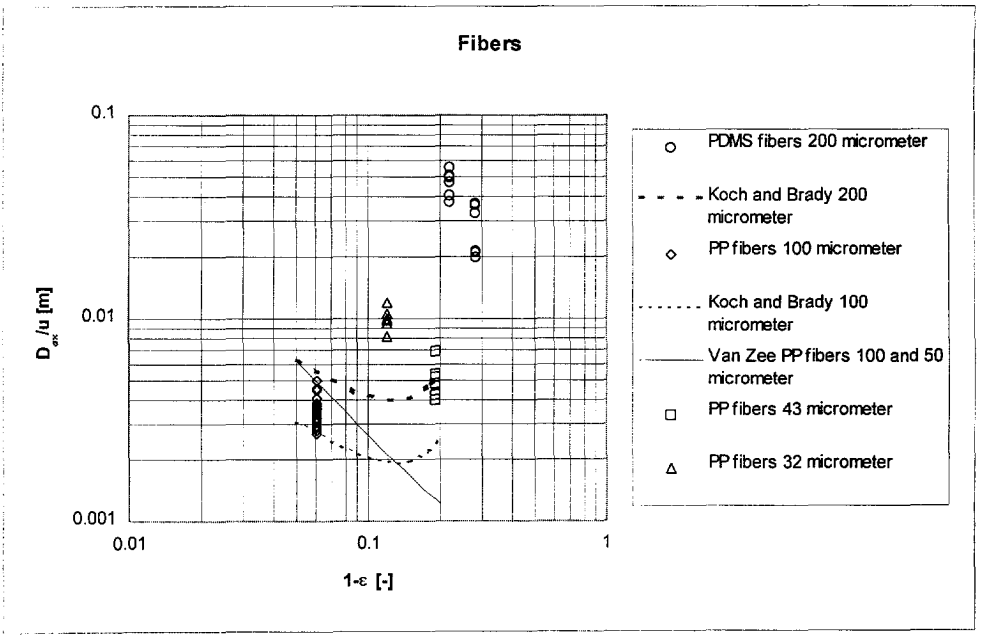

Figure 3.15: Axial dispersion for fiber materials

The results for the 100 μm PP fibers, determined with the vertical perspex tube, are near to the results according to Van Zee (who used the horizontal PVC tube). These 100 μm PP fibers are also near to the relation according to Koch and Brady (with $u=10^{-2}$ m/s and $D=10^{-9}$ m^2/s). In contrast, the results for the 43 μm and 32 μm PP fibers are not only greatly deviating from Van Zee's relation but also have larger instead of smaller values than the 100 μm PP fibers results as one would expect using the relation according to Koch and Brady (Koch and Brady predict smaller values for D_{ax}/u for smaller fiber diameters, depicted in figure 3.15 by the difference between 200 μm and 100 μm fibers).
PDMS fibers show substantially larger axial dispersion than PP fibers, the difference in D_{ax}/u with 100 μm PP fibers amounts to one to two decades. As with the 43 μm and 32 μm PP fibers, the PDMS fibers do not follow Koch and Brady's relation.

The differences between the results of the 32 μm, 43 μm and 100 μm PP fibers point to a dominant influence of the fiber bed structure. The supplied structure of the 32 μm and 43 μm fiber materials is different from the 100 μm fiber material. The discrepancy between the experimental results and Koch and Brady's theory can be attributed to differences in packed fiber bed structure as well, since Koch and Brady's theory assumes a homogeneous structure of the bed. The packed PDMS fiber beds show relatively large inhomogenuities caused by the slackness and the friction of the silicone rubber fibers and their production method, and therefore show the largest axial dispersion.

The results for foam material (see figures 3.12 through 3.14) show considerable spread, even larger than with fibers, so they should be used for comparison with the other

experimentally determined values rather than considering them as absolute values. Figure 3.16 shows the results for foam materials as a function of the bed packing density for mutual comparison as well as comparison with the experimental result of Montillet et. al. (equation 3.31):

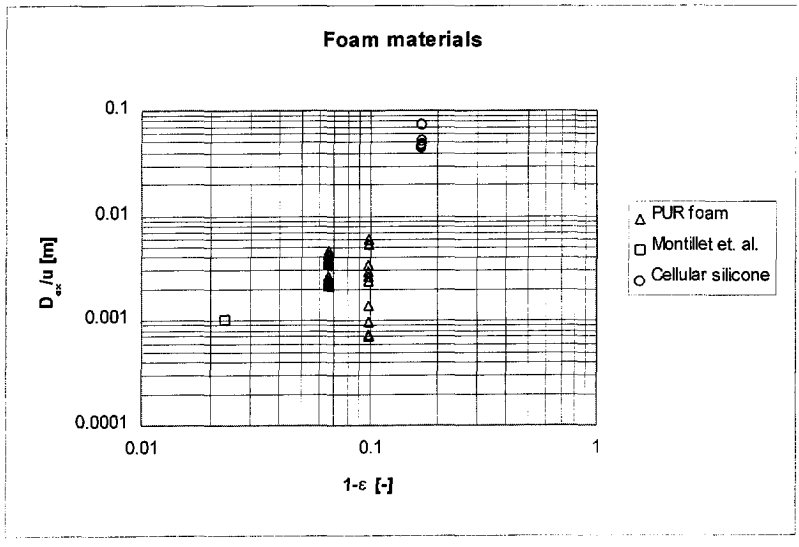

Figure 3.16: Axial dispersion for foam materials

PUR foam has D_{ax}/u values comparable with 100 μm PP fibers. The lowest experimental values agree with the results for reticulated nickel foam (Montillet et. al.), which has the same structure as PUR foam from which it is made (nickel is deposited on PUR foam which is pyrolysed afterwards). The nickel foam has a D_{ax}/u value lower than the average D_{ax}/u value of PUR foam, probably because the nickel foam is more rigid and will therefore retain its regular structure under external forces. In contrast, the PUR foam is more flexible so that the liquid flow may cause structural deformations (deformed cell shapes). Cellular silicone shows D_{ax}/u values 1 to 2 decades higher than for PUR foam, caused by its irregular cell structure with partially intact cell membranes.

3.3.5 Conclusions

The axial dispersion in open materials can be described by the axially dispersed plug flow model, using the axial dispersion coefficient D_{ax} as the only parameter. D_{ax} was determined for a number of fiber and foam materials using open-open type tracer pulse response experiments. The ratio of the axial dispersion coefficient and the superficial water velocity, D_{ax}/u, ranges from approximately $3 \cdot 10^{-3}$ for PUR foam (porosity 0.9) to approximately $5 \cdot 10^{-2}$ for cellular silicone (porosity 0.83). These values are average values and it should be noted that the spread of these results is quite large. The results for PP fibers approximate those for PUR foam and the results for PDMS fibers are close

to those for cellular silicone. The high D_{ax}/u values for cellular silicone are caused by the irregular cell structure with partially intact cell membranes, the high D_{ax}/u values for packed PDMS fiber beds are caused by the large inhomogenuities in these beds due to the slackness of the silicone rubber fibers.
Axial dispersion in packed PP fiber beds with different fiber diameters each, can not be described by Koch and Brady's theory. The 32 μm and 43 μm fiber beds, which have a less regular structure, have a higher dispersion than the 100 μm fiber bed. For packed PDMS fiber beds with even larger inhomogenuities the dispersion is also higher. Foam shows a similar dependence between dispersion and inhomogenuity of the bed structure. Hence experimental determination of the axial dispersion coefficient of a packed fiber or foam bed is inevitable to obtain an accuracy better than order of magnitude. Care should be taken to correctly pack the fiber or foam beds for experiments to avoid a large discrepancy between experimentally established and actual dispersion in packed fiber or foam beds and to avoid a large spread in experimental results.

3.4 Conclusions

In this chapter the pressure drop and the axial dispersion in both packed fiber beds and open-cell foam beds have been investigated. Comparisons have been made between theoretical and empirical predictions from literature and experimental results. Generally, the agreement between the predictions and the experimental results is poor and the predictions will only serve as order of magnitude estimates. As a consequence, experimental determination of both the pressure drop and the axial dispersion coefficient of packed beds of slack polymeric fibers (like silicone rubber fibers) or open-cell foam beds (like PUR foam and cellular silicone) is inevitable to obtain an accuracy better than an order of magnitude.

The deviations between theoretical and empirical predictions from literature and experimental results are mainly caused by differences in packed bed structure. Also, due to these differences in packed bed structure, the packed beds consisting of silicone rubber (PDMS) material (both fibers and foam) show considerably higher pressure drop and axial dispersion than the packed beds consisting of crystalline fibers and PUR foam. The PDMS fiber beds show relatively large inhomogenuities compared with the crystalline fiber beds, caused by the slackness and the friction of the silicone rubber fibers and their production method. The cellular silicone has a structure in which only the thin parts of the cell membranes were removed, whereas in reticulated foam only the cell struts were left

The pressure drop of a packed bed of open material can be described by equation (3.6). This relation is valid for both fiber and foam materials by using an equivalent fiber diameter for foam. The pressure drop in the laminar flow regime is characterised by a single structural parameter C_1. For crystalline fibers, C_1 can be estimated by the relation according to Jackson and James (equation 3.15). For PUR foam, C_1 has a value increasing from about 20 to 40 for porosities of around 0.92 and higher. A value of C_1 of 10^3 can be used as an order of magnitude estimate for cellular silicone.

The axial dispersion of a packed bed of open material can be described by the axially dispersed plug flow model, using the axial dispersion coefficient D_{ax} as a single parameter. The axial dispersion coefficient divided by the superficial water velocity, D_{ax}/u, ranges from approximately $3 \cdot 10^{-3}$ for PUR foam (porosity 0.9) to approximately $5 \cdot 10^{-2}$ for cellular silicone (porosity 0.83) based on measurements with velocities for which the pressure drop is proportional to the mass flow rate. The results for the used PP fiber beds approximate those for PUR foam and the results for the used PDMS fiber beds lie close to those for cellular silicone.

References

[1] Darcy, H.P.G., *Les fontaines publiques de la ville de Dijon. Exposition et application à suivre et des formules à employer dans les questions de distribution d'eau*, Victor Dalamont, Paris, 1856

[2] Kozeny, J., *Über kapillare Leitung des Wassers im Boden (Aufstieg, Versicherung und Anwendung auf die Bewässerung)*, Sitzb.Akad.Wiss., Wien, Math.-naturw. Kl. **136** (Abt, IIa), 1927, pp. 271-306

[3] Kozeny, J., *Über Bodendurchlässigkeit*, Pfl.-Ernähr.Düng.Bodenk., **28A** (1933), pp. 54-56

[4] Ergun, S., *Fluid flow through packed columns*, Chem.Eng.Prog., **48** (1952), pp. 89-94

[5] Montillet, A., Comiti, J., Legrand, J., *Axial dispersion in liquid flow through packed reticulated metallic foams and fixed beds of different structures*, Chem.Eng.J., **52** (1993), pp. 63-71

[6] Coulson, J.M., Richardson, J.F., Backhurst, J.R., Harker, J.H., *Chemical engineering, Volume 1 (5th ed.)*, Butterworth-Heinemann, Oxford, 1996, ISBN 0-7506-2557-0

[7] Coulson, J.M., Richardson, J.F., Backhurst, J.R., Harker, J.H., *Chemical engineering, Volume 2 (4th ed.)*, Butterworth-Heinemann, Oxford, 1996, ISBN 0-7506-2942-8

[8] Happel, J., *Viscous flow relative to arrays of cylinders*, AIChE J., **5** (1959), pp. 174-177

[9] Happel, J., Brenner, H., *Low Reynolds number hydrodynamics (2nd ed.)*, Noordhoff International Publishing, Leyden, 1973, ISBN 90-01-37115-9

[10] Jackson, G.W., James, D.F., *The permeability of fibrous porous media*, Can.J.Che.Eng, **64** (1986), pp. 364-374

[11] Davies, C.N., *The separation of airborne dust and particles*, Proc., Inst.Mech.Eng.(London), **B1** (1952), pp. 185-213

[12] Du Plessis, P., Montillet, A., Comiti, J., Legrand, J., *Pressure drop prediction for flow through high porosity metallic foams*, Chem.Eng.Sci., **49** (1994), pp. 3545-3553

[13] Gent, A.N., Rusch, K.C., *Permeability of open-cell foamed materials*, J.Cell.Plast., **2** (1966), pp. 46-51

[14] Liu, S., Afacan, A., Masliyah, J., *Steady incompressible laminar flow in porous media*, Chem.Eng.Sc., **49** (1994), pp. 3565-3586

[15] Hilyard, N.C., Collier, P., A *structural model for air flow in flexible PUR foams*, Cellular Polymers, **6**-6 (1987), pp. 9-26

[16] Westerterp, K.R., *Chemical reactor design and operation (2nd ed.)*, John Wiley & Sons Ltd., Chichester, 1984, ISBN 0-471-90183-0

[17] Koch, D.L., Brady, J.F., *The effective diffusivity of fibrous media*, AIChE Journal, **32** (1986), pp. 575-591

[18] Zee, G. van, *Counter current sorption using fiber sorbents (Ph.D.-thesis)*, Delft University Press, 1996, ISBN 90-407-1328-6

[19] Zee, G. van, Veenstra, R., Graauw, J. de, *Axial dispersion in packed fiber beds*, Chem.Eng.J., **58** (1995), pp. 245-250

4

Mass transfer

4.1 Introduction

This chapter describes the mass transfer model and the parameters involved that will be used to evaluate the countercurrent mass transfer experiments with the pilot unit (Chapter 5) and to scale the separation equipment up to an industrial feed flow rate (Chapter 6). The model assumes both diffusive and dispersive transport of matter to be proportional to the concentration gradient and also assumes concentration independence of phase flow rates, the overall mass transfer coefficient and the distribution coefficient. The dispersive transport of matter is described using an axial dispersion coefficient (axially dispersed plug flow model). The phenomena of axial dispersion were treated in detail in Chapter 3.

Section 4.2 gives the process scheme for which the mass transfer model applies. Next, in section 4.3 the model for both the sorption and the regeneration section is derived. The mass transfer parameters are explained and estimates are given for these parameters. Subsequently, in section 4.4 some of these parameters are established by experiment. This chapter is concluded in section 4.5.

4.2 Process scheme

The principle of countercurrent sorption using an endless packed bed of sorbent material is pictured in figure 4.1. The sorbent material is transported in continuous and countercurrent operation through a sorption section and a regeneration section. Regenerated clean sorbent material entering the sorption section gradually removes the component polluting the aqueous feed. The laden sorbent material then enters the regeneration section in which this component is removed again by a regenerant phase. Next, the stripped sorbent material enters the sorption section, by which the cycle is completed.

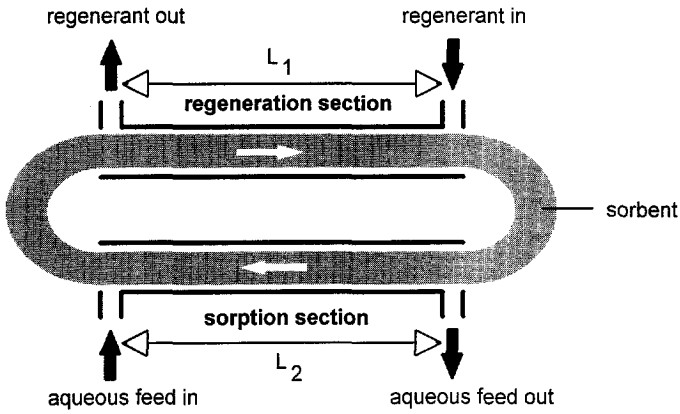

Figure 4.1: Process scheme

When the component to be removed has a low solubility in the aqueous phase and a high solubility in the regenerant phase (for instance a volatile organic compound) it is preferable to use steam as a regenerant as this would allow condensation of the laden steam resulting into phase separation of a saturated water-phase and a phase containing high concentrations of the component removed. The relatively small flow of saturated water can be recycled to the aqueous feed.

4.3 Mass transfer model

4.3.1 Introduction

This section describes a mass transfer model for countercurrent sorption which can be applied to equipment operated according to the process scheme described in section 4.2. Due to various assumptions with respect to the description of the mass transfer phenomena, the derivation of the mass balances, the solution of the subsequent differential equations and - particularly - the application of estimated mass transfer properties, the resulting practical model gives only a rough estimation of the performance of the separation process. For a more accurate estimation of the separation performance experimental determination of individual mass transfer properties is required. Although less suitable for accurate calculations, the resulting model is very useful for examining the response of the system to parameter variations and gives a prediction of the behaviour of the system.

4.3.2 Sorption section

In figure 4.2, a cylindrical countercurrent sorption column of height H is depicted. Net mass transfer of component "j" takes place from the (liquid) feed (subscript L) to the sorbent phase (subscript S):

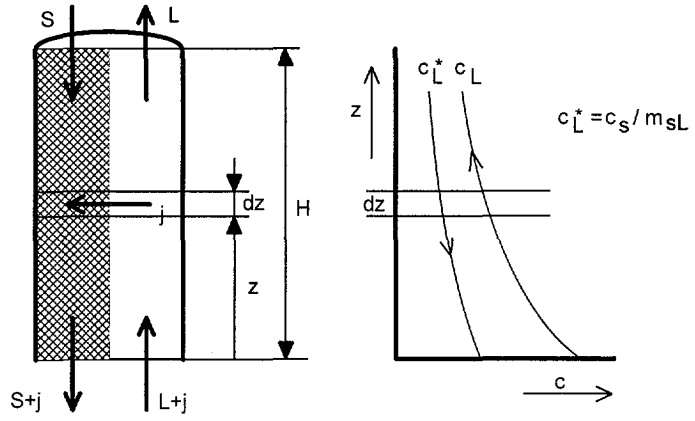

Fig. 4.2: Countercurrent sorption column

Under the following conditions, we can derive the mass balances over a column segment:

- only transfer of a single component is considered
- both the diffusive transport rate and the dispersive transport rate of matter are proportional to the concentration gradient
- the flow pattern has not too large deviations from ideal plug flow
- uniform concentration in both phases in radial column direction
- concentration independence of phase flow rates, overall mass transfer coefficient and distribution coefficient

Mass balance over column segment z, z + dz:

Liquid phase:

$$[\frac{u}{\varepsilon}\cdot(c_L)_z\cdot\varepsilon\cdot A - D_{ax}\cdot(\frac{\partial c_L}{\partial z})_z\cdot\varepsilon\cdot A]$$
$$-[\frac{u}{\varepsilon}\cdot(c_L)_{z+dz}\cdot\varepsilon\cdot A - D_{ax}\cdot(\frac{\partial c_L}{\partial z})_{z+dz}\cdot\varepsilon\cdot A + k_{oL}\cdot a_S\cdot(c_L - \frac{c_S}{m_{SL}})\cdot A\cdot dz] = \frac{\partial c_L}{\partial t}\cdot\varepsilon\cdot A\cdot dz \qquad (4.1)$$

Sorbent phase:

$$[v\cdot(c_S)_{z+dz}\cdot(1-\varepsilon)\cdot A + k_{oL}\cdot a_S\cdot(c_L - \frac{c_S}{m_{SL}})\cdot A\cdot dz] - v\cdot(c_S)_z\cdot(1-\varepsilon)\cdot A = \frac{\partial c_S}{\partial t}\cdot(1-\varepsilon)\cdot A\cdot dz \qquad (4.2)$$

u:	superficial flow velocity relative to fixed co-ordinates	[m/s]
v:	sorbent transport velocity	[m/s]
ε:	bed porosity	[-]
A:	phase boundary surface area	[m^2]
c_L:	concentration in liquid phase	[kg/m^3]
c_S:	concentration in sorbent phase	[kg/m^3]
D_{ax}:	axial dispersion coefficient (see section 3.3)	[m^2/s]
k_{oL}:	liquid side overall mass transfer coefficient	[m/s]
a_S:	specific sorbent surface area	[m^2/m^3]
m_{SL}:	distribution coefficient (=(c_S/c_L) at equilibrium)	[(kg/m^3)/(kg/m^3)]
t:	time	[s]

Since there is no accumulation in time in the liquid or sorbent phase in any segment between z and z + dz (stationary condition), the resulting differential equations are:

Liquid phase:

$$-u\cdot\frac{dc_L}{dz}+\varepsilon\cdot D_{ax}\cdot\frac{d^2c_L}{dz^2}-k_{oL}\cdot a_S\cdot(c_L-\frac{c_S}{m_{SL}})=0 \qquad (4.3)$$

Sorbent phase:

$$(1-\varepsilon)\cdot v\cdot\frac{dc_S}{dz}+k_{oL}\cdot a_s\cdot(c_L-\frac{c_S}{m_{SL}})=0 \qquad (4.4)$$

An analytical solution of these equations is given by Miyauchi and Vermeulen [1], using the following boundary conditions:

$$z=0: \qquad \frac{dc_L}{dz}=\frac{u}{\varepsilon\cdot D_{ax}}\cdot(c_{L,z=0}-c_L^0), \quad \frac{dc_S}{dz}=0 \qquad (4.5)$$

$$z=H: \qquad \frac{dc_L}{dz}=0, \quad \frac{dc_S}{dz}=-\infty \qquad (4.6)$$

The condition according to the right hand side of equation (4.6) corresponds with the assumption that there is no axial dispersion in the sorbent phase.

The solution is as follows. Equation (4.7) gives the concentrations c_L in the liquid phase and c_S in the sorbent phase as a function of the position "z" (see figure 4.2) relative to the column:

$$c_L(\frac{z}{H})=X\cdot(c_L^0-\frac{c_S^0}{m_{SL}})+\frac{c_S^0}{m_{SL}}, \qquad c_S(\frac{z}{H})=Y\cdot(m_{SL}\cdot c_L^0-c_S^0)+c_S^0 \qquad (4.7)$$

c_L^0: feed inlet concentration outside the column [kg/m^3]

c_S^0: sorbent inlet concentration outside the column [kg/m^3]

with

$$X = \sum_{i=1}^{3} \frac{D_i}{D} \cdot \exp(\lambda_i \cdot \frac{z}{H}), \qquad Y = \sum_{i=1}^{3} f_i \cdot \frac{D_i}{D} \cdot \exp(\lambda_i \cdot \frac{z}{H}) \tag{4.8}$$

$$D = D_1 + \lambda_3 \cdot (1 - \frac{\lambda_2}{Pe}) \cdot \exp(\lambda_3) - \lambda_2 \cdot (1 - \frac{\lambda_3}{Pe}) \cdot \exp(\lambda_2) \tag{4.9}$$

$$D_1 = \Lambda \cdot (\lambda_2 - \lambda_3) \cdot \exp(a), \quad D_2 = \lambda_3 \cdot \exp(\lambda_3), \quad D_3 = -\lambda_2 \cdot \exp(\lambda_2) \tag{4.10}$$

$$f_i = 1 + \frac{\lambda_i}{N_{oL}} - \frac{\lambda_i^2}{N_{oL} \cdot Pe} \tag{4.11}$$

$$a = Pe + \Lambda \cdot N_{oL}, \qquad b = (1 - \Lambda) \cdot N_{oL} \cdot Pe \tag{4.12}$$

$$\lambda_1 = 0, \qquad \lambda_2 = \frac{a}{2} + \sqrt{[(\frac{a}{2})^2 + b]}, \qquad \lambda_3 = \frac{a}{2} - \sqrt{[(\frac{a}{2})^2 + b]} \tag{4.13}$$

The dimensionless Péclet number "Pe" represents the ratio between convective and dispersive mass transfer in the liquid phase:

$$Pe = \frac{u \cdot H}{\varepsilon \cdot D_{ax}} \tag{4.14}$$

N_{oL} is the liquid side number of overall mass transfer units in the column:

$$N_{oL} = \frac{k_{oL} \cdot a_S \cdot H}{u} \tag{4.15}$$

with the liquid side overall mass transfer coefficient k_{oL} defined as follows:

$$k_{oL} = [\frac{1}{k_L} + \frac{1}{m_{SL} \cdot k_S}]^{-1} \tag{4.16}$$

k_L: liquid side mass transfer coefficient [m/s]
k_S: sorbent side mass transfer coefficient [m/s]

The dimensionless parameter Λ is the capacity ratio and is the inverse of the sorption factor "S":

$$\Lambda = \frac{1}{S}\ (S \neq 1), \quad S = \frac{m_{SL} \cdot (1-\varepsilon) \cdot v}{u} \tag{4.17}$$

4.3.3 Regeneration section

In figure 4.3, a cylindrical countercurrent regeneration column of height H is depicted. Net mass transfer of component "j" takes place from the (sorbent) feed (subscript S) to the (gaseous) regenerant phase (subscript G):

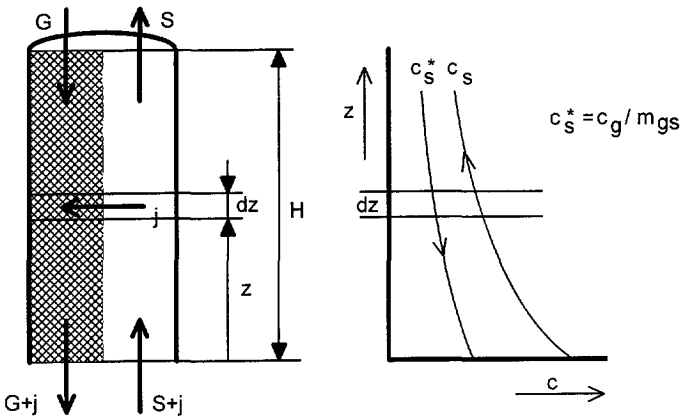

Fig. 4.3: Countercurrent regeneration column

The resulting differential equations are:

Sorbent phase:

$$(1-\varepsilon) \cdot v \cdot \frac{dc_S}{dz} + k_{oS} \cdot a_S \cdot (c_S - \frac{c_G}{m_{GS}}) = 0 \tag{4.18}$$

Regenerant phase:

$$-u \cdot \frac{dc_G}{dz} + \varepsilon \cdot D_{ax} \cdot \frac{d^2 c_G}{dz^2} - k_{oS} \cdot a_s \cdot (c_S - \frac{c_G}{m_{GS}}) = 0 \tag{4.19}$$

Equations (4.18) and (4.19) are comparable with equations (4.3) and (4.4), so the solution can be described by equations (4.7) through (4.17) for the sorption column using k_{oS} instead of k_{oL} and m_{GS} instead of m_{SL}:

$$k_{oS} = [\frac{1}{k_S} + \frac{1}{m_{GS} \cdot k_G}]^{-1} \qquad (4.20)$$

k_{oS}:	sorbent side overall mass transfer coefficient	[m/s]
m_{GS}:	distribution coefficient (=(c_G/c_S) at equilibrium)	[(kg/m^3)/(kg/m^3)]
c_G:	concentration in regenerant phase	[kg/m^3]
k_G:	mass transfer coefficient for the regenerant phase	[m/s]

The regenerant phase now enters the column at z = 0 and the sorbent phase enters the column at z = 1, in accordance with figure 4.2. The calculated concentration c_L now represents the concentration in the regenerant phase.
For the sake of clarity, the mass transfer model for regeneration used in Chapter 6 (Appendix D.1) is expressed in terms of sorbent side mass transfer properties, applying the appropriate inversion relations to equations (4.7) through (4.17) according to Miyauchi and Vermeulen [1].

4.3.4 Estimated mass transfer properties

In order to allow application of the mass transfer model described in the previous paragraphs, a number of the mass transfer parameters involved are evaluated in this paragraph.

Mass transfer coefficient for the liquid phase: k_L
The liquid side mass transfer coefficient k_L may be obtained from empirical relations for forced convection mass and heat transfer in packed fiber beds and porous materials of resembling structure. Van Zee [2] established the following empirical relation representing the various relations found in literature:

$$Sh_L = \frac{k_L \cdot d}{D_L} = 0.7 \cdot Re^{0.4} \cdot Sc^{0.33} \qquad (4.21)$$

with

$$Re = \frac{u \cdot d}{\nu}, \qquad Sc = \frac{\nu}{D_L} \qquad (4.22)$$

Sh:	Sherwood no (total mass transfer / diffusive mass transfer)	[-]
k_L:	mass transfer coefficient of the continuous phase	[m/s]
d:	fiber diameter or equivalent fiber diameter d_{eq} for foam (see equation 4.25)	[m]
D_L:	diffusion coefficient in the continuous phase	[m^2/s]
Re:	Reynolds no (inertia forces / viscous forces)	[-]
Sc:	Schmidt no (hydrodynamic boundary layer / mass transfer bound.l.)	[-]
ν:	kinematic viscosity of the continuous phase	[m^2/s]

Experiments with a single carbon fibre electrode gives the same result for Sc=1000 [3]:

$$Sh_L = 7 \cdot Re^{0.4} \qquad (0.04 \leq Re \leq 0.2) \qquad (4.23)$$

It should be noted that the definition of the Reynolds number as employed in equations (4.21) through (4.23) is based on the superficial liquid velocity and the particle diameter. In contrast, the Reynolds number used elsewhere in this thesis is based on the interstitial liquid velocity and the hydraulic mean diameter (see §3.2.2).
Although the empirical relation according to equation (4.21) has been established with liquid media, for lack of alternatives this relation will also be used to estimate the gas side mass transfer coefficient k_G for the regeneration section in Chapter 6.
If the diffusion coefficient D_L in the continuous phase is known, k_L can be estimated from Sh_L for a given fiber or equivalent fiber diameter (see equation 4.21). D_L is obtained or estimated from literature and can be calculated using the relation according to Wilke and Chang [4].

According to equation (4.21), the liquid side mass transfer coefficient k_L for fibers with a diameter of 200 μm, a diffusion coefficient of $7.6 \cdot 10^{-10}$ m^2/s for water/ ethylbenzene at room temperature and a kinematic viscosity of $1 \cdot 10^{-6}$ m^2/s for water is equal to:

$$k_L = 2.37 \cdot 10^{-4} \cdot u^{0.4} \qquad (4.24)$$

This value for k_L for PDMS / ethylbenzene (PDMS: Poly Di Methyl Siloxane, a silicone rubber) will be used in the modelling of mass transfer experiments conducted with the pilot unit (Chapter 5).

For open-cell foam materials, the equivalent fiber diameter d_{eq} is used instead of the fiber diameter d in equation (4.21), thus assuming the foam to be equivalent to a fiber mass consisting of fibers with diameter d_{eq}. d_{eq} is derived by treating the definitions of specific sorbent surface area for open-cell foam and for fiber beds as equals, resulting in the following relation for d_{eq} (see §3.2.2):

$$d_{eq} = \frac{1-\varepsilon_0}{\varepsilon_0} \cdot d_p \qquad (4.25)$$

ε_0:	initial porosity (supplied / uncompressed condition)	[-]
d_p:	mean pore diameter (empty space based) at $\varepsilon = \varepsilon_0$	[m]

Mass transfer coefficient for the sorbent phase: k_S
The sorbent side mass transfer coefficient k_S can be derived from the outlet concentration profile obtained from fixed bed experiments, together with the distribution coefficient "m" (see §4.4.3).

A rough estimate can be made using a Sherwood number of 8 for fiberlike polymeric sorbents [5]:

$$Sh_S = \frac{k_S \cdot d}{D_S} = 8 \qquad (4.26)$$

k_S:	mass transfer coefficient of the sorbent phase	[m/s]
D_S:	diffusion coefficient in the sorbent phase	[m^2/s]
d:	fiber diameter or equivalent fiber diameter d_{eq} for foam (see equation 4.25)	[m]

If the diffusion coefficient D_S in the sorbent (polymer) phase is known, k_S can be estimated from Sh_S. D_S can be obtained or estimated from literature.
The k_S for PDMS fibers with a fiber diameter of 200 μm and ethylbenzene is $8.8 \cdot 10^{-7}$ m/s, based on a diffusion coefficient D_S of $2.2 \cdot 10^{-11}$ m^2/s [2]. This value for k_S for PDMS / ethylbenzene will be used in the modelling of mass transfer experiments conducted with the pilot unit (Chapter 5).

Distribution coefficient: m
The sorbent / water distribution coefficient m_{SL} can be determined by a relatively simple equilibrium experiment, see §4.4.2. Also, m_{SL} (together with k_S) can be derived from the outlet concentration profile obtained from fixed bed experiments, see §4.4.3.

m_{SL} for PDMS / water / ethylbenzene is estimated at 1,300 according to [2]. This value will be used in the modelling of mass transfer experiments conducted with the pilot unit (Chapter 5).

For the regeneration section, the steam/sorbent distribution coefficient m_{GS} can be calculated from the product of m_{GL} and m_{LS} (the steam / water respectively the water / sorbent distribution coefficient), both at 100°C. We will calculate m_{GS} for toluene and a sorbent material consisting of PDMS, because this data is required for the design study of Chapter 6.

m_{GL} is defined as:

$$m_{GL} = K \cdot \frac{M_L}{M_G} \cdot \frac{\rho_G}{\rho_L} \qquad (4.27)$$

m_{GL}:	distribution coefficient (= (c_G/c_L) at equilibrium)	[$(kg/m^3)/(kg/m^3)$]
K:	mole fraction based distribution coefficient	[-]
M_L:	molecular weight of the liquid phase	[kg/kmole]
M_G:	molecular weight of the gas phase	[kg/kmole]
ρ_G:	density of the gas phase	[kg/m^3]
ρ_L:	density of the liquid phase	[kg/m^3]

For a dilute aqueous solution at 100°C, K for toluene is given by Hwang et. al. [6]: $K = 10^{3.5}$. M_L equals M_G, ρ_G and ρ_L are given by [7] and are 0.598 kg/m^3 and 958.3 kg/m^3 respectively at 1 bar and 100°C. Thus, according to equation (4.27) $m_{GL} \approx 2$.

m_{LS} can be estimated using the following approximate equation for low toluene concentrations in both the water and the sorbent phase:

$$m_{LS} = (\gamma'/\gamma) \cdot \frac{M_i}{M_L} \cdot \frac{\rho_L}{\rho_S} \qquad (4.28)$$

m_{LS}:	reciprocal value of m_{SL}	$[(kg/m^3)/(kg/m^3)]$
γ':	component's activity coefficient in the sorbent phase	[-]
γ:	component's activity coefficient in the liquid phase	[-]
M_i:	molecular weight of component to be desorbed	[kg/kmole]
ρ_S:	density of the sorbent phase	$[kg/m^3]$

Van Zee [2] established a value for m_{LS} of 0.005 at room temperature for PDMS / toluene. This means that for toluene ($M_i = 92 \cdot 10^{-3}$ kg/mole) and PDMS sorbent material ($\rho_S = 1.1 \cdot 10^3$) and with $\gamma = 7.3 \cdot 10^3$ at 25°C according to Hwang et. al. [6], γ' has an apparent value of 7.86 at room temperature. If we assume that γ' at 100°C will be equal to γ' at room temperature, we can estimate m_{LS} for 100°C. Then, according to equation (4.28) and with $\gamma = 3.4 \cdot 10^3$ at 100°C according to Hwang et. al. [6], $m_{LS} \approx 0.01$.

This results in an estimated value of 0.02 for the steam/sorbent distribution coefficient m_{GS} ($m_{GS} = m_{GL} \cdot m_{LS} \approx 2 \cdot 0.01$) when toluene has to be stripped from PDMS sorbent material (to be used in Chapter 6).

Specific sorbent surface area: a_S

The specific surface area of a packed fiber bed is given by equation (4.29):

$$a_S = \frac{4 \cdot (1 - \varepsilon)}{d} \qquad (4.29)$$

in which "d" represents the fiber diameter. For open-cell foam "d" is replaced by the equivalent fiber diameter d_{eq} for foam according to equation (4.25).

When k_S and m_{SL} are determined by fixed bed experiments (§4.4.3), the specific sorbent surface area of the packed sorbent bed "a_S" is larger than of the uncompressed sorbent material in the supplied state. This should be accounted for by equation (4.29) because the packed bed porosity ε is smaller than the initial porosity ε_0 of the uncompressed sorbent material prior to filling of the column. Because some concern may exist whether the increase in a_S due to compression of the foam material is correctly accounted for by equation (4.29) which is based on the assumption that the foam structure can be treated as a fiber mass, a comparison is made with the relation between packed bed porosity and mean pore diameter according to Hilyard and Collier [8]:

$$d'_p = \left(\frac{\varepsilon}{\varepsilon_0}\right)^2 \cdot \left(\frac{1 - \varepsilon_0}{1 - \varepsilon}\right)^3 \cdot d_p \qquad (4.30)$$

d'_p:	compressed mean pore diameter at $\varepsilon < \varepsilon_0$	[m]
d_p:	uncompressed mean pore diameter at ε_0	[m]

Equation (4.30) is based on a structural model and is valid for compression up to 60%. The compressed mean pore diameter d'_p is used to calculate the specific sorbent surface area for a compressed open-cell foam as follows (see §3.2.2):

$$a_S = 4 \cdot \varepsilon / d'_p \tag{4.31}$$

Comparison for all fixed bed experiments of §4.4.3 between a_S according to equation (4.29) and a_S according to equation (4.31) shows a maximum difference of only 5% between the two equations, so we will use equation (4.29).

Axial dispersion coefficient for the continuous phase: D_{ax}
It is recommendable to determine this coefficient by experiment because estimation of D_{ax} using relations obtained from literature gives large deviations from measured values for D_{ax} (see Chapter 3 section 3.3). However, this does not always mean that the measured D_{ax} is accurate. The purpose of determining D_{ax} experimentally is to establish the relative difference in D_{ax} between different sorbent beds.
It is arguable whether D_{ax} doesn't also include some effects already accounted for by k_L, since the empirical relation for Sh_L used for estimation of k_L is established under conditions which are very likely to be different from perfect plug flow. For higher flow velocities ($> 10^{-2}$ m/sec in packed beds of open materials), this potential overlap in accounting for dispersive effects will probably decrease. Application of D_{ax} together with k_L as derived from the empirical relation for Sh_L has to be regarded as only a rough estimation of the contribution of dispersion and continuous phase side mass transfer resistance to the behaviour of the concerning system.

4.4 Experimental determination of mass transfer properties

4.4.1 Introduction

This section discusses the experiments performed to determine the sorbent / water volumetric distribution coefficient m_{SL} and the sorbent side mass transfer coefficient k_S. First, m_{SL} will be established using simple batch equilibrium tests. Next, both m_{SL} and k_S will be determined by fitting experimentally established fixed bed outlet concentration profiles to model curves. The mass transfer parameters m_{SL} and k_S established for PUR (polyurethane) foam and ethylbenzene will be used in the modelling of mass transfer experiments conducted with the pilot unit (Chapter 5). The parameters m_{SL} and k_S established for cellular silicone (PDMS) and toluene will be used in the dimensioning of an industrial-scale separation unit for countercurrent foam absorption (Chapter 6).

4.4.2 Distribution coefficient at equilibrium

The sorbent / water volumetric distribution coefficient m_{SL} can be determined with a simple batch experiment. A certain amount of tap water in which a specific amount of a component to be absorbed has been solved (ethylbenzene or toluene), is brought into contact with a specific amount of sorbent material for sufficiently long time for the system to reach equilibrium. m_{SL} follows from the following relation:

$$m_{SL} = \frac{c_S}{c_L} \tag{4.32}$$

c_S:	concentration in the sorbent phase	[kg/m^3]
c_L:	concentration in the liquid phase	[kg/m^3]

The concentration ethylbenzene or toluene in the liquid phase is measured with an UV-spectrophotometer. Because it is not possible to measure the concentration in the sorbent material in a similar way, this relation is rewritten to the following equation, using the proportionality of the relation between the UV-spectrophotometer signal and the component's concentration:

$$m_{SL} = \frac{UV_0 - UV_e}{UV_e} \cdot \frac{W_L}{W_S} \cdot \frac{\rho_S}{\rho_L} \tag{4.33}$$

UV_0:	UV-signal at the start of the experiment	[-]
UV_e:	UV-signal at the end of the experiment	[-]
W_L:	weight of the liquid phase	[kg]
W_S:	weight of the sorbent phase	[kg]
ρ_S:	density of the sorbent phase (solid based)	[kg/m^3]
ρ_L:	density of the liquid phase	[kg/m^3]

PUR foam

For PUR (polyurethane) foam, type BPS90 supplied by Recticel, Belgium, 8 batch experiments were conducted with ethylbenzene with concentrations from about 25 to 110 wt.ppm. The water / ethylbenzene mixture was stirred for 10 hours to dissolve the ethylbenzene into the water. Next, small pieces of PUR foam of a previously determined total weight were added to the aqueous solution. The initial ethylbenzene concentration in the liquid phase was determined with an UV-spectrophotometer (Hitachi U1100) at a wave length of 254 nm, just before and just after adding the foam. The proportionality factor between the UV-spectrophotometer signal and the component concentration was established using standard ethylbenzene / tap water solutions. The ethylbenzene concentration was measured after 1 and 2 days.

The results for PUR foam are given in the table 4.1. For PUR foam, the solid based density used in equation (4.33) is 1070 kg/m^3.

Table 4.1: distribution coefficient from simple batch experiments for PUR / water / ethylbenzene

W_L [kg]	W_S [kg]	UV_0	UV_e 1 day	UV_e 2 days	m_{SL} 1 day	m_{SL} 2 days
2.047	$2.585 \cdot 10^{-3}$	0.068	0.063	0.066	67	26
1.009	$1.301 \cdot 10^{-3}$	0.131	0.103	0.106	226	196
1.011	$1.335 \cdot 10^{-3}$	0.207	0.170	0.167	176	194
1.016	$1.373 \cdot 10^{-3}$	0.258	0.230	0.216	96	154
1.026	$1.293 \cdot 10^{-3}$	0.312	0.263	0.255	158	190
0.990	$1.316 \cdot 10^{-3}$	0.092	0.081	0.070	109	253
0.993	$1.313 \cdot 10^{-3}$	0.091	0.070	0.078	243	135
0.946	$1.314 \cdot 10^{-3}$	0.186	0.145	0.168	218	83
0.933	$1.333 \cdot 10^{-3}$	0.253	0.220	0.218	112	120

The results for PUR foam not only show a large spread, but also point to experimental error for some experiments since they appear to have a smaller instead of a larger m_{SL} after 2 days compared with m_{SL} after 1 day. The mean value of m_{SL} for PUR / water / ethylbenzene according to the values in table 4.1 is approximately 150. m_{SL} derived from fixed bed outlet concentration profiles has a mean value of 465 (see §4.4.3), which is considerably higher. The results according to fixed bed experiments are much more reliable than the results from the simple batch experiments because with fixed bed experiments it is clearly visible whether an experiment is valid or not.

Cellular silicone

For cellular silicone, PDMS silicone rubber foam DC8157 supplied by Dow Corning, Germany, 4 different batch experiments were conducted with toluene with concentrations from about 90 to 150 wt.ppm. The water / toluene mixture was stirred for 1 day to dissolve the toluene into the water. The test procedure was the same as with PUR foam. The toluene concentration was measured after 4 hours, 1 day and 1.5 days.

The results for cellular silicone are given in Table 4.2. The measured concentrations after 1.5 days appear to be equal to the concentrations after 1 day and are therefore left out of the table. The solid phase based density of the silicone rubber foam used in equation (4.33) is 1030 kg/m^3.

Table 4.2: distribution coefficient from simple batch experiments for cellular silicone / water / toluene

W_L [kg]	W_S [kg]	UV_0	UV_e 4 hours	UV_e 1 day	m_{SL} 4 hours	m_{SL} 1 day
1.049	$3.53 \cdot 10^{-3}$	0.313	0.184	0.174	215	245
1.021	$3.42 \cdot 10^{-3}$	0.287	0.157	0.151	255	277
1.012	$1.98 \cdot 10^{-3}$	0.200	0.137	0.131	242	277
1.014	$2.14 \cdot 10^{-3}$	0.182	0.120	0.115	252	284

The results for cellular silicone show a relatively small spread and appear to be consistent (m_{SL} increases with time and reaches equilibrium, according to the observation that m_{SL} after 1.5 days equals m_{SL} after 1 day). The mean value of m_{SL} for

cellular silicone / water / toluene is approximately 270, which is only slightly higher than the value of m_{SL} = 260 derived from fixed bed outlet concentration profiles (see §4.4.3).

4.4.3 Fixed bed outlet concentration profiles

The mass transfer properties m_{SL} and k_S for packed beds of open sorbent material can be determined or verified by analysing the outlet concentration profiles (breakthrough curves) for a constant feedwater flow rate with a stepwise increase of VOC concentration. The equipment for determining outlet concentration profiles is shown in figure 4.4. Experiments were carried out with open-cell foam materials (PUR foam and cellular silicone) at room temperature in a vertical glass column (diameter $16.6 \cdot 10^{-3}$ m and maximal length 0.51 m). The feed preparation is done batchwise in a feedstock solution reservoir (order of magnitude 100 wt.ppm VOC in tap water). The feed is pumped through the column, where the VOC (toluene or ethylbenzene) is absorbed by the sorbent material. The VOC concentration in the column is measured periodically by UV spectrophotometry (at a wavelength of 254 nm) by withdrawal of samples from the effluent of the column every 17 seconds, using a sipper sampler device. The time for the outlet concentration to reach its steady state maximum value ranges from 26 to 75 minutes. Before the first sorption experiment and after each next sorption experiment, the bed is regenerated with steam.

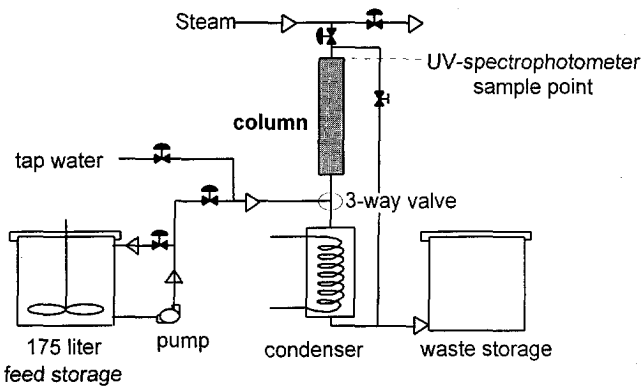

Figure 4.4: Fixed bed equipment

Figure 4.5 gives an example of a measured normalised outlet concentration profile (dashed line in figure 4.5) and a fitted normalised outlet concentration profile (C(t) in figure 4.5) as a function of time "t" (in seconds), using a simple linear rate adsorption model discussed by Ruthven and Ching [9]:

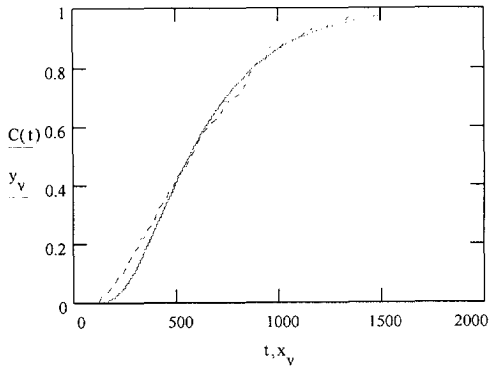

Figure 4.5: Example of measured and fitted outlet concentration profile

The model is based on a linear equilibrium relationship and uses Lapidus and Amundson's solution for a step response for a sufficiently long column [10], approximated by Van Deemter et. al. as follows [11, 9]:

$$C(t) = \frac{1}{2} \cdot \left[1 - \mathrm{erf}\left(\frac{1 - \frac{t}{t_R}}{\sqrt{2 \cdot \sigma_0^2 \cdot \frac{t}{t_R}}} \right) \right] \tag{4.34}$$

with

$$\sigma_0 = \sqrt{2 \cdot \frac{u}{L} \cdot \left(\frac{\varepsilon \cdot D_{ax}}{u^2} + \frac{1}{k_L \cdot a_S} + \frac{1}{m_{SL} \cdot k_S \cdot a_S} \right)} \tag{4.35}$$

$$t_R = \frac{L}{u} \cdot (\varepsilon + (1 - \varepsilon) \cdot m_{SL}) \tag{4.36}$$

L: packed bed length [m]

The calculated outlet concentration profiles according to the model (equations 4.34 through 4.36) are a function of the sorbent side mass transfer coefficient k_S, the liquid side mass transfer coefficient k_L, the axial dispersion coefficient D_{ax} and the volumetric sorbent/water distribution coefficient m_{SL}. The specific sorbent surface area a_S is given by equation (4.29). The area under the outlet concentration profile is a measure for the fraction VOC not absorbed by the sorbent material. This area depends on the value of m_{SL}, but is independent of the other parameters for sufficiently long time. The distribution coefficient m_{SL} is determined by application of the condition of equal surface areas under the experimental and predicted outlet concentration profiles. The sorbent side mass transfer coefficient k_S is determined by subsequently fitting the shape of the model curve to the experimental curve using estimated values for the liquid side

mass transfer coefficient k_L (from equation 4.21) and the axial dispersion coefficient D_{ax} (from Chapter 3 section 3.3).

PUR foam

The PUR foam has a mean pore diameter (empty space based) of 294 μm (determined by microscope). The supplied porosity is 0.972. The glass column is filled with foam by consecutively inserting and gently pressing cylindrical plugs into the tube with a piston. The bed is supported at the top by a polyester screen. Visual inspection ensures equal packed plug heights. Before the sorption experiment starts, the packed foam bed is slowly flooded and rinsed with tap water to purge all air from the foam. A number of fixed bed experiments were conducted with ethylbenzene as the component to be removed from the water.

The liquid side mass transfer coefficient k_L is estimated using equation (4.21). With an equivalent fiber diameter d_{eq} of 8.5 μm for the supplied PUR-foam according to equation (4.25), a kinematic viscosity of $1 \cdot 10^{-6}$ m^2/s for water and a diffusion coefficient of $7.6 \cdot 10^{-10}$ for water / ethylbenzene at room temperature, k_L for the PUR foam experiments has been estimated as follows:

$$k_L = 1.58 \cdot 10^{-3} \cdot u^{0.4} \tag{4.37}$$

The axial dispersion coefficient D_{ax} is estimated based on experiments (see §3.3.3). Because the results for PUR foam approximate the results for crystalline fibers, the corresponding empirical relation according to Van Zee (see Chapter 3) is used to estimate D_{ax} for the PUR foam experiments:

$$D_{ax} = 1.2 \cdot 10^{-4} \cdot \frac{u}{\varepsilon \cdot (1-\varepsilon)^{1.3}} \tag{4.38}$$

Table 4.3 gives the fit results for the fixed bed experiments with PUR foam, using equations (4.37) and (4.38) for k_L and D_{ax}. All experiments were conducted with the same packed bed. The measured and fitted outlet concentration profiles are given in Appendix B.1.

Table 4.3: results of fixed bed experiments with PUR foam / water / ethylbenzene

experiment number	packed bed length L [m]	packed bed porosity ε [-]	superficial water velocity u [cm/s]	fit parameters	
				m_{SL} [-]	k_S [m/s]
PUR1	0.5	0.932	3.06	500	$3 \cdot 10^{-8}$
PUR2	0.5	0.932	2.63	500	$3 \cdot 10^{-8}$
PUR3	0.5	0.932	2.87	470	$2.5 \cdot 10^{-8}$
PUR4	0.5	0.932	3.06	430	$2.5 \cdot 10^{-8}$
PUR5	0.5	0.932	2.56	400	$1.5 \cdot 10^{-8}$
PUR6	0.32	0.895	1.93	500	$1.5 \cdot 10^{-8}$
PUR7	0.29	0.884	2.87	440	$1.5 \cdot 10^{-8}$

The overall fit parameters for which all experimental outlet concentration profiles can be approximated are:

$m = 465$
$k_S = 2.2 \cdot 10^{-8}$

and are equal to the mean value of the corresponding fit parameters for all experiments.

Cellular silicone
The cellular silicone, mainly consisting of PDMS, has a supplied porosity of 0.87 and a mean pore diameter (empty space based) of approximately 700 μm. The bed is supported at the top by a sieve plate instead of a polyester screen as with PUR foam, due to the higher pressure drop of the cellular silicone. The test procedure is the same as with PUR foam. A number of fixed bed experiments were conducted with toluene as the component to be removed from the water.

The liquid side mass transfer coefficient k_L is estimated using equation (4.21). With an equivalent fiber diameter d_{eq} of 104.6 μm for the supplied cellular silicone according to equation (4.25), a kinematic viscosity of $1 \cdot 10^{-6}$ m^2/s for water and a diffusion coefficient of $8.5 \cdot 10^{-10}$ for water / toluene at room temperature, k_L for the cellular silicone experiments has been estimated as follows:

$$k_L = 3.77 \cdot 10^{-4} \cdot u^{0.4} \qquad (4.39)$$

The difference between this k_L and the k_L for PUR foam is mainly caused by the difference in equivalent fiber diameter of the foam (104.6 μm instead of 8.5 μm).

The axial dispersion coefficient D_{ax} is estimated on the basis of experiments (see §3.3.3), resulting in the following equation:

$$D_{ax} = 0.05 \cdot u \qquad (4.40)$$

Table 4.4 gives the fit results for the fixed bed experiments with cellular silicone, using equations (4.39) and (4.40) for k_L and D_{ax}. All experiments were conducted with the same packed bed. The measured and fitted outlet concentration profiles are given in Appendix B.2.

Table 4.4: results of fixed bed experiments with cellular silicone / water / toluene

experiment number	packed bed length L [m]	packed bed porosity ε [-]	superficial water velocity u [cm/s]	fit parameters m_{SL} [-]	fit parameters k_S [m/s]
SIL1	0.28	0.806	1.02	260	$1 \cdot 10^{-6}$
SIL2	0.265	0.795	1.27	260	$1 \cdot 10^{-6}$
SIL3	0.265	0.795	1.49	260	$1 \cdot 10^{-6}$

4.4.4 Discussion

The results for m_{SL} from the batch equilibrium tests for PUR foam lack reliability due to the observed decrease of m_{SL} in time for some of the experiments and the large spread in results. In contrast with the results for PUR foam, the results for cellular silicone which were established using the same test procedure show a relatively small spread and an increasing m_{SL} during time, reaching equilibrium within 1.5 days. Also, for cellular silicone the average value of m_{SL} according to the batch equilibrium tests is nearly the same as the mean value established with fixed bed experiments. A clear explanation for the poor results with PUR foam is not available. Maybe the results would have been better if larger amounts of PUR foam had been used for the batch equilibrium tests (for instance twice as much), thus increasing the difference between initial and final ethylbenzene concentrations in the water. Since the results according to fixed bed experiments are more reliable than the results from the simple batch experiments due to the fact that it is clearly visible if a fixed bed experiment is valid or not, we will use the more reliable fixed bed results. These results are:

PUR foam / ethylbenzene: $m_{SL} = 465$.
Cellular silicone (PDMS) / toluene: $m_{SL} = 260$.

The fixed bed outlet concentration profiles can be adequately described by a model discussed in §4.4.3. The measured outlet concentration profiles were fitted by the model curves assuming that the liquid side mass transfer coefficient k_L can be described by equation (4.21). It should be noted however that the fitted model curves are rather insensitive to small variations of the mass transfer parameters. On the other hand, the mass transfer model for countercurrent sorption equipment (§4.3.2 and §4.3.3) is rather insensitive to small variations of the mass transfer parameters as well, so the accuracy of the mass transfer model is not largely affected by the accuracy of the applied fitting method.

The established value of $2.2 \cdot 10^{-8}$ m/s for k_S for PUR foam / ethylbenzene corresponds with a sorbent phase diffusion coefficient D_S of $2.3 \cdot 10^{-14}$ m^2/s according to equation (4.26). The order of magnitude is comparable with the value of $D_S = 3 \cdot 10^{-14}$ m^2/s for polyurethane (Lycra) fibers / toluene established by Van Zee [2].
The established value of $1 \cdot 10^{-6}$ m/s for k_S for cellular silicone / toluene corresponds with a sorbent phase diffusion coefficient D_S of $1.3 \cdot 10^{-11}$ m^2/s. This is almost one order of magnitude smaller than the value of $D_S = 7.7 \cdot 10^{-11}$ m^2/s for sheets of PDMS (Silopren) / toluene established by Van Zee [2]. Silicone rubber (PDMS) is a far better sorbent material than PUR owing to its relatively high diffusion coefficient.

It is unknown to which extent the established mass transfer properties will change during service life of the sorbent material because it can be expected that the sorbent will slowly degenerate chemically with large numbers of sorption / desorption cycles. Further research on this issue is recommended.

4.5 Conclusions

A model describing countercurrent mass transfer of a single component, including axial dispersion in the liquid (or gaseous) phase, is given by Miyauchi and Vermeulen (§4.3.2 and §4.3.3). This model will be used to evaluate the separation efficiency of the pilot unit (Chapter 5) and a scaled-up and improved version of this equipment (Chapter 6). The axial dispersion is accounted for by the axial dispersion coefficient D_{ax}, which is established by experiment (Chapter 3 section 3.3).

The model uses a number of mass transfer properties which will have to be estimated or determined by experiment for each specific separation problem.
The liquid side mass transfer coefficient k_L can be estimated using an empirical relation (equation 4.21) representing the various mass transfer correlations for the liquid phase found in literature. For the gaseous regenerant phase the same empirical relation will be used.
The sorbent side mass transfer coefficient k_S can be estimated from the Sherwood number, which is assumed to have a value of 8 for fiberlike polymeric sorbents, but can also be experimentally determined by fitting outlet concentration profiles of fixed bed experiments.
The sorbent / water distribution coefficient m_{SL} can be determined either by simple batch equilibrium tests or by fitting outlet concentration profiles of fixed bed experiments. The latter method is more reliable and is therefore preferred. The steam / sorbent distribution coefficient m_{GS} for the regeneration section can be calculated by multiplying the steam / water and water / sorbent distribution coefficients, both at 100°C. For cellular silicone (PDMS) / toluene, m_{GS} is estimated at 0.02 (used in Chapter 6).

The results from fitting fixed bed outlet concentration profiles are:

PUR foam / ethylbenzene (used in Chapter 5):
$m_{SL} = 465$
$k_S = 2.2 \cdot 10^{-8}$ m/s

Cellular silicone (PDMS) / toluene (used in Chapter 6):
$m_{SL} = 260$
$k_S = 1 \cdot 10^{-6}$ m/s.

References

[1] Miyauchi, T., Vermeulen, T., *Longitudinal dispersion in two-phase continuous-flow operations*, I&EC Fundamentals, **2** (1963), pp. 113-126

[2] Zee, G. van, *Counter current sorption using fiber sorbents (Ph.D.-thesis)*, Delft University Press, 1996, ISBN 90-407-1328-6

[3] Schmal, D., Erkel, J. van, Duin, J. van, *Mass transfer at carbon fibre electrodes*, Journal of applied electrochemistry, **16** (1986), pp. 422-430

[4] Sinnot, R.K., *Coulson & Richardson's Chemical Engineering, Volume 6 (2nd ed.)*, Pergamon Press, Oxford, 1993, ISBN 0-08-041866x

[5] Zee, G. van, Bisschops, M., Graauw, J. de, *Internal Sherwood numbers for diffusion in sorption operations*, Chem. Engng. Proc., **36** (1997), pp. 201-208

[6] Hwang, Y., Olson, J.D., Keller, G.E., *Steam stripping for removal of organic pollutants from water. 2. vapor-liquid equilibrium data*, Ind.Eng.Chem.Res, **31** (1992), pp.1759-1768

[7] Janssen, L.P.B.M, Warmoeskerken, M.M.C.G., *Transport phenomena data companion*, Delftse Uitgevers Maatschappij b.v., Delft, 1987, ISBN 90-6562-074-5

[8] Hilyard, N.C., Collier, P., *A structural model for air flow in flexible PUR foams*, Cellular Polymers, **6**-6 (1987), pp. 9-26

[9] Ruthven, D.M., Ching, C.B., *Modelling of chromatographic processes*, in:Ganetsos, G. and Barker, P.E. (eds), *Preparative and production scale chromatography*, Marcel Dekker Inc., New York, 1993, ISBN 0-8247-8738-2

[10] Lapidus, L., Amundson, N.R., *Mathematics of adsorption in beds. VI. The effect of longitudinal diffusion in ion exchange and chromatographic columns*, J.Phys.Chem., **56** (1952), pp. 984-988

[11] Deemter, J.J. van, Zuiderweg, F.J., Klinkenberg, A., *Longitudinal diffusion and resistance to mass transfer as causes of nonideality in chromatography*, Chem.Eng.Sci., **5** (1956), pp. 271-289

5

Pilot unit

5.1 Introduction

After preliminary studies on countercurrent sorption using a tubular sorbent bed transported through a straight cylindrical column [1], a pilot unit was developed using an annular sorbent bed transported through a circular column. By using a circular column in which the packed sorbent bed is transported concentric, mechanical degradation of the open sorbent material and hence the occurrence of unacceptable by-pass flows as with the tubular sorbent bed is prevented. The purpose of the pilot unit is to prove the technical feasibility of continuous countercurrent sorption equipment using mechanical transport of the sorbent bed and to establish the separation performance and investigate the possible improvements when using this kind of equipment.

Section 5.2 gives a description of the basic design and operation of the pilot unit. Next, section 5.3 discusses a number of relevant design details and section 5.4 gives a more detailed description of the operation of the pilot unit. Section 5.5 presents the results for mass transfer experiments conducted with this new separation equipment. The results are evaluated in section 5.6. Finally, conclusions are given in section 5.7.

5.2 Basic design

For research and for demonstration purposes a new kind of separation equipment was developed in co-operation with the Central Workshop of Delft University of Technology. This experimental demonstration unit or pilot unit is based on the principle of continuous countercurrent sorption. The implementation and basic operation of the pilot unit will be discussed in this section. Further details will be discussed in section 5.3.

The packed bed consists of open sorbent material and is located in the annular space between a slowly rotating housing, shaped like a spool, and a static cylinder, see figures 5.1 and 5.2. The sorbent bed is attached to the rotating housing and is transported clockwise according to figure 5.1. The inlet and outlet ports for the process media (water and steam) are placed on the static cylinder. Perpendicular to the direction of fluid flow a number of check valve plates are placed at equal distances throughout the annulus, dividing the annular sorbent into similar bed segments. These plates are

provided with check valves (non-return valves) which allow fluids only to pass the plates in the direction opposite to the direction of sorbent transport. Accordingly the process media only flow anti-clockwise so countercurrent operation is achieved. The check valves are self-sealing and are opened by pressure differences across the plates caused by the flowing process media. The number of check valve plates (12) and the positions of the inlet and outlet ports are chosen in such a way that during rotation always at least one check valve plate is present between neighbouring ports to secure countercurrent operation.
The application of self-sealing check valves integrated with the packed bed is unique, in contrast to the application of external cam-driven poppet valves between the bed segments for sorption or chromatography separation processes [2,3]. An international patent application for our design of the rotating annular sorbent apparatus for countercurrent sorption has been filed [4].

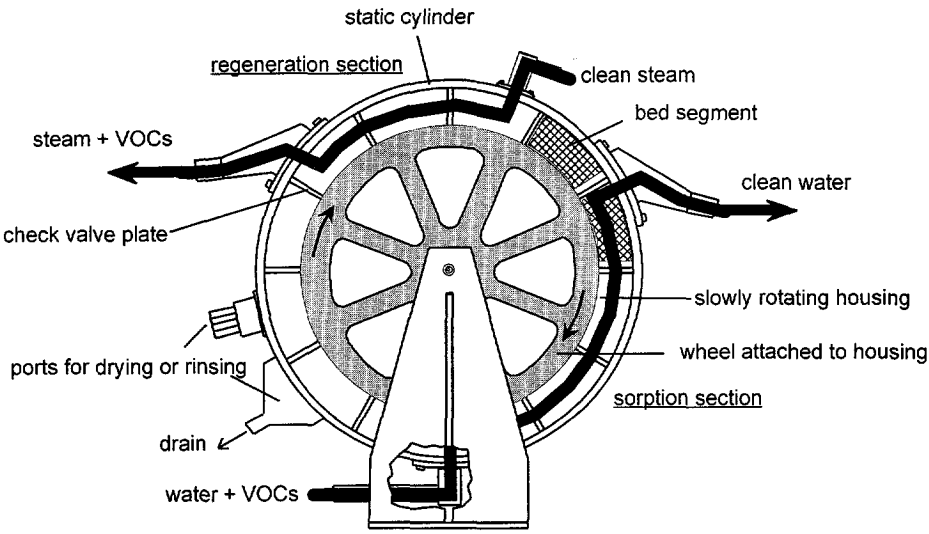

Figure 5.1: Front-view of the pilot unit

Removal of sparingly soluble VOCs (Volatile Organic Compounds) from waste water was chosen as application for this study (see Chapter 1). The feed water, typically containing up to around 100 wt.ppm toluene or ethylbenzene, is pumped through the sorption section. Due to the check valves the water only flows countercurrent with the transported packed bed which sorbs the VOCs from the feed water. The purified water leaves the separation unit through an outlet port in the static cylinder. The packed sorbent bed containing the VOCs is transported from the sorption to the regeneration section.
Between the sorption and regeneration section additional ports are provided for optional drying or rinsing of the sorbent before entering the regeneration section.
In the regeneration section steam stripping is applied to remove the VOCs from the sorbent. Countercurrent operation is enforced in a similar way as in the sorption section.

Owing to the high temperature in the regeneration section (approximately 110°C) the concentration of VOCs in the steam will be high, so after condensation phase separation into an organic phase and a water phase will take place. This organic phase can be isolated by a decanter. The relatively small amount of condensed steam saturated with VOCs can be recycled to the feed water inlet port.

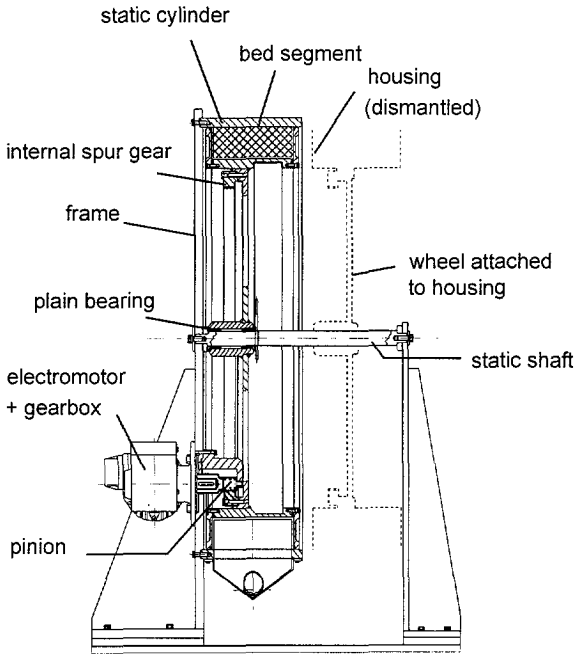

Figure 5.2: Side-view of the pilot unit

The dimensions of the pilot unit were based on preliminary mass transfer calculations using a simplified mass transfer model and assuming application of silicone rubber fibers with a packed bed porosity of 0.9, a fiber diameter of $50 \cdot 10^{-6}$ m and a pressure drop of $3.2 \cdot 10^{4}$ Pa/m.
The circumference of the annulus is divided into 12 compartments of 30 degrees each, the bed segments cover 21.82 degrees per compartment. At a mean annulus diameter of 0.65 m the curved length of a bed segment is 0.124 m. The total packed bed length in the sorption section (110 degrees) is 0.45 m at this diameter and in the regeneration section (60 degrees) this length is 0.25 m. The cross-sectional area of the packed bed is determined by the height and the width of the bed segments. The inner diameter of the annulus (housing inner face) is 0.6 m, the outer diameter of the annulus (static cylinder) is 0.7 m, so the height of the packed bed is 0.05 m. The width of the packed bed is 0.15 m. With a nominal flow rate of 1 m^3/h, the superficial water velocity is approximately 3.7 cm/s. The nominal transport velocity of the sorbent at the mean diameter (0.65 m) is approximately 2.3 mm/s, corresponding with a rotational speed of around 4 revolutions per hour.

Figure 5.3 gives a schematic representation of the pilot unit plus ancillary equipment. The VOC-concentration in the purified water is monitored by a gas chromatograph (GC), see section 5.4.

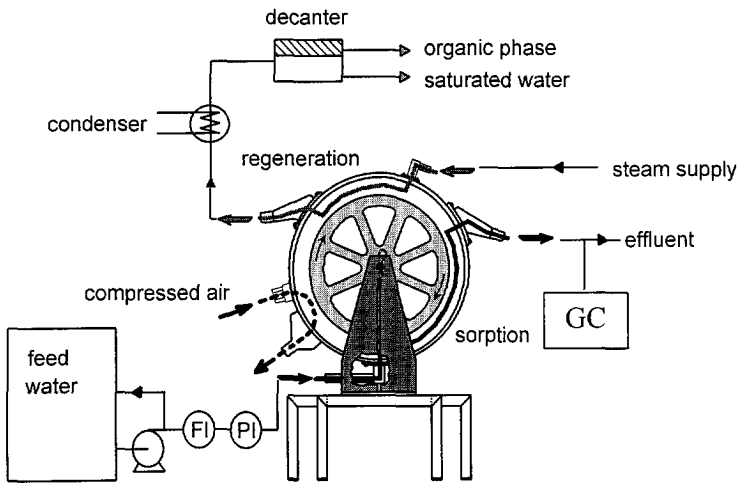

Figure 5.3: Schematic representation of the equipment

Figure 5.4 shows a photo of the pilot unit. The photo according to figure 5.5 displays the dismantled housing, exposing a number of bed segments separated by check valve plates.

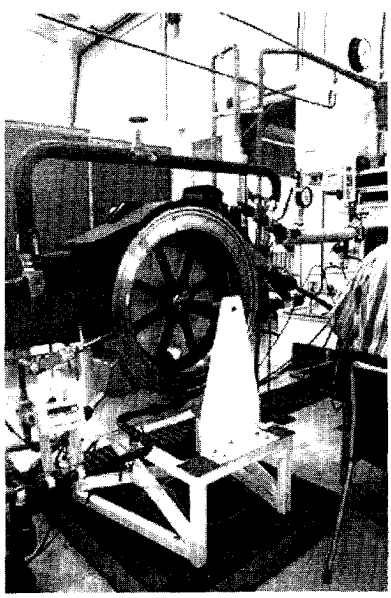

Figure 5.4: Pilot unit

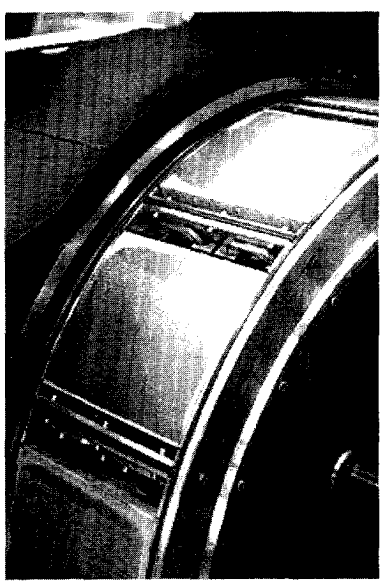

Figure 5.5: Housing (dismantled)

5.3 Design details

Drive
For the chosen application the rotational speed of the housing is low (maximal 8 revolutions per hour, adjustable to zero), at the same time a large enough driving torque has to be available to overcome the frictional resistance between the slowly rotating housing and the static cylinder and the flow resistance of the bed segments and the check valves. By choosing a large reduction ratio (9375 to 1) the housing can be driven by a relatively small electromotor (60 W). The large reduction ratio is realised by linking the electromotor to a compact reduction gearbox with a double worm gear and a ratio of 375 to 1, which in turn is connected to a pinion which drives the internal spur gear attached to the rotating housing with a ratio of 25 to 1 (see figure 5.2). The maximal driving torque is 300 Nm.

The housing can be simply disassembled from the pilot unit by translating the housing outside the static cylinder (see figure 5.2). The housing is then supported on a static shaft via a wheel and a plain bearing. With the housing disassembled the annulus is accessible for inspection and maintenance (see figure 5.5).

Seals
To prevent leakage of process media through the circular gaps between housing side faces and static cylinder (see figure 5.6), these gaps have to be sealed. Also the straight gaps between check valve plates and static cylinder (see figure 5.7) have to be sealed to prevent leakage around these plates.

These seals have to comply with the following requirements:
- the seals have to bridge variations in gap height as a result of manufacturing tolerances and differences in thermal expansion
- low friction to restrict the required driving torque
- no lubricants other than water
- suitable for both rotation (normal operation) and translation (disassembly and assembly of the housing).

A combination has been chosen of a teflon compound (glass filled teflon) and steam resistant EP-rubber (Ø4 mm, 60° Shore A) which supports the teflon. The teflon makes contact with the static cylinder and has low friction, the rubber ensures sufficient contact pressure for correct sealing and bridges the differences in gap height between housing or check valve plates and static cylinder. All main parts of the separation drum (the static cylinder, the housing, the check valves and the check valve plates) are made of stainless steel (AISI 316). The inner surface of the static cylinder is grinded to a surface roughness of 0.3 μm. The diametrical tolerance between static cylinder and housing side faces is 0.4 mm due to manufacturing tolerances and approximately another 0.4 mm due to differences in thermal expansion during operation (observed during experiments).
The gap between housing and static cylinder is sealed by a teflon ring (ER 48-820-700 L=4.2 mm supplied by Eriks B.V., Alkmaar, The Netherlands) plus a rubber ring (made from O-ring cord) according to figure 5.6. The rubber O-ring is shortened by 13 cm to

adjust the thickness and hardness of the O-ring cord to realise sufficient sealing at minimal friction. The gap between check valve plates and static cylinder is sealed by a teflon strip plus rubber strip according to figure 5.7.

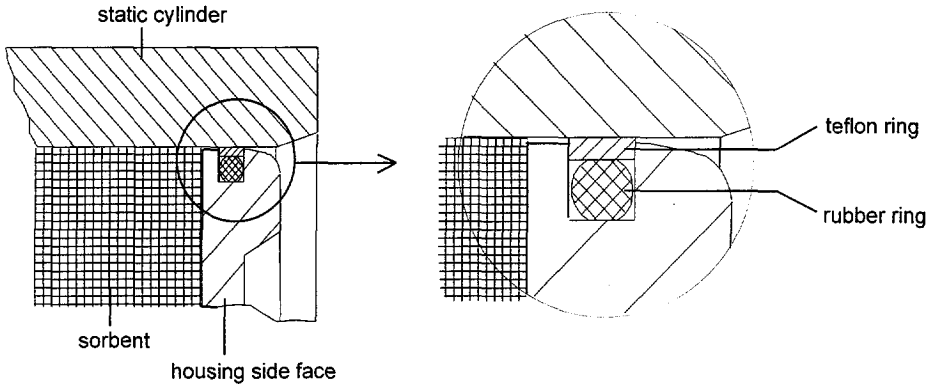

Figure 5.6: Sealing between housing and static cylinder

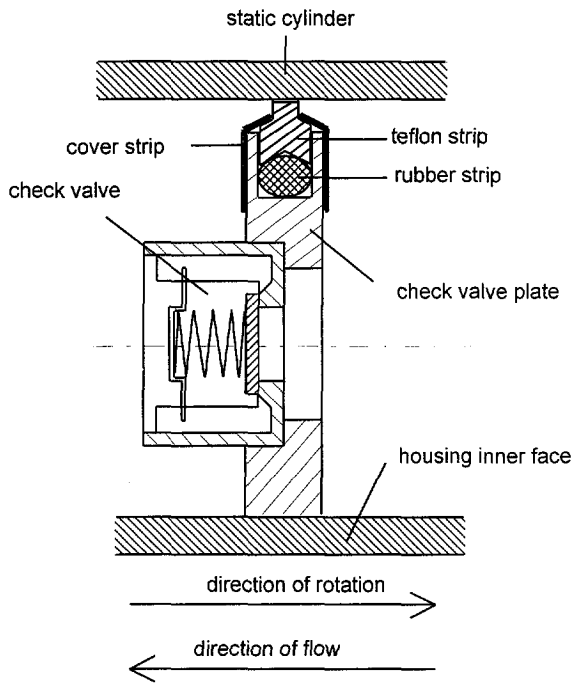

Figure 5.7: Sealing between check valve plate and static cylinder

The gap between the straight seals on top of the check valve plates and the circular seals of the housing side faces has to be as small as possible to prevent leakage across the check valve plates. Therefore the joining of these seals is implemented according to figure 5.8:

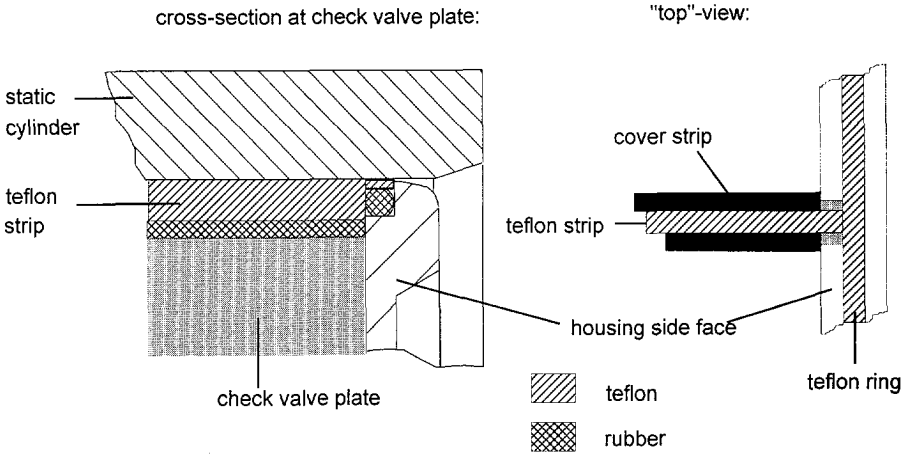

Figure 5.8: Joining of straight and circular seals

For future improved or scaled-up equipment the circular seals between housing and static cylinder (see figure 5.6) have to be improved on a number of items. First, the durability of the teflon and rubber O-ring has to be sufficiently high. During assembly and disassembly the teflon ring at the side of the frame has to pass various openings in the static cylinder at the inlet and outlet ports, causing damage to the teflon ring. Also, a rubber O-ring made in one piece has to be used instead of a vulcanised O-ring cord to prevent the O-ring from tearing at the vulcanised spot after exposure to steam for several hours. This requires a design adapted to standard O-ring sizes or requires a tailor-made mould for the O-ring. Secondly, the inner surface of the static cylinder which is in contact with the teflon seals has to be hardened or a teflon compound other than glass-filled teflon has to be used, to prevent wear of the stainless steel contact surface area. Finally, the teflon ring may no longer rotate relative to the rubber O-ring as was observed during the experiments, to prevent wear of the O-ring and to enable correct functioning of the seal.

Check valve plates

To prevent the housing side faces from deflecting as a result of the liquid pressure, these side faces are bolted to the check valve plates, see figure 5.9. The check valves (Convey CVD DN15 Austi/Austi PN 6/40 supplied by Eriks B.V., Alkmaar, The Netherlands) have an opening of Ø15 mm. Each plate is provided with 2 check valves. The valves are self-sealing (spring loaded) and have an opening pressure of approximately $2.5 \cdot 10^3$ Pa.

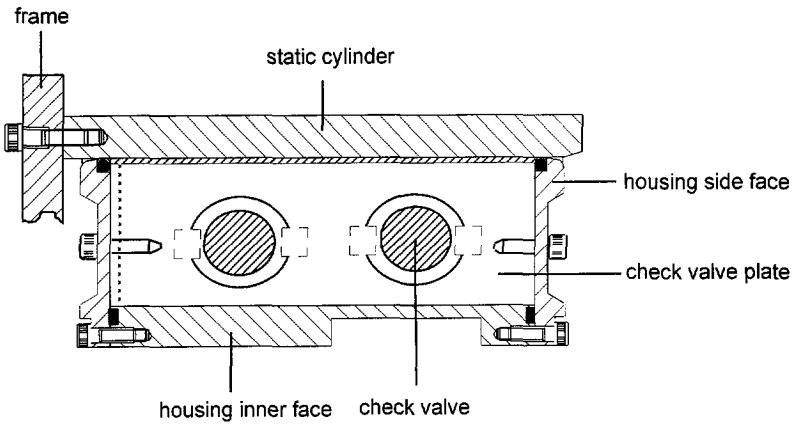

Figure 5.9: Check valve plate

Packed bed

The packed bed is segmented by check valve plates to enable countercurrent operation. Each bed segment is fenced in by two sieve plates (80 holes Ø6 mm), the downstream sieve plate balances the forces due to the flow resistance of the bed segment. The check valve plates are mounted between the sieve plates of successive bed segments (see figure 5.5). The bed segments are covered with polyester screens to minimise friction with the static cylinder and to protect the sorbent material from wear. So the bed segments are confined within the housing (inner face and side faces), the sieve plates (upstream and downstream face) and the polyester screen (top face), see figures 5.10 and 5.11:

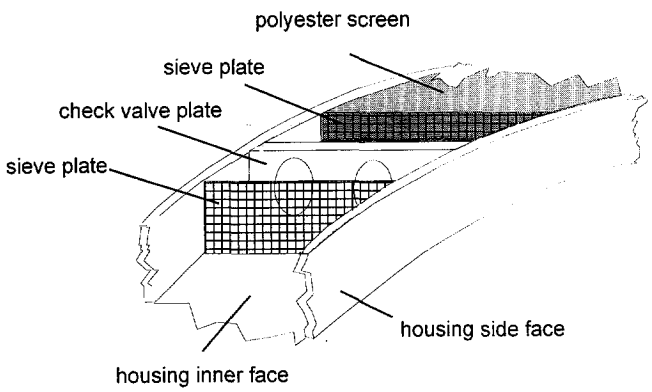

Figure 5.10: Confinement of bed segments

The polyester screen (Scrynel PE-100-HD by ZBF, Rüschlikon, Switzerland), see figure 5.11, is attached to the sieve plates by means of thin rods which fit into narrow sleeves at both ends of the screen. These rods are hooked to pins attached to the lower part of the sieve plates.

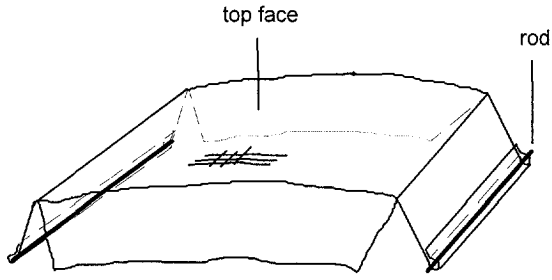

Figure 5.11: Polyester screen

Because the screen is mounted under slight compression of the packed bed, the bed segments exert an elastic pressure on the static cylinder which is needed to prevent by-pass of process media between the packed bed and the static cylinder.

5.4 Operation

Feed water route

The pilot unit has a nominal flow rate of 1 m^3/h (maximal 2 m^3/h). The flow rate to the separation drum is adjusted by valve V12 in the return pipe of the feed pump to the feed water buffer vessel (see figure 5.12). The contents of the feed water buffer vessel is limited (approximately 1 m^3) so additional equipment has been provided to facilitate continuous operation with constant feed water composition. The organic compound, for instance ethylbenzene, is pumped by a membrane pump (P3) through a capillary tube into a T-joint (B in figure 5.12) and mixed with a small water flow supplied by a gear pump (P2). The ethylbenzene droplets are reduced in size by an orifice (A in figure 5.12, Ø1.8 mm) after which the ethylbenzene-water mixture enters the top of the buffer vessel as a jet. This jet is thoroughly mixed with a tap water jet perpendicular to the first one. By supplying the ethylbenzene in this way and by the continuous circulation at the bottom of the buffer vessel by the return pipe (valve V12) of the feed pump (P1), the small ethylbenzene droplets will dissolve well within the residence time of the feed water in the vessel.

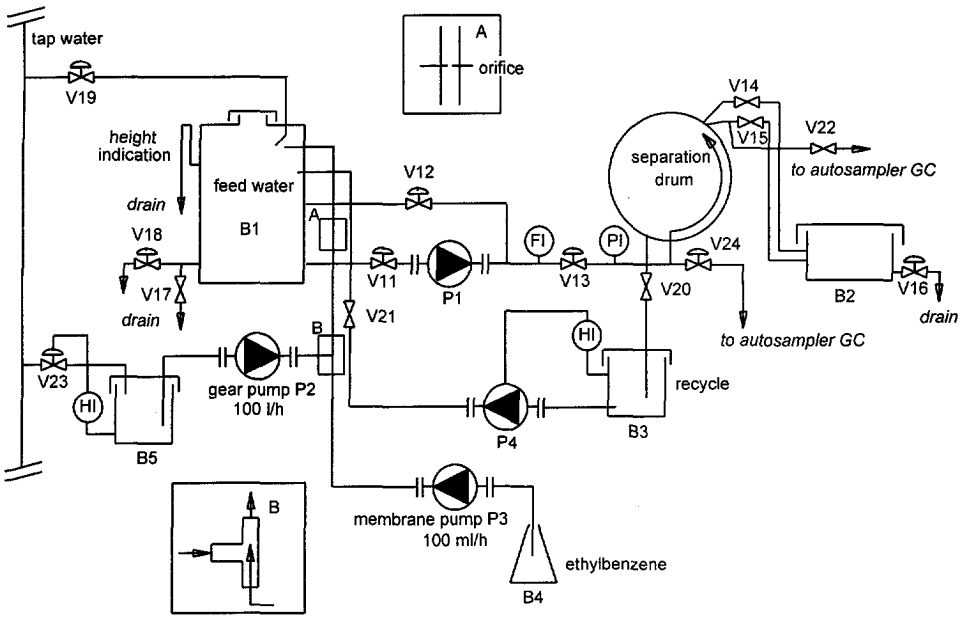

Figure 5.12: Feed water route

The water which is carried along with the packed bed and which is partly drained by gravity at the outlet port left from the feed water inlet port, still has the desired feed water composition and is therefore recycled via buffer vessel B3 and pump P4. The purified feed water, leaving the separation unit at V14 and V15, is replenished by tap water (V19) to prevent accumulation of pollutants or dirt particles in the system. At valves V22 respectively V24 small flows can be directed towards the flow cell of the autosampler of the gas chromatograph (GC) to determine the effluent composition respectively the feed water composition.

Steam route

Steam is available at 10 bar and is supplied to the separation unit by a metering valve (V41 in figure 5.13). First, the steam pressure is reduced at reducing valve R2 to approximately 3 bar. When the system has to be heated (start-up), valves V39, V40 and V36 are opened and V35 is closed. During normal operation, V35 is open and V39, V40 and V36 are closed. Now the steam flow rate through the separation unit is adjusted by choosing the proper setting of V41 in relation to the pressure difference between PI 22 and PI 23. The system was calibrated by leading steam via the by-pass (V36 open) to the condenser and weighing the condensate. The pressure at PI 23 is 1.5 bar at the most under normal operating conditions.

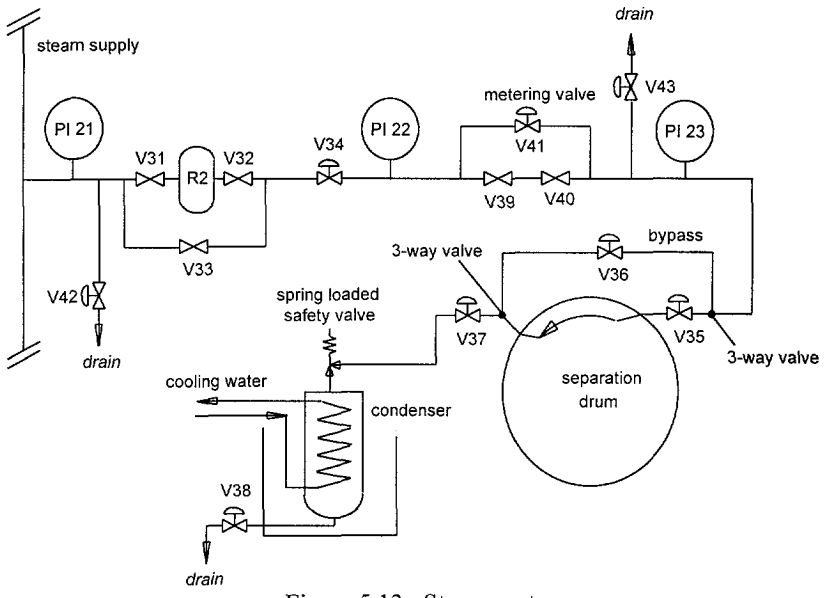

Figure 5.13: Steam route

Regeneration

The pilot unit was provided with a drying section using compressed air (see figure 5.3). However, since the compressed air strips most of the ethylbenzene from the packed beds, this section was not used for regular mass transfer experiments. In all cases only steam was used as stripping agent. The adhering water which remained in the packed bed after draining by gravity had to be stripped in the regeneration as well.

Experiments with PDMS fibers (Poly Di Methyl Siloxane, a silicone rubber) and PUR foam (PolyURethane) show that the steam flow rate through the metering valve has to be about 20 kg/h to maintain normal steady state operating conditions. At lower steam flow rates it may occur that only water instead of steam plus water leaves the regeneration section of the separation drum. In that case the sorbent leaving the regeneration section is not clean enough to achieve the required removal efficiency in the sorption section. The required steam supply for stripping of the sorbent material is estimated by experiments and calculations at some 25% maximally of the required total steam supply, the rest of the steam is required to heat the rotating parts (steel and sorbent material) and the adhered water. The steam leaving the regeneration section has a superficial velocity of approximately 0.3 m/s. This steam velocity of 0.3 m/s will be sufficient to strip the sorbent material under practical conditions. This value will be used for an improved and scaled-up design (Chapter 6).

Gas chromatograph

The concentration of dissolved VOCs in the effluent (valve V22 at the right of figure 5.12) is monitored every 2.5 to 3 minutes by a gas chromatograph (Chrompack CP-9001) using an autosampler (CTC A200S). The feed water concentration is monitored

by the GC as well. A sample of 0.2 microliter is injected into the wide bore capillary column of the GC (Chrompack 10 m x 0.53 mm WCOT Fused Silica, stationary phase: CP-Sil-5 CB). The injector temperature and the FID detector (Flame Ionisation Detector) temperature are 250°C, the temperature of the oven is 100°C. The peak surface area of the chromatogram at the retention time of the concerning VOC is proportional to the concentration of the VOC in the sample.
Ethylbenzene was chosen for mass transfer experiments instead of toluene because the chromatograms showed inexplicable disturbances at the retention time of toluene.

5.5 Mass transfer experiments

Sorbent materials
As planned, mass transfer experiments were conducted with PDMS fibers. Since these fibers are not commercially available, we made PDMS fibers at our laboratory [1]. These self-made fibers however did not have structural properties according to the desired specifications which were used for preliminary mass transfer calculations for the equipment design. The fibers had a diameter of 200 μm instead of 50 μm and a packed bed porosity of 0.77 instead of 0.9. PDMS fibers with a diameter smaller than 200 μm and a packed bed porosity higher than 0.77 caused too many problems with respect to fiber production and compressibility of the packed bed.
Because the PDMS fiber beds showed a poor removal efficiency caused by the large compressibility of the beds (see section 5.6), next an alternative sorption material was used which is commercially available and has a smaller compressibility: open-cell PUR foam (BPS 90 by Recticel, Belgium) with 90 pores per inch and an unpacked porosity of 0.972. The PUR foam has a mean pore diameter (empty space based) of 294 μm and an equivalent fiber diameter of 8.5 μm (see Chapter 4). The pressure drop of the sorption section is approximately $2.5 \cdot 10^4$ Pa at 3.7 cm/s. Although the PUR foam is not steam resistant and therefore unsuitable for practical application, this foam is suitable for study of the behaviour of the pilot unit and for mass transfer experiments.
In a later stage, samples of cellular silicone (open-cell silicone rubber foam), steam resistant and with a smaller compressibility than PDMS fiber beds, were supplied by Dow Corning, Germany. However, these samples could not be used in the pilot unit due to the relatively high pressure drop of these samples. The mass transfer properties of cellular silicone were characterised by separate experiments (see Chapter 4), showing that cellular silicone is a far better sorbent material than PUR foam owing to its relatively high diffusion coefficient for VOCs. The scaled-up and improved design (Chapter 6) will be based on application of cellular silicone.

Calculations
The calculations for the sorption section for every first experiment with PDMS fibers and PUR foam are given in Appendix C.1. These calculations are made using the mass transfer model for countercurrent fiber sorption (Chapter 4). For PUR foam the equivalent fiber diameter was used, derived from the structural foam properties as described in Chapter 4.

The sorption section has an averaged total packed bed length of 0.45 m at the mean diameter of the annulus (0.65 m). This value of 0.45 m is an averaged value since the number of check valve plates located in the sorption section varies between 3 and 4 (see figure 5.1). The effluent concentration will show some fluctuation due to the position of the slowly rotating housing relative to the static cylinder.
According to the experimental conditions, calculation of the mass transfer phenomena in the separation unit assumes a steam flow rate high enough to clean the sorbent material. Therefore the VOC-concentration of the sorbent entering the sorption section is assumed to be 0.01 kg/m^3 solid based.

PDMS fibers, ethylbenzene
The experiments with PDMS fibers were conducted prior to the availability of facilities for continuous feed water production, so these experiments had a limited duration of approximately 1 hour. Effluent measurements were made every 2.5 minutes.
The following parameters apply to the experiments conducted with PDMS fibers (see Chapters 3 and 4):

packed bed properties:		
porosity of packed fiber bed:	$\varepsilon = 0.77$	[-]
fiber diameter:	$d = 200 \cdot 10^{-6}$	[m]
specific bed surface area:	$a_S = \frac{4 \cdot (1-\varepsilon)}{d} = 4.6 \cdot 10^3$	[m^2/m^3]
mass transfer properties:		
sorbent/liquid distribution coeff.:	$m_{SL} = 1{,}300$	[(kg/m^3)/(kg/m^3]
sorbent side mass transfer coeff.:	$k_S = 8.8 \cdot 10^{-7}$	[m/s]
liquid side mass transfer coeff.:	$k_L = 2.37 \cdot 10^{-4} \cdot u^{0.4}$	[m/s]
axial dispersion coefficient:	$D_{ax} = 0.05 \cdot u$	[m^2/s]
other parameters:		
superficial flow velocity	u	[m/s]
sorbent transport velocity:	$v = 2.14 \cdot 10^{-4}$	[m/s]
sorption factor	$S = \frac{m_{SL} \cdot (1-\varepsilon) \cdot v}{u}$	[-]
water input concentration:	C_{L0} (or C_{IN})	[kg/m^3]
sorbent input concentration:	$C_{S0} = 10^{-2}$	[kg/m^3 solid based]

The results are summarised as follows:

Table 5.1: removal efficiency "E", experiment versus calculation, PDMS fibers

u [m/s]	S [-]	C_{IN} [wt.ppm]	C_{OUT} [wt.ppm] experimental	$E = 1-C_{OUT}/C_{IN}$ [-] experimental	$E = 1-C_{OUT}/C_{IN}$ [-] model
0.0443	1.44	16.5	7.4	0.55	0.786
0.034	1.88	37.1	8.7	0.77	0.885
0.0293	2.18	24.8	3.0	0.88	0.887
0.0245	2.61	45.2	5.4	0.88	0.918
0.021	3.05	24.3	0.6	0.975	0.939

Figure 5.14 gives the removal efficiency E (the difference between inlet and outlet concentration, divided by the inlet concentration) as a function of the sorption factor S. The continuous line is predicted by the model according to Chapter 4 (see example calculation in Appendix C.1), the dotted straight line represents equilibrium at infinite packed bed length. The sorption factor S decreases with increasing superficial water velocity "u".

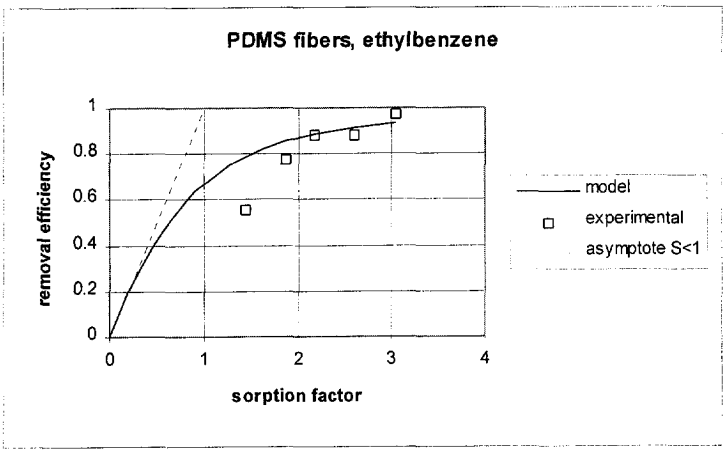

Figure 5.14: Removal efficiency, experiment versus calculation, PDMS fibers

PUR foam, ethylbenzene

The experiments with PUR foam were conducted with continuous feed water production (see section 5.4) allowing for an experiment duration of several hours. The time interval between two effluent measurements was 3 minutes. Figure 5.15 gives as an example the measured feed water and effluent concentrations of the first experiment with PUR foam.

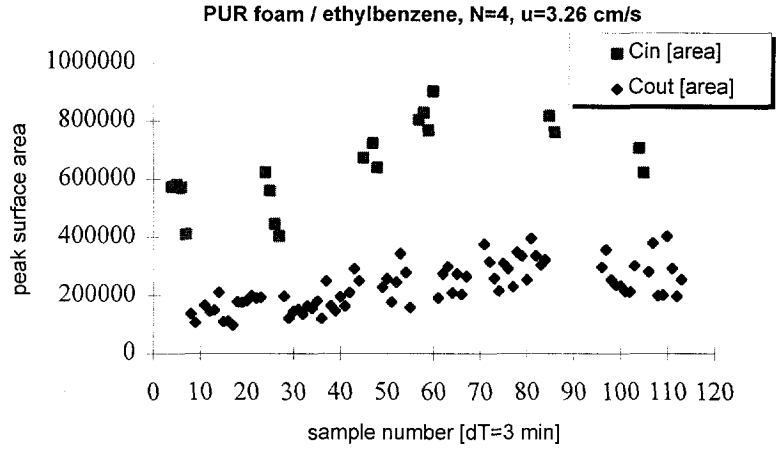

Figure 5.15: Example of measured feed water and effluent concentrations for PUR foam experiments

The concentrations in figure 5.15 are given as peak surface areas of the corresponding chromatograms. The feed water concentration is given by Cin, the effluent concentration is given by Cout. These area values have to be corrected for the peak surface area of clean tap water and are then converted into a wt.ppm concentration by comparison with a standard.

The following parameters apply to the experiments conducted with PUR foam (see Chapters 3 and 4; D_{ax} for PUR foam was estimated using an empirical relation according to Van Zee, see Chapter 4):

<u>packed bed properties:</u>		
porosity of packed foam bed:	ε (see tables 5.2 and 5.3)	[-]
specific surface area:	a_S (see tables 5.2 and 5.3)	$[m^2/m^3]$
	$a_S = \frac{4\cdot(1-\varepsilon)}{d_{eq}}$ ($d_{eq} = 8.5\cdot10^{-6}$ [m])	
<u>mass transfer properties:</u>		
distribution coefficient	$m_{SL} = 465$	$[(kg/m^3)/(kg/m^3)]$
sorbent side mass transfer coeff.:	$k_S = 2.2\cdot10^{-8}$	[m/s]
liquid side mass transfer coeff.:	$k_L = 1.58\cdot10^{-3}\cdot u^{0.4}$	[m/s]
axial dispersion coefficient:	$D_{ax} = 8.8\cdot10^{-3}\cdot u$	$[m^2/s]$
<u>other parameters:</u>		
superficial flow velocity	u	[m/s]
sorption factor	$S = \frac{m_{SL}\cdot(1-\varepsilon)\cdot v}{u}$	[-]
water input concentration:	C_{L0} (or C_{IN})	$[kg/m^3]$
sorbent input concentration:	$C_{S0} = 10^{-2}$	$[kg/m^3$ solid based]

The experiments were conducted with two different bed transport velocities: 4 rev/h (N=4) and 8 rev/h (N=8).

4 revolutions per hour (N=4):
sorbent transport velocity: $v = 2.27 \cdot 10^{-3}$ [m/s]

Table 5.2: removal efficiency "E", experiment versus calculation, PUR foam, N=4, ε=0.963, $a_S = 1.741 \cdot 10^4$

u [m/s]	S [-]	C_{IN} [wt.ppm]	C_{OUT} [wt.ppm] experimental	$E = 1-C_{OUT}/C_{IN}$ [-] experimental	$E = 1-C_{OUT}/C_{IN}$ [-] model
0.0326	1.2	109.1	29.1	0.733	0.736
0.0099	3.95	116.5	6.2	0.947	0.995
"	"	47.3	6.2	0.869	"
0.0193	2.02	52.2	7.3	0.861	0.918
"	"	67.3	14.5	0.784	"
"	"	79.6	27.6	0.653 *)	"
"	"	78.2	16.5	0.788	"

*) deliberately poor regeneration

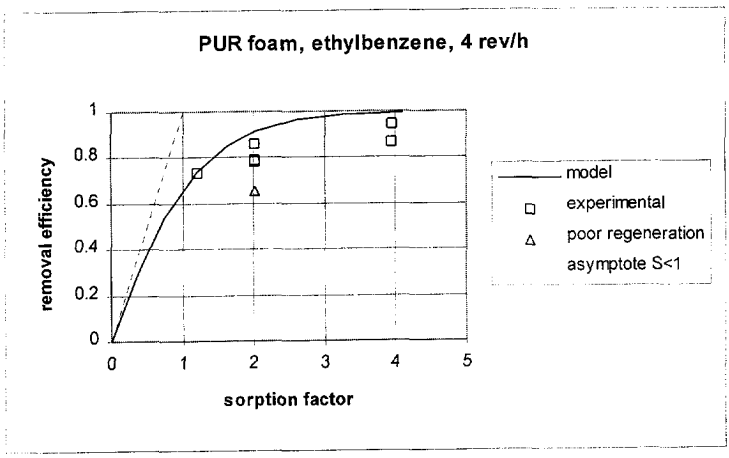

Figure 5.16: Removal efficiency, experiment versus calculation, PUR foam, N=4

8 revolutions per hour (rev/h):
sorbent transport velocity: $v = 4.54 \cdot 10^{-3}$ [m/s]

Table 5.3: Removal efficiency "E", experiment versus calculation, PUR foam, N=8

ε [-]	a_S [m^2/m^3]	u [m/s]	S [-]	C_{IN} [wt.ppm]	C_{OUT} [wt.ppm] experimental	E = 1-C_{OUT}/C_{IN} experimental	E = 1-C_{OUT}/C_{IN} model
0.963	$1.741 \cdot 10^4$	0.0185	4.22	227.3	11.6	0.949	0.961
"	"	"	"	100.5	48.9	0.514 *)	"
"	"	"	"	101.8	22.9	0.775	"
"	"	0.0361	2.16	100	18.2	0.818	0.794
0.961	$1.835 \cdot 10^4$	0.0278	2.96	100.9	6.7	0.933	0.891
"	"	0.0307	2.68	70.9	11.8	0.833	0.864
"	"	"	"	159.1	18.2	0.886	"
"	"	"	"	138.2	"	0.868	"
"	"	"	"	112.7	"	0.839	"
"	"	"	"	83.6	"	0.783	"

*) deliberately poor regeneration

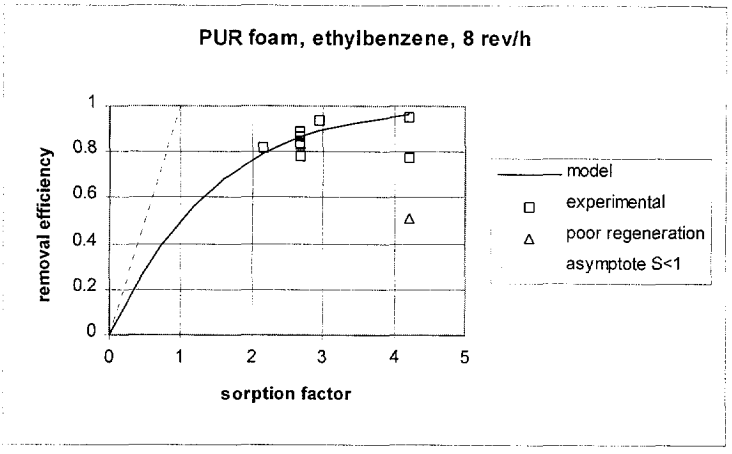

Figure 5.17: Removal efficiency, experiment versus calculation, PUR foam, N=8

5.6 Discussion

Figure 5.14 gives the removal efficiency E as a function of the sorption factor S for experiments as well as calculations using the model for countercurrent fiber sorption (Appendix C.1). It appears that the removal efficiency for PDMS fibers is not as good as expected. The main reason for this is the compressibility of the fiber bed. The PDMS fibers are slightly compressed into the bed segments so that the packed fiber bed exerts an elastic pressure on the screen covering the bed segments. Due to the high compressibility (low stiffness) of the fiber bed the packed bed porosity is relatively low (0.77). The elastic compression of the fiber bed presses the screen covering the bed segments against the static cylinder, thus preventing by-pass of water between screen and static cylinder or between packed bed and screen. However, it appeared that during operation the fiber beds were compacted as a result of the pressure drop, possibly accelerated by stress relaxation in the silicone rubber fibers caused by the high temperature in the regeneration section (110°C). As a result, by-pass between the packed bed and screen or static cylinder occurred, particularly at higher water velocities due to the high compressibility (low stiffness) of the fiber bed. This is in agreement with the experimental results according to figure 5.14 which shows larger differences between calculated and measured removal efficiencies at smaller sorption factors (higher water velocities).

The results for PUR foam (figures 5.16 and 5.17) also show differences between predicted and measured removal efficiencies. The PUR bed segments gradually shrink when exposed to steam (the PUR foam is not steam resistant). This results in by-pass of water between foam bed and screen or static cylinder. Thanks to the smaller compressibility of the foam, the PUR foam beds do not clearly exhibit increased by-pass at higher water velocities (smaller sorption factors) in contrast to the PDMS fiber beds. The PUR foam beds were replaced once during experiments. The first experiment with PUR foam (table 5.2 E-experimental = 0.733) and the first experiment immediately after replacement of the foam beds (table 5.3 E-experimental = 0.933) show good agreement between model and experiment. The experiments often (but not always) show larger differences between calculated and measured removal efficiencies as the packed foam beds are longer in use and shrinkage of the bed segments progresses. So it seems that despite the observed differences between model and experiments, the model is suitable to predict the removal efficiency in the absence of the unwanted by-pass flows. Based on both the model and the experiments, with unshrinked PUR foam beds removal efficiencies of 0.95 seem to be feasible.

Besides by-pass flow between packed bed and screen or static cylinder, by-pass can also occur at two other places. The slots in the housing side faces to fit the sieve plates expose the O-ring slot, see figure 5.18. In this way feed water can by-pass the packed bed all the way to the water outlet port.

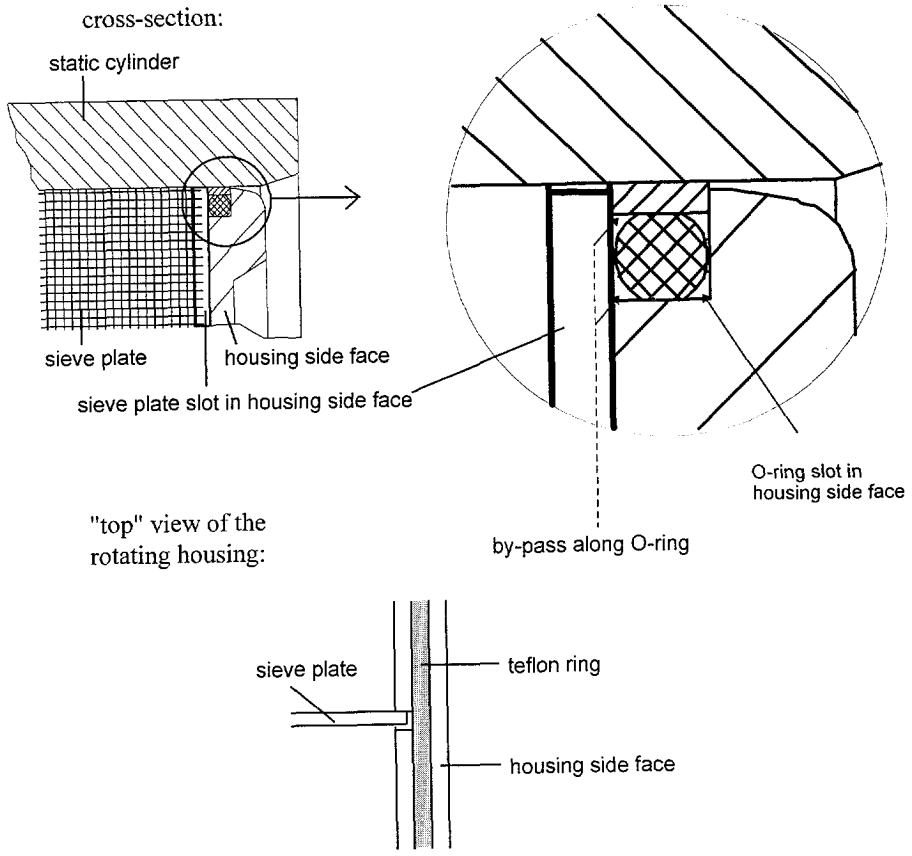

Figure 5.18: By-pass along O-ring via sieve plate attachment

Another place where by-pass can occur is the small slot between packed bed and main seal, see figure 5.19. This by-pass channel is interrupted at the check valve plates, so the water flowing through this channel will be mixed with the main stream several times before leaving the sorption section.

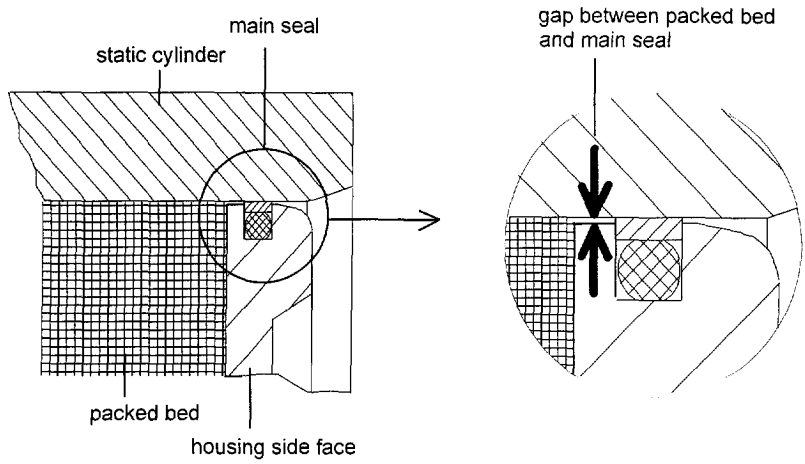

Figure 5.19: Small slot between packed bed and main seal

Because the cross-sectional area for by-pass along the O-ring slot and the cross-sectional area of the slot between packed bed and main seal are small compared to the total cross-sectional area of the packed bed, by-pass along these channels in the direction opposite to the transported packed bed will be limited and small compared with the by-pass observed between the packed PDMS fiber beds or PUR foam beds and the static cylinder. However, because of this limited by-pass the feasible removal efficiency is restricted to values below 0.99, which is the desired removal efficiency of the pilot unit. In a scaled-up and improved design, the concerning by-pass channels should be avoided, although their relative importance decreases as the cross-sectional area of the packed bed increases.
At the inlet port for water, where a relatively large pressure gradient exists over the check valve plate located between feed water inlet port (maximum pressure) and drain outlet port (atmospheric pressure), larger amounts of water will flow along the concerning channels in the direction of the drain outlet port. These larger by-pass flows are simply recycled to the feed water inlet port and will not affect the removal efficiency of the sorption section.

The large spread in measured concentrations and removal efficiencies (see figures 5.14 to 5.17) can be largely attributed to shortcomings of the sampling procedure and the analysis with the GC. Because the sample volume is very small (0.2 microliter), the determination of the ethylbenzene concentration is susceptible to various disturbances given the low ethylbenzene concentrations (order of magnitude 100 wt.ppm):

- the septum of the flow cell of the autosampler can get leaky causing evaporation of a part of the ethylbenzene, resulting in lower measured concentrations
- the feed or effluent water quickly erodes the needle bore and the small needle is sensitive to scaling, possibly causing both higher and lower sample volumes
- the peak surface area can be taken both too high and too low because it is difficult to determine the right base line due to other peak areas around the retention time of ethylbenzene

- the retention time of the ethylbenzene peak area in the chromatogram shows a relatively large spread, possibly causing missing of a part of the ethylbenzene peak surface area

The water sample is restricted to a very small volume because the water has to be vaporised in the GC. Afterwards we realise that the ethylbenzene concentration can be more accurately determined by the GC when using a small stripper device instead of a flow cell, thus increasing the ethylbenzene concentration in the sample.

5.7 Conclusions

It seems that despite the observed differences in removal efficiencies between model and experiments, the model is suitable to predict the removal efficiency for packed sorbent beds in the absence of the unwanted by-pass flow caused either by too large compressibility (PDMS fibers) or shrinkage (PUR foam). With fresh PUR foam beds (no shrinkage), removal efficiencies of 0.95 seem to be feasible. The desired removal efficiency of 0.99 can not be achieved due to by-pass flows along small channels alongside the packed bed. The large spread in measured concentrations and removal efficiencies can be largely attributed to shortcomings of the sampling procedure and the analysis with the GC and are directly related to the small sample volume. Better results may be achieved with cellular silicone (PDMS foam), which has a smaller compressibility than packed PDMS fiber beds, in combination with a stripping device added to the analytical equipment to increase the VOC-concentration in the sample injected into the GC. The by-pass flows along the small channels alongside the packed bed can be prevented by adapting the design. Their relative importance will decrease anyway as the cross-sectional area of the packed bed increases when scaling-up the equipment. Another item to be considered for improvement is the main seal between the slowly rotating housing and the static cylindrical casing. The durability of both the teflon ring and the rubber O-ring has to be increased and wear of the inner surface of the static cylinder making contact with the teflon rings has to be restricted.

The concept of the countercurrent circular sorption column was demonstrated to function correctly. With suitable sorbent material (for instance cellular silicone) and with a scaled-up design with the improvements suggested above, a removal efficiency of 0.99 is expected to be feasible with our continuous countercurrent sorption equipment based on the concept of a rotating circular packed bed segmented by check valve plates. More certainty about the feasible removal efficiency can be obtained using a small air stripper device instead of a flow cell for the GC, thus avoiding the large spread in measured concentrations and removal efficiencies.

References

[1] Zee, G. van, *Counter current sorption using fiber sorbents (Ph.D.-thesis)*, Delft University Press, 1996, ISBN 90-407-1328-6

[2] Barker, P.E., *Continuous chromatographic refining*, in: Preparative and production scale chromatography (Chapter 10), Zlatkis, A. and Pretorius, V. (Eds.), Wiley-Interscience, New York, 1971

[3] Barker, P.E., *Developments in continuous chromatographic refining*, in: Developments in chromatography Vol. 1 (Chapter 2), Knox, J.H. (Ed.), Applied Science Publishers, Barking, Essex, England, 1978

[4] Diederen, A.M., Zee, G. van, *Apparatus for separating a fluidum in at least two components*, international patent application PCT/NL97/00189, Delft University of Technology, 1997

6

Design considerations

6.1 Introduction

This chapter is concerned with the practical implementation of countercurrent sorption, based on absorption of dissolved toluene from water into cellular silicone (silicone rubber foam). This process will be called "countercurrent foam absorption", abbreviated by "CFA". The high compressibility of a packed bed of silicone rubber fibers preclude the practical application of these fibers in countercurrent sorption equipment. Cellular silicone has a much lower compressibility and for this reason application of foam instead of fibers was chosen.

The design for CFA equipment is based on the proven concept of the pilot unit (Chapter 5) and will be scaled up to a larger flow rate and modified on a number of items needed to be improved. The design is based on regular components and on (sub)structures which are clearly realisable or have been demonstrated to function correctly (Chapter 5). With this approach a realistic picture can be given of the practically feasible equipment specification and design for a given separation performance. On the basis of this design, cost and size estimates for CFA relative to alternative techniques for VOC-removal from water will be evaluated in Chapter 7.

For the determination of the mass transfer parameters, needed to establish the main equipment dimensions, it has been assumed that for dedicated batches of cellular silicone its structure can be slightly improved in order to lower the pressure drop and the axial dispersion in cellular silicone. This can be achieved by increasing the uncompressed porosity from 0.87 to around 0.9, decreasing the spread in pore diameter and particularly by removing larger parts of the cell membranes as compared with the cellular silicone samples tested in Chapter 3. It is assumed that this improved cellular silicone has a smaller pressure drop ($C_1 = 10^3$) and a smaller axial dispersion ($D_{ax}/u = 10^{-2}$) than the samples tested earlier in this research (see Chapter 3).

In section 6.2 the requirements for CFA are established. Section 6.3 gives a description of the concept of the CFA equipment which is basically similar to the concept of the pilot unit (Chapter 5). In this section the main dimensions of the design are assessed. Section 6.4 discusses a number of design details. Section 6.5 provides a short evaluation of the column size of CFA compared to the column size of the traditional granular

activated carbon separation technique for the same separation problem. Finally, in section 6.6 conclusions are given regarding the design for CFA equipment.

6.2 Requirements

As already mentioned in Chapter 1, we chose to focus on the removal of low concentrations of VOCs from large flows of water for mass transfer modelling. Toluene was chosen as the component to be removed from water, since besides being an existing waste water component, toluene is a frequently used compound with many available references. The maximum solubility of toluene in water at ambient temperature is approximately 550 wt.ppm, so a value around 100 wt.ppm seems a realistic measure for common concentrations in waste water. A removal efficiency of 99% has been chosen, so the effluent concentration in case of a feed concentration of 100 wt.ppm may not exceed 1 wt.ppm. Because in theory countercurrent sorption using transported open sorbent material enables compact equipment compared to granular sorption processes [1], it is expected that CFA will be more competitive for larger flow rates because of this compactness. For this reason, the design of one CFA unit assumes an application with a flow rate of 10 m^3/h. For larger flow rates, a number of CFA units will operate in parallel.

Generally the novel CFA equipment has to be reliable, compact, have a low energy consumption and has to treat the waste water at minimal cost.
More specific requirements result from findings with the pilot unit (see Chapter 5). In the first place the circular seals between the slowly rotating housing and the static cylinder have to be improved:
- the durability of the teflon and rubber O-ring has to be sufficiently high
- the teflon ring is not allowed to rotate relative to the rubber O-ring to prevent wear of the O-ring and to enable correct sealing
- the inner surface of the static cylinder and the outer rims of the housing side faces are no longer allowed to be subject to wear
- the teflon rings are no longer allowed to be translated along the openings in the static cylinder during assembly and disassembly to prevent damage to these teflon rings.

Furthermore it has to be possible to move the entire housing outside the static cylinder (see figure 5.2) from one side. The angular position of the housing before disassembly has to be reproducible in order to fit the drive of the housing (pinion) into the internal spur gear during reassembly.

6.3 Basic design

Concept
The concept of countercurrent sorption by means of rotation of an annular sorbent shaped as a series of bed segments separated by check valves, was demonstrated to function correctly (see Chapter 5). A number of alternative concepts are possible, among others transportation of an endless tubular sorbent through straight tubes.

However, the tubular sorbent bed suffers permanent damage from repeated contraction of the sorbent material around the transport wheels between sorption and regeneration section [1]. The circular shape is preferred because in that case external forces acting on the bed due to confinement and transportation remain constant.
For these reasons, a concept corresponding with the principle of the pilot unit has been chosen: a circular series of compartments, separated by check valves (non-return valves), slowly rotates in a static cylinder (see figures 5.1, 5.2 and 5.5). The packed bed is divided into a number of bed segments, equal to the number of compartments (twelve for the pilot unit). A single compartment ranges from the centre of a check valve plate to the centre of the next check valve plate and thus contains one bed segment surrounded by two sieve plates and altogether one check valve plate. In figure 5.5 one entire compartment can be seen (and large parts of the two neighbouring compartments). This figure also shows the permeable polyester screens between the sieve plates covering the packed foam beds. The housing together with its internals is called the rotating drum, which can be translated outside the static cylinder as can be seen from figures 5.2 and 5.5.

Horizontal arrangement
The static shaft can be positioned vertical as well as horizontal (pilot unit) with the packed bed rotating in a vertical plane. The horizontal shaft arrangement is preferred, because in case of a vertical shaft arrangement with the packed bed rotating in a horizontal plane, a pressure gradient perpendicular to the plane of transportation is present. This vertical pressure gradient is caused by gravity. Because the pressure gradient in the plane of transportation, caused by the flow resistance of the packed bed, is relatively low for open sorbent materials, the pressure gradient caused by gravity causes a velocity distribution differing from desired plug flow conditions along the cross-section of the bed in case of a vertical shaft arrangement.

Removal of adhered water
To restrict the amount of steam needed to regenerate the bed segments leaving the sorption section, drying of the sorbent between sorption and regeneration section could be considered to diminish the quantity of adhered water taken along into the regeneration section by the foam. However, a facility for drying will make the separation unit more complex, all the more because obvious methods like squeezing or compressed air drying are not applicable. Squeezing will cause permanent damage to the foam structure and compressed air drying will take along at least a significant part of the VOCs, thus creating an additional VOC-polluted stream. Moreover, comparison with the calculated quantity of steam needed to strip the toluene from the cellular silicone shows that heating of the adhered water is only a relatively small part of the total steam quantity needed for the regeneration section (see Appendix E.4). For these reasons a surplus of steam will be used in the regeneration section to heat and strip the adhered water, instead of installing facilities to remove the adhered water before the regeneration section other than draining by gravity. Hence, from the ports for drying or rinsing shown in figure 5.1 only the drain will be used and drying is no longer considered as an option.

Height (inner and outer diameter) of the packed bed

For a high separation performance of the countercurrent equipment a large number of compartments in the sorption section is favourable because concentration gradients caused by length variation of the flow path along the height (diameter) of the packed bed (see later in this section) are balanced by mixing at the check valve plates. The number of compartments however is limited by space requirements for check valve plates and sieve plates. Especially near the inner diameter D_{in} of the packed bed this is important because here the space left for the sorbent is minimal. Moreover, near D_{in} the transport velocity (the circumferential speed) of the sorbent is minimal and the liquid velocity is maximal, resulting in a relatively poor separation efficiency of the inner layers of the bed segments. This effect is more significant as the ratio $1-D_{in}/D_{out}$ becomes larger (D_{out} is the outer diameter of the packed bed). For this reason D_{in} should be chosen not too small and D_{out} should be chosen not too large.

D_{in} should be chosen not too small for another reason as well. A drive with dimensions large enough to both withstand the required driving torque and realise a torque reduction around ten to one has to fit inside the drum. In this way, a large drive outside the drum can be avoided and the required output torque and consequently the dimensions of the electromotor-gearbox combination outside the drum (see figure 5.2) will be relatively small.

D_{out} should be chosen not too large for other reasons than mentioned above as well. The teflon part of the main seal is cut from a thin-walled teflon cylinder, diameters much larger than 1 m should therefore be avoided. Diameters much larger than 1 m should also be avoided because accurate machining operations at the inner surface of the static cylinder and at the outer rims of the housing side faces are relatively difficult and expensive at large diameters. Finally, the required driving torque (frictional resistance of seals and screens, flow resistance of bed segments and check valves) of a scaled-up and thus relatively wide packed bed with an outer diameter much larger than 1 m will become too large to be able to realise the chosen concept.

Considering the above, D_{in} is established at 0.5 m and D_{out} is established at 1 m. As a result, the packed bed height is 0.25 m.

Width of the packed bed

With a fixed bed height (0.25 m) and a fixed flow rate (10 m^3/h), the required width of the packed bed follows from the superficial liquid velocity through the bed. For the applied cellular silicone the liquid velocity relative to the fixed column (the static cylinder) is limited to approximately 1 cm/s. Consequently, the width of the packed bed is established at 1 m.

The value of 1 cm/s is estimated on the basis of the 1-dimensional model discussed in Chapter 2 which predicts the maximum allowable liquid velocity u_{max} through a packed bed of open material for which the bed remains uncompressed and for which its high porosity is maintained. Although this model appeared to be less suitable for foam materials (the predicted u_{max} can be both too high and too low for foam beds), it is still considered to be suitable for order of magnitude estimates for u_{max}. A u_{max} higher than 1 cm/s is desirable, but not practically feasible yet as a result of the structural properties of currently available cellular silicone, even with the small improvements as discussed in

section 6.1. Higher liquid velocities would first of all result in axial dispersion to such an extent that the required effluent concentration can not be achieved with one single CFA unit. Secondly, the bed segments would be subject to compression, resulting in an even higher dispersion and flow resistance. Apart from that, a higher liquid velocity in combination with the large cross-sectional area of the bed segments would lead to a substantial increase of the required driving torque (due to the high pressure drop) of the separation equipment.

Transport velocity of the sorbent

The optimal transport velocity of the sorbent is now determined using the mass transfer model for countercurrent fiber sorption (Chapter 4). The removal efficiency per unit of packed bed length in the sorption section is higher when the bed transport velocity in the sorption section is higher. In the regeneration the opposite applies. A small bed transport velocity results in a sorption section too long to fit within the established outer diameter. On the other hand a high sorbent velocity results not only in a regeneration section too long to fit within the established outer diameter but also in more frequent heating and cooling of the rotating parts, leading to a significant increase in the required steam supply which determines a substantial part of the operating cost (see Chapter 7). A compromise is found at a sorbent velocity of around 1 mm/s at the mean diameter D_G of the packed bed ($D_G = (D_{out}+D_{in})/2 = 0.75$ m), that is a rotational speed of approximately 1.5 revolutions per hour. This mean sorbent velocity is about 2.5 times higher than the minimum required sorbent velocity to remove 99% of the supplied toluene.

The following mass transfer properties were used:

porosity:	0.9
mean pore diameter:	700 μm
equivalent fiber diameter:	77.8 μm (equation 3.9 or 4.25)
<u>sorption section:</u>	
liquid velocity:	0.01 m/s
liquid side mass transfer coefficient k_L:	10^{-4} m/s
sorbent side mass transfer coefficient k_S:	10^{-6} m/s
sorbent/water distribution coefficient m_{SL}:	260 $(kg/m^3)/(kg/m^3)$
D_{ax}/u:	10^{-2} m^2/s
<u>regeneration section:</u>	
steam velocity:	0.3 m/s
gas side mass transfer coefficient k_G:	10^{-2} m/s
sorbent side mass transfer coefficient k_S:	10^{-6} m/s
steam/sorbent distribution coefficient m_{GS}:	0.02 $(kg/m^3)/(kg/m^3)$
D_{ax}/u:	10^{-1} m^2/s

The packed (precompressed) bed porosity is assumed to be approximately equal to the uncompressed porosity (0.9), because only a small compression of the bed is needed to obtain sufficient contact stress between the static cylinder and the screen covering the bed to prevent bypass flows.
The steam velocity in the regeneration section is estimated at 0.3 m/s, based on experiments with the pilot unit (see Chapter 5) which show that stationary conditions can not be established at lower steam velocities because of inadequate stripping of the sorbent resulting in insufficient removal efficiency of the sorption section.
The liquid side mass transfer coefficient k_L for cellular silicone is estimated at 10^{-4} m/s at a liquid velocity of 1 cm/s, using equation (4.21) with a diffusion coefficient in the liquid phase of approximately 10^{-9} m²/s. Although equation (4.21) was established for liquids, the gas side mass transfer coefficient k_G is also estimated using this equation, resulting in a value of approximately 10^{-2} m/s.
The sorbent side mass transfer coefficient k_S is supposed to be the same for both the sorption and the regeneration section and is estimated at approximately 10^{-6} m/s, using equation (4.26) with a diffusion coefficient in the sorbent phase of approximately 10^{-11} m^2/s (see §4.4.4).
The distribution coefficient m_{SL} of toluene for cellular silicone/water at ambient temperature was established at 260 (kg toluene / m^3 cellular silicone solid based) / (kg toluene / m^3 water), see Chapter 4. The distribution coefficient m_{GS} of toluene for steam/cellular silicone at 100°C was estimated as the product of the distribution coefficients m_{GL} and m_{LS} for steam/water and water/cellular silicone respectively, both at 100°C. Based on estimates and experimental results from literature, this resulted in an estimated value for m_{GS} of 0.02 (see Chapter 4).
The ratio D_{ax}/u of the axial dispersion coefficient and the superficial liquid velocity is estimated at 10^{-2} m/s, because the cellular silicone with improved structure will have a D_{ax}/u smaller than the established value of $5 \cdot 10^{-2}$ m/s for the sample material (Chapter 3), but larger than the established value of $3 \cdot 10^{-3}$ m/s for PUR foam with a packed bed porosity of 0.9. D_{ax}/u for steam is estimated one order of magnitude larger than for water.

Required bed lengths
With the established sorbent velocity of 1 mm/s at the mean diameter D_g of the bed segments, a first estimate can be made with the mass transfer model for countercurrent fiber sorption for the required total packed bed length at this mean diameter without taking into account effluent concentration variations along the packed bed height caused by differences in fluid (water or steam) flow velocity and sorbent velocity in the various layers between the inner and outer diameter of the packed bed (see figure 6.1). In this way, the required packed bed length for the sorption section would be 0.24 m, for the regeneration section the required packed bed length would be 0.14 m (see Appendix D.1).

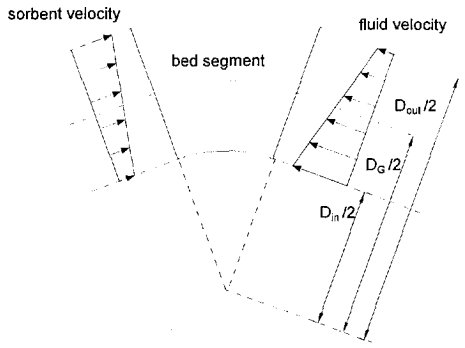

Figure 6.1: Front view of a bed segment

If the aforementioned velocity differences are accounted for, the required bed length to achieve a given removal efficiency appears to be considerably larger, in particular for the sorption section. The fluid velocity in the inner layers is higher than the velocity in the outer layers because the circumferential or arched length decreases with the diameter whereas the pressure both before and after a bed segment is approximately uniform and thus equal per side for all layers. For laminar flow this results in a linear velocity distribution along the diameter:

$$u(D) = \frac{D_{in} + D_{out} - D}{0.5 \cdot (D_{in} + D_{out})} \cdot u_G \qquad (D_{in} \le D \le D_{out}) \qquad (6.1)$$

u_G: fluid velocity at D_G

At the same time the quantity of sorbent supplied per unit of time (the sorbent velocity) is reversibly proportional to the diameter. For the sorption section this combination of higher liquid velocity and lower sorbent velocity results in a diminished separation performance of the inner layers relative to the outer layers of the bed segments. As a result the output concentration at the end of a bed segment is higher at the inner layers and lower at the outer layers than calculated for a straight bed segment with an arched length and with velocities based on D_G. These concentrations are balanced by mixing between the bed segments. Because per unit of time more liquid flows through the inner layers than through the outer layers, the mean output concentration after a bed segment is higher than calculated for a straight bed segment. For this reason the sorption section requires a larger total packed bed length, namely 0.3 m instead of 0.24 m based on D_G as will be seen later in this section

In the regeneration section a similar effect takes place, but less pronounced than in the sorption section. The maximal sorbent concentration arising from transportation through the sorption section and present in the inner layers of the bed segments is taken as sorbent input concentration for the regeneration section to be on the safe side. The total packed bed length for the regeneration section is only a fraction larger by the effect of velocity gradients, namely 0.15 m instead of 0.14 m at D_G as will be seen later in this

section. This means that the regeneration section can be modelled as a straight column with a length equal to the arched length at the mean diameter D_G.

Number and distribution of compartments

Before final calculations of the required total packed bed lengths of the sorption and regeneration section can be made, first the number of compartments has to be determined to establish the length of a bed segment and the number of mixing steps per section.

A compartment ranges from the centre of a check valve plate to the centre of the next check valve plate and thus contains one bed segment surrounded by two sieve plates and altogether one check valve plate (see figures 5.5 and 6.2). For enabling countercurrent operation, the ports in the static cylinder have to be always at least one compartment apart, thus preventing bypass flows in the direction of rotation of the drum. This results in more than three required compartments between the three consecutive sections (sorption section, drain section and regeneration section), see figure 6.2. The inlet and outlet ports for the sorption and regeneration section and the longer port for the drain section together are covering another two to three compartments (see figure 6.2). Supposing the sorption section requires at least three mixing steps (balancing of concentration differences) to achieve the required removal efficiency and for the regeneration section one mixing step is required, then these sections should cover almost four respectively almost two compartments. This means that in total a minimum number of 12 compartments is required. A number of 14 compartments would give the opportunity to provide a margin for the sorption and regeneration section by supplying both sections with an additional compartment. This results in a larger total packed bed length and one extra mixing step per section, the latter being especially important in the sorption section. At a number of 16 compartments the arched length of the bed segments relative to the arched length of the compartment diminishes too much because the absolute space requirements for the check valve plates and sieve plates per compartment remain constant. Therefore a number of 14 compartments has been chosen (for comparison: the pilot unit has 12 compartments). The compartments remaining after subtraction of the compartments between the different sections and the required circumference for the inlet and outlet ports (including drain) are divided among the sorption and regeneration section in proportion of the required bed lengths (estimated at 2 to 1), resulting in a sorption section of 2.2 radians (almost 5 compartments) and a regeneration section of 1.1 radians (about 2½ compartments), see figure 6.2:

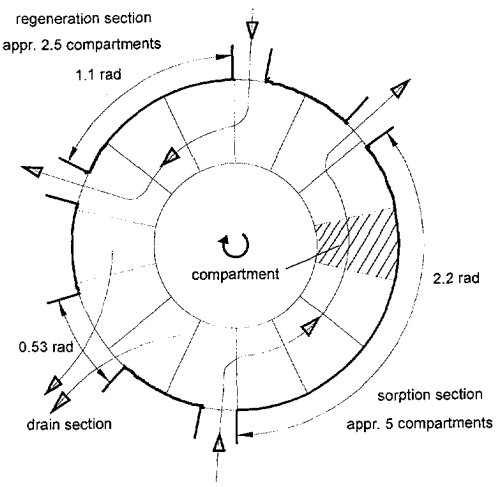

Figure 6.2: Design with 14 compartments (front view, schematic)

Final calculation of required bed lengths

Each compartment now consists of a bed segment of about 0.3 rad (about 0.11 m at D_G) and an arc of about 0.14 rad for two sieve plates and altogether one check valve plate. The bed segments are now divided into a number of layers for mass transfer calculations. Each layer has a different fluid (water or steam) velocity, arched bed length and sorbent velocity (see figure 6.1), resulting in different fluid and sorbent output concentrations for each layer at the end of a bed segment. Between two bed segments the fluid output concentrations of the different layers are averaged (mixing at the check valve plates) and the fluid input concentrations of the various layers of the next bed segment are equal to this averaged value. To avoid extra iteration loops for the consecutive bed segments the highest sorbent output concentration is used as input value for all layers of the next bed segment (in practice the situation is more favourable). A number of 11 layers appears to be sufficiently accurate to account for the effluent concentration variations along the packed bed height. The calculations are given in Appendix D.2.

For the sorption section the first bed segment leaving the regeneration section and entering the sorption section has a sorbent input concentration of 0.01 wt.ppm (0.01 kg toluene per m^3 solid sorbent material) and an liquid input concentration of 8 wt.ppm (see figure 6.3). Based on a straight bed segment with uniform liquid and sorbent velocity and a length equal to the arched length at D_G, the liquid outlet concentration would be 0.71 wt.ppm, but for the curved bed segment 1.05 wt.ppm is calculated. The maximum sorbent concentration is about 1 kg/m^3 (at the inner layer at D_{in}) and this value is taken as input sorbent concentration for all layers of the next bed segment. This second bed segment purifies the water from 40 to 8.43 wt.ppm (straight bed segment: 6.9 wt.ppm) and the maximum sorbent concentration (inner layer) becomes 5.8 kg/m^3. The third bed segment purifies the water from 120 to 37.8 wt.ppm (straight bed segment: 32.3 wt.ppm) and the maximum sorbent concentration (inner layer) becomes

21.5 kg/m³. So apparently three consecutive bed segments can purify the water from 120 to 1 wt.ppm. From this result follows a required total packed bed length of approximately 0.3 m at D_G for the purification from 100 to 1 wt.ppm. This is some 25% more than predicted on the basis of a straight packed bed (0.24 m).

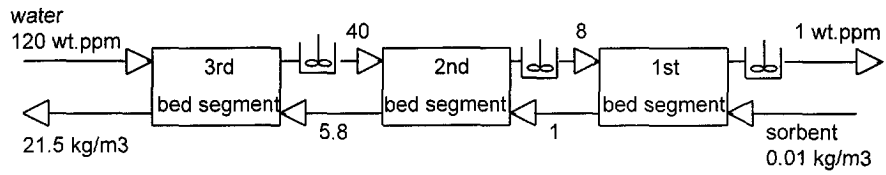

Figure 6.3: Calculation of sorption section

For the applying process conditions and mass transfer properties, the regeneration section appears to have neither significant differences in output steam concentrations nor in sorbent output concentrations at the end of the various layers. For this reason the simple calculation for a straight packed bed is a good approximation for the regeneration section. In this section the check valve plates merely serve to enforce countercurrent operation, they do not have to compensate for concentration differences in the continuous phase as in the sorption section. When the regeneration section is calculated with an input sorbent concentration equal to the maximal concentration of the inner layer, following from calculations for the sorption section, the total packed bed length is only a fraction larger than calculated for a straight packed bed, namely 0.15 m instead of 0.14 m at D_G.

Potential removal efficiency

With the applying process conditions and mass transfer properties, in theory a removal efficiency of 99.9% instead of the required 99% can be achieved with the design.

For the purification from 1000 to 1 wt.ppm and assuming that the sorbent has sufficient sorption capacity, the required total packed bed length for sorption with a curved packed bed can be roughly estimated by multiplying the calculated length for a straight packed bed with a factor 1.25, this factor being derived from the calculation for the purification from 100 to 1 wt.ppm. This results in a total packed bed length of 0.46 m, corresponding with over 4 compartments for this separation and thus fitting into the current sorption section of almost 5 compartments. The higher sorbent output concentration (100 kg/m³) can be stripped with a total packed bed length of 0.19 m, corresponding with 1¾ compartments and thus fitting into the current regeneration section of about 2½ compartments.

In a similar way for a purification from 100 to 0.1 wt.ppm it can be estimated that the required total packed bed length in the sorption section corresponds with around 4½ compartments which also fits into the current sorption section of almost 5 compartments. The required total packed bed length in the regeneration section remains the same in this case.

In practice a removal efficiency of 99.9% probably will not be achieved, among others due to flow patterns deviating from plug flow, especially near the inlet and outlet ports, and due to (small) bypass flows along the packed beds. On the other hand, because the sorption section provides at least 4 mixing steps, the required effluent concentration of 1 wt.ppm will be achieved even at a bypass flow of 5% of the feed flow rate. This means that the design has a wide safety margin for the required removal efficiency of 99%.

6.4 Design details

The drawings of the static cylinder and the parts of the rotating drum (housing inner face, housing side faces, check valve plates and sieve plates) are given in Appendix D.3. The cost estimates of the main parts of the actual separation equipment (excluding drive) are estimated based on these drawings (see Chapter 7).

Drive

The required driving torque of the rotating drum follows from the frictional resistance of the teflon seals and the screen-covered bed segments and the flow resistance of the bed segments and check valve plates (the flow resistance of the sieve plates and screens is negligible).

The frictional resistance of the design is estimated on the basis of the maximum applied driving torque for seals and screens of the pilot unit, firstly to be sure of correct sealing and secondly to be sure of the availability of sufficient driving torque. The sealing of the teflon compound on polished stainless steel at low liquid and gas pressures as applied in our equipment appears sufficient even at a relatively low constant stress of approximately $2 \cdot 10^5$ Pa. This value is estimated from experiments with the pilot unit. The friction coefficient between teflon and stainless steel at low contact stress and for boundary lubrication with water or steam is estimated at 0.1. The required driving torque for sealing of the scaled-up separation unit follows from the total contact surface area between teflon and stainless steel multiplied with the contact stress, the friction coefficient and the outer radius of the bed segments, resulting in a driving torque of 870 Nm. In a similar way the driving torque for the screens covering the bed segments is estimated at 630 Nm via a contact stress of $2 \cdot 10^3$ Pa (estimated from experiments with the pilot unit) and a friction coefficient of around 0.3 (established with the test equipment according to Appendix A.2). The total frictional resistance of the teflon seals and the screens results in a driving torque of about 1,500 Nm.

For a packed bed porosity of 0.9, an equivalent fiber diameter of 77.8 μm (mean pore diameter 700 μm) and a C_1-value of 10^3 (see Chapter 3), the flow resistance of the packed beds in the sorption section results via the pressure drop of $2.3 \cdot 10^4$ Pa/m at 1 cm/s, a mean bed length of 0.6 m, a cross-sectional area of 0.25 m² and a mean radius of 0.375 m in a driving torque of approximately 1,300 Nm. It is obvious that the liquid velocity has a large impact on the required driving torque. This is not only to be blamed on the pressure drop itself, but also on the large cross-sectional area in combination with the distance to the axis of rotation. For the regeneration section the flow resistance results via a pressure drop of $8.5 \cdot 10^3$ Pa/m at 0.3 m/s and a mean bed length of 0.3 m in a driving torque of approximately 240 Nm. In total averagely 7 check valve plates are

passed by liquid or gas, each with an opening pressure (that is the opening pressure of one check valve) of 10^3 Pa, resulting in a driving torque of approximately 660 Nm. Again, this torque is relatively high due to the large cross-sectional area of the packed bed. The total flow resistance of the sorption and regeneration section results in a design torque of approximately 2,200 Nm
In total a driving torque of around 3,700 Nm is required to drive the drum. For comparison: for the pilot unit the drum requires 300 Nm at similar conditions.

The rotating drum is driven by an internal spur gear (see figure 5.2). In the scaled-up version of the pilot unit the internal spur gear will no longer be driven by a pinion but by a planetary gear system (see figure 6.4) to be able to cope with the much larger driving torque (3,700 Nm instead of 300 Nm):

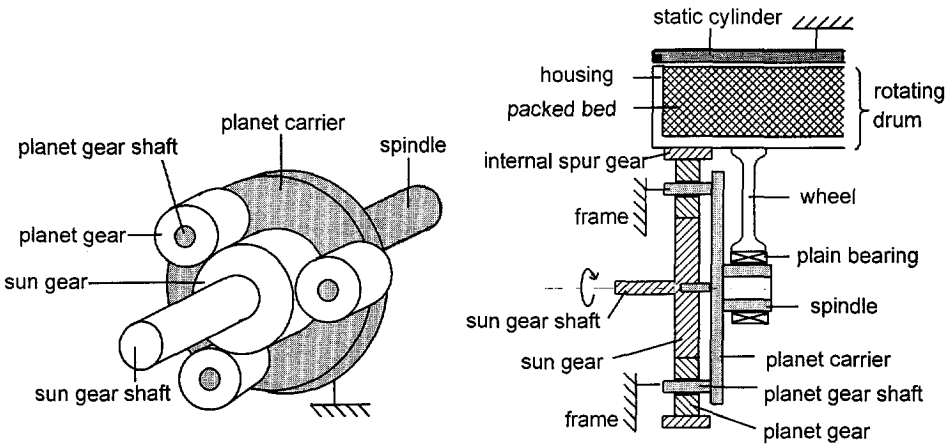

Figure 6.4.: Planetary gear system

The planetary gear system is driven by a central shaft (the sun gear shaft, supported by the planet carrier, see figure 6.4), which is linked with the output shaft of the electromotor/gearbox combination. The shafts of the planet gears are rigidly connected to the planet carrier and the static spindle of the planet carrier, and at the side of the sun gear shaft they are connected to the static frame of the separation equipment (see also figure 6.7).
With the available space under the housing inner face, a planetary gear system with a reduction ratio of around 9 to 1 can be constructed to transmit the required driving torque of approximately 3,700 Nm [2]. The sun gear has 16 teeth, the planet gears have 65 teeth each and the internal spur gear has 146 teeth. The required output torque of the motorreductor (electromotor + gearbox combination) is about 400 Nm with this reduction ratio. With a rotational speed range from 0 to 3 revolutions per hour of the internal spur gear (the rotating drum requires a nominal rotational speed of around 1½ revolutions per hour), the required rotational speed at the output shaft of the motorreductor is 0 to 27 revolutions per hour. A motorreductor with a frequency

regulator, a power of 0.12 kW and a reduction ratio of 2768 to 1 satisfies the requirements [3]. This motorreductor measures 0.65 m x 0.34 m x 0.3 m and has a weight of 59 kg. The planetary gear system is protected against overload by a safety coupling (400 Nm) between sun gear shaft and motorreductor output shaft.

Sealing

In order to comply with the requirements with respect to sealing and assembly or disassembly, the main seal consisting of a combination of teflon plus rubber O-ring has been replaced by a so called R-omniring (see figure 6.5) in a modified construction (see figure 6.6).

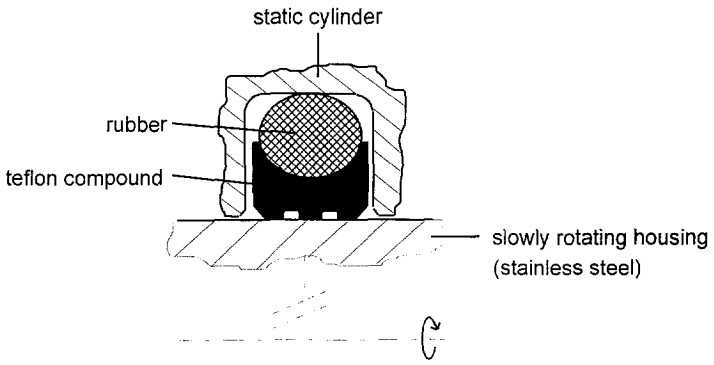

Figure 6.5: R-omniring

Just like the main seal used in the pilot unit, the R-omniring consists of a combination of a teflon compound and a rubber ring, but rotation of the teflon ring relative to the rubber ring is now prevented by the shape of these rings: a small contact surface area between teflon and stainless steel, a large contact surface area between teflon and rubber and a favourable shape for both rings with regard to stress distribution. Another important improvement is the increased thickness of the rubber ring so that a wider gap can be bridged before leakage takes place between the static teflon ring and the slowly rotating housing. The R-omnirings are fitted into the static cylinder instead of the rotating housing and the cylinder is divided into two different parts, so the teflon rings no longer have to be translated along the openings in the cylinder during assembly or disassembly, see figure 6.6:

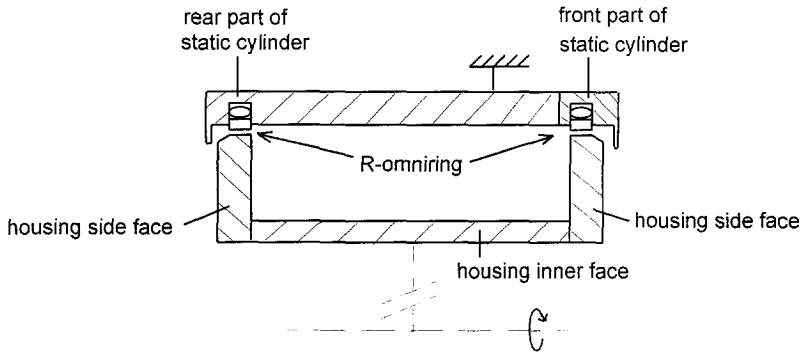

Figure 6.6: Modified construction of the static cylinder and the main seal

During assembly the drum is translated into the rear part of the static cylinder which is already provided with an R-omniring. Subsequently the front part of the static cylinder (including R-omniring) is mounted. For disassembly obviously the opposite procedure applies. Both side faces of the rotating housing are provided with a cone to guide the R-omnirings.
The sealing of the bed segments is now completed by straight seals on top of the check valve plates, composed of the tried and tested combination of teflon and rubber strips (see Chapter 5). Because the teflon strips on top of the check valve plates move relative to the R-omnirings fitted into the static cylinder, always a small gap has to be present between teflon strip and teflon ring (R-omniring). This gap must be enforced by a small stop at both ends on top of the check valve plate, to prevent the teflon strip from jamming between both R-omnirings in the regeneration section where the thermal expansion of the teflon strip is larger than the thermal expansion of the stainless steel check valve plate.

Both parts of the static cylinder (see Appendix D.3) have to be honed inside for correct sealing of the check valve plates. The teflon compound is filled with graphite instead of glass as with the pilot unit to prevent wear of the stainless steel contact surface area. An alternative way to protect the contact surface area against wear would be a combination of glass-filled teflon and stainless steel, hardened to prevent wear of the stainless steel, but the static cylinder has too large dimensions to be hardened at reasonable cost. The same considerations apply for the main seals in contact with the housing side faces, resulting in graphite-filled teflon for the R-omnirings in combination with polishing of the housing side faces at the outer diameter (see Appendix D.3).

Disassembly / reassembly
For assembly and disassembly of the drum a separate assembly unit can be used so the separation equipment can be less complex. This assembly unit has to be used only a few times a year for inspection, maintenance and replacement of sorbent material and can therefore be used for a large number of CFA units. This assembly unit has to be equipped with a driven shaft which can be positioned in line with the static shaft of the

drum and which can support this drum. Furthermore, the assembly unit is provided with hydraulic cylinders to translate the drum in and out of the static cylinder.
During operation the rotating drum is mainly supported by the internal spur gear through the planet gears (see figure 6.4), but at the beginning of disassembly and at the end of reassembly the drum is supported by the static spindle of the planet carrier by means of a plain bearing and a wheel connected to the drum (comparable with the pilot unit, see figure 5.2). During assembly and disassembly of the drum, the spindle of the planet carrier is extended by the shaft of the assembly unit, so the drum can be moved onto and from the shaft of the assembly unit. The assembly unit is equipped with a blocking device that can reproduce the exact angular orientation of the drum during disassembly, so during reassembly the internal spur gear can be translated back over the planet gears without elaborate positioning.

Frame
The driving mechanism (the motorreductor and the planet carrier with planet gears and sun gear) is attached to the rear side frame, see figure 6.7. The rear part of the static cylinder is bolted to the rear side frame as well.

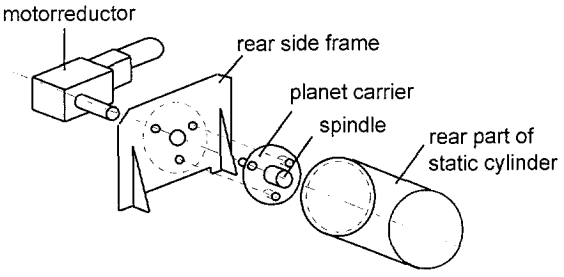

Figure 6.7: Rear side frame

The front part of the static cylinder is bolted to both the rear part of the cylinder and the front side frame, see figure 6.8. The rear and front side frames support both the dead weight and the reaction torque of the static cylinder. For assembly and disassembly of the drum the front side frame and the front part of the static cylinder are removed and the cylinder is supported by blocks instead. The axial forces on the static cylinder during assembly and disassembly are supported only by the rear side frame.

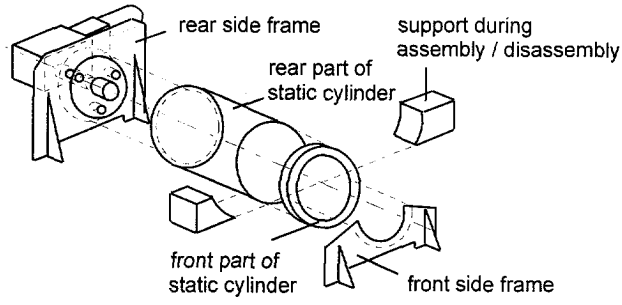

Figure 6.8: Front side frame

Check valve plates

The check valve plates (see figure 5.7 and Appendix D.3) are bolted to the housing inner face and the housing side faces to stiffen the rotating drum. Sealing is achieved here by applying steam resistant packing between check valve plate and housing. The check valve plates are equipped with standard stainless steel check valves (non-return valves) with an opening of Ø50 mm and a short length. At customer's request the opening pressure of the check valves can be adapted and diminished to around 10^3 Pa. The check valves are sealed with an EP-rubber O-ring onto the chamfered openings in the check valve plates. Similar to the pilot unit, at the top of the check valve plate a seal is mounted consisting of an EP-rubber O-ring cord and a teflon strip. Instead of glass-filled teflon (pilot unit) graphite filled teflon will be used to diminish friction and wear.

Teflon - stainless steel: differences in thermal expansion

Because of different thermal expansion coefficients of stainless steel and teflon, differences in thermal expansion between stainless steel and the teflon strips on top of the check valve plates (1 mm respectively 9 mm expansion in the regeneration section) have to be bridged. To allow the teflon strips to expand between the R-omnirings when heated in the regeneration section, they can be shaped according to figure 6.9:

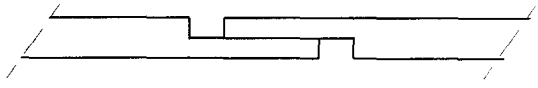

Figure 6.9: Teflon strip allowing for thermal expansion

The circular teflon part of the R-omniring will lengthen approximately 7 mm due to expansion near and in the regeneration section. Looking at the experiences with the pilot unit, no problems are expected at this point.

Sieve plates

The sieve plates are no longer fitted only into slots in the housing side faces, but also in slots in the housing inner face to be able to support the flow resistance of the bed

segments acting on the relatively large sieve plate surface area. To fix the sieve plate after assembly, two bolts attached to the housing side faces support the sieve plate by two small brackets attached to both sides of the sieve plate (see Appendix D.3). The polyester screen covering the bed segments is attached to clamps on the sieve plates by means of a strip at the ends of the screen, see figure 6.10:

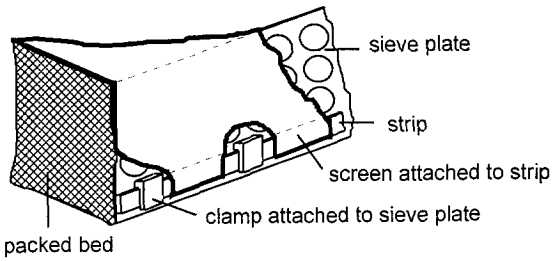

Figure 6.10: Connection between screen and sieve plates

Ancillary equipment
The CFA unit has to be equipped with a feed water filter to prevent fouling or plugging of screens and sorbent material. To determine the influent and effluent concentrations a small air-stripper combined with gas-chromatography can be applied.

Weight
The total weight of the CFA unit has to be minimal to cut cost and to restrict the amount of steam required to heat the rotating drum. The total weight of the main equipment (static cylinder plus drum, see the drawings in Appendix D.3) is about 1,200 kg. The total weight of the corresponding parts of the pilot unit is about 120 kg:

	design (Ø0.5 x Ø1 x 1, 14 compartments):	pilot unit (Ø0.6 x Ø0.7 x 0.15, 12 compartments):
static cylinder:	400	51
housing inner face:	170	40
housing side faces:	80	15
check valve plates (incl. valves):	440	8
sieve plates:	110	2
	------ +	------ +
	≈ 1,200 kg	≈ 120 kg

Actual liquid velocity
With the established dimensions and process conditions a flow rate of 9 m^3/h is realised at a liquid velocity of 1 cm/s. For a flow rate of 10 m^3/h either the width and thus the cross-section of the packed beds has to be increased or the liquid velocity has to be

increased. An increase in liquid velocity was chosen because a larger cross-section (and an unchanged liquid velocity) would result in a larger driving torque. The actual liquid velocity then becomes 1.11 cm/s, still achieving a removal efficiency of 99%, the driving torque increases by 140 Nm which is an increase of less than 4%.

Summary of design specifications

Sorbent	
material:	cellular silicone
porosity:	0.9
mean pore diameter:	700 μm
Sorption section	
water flow rate:	10 m^3/h
water input concentration:	100 wt.ppm
sorbent input concentration:	0.01 kg/m^3
water output concentration:	1 wt.ppm
total packed bed length (at D_G):	≈ 0.56 m (almost 5 compartments)
mean liquid velocity:	0.011 m/s
pressure drop (incl. check valves):	≈ 20 kPa
Regeneration section	
steam flow rate (see Appendix E.4):	223 kg/h
steam input concentration:	10^{-6} kg/m^3
sorbent input concentration:	10 kg/m^3
steam output concentration:	$3 \cdot 10^{-3}$ kg/m^3
total packed bed length (at D_G):	≈ 0.3 m (about 2.5 compartments)
mean steam velocity:	0.3 m/s
pressure drop (incl. check valves):	≈ 5 kPa
Equipment	
packed bed outer diameter:	1 m
packed bed inner diameter:	0.5 m
packed bed width:	1 m
mean sorbent velocity:	1 mm/s
nominal rotational speed:	1.5 rev/h
maximum driving torque:	3,700 Nm
electric power consumption:	< 0.5 kW

Reliability

The CFA design as outlined so far is expected to function as required. This confidence is based on the experiences with the pilot unit and the proposed improvements for the scaled-up equipment. However, it has yet to be verified whether the chemical durability of the cellular silicone (sorption properties) and the physical durability of the foam-shaped sorbent (lasting resistance to compressibility) is sufficient under practical

conditions. A life of one year for the sorbent material is aimed at. It has also yet to be verified that the seals and the screens covering the bed segments have sufficient life under practical conditions. The expected lifespan for the system as such is 10 years.

6.5 Equipment size evaluation

The traditional granular activated carbon adsorption technique (abbreviated by GAC) acts as a primary reference for our countercurrent foam absorption technique (abbreviated by CFA). Van Zee [1] poses a possible reduction in column volume with an order of magnitude of 10 for countercurrent fiber sorption processes compared to GAC. This should also apply to CFA, since the open-cell foam sorbent material used for CFA has a porosity and specific surface area comparable with packed beds of fibers. For our design specifications, treating 10 m^3/h water with 100 wt.ppm toluene and a removal efficiency of 99%, preliminary design calculations have been made for GAC as well (see Chapter 7 and Appendix E.1). In this way, a direct comparison between CFA and GAC can be made for space requirements.
The annular column for CFA seizes a volume of 0.6 m^3 (0.4 m^3 for the sorbent). The column volume of the 2 GAC contactors is 4.2 m^3 (1.7 m^3 for the carbon and 2.5 m^3 for the rounded bottom and top sections). This means that for the given separation problem the required column volume can be decreased by a factor 7 when applying CFA instead of GAC. Considering the fact that the CFA-system can treat larger feed flow rates with the same equipment size when further developments of open sorbent materials allow higher liquid velocities through these materials (further reduced axial dispersion and pressure drop, smaller compressibility), the predicted reduction in column size with an order of magnitude of 10 is feasible.
However, as will be discussed in Chapter 7 the footprint and the total volume occupied by the complete system (that is the footprint multiplied with the maximum height) are of more practical importance than column volume. Possible profits in column size fall into the background when footprints are considered, because the footprint comprises the total separation system and includes an additional free space of 1 m around the system. The footprint of the CFA-system is equal to the footprint of the GAC-system (17 m^2, see Chapter 7 and Appendices E.1 and E.4), the total volume of the CFA-system is slightly less because of a maximum height of 2.5 m for CFA and a maximum height of 3.3 m for GAC. Again, when further developments of open sorbent materials allow for higher liquid velocities, the compactness of CFA increases proportional to the liquid velocity.

6.6 Conclusions

The design for countercurrent sorption equipment using transported open sorbent material is based on the application of cellular silicone with slightly improved structure related properties compared with the sample material tested earlier. The design is an improved and scaled-up version of the pilot unit with its proven concept of rotation of an annular sorbent shaped as a series of bed segments separated by check valves. Improvements particularly refer to the sealing between the rotating drum and the static

cylinder and the improved assembly/ disassembly procedure for the drum. Scaling-up has taken place in both radial and axial direction: the outer diameter of the packed bed has increased to 1 m, the inner diameter has decreased to 0.5 m and the width of the packed bed has increased to 1 m. The design can handle a feed flow rate of 10 m^3/h with an input concentration of 100 wt.ppm toluene. In theory, a removal efficiency of 99.9% is possible with the design, under practical conditions the required removal efficiency of 99% will be realised with a relatively large safety margin. A sufficient service life, particularly of the sorbent material (plus covering screens) and the seals, has yet to be verified.

Calculations of the curved sorption section taking into account concentration differences along the diameter of the bed segments and balancing of these concentration differences by mixing between the compartments, show an increase of the total required packed bed length of approximately 25% compared to the calculated required packed bed length for straight bed segments with velocities and lengths applying for the mean diameter.

The required column volume can be decreased by a factor 7 when applying countercurrent foam absorption instead of granular activated carbon adsorption, however this profit in column size falls into the background when the footprints of the complete systems are considered. The compactness of the countercurrrent sorption column will increase as cellular silicone with more favourable structural properties regarding pressure drop, compressibility and dispersion will be available, allowing a higher mean liquid velocity in the column (now restricted at approximately 1 cm/s).

References

[1] Zee, G. van, *Counter current sorption using fiber sorbents (Ph.D.-thesis)*, Delft University Press, 1996, ISBN 90-407-1328-6.

[2] Information provided by Stork Gears & Services B.V., Rotterdam, The Netherlands, January 1997.

[3] Information provided by Vector Aandrijftechniek B.V., Schiedam, The Netherlands, December 1996.

7

Techno-economic evaluation

7.1 Introduction

In this techno-economic evaluation it will be examined whether Countercurrent Foam Absorption (CFA), using our new separation equipment based on the design presented in Chapter 6 and filled with cellular silicone as a sorbent material, is economically attractive for the removal of low concentrations of VOCs from large flows of water. In section 7.2 the target application is defined. Also the potential market is briefly explored. Section 7.3 presents a survey of applicable techniques for the target application defined in section 7.2. A distinction is made between traditional techniques which act as a primary reference for CFA and a number of new and emerging techniques. These techniques are evaluated in section 7.4 with respect to cost and size. The first part of section 7.4 concerns the method used for cost and size estimations. Next, successively the traditional techniques, CFA and the other alternative techniques are discussed. In the final part of section 7.4 a summary of all cost and size estimates is given, together with an evaluation of the results. Subsequently section 7.5 provides a short evaluation of other criteria. In section 7.6 a number of alternative applications for CFA are given. Finally, in section 7.7 conclusions are drawn from this techno-economic evaluation.

7.2 Application

Target VOCs

As already stated in Chapter 1, we have chosen to focus on the removal of low concentrations of VOCs from large flows of water for mass transfer modelling, experiments and feasibility studies. During this study, silicone rubber proved to be the choice sorbent material, combining resistance to steam regeneration and availability of fiber and foam structures with high capacity for VOC absorption and low capacity for water absorption. Countercurrent foam absorption (CFA) using steam regeneration followed by phase separation through condensation is most effective if the components to be absorbed have a low solubility in water and are sufficiently volatile to perform the regeneration step. It is estimated that meaningful application of CFA using cellular silicone and steam regeneration is restricted to volatile organic compounds with a water solubility less than approximately 2,000 wt.ppm and a boiling point less than around

150°C. The most important volatile organic compounds which comply with these criteria, are given in table 7.1:

Table 7.1: target VOCs

VOCs	water solubility (wt.ppm) at 25°C [1]	boiling point (°C) [1]
monocyclic aromatics (BTEX):		
benzene	1,800	80
toluene	520	111
ethyl benzene	200	136
xylenes	200	138
chlorinated hydrocarbons:		
1,1,1-trichloroethane (TCA)	1,300	74
trichloroethylene (TCE)	1,100	87
perchloroethylene (PCE)	150	121

Less toxic VOCs complying with above mentioned restrictions are (among others): n-pentane, n-hexane, n-heptane and cyclohexane.
Although carbon tetrachloride (CCl_4) has a water solubility smaller than 2,000 wt.ppm and a boiling point less than 150°C, it is not considered a primary target VOC because in that case our separation equipment using steam regeneration must be made from an alloy resistant to hydrochloric acid.

Target application
VOCs are mainly used as a solvent (cleaning, degreasing and painting) or as a feedstock material used in the production of chemicals (benzene, toluene). Benzene and TCA have been replaced or are being replaced as a solvent, but are still common volatile organics in polluted ground water.

Potential applications can be found at places where VOCs are used as a solvent or as a feed stock material. The most important groups of industry are:
- chemical industries
- petrochemical industries
- oil and gas production.

Other places where applications of VOC-removal from water can be found are:
- paint- and coating industries
- metal industries
- electronics industries
- chemical dry-cleaning
- printing industries
- pharmaceutical industries.

Potential applications can also be found at places where VOCs have been spilled:
- ground water (e.g. former gasworks, former paint factories, petrol stations)
- drainage water (e.g. chemical and petrochemical plants)
- percolation water from refuse dump sites

or where VOCs are always present:

- produced water with natural gas production.

The competitiveness of CFA is expected to be most favourable with large flow rates. Large industrial waste water flow rates have an order of magnitude of 10 to 100 m^3/h (for ground water treatment a flow rate of 10 m^3/h is rather large). Therefore flow rates of both 10 m^3/h and 100 m^3/h are taken into consideration for economic evaluation of CFA. Toluene has been chosen as the component to be removed from water, since besides being an existing waste water component, toluene is a frequently used compound not only in our own experiments but also in other investigations, so many references are available. Since the potential benefits of CFA are best exploited at higher concentrations and CFA is able to achieve a removal efficiency of 99% (see Chapter 6), we choose the removal from 100 wt.ppm to 1 wt.ppm toluene in water (at a flow rate of 10 m^3/h or 100 m^3/h) as our primary application. A temperature of 12°C is assumed to be representative for waste water.

Potential market

It is difficult to estimate the potential market for the removal of VOCs from water since figures for VOC-pollution of water most often are not given explicitly and a large part of the emissions originate from diffuse sources. However, some general estimates can be given.

According to Statistics Netherlands (CBS) [2], the Dutch industry invested approximately NLG 230 million in environmental protection related waste water treatment in 1993. This figure is the summation of the differences between actual investments and fictitious investments without environmental considerations. Only part of this annual investment, an estimated 25% [3], concerns VOC-removal.

Another indication is given by Akzo Nobel [4]. The current market in Western Europe (Benelux, Germany, United Kingdom, France and Sweden) for treatment of industrial waste water is about NLG 4 billion annually. Again, some 25% of these investments concern VOC-removal, leading to a current market for Western Europe of approximately NLG 1 billion annually for VOC-removal from industrial waste water. The current market for ground water treatment in this region is estimated at approximately NLG 400 million annually. Some 50% of this amount or approximately NLG 200 million annually concerns VOC-removal.

Approximately 10% of annual investments in VOC-removal is concerned with design, some average 5% [5] of design cost involves research, leading to a limited research budget from the current market. This is why it is obvious that new techniques can only be developed with support of public authorities, or by companies who are convinced of the profitability of such new business and are therefore prepared to take risks.

Market perspectives

Investments in systems for removing VOCs from water are mainly legislation-driven or cost-driven. Incentives are:

- comply with (more stringent) legislation
- reduction of operating cost by replacement of conventional methods by cheaper new methods
- water treatment or water recycling to avoid the (increasing) cost associated with discharging waste water
- water recycling to avoid the (increasing) cost of taking in ground water or tap water.

Conditions favouring replacement of conventional separation processes include a relatively low energy consumption and a smaller size of the separation unit. Low total cost are essential, especially since the market for end-of-pipe techniques and ground water remedation techniques is reaching saturation.

Furthermore, reliability of the separation system is imperative. Frequently, proven technology is preferred to new techniques for this reason. In many cases one must have quickly at one's disposal a cost-effective solution to handle a certain problem. Adaptation of existing technology is often the most reliable and efficient solution. The danger of interference with or even shutdown of the main operation has to be minimal. In many environmental situations, technological risks are also avoided as much as possible to prevent liability in the event of exceeding legal requirements.

The cost estimates for CFA and alternative techniques will be made for the removal of one specific component (toluene) with one specific technique so that a well-defined comparison can be made. However, waste water often contains diverse pollutants such as mineral salts, trace metals, organic compounds, dissolved gases, colloidal matter, particles in suspension and micro-organisms. Removal of volatile organic compounds often is only a part of the total required separation effort. To minimise the cost per m^3 treated water it is often better to use a combination of techniques. Such integrated systems require compact, modular and easy to install preassembled devices to cut equipment and installation cost. Benefits of integrated waste water treatment systems are lower operating cost, higher efficiencies and longer life and smaller space requirements.
An example of a meaningful combination of techniques is a pre-treatment of organic compounds containing waste water by a light dose of ozone (for a light oxidation of the organic contaminants) followed by activated carbon adsorption together with biodegradation of the adsorbed organic compounds. This results in a strongly extended carbon life [6]. An example of a desired combination of techniques is one which can remove both dissolved aromatics and trace metals from produced water with natural gas production [7].

7.3 Applicable techniques

Traditional techniques
For our target application, removing dissolved toluene from water at flow rates of 10 m^3/h or 100 m^3/h, a concentration of 100 wt.ppm and a removal efficiency of 99%, a number of traditional techniques are applicable: granular activated carbon adsorption,

air stripping and steam stripping. These traditional techniques will act as primary reference to evaluate the economic applicability of countercurrent foam absorption (CFA) for waste water treatment. Preliminary design studies will be made for both these traditional techniques and CFA (see section 7.4).
The United States Environmental Protection Agency (EPA) accepts both granular activated carbon (GAC) and packed tower aeration as "best available technology" for treatment of VOCs in water. Packed tower aeration is the most commonly applied air stripping technique for the removal of VOCs from water. For additional treatment of the off-gas, air-phase granular activated carbon adsorption is the commonly applied method. As abbreviation "PTA+" (Packed Tower Aeration + gas-phase GAC) will be used.
Steam stripping will be competitive for the VOC concentrations concerned if operated under reduced pressure (lower boiling point) to minimise the required heat exchange surface area for feed preheating. As abbreviation "VSS" (Vacuum Steam Stripping) will be used.

New and emerging techniques
Besides GAC, PTA+ and VSS, a number of other techniques are applicable for our target application and are potential competitors to our own CFA technique: macro porous polymer extraction, aerobic biological treatment, pertraction, pervaporation, thick film absorption and chemical oxidation. These techniques will not be evaluated using preliminary design calculations, but will be evaluated on the basis of supplier information (see section 7.4).

Macro porous polymer extraction uses extraction liquid immobilised in the pores of polymer particles. For aerobic biological treatment, a biorotor system has been chosen for our target application. The biorotor is a biofilmreactor in which the micro-organisms are attached to a supporting packing material which is rotated alternately through waste water and through air. Pertraction is a hollow membrane extraction process in which the phases are separated by a non-selective membrane. Pervaporation is a membrane process in which the VOCs permeate through a non-porous organophilic membrane and evaporate on the other side. Thick film absorption resembles our own CFA technique using sheets of silicone rubber instead of cellular silicone rubber. For chemical oxidation, application of hydrogen peroxide + UV-light has been chosen since the operating cost of hydrogen peroxide based systems are generally lower than those employing ozone, chlorine, chlorine dioxide, or potassium permanganate [8].
In addition to these techniques, a number of other techniques are under development such as supercritical extraction, polymeric resin adsorption and adsorbent-filled membranes. Some may eventually prove to be competitive to the techniques mentioned above.

Table 7.2 gives an overview of the applicable techniques, their abbreviation and the primary source of information used for evaluation:

Table 7.2: applicable techniques

Technique	Abbreviation	Source of information
Traditional techniques:		
Granular Activated Carbon adsorption	GAC	preliminary design study
Packed Tower Aeration + GAC	PTA+	preliminary design study
Vacuum Steam Stripping	VSS	preliminary design study
Countercurrent Foam Absorption	CFA	preliminary design study
New and emerging techniques:		
Macro Porous Polymer Extraction	MPPE	AKZO NOBEL
aerobic biological treatment (BIOrotor)	BIO	TAUW Milieu
PerTrACtion	PTAC	TAUW Milieu
PerVAPoration	PVAP	SETEC
Thick Film Absorption	TFA	EnviroSep
chemical oxidation (H_2O_2 + UV)	H_2O_2+	KEMIRA

Generally, all these techniques typically involve passing the contaminated water through or over a large surface area to facilitate the separation.

In section 7.4, for all of the above techniques cost and size estimates will be given to evaluate the attractiveness of the various techniques relative to one another, and to position our own CFA technique. In section 7.5, the evaluation of the techniques from table 7.2 will be extended with other selection criteria.

7.4 Cost and size estimation

7.4.1 Introduction

Cost and size estimates from open literature for comparable systems vary widely, even for similar cases. In order to obtain more reliable cost and size estimates it is necessary to make preliminary design studies or to ask supplier information for one specific case.

In our specific case all systems are specified for 99% removal of toluene from water with a feed concentration of 100 wt.ppm, a feed water temperature of 12°C and a flow rate of 10 m^3/h or 100 m^3/h (see section 7.2).

Cost estimates are based on a 10 year period regarding capital cost. Except for GAC and PTA+, (see §7.4.3), the fixed capital investment is derived from the estimated uninstalled or purchased equipment cost by multiplication with a Lang factor or by multiplication with an installation factor (see §7.4.2). The treatment cost per m^3 water is the sum of annual capital and operating cost, divided by the annual volume of treated water.

For the traditional techniques (GAC, PTA+ and VSS) and for CFA, cost and size estimates are obtained by preliminary design calculations. These calculations are available in appendices E.1 through E.4.

Cost and size estimates for new and emerging techniques applied to our specific case are given by suppliers of know-how {(TAUW Milieu, Deventer, The Netherlands), (SETEC, Voorschoten, The Netherlands), (EnviroSep Inc, Corvallis, Oregon, USA)}, suppliers of raw materials (KEMIRA, Rozenburg, The Netherlands) or suppliers of complete systems (AKZO NOBEL, Arnhem, The Netherlands). They all offer complete preassembled or skid-mounted systems.

The general conditions applying to the preliminary design calculations and the estimates from the suppliers are given in §7.4.2. In §7.4.3 through §7.4.5, all techniques listed in table 7.2 will be discussed separately. Finally, the results of the cost and size estimates are evaluated in §7.4.6.

7.4.2 General conditions for cost and size estimations

For all techniques, foreign matter which can foul the surface area and plug the tortuous passages through packing materials is assumed to be already removed using gravity separation or filtration. This pre-treatment is not included in the cost estimates.

The fixed capital investment "I" includes (if applicable):

- purchased equipment
- purchased equipment installation
- instrumentation & controls (installed)
- piping (installed)
- electrical (installed)
- buildings & building services
- yard improvements
- service facilities (installed)
- land
- engineering
- construction expense
- contractor's fee
- contingency

The fixed capital investment "I" including all the cost items mentioned above can be estimated from the purchased equipment cost alone by multiplication with a so-called Lang factor. This Lang factor accounts for all the other cost items mentioned above. "I" for both GAC and PTA+ are based on evaluation of realised GAC- and PTA+ applications (see §7.4.3). The equivalent Lang factor, based on purchased main equipment cost, appears to be approximately 3 for both techniques. For VSS the fixed capital investment "I" is derived from purchased main equipment cost by multiplication with the same Lang factor of 3. Although a Lang factor of 3 is relatively low for fluid

processing equipment, this value for VSS is chosen for direct comparison with GAC and PTA+. For the other techniques the purchased equipment cost involves complete preassembled or skid-mounted systems, but does not include (as far as applicable) buildings & building services, yard improvements, service facilities (installed) and land. For these techniques the preassembled/skid-mounted equipment cost are multiplied with an installation factor of 1.5 to obtain a fixed capital investment "I" which can be compared to "I" for GAC, PTA+ and VSS.

For CFA and H_2O_2+, both techniques that are using modular systems where the number of units is proportional to the feed rate, the fixed capital investment "I" for the 100 m³/h case is not available and is estimated at seven times "I" known for the 10 m³/h case. The figure seven is based on a weighed average derived from a number of quotations. For all other techniques using modular systems (BIO, PTAC, PVAP and TFA) "I" for the 100 m³/h case is given by suppliers and does not exceed eight times "I" for the 10 m³/h case.

The fixed capital investment "I" is converted into a fixed annual charge by multiplication with a factor "a". The resulting annualised capital cost (I x a) together with the annual operating cost are the annual treatment cost. The operating cost include maintenance and repair (% of I), operating labour, utilities (steam and electric power) and replacements (carbon, membranes, etc.).

A coarse shortcut method to derive the factor "a" is given by the annuity equation (7.1):

$$a = \frac{i}{1-(1+i)^{-N}} \qquad (7.1)$$

At a cost of capital of 15% (i=0.15) and a 10 year project period (N=10) "a" is 20%.

Maintenance and repair cost range from 3% (simple process) to 8% (complex process) of fixed capital investment, depending on the system.

The systems are assumed to be employed at an industrial location without the need for sophisticated instrumentation and controls. For GAC, PTA+, VSS and MPPE, operating labour cost are estimated at 500 man-hours per year (0.5 hours per shift, 3 shifts a day, 8,000 operating hours per year, continuous operation) at 70 NLG/h. No distinction is made for the two different feed rates (10 m³/h and 100 m³/h) since the required operating labour will be approximately equal (roughly only column diameters will change considerably). However, all other techniques use modular systems. For modular systems where the number of units is proportional to the feed rate (CFA, PTAC, PVAP, TFA and H_2O_2+), the operating labour cost for a feed rate of 10 m³/h is also estimated at 500 man-hours per year, but for the 100 m³/h case (10 times as many units) the operating labour cost is estimated at three times the operating labour cost for the 10 m³/h case. An exception is made for BIO. Because for the 100 m³/h case BIO uses twice as many units instead of 10 times as many units, the operating labour cost is estimated at 1.5 times the operating labour cost for the 10 m³/h case.

Low pressure steam (approximately 2 bar and 120°C) is assumed to be available at the site at a cost of 30 NLG/ton, electric power at 0.18 NLG/kWh [9].

The exchange rate is assumed to be 1.7 NLG/$ (1996).

All cost are valid for the year 1996.

Possible revenues of recovered toluene or possible cost involved with disposal of toluene concentrate are neglected.

For the footprint of the system a free space of 1 m around the main equipment (columns, large heat exchangers, pre-treatment buffer vessels for H_2O_2+) and around skid-mounted units or arrays of units is assumed. Also the maximum height of the system will be given. The system will approximately take a volume corresponding to the product of the footprint and the maximum height (this volume will not be given explicitly).

7.4.3 Traditional techniques

Granular activated carbon adsorption (GAC)
The system consists of two down-flow fixed bed adsorbers: one column is in operation, the carbon of the other column can be regenerated on-site or can be replaced with fresh carbon instead of on-site regeneration. In the latter case, the spent carbon can be landfilled, incinerated as a solid waste or reactivated off-site. After carbon exchange, the column with the fresh carbon is then used in series with the other column to be able to use the full packed height of the carbon bed, see figure 7.1:

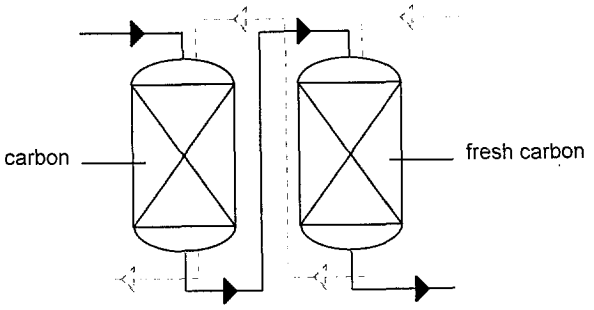

Figure 7.1: Granular activated carbon adsorption with carbon exchange instead of on-site regeneration

As a rule, the load capacity of the carbon increases with decreasing water solubility and decreasing polarity of the component to be adsorbed.
Important parameters determining the adsorber effectiveness are the Freundlich isotherm parameters "K" and "1/n" (see equation 7.2). The Freundlich isotherm provides a good estimate of the equilibrium capacity of carbon for the compound to be removed:

$$q = K \cdot c^{1/n} \qquad (7.2)$$

q:	amount of compound adsorbed per unit weight of carbon	[μg/g]
K:	adsorbability of the compound	$[(\mu g/g)/(\mu g/L)^{1/n}]$
c:	concentration of unadsorbed compound in equilibrium with the carbon	[μg/L]
1/n:	concentration sensitivity exponent	[-]

Because the assumed adsorption isotherm has a major influence on the estimated performance of the system, an isotherm determined for conditions matching our case (among others a feed water temperature of 12°C) as close as possible has been used. For concentrations of 0.005 to 3.45 wt.ppm toluene in distilled water of 14°C, Filtrasorb 400 carbon has the following Freundlich isotherm parameters [10]:

1/n	= 0.328	[-]
K	= 9910	$[(\mu g/g)(L/\mu g)^{1/n}]$

At a 100 wt.ppm toluene feed concentration the carbon load at equilibrium is 433 mg/g, according to equation (7.2). For comparison, Stenzel [11] gives 1/n = 0.729 and K = 195 (K = 30 on mg-basis instead of μg-basis) as typical Freundlich isotherm constants for toluene, leading to a carbon load at equilibrium of 861 mg/g.

The calculation of the adsorption system, together with all assumed parameters, is given in Appendix E.1. The calculation has been performed using a program for drinking water and ground water remedation cost evaluation made by the U.S. EPA (Environmental Protection Agency) [12]. Spent carbon is replaced with virgin carbon since this is the cheapest option for both feed rates (10 m^3/h and 100 m^3/h).
For a range of empty bed contact times (EBCTs) the total cost together with the GAC bed height has been calculated. The program yields results for one contactor. Fixed capital investment and operation & maintenance cost (excluding carbon replacements) have to be doubled because our system has two contactors.

With increasing empty bed contact time (EBCT), the replacement frequency and hence the cost of spent carbon will decrease but the construction cost will increase. The optimal EBCT has been determined by calculating the treatment cost per m^3 feed water for a range of EBCT's, see Appendix E.1. For a feed rate of 10 m^3/h an optimal EBCT of 5 minutes has been established, for a feed rate of 100 m^3/h the optimal EBCT turns out to be 6 minutes.

Cost and size estimates are based on calculations accounted for in Appendix E.1.
The treatment cost for GAC are derived as follows:

	10 m³/h	100 m³/h
fixed capital investment "I" (NLG):	385,000	1,135,000
fixed annual charge at 20% of I:	77,000	227,000
operation and maintenance including labour:	99,000	144,000
electric power:	4,000	20,000
GAC replacements:	93,000	806,000
	---------- +	---------- +
annual treatment cost (NLG/y):	273,000	1,197,000
volume of treated water (m³/y):	80,000	800,000
treatment cost (NLG/m³):	3.4	1.5

For the 10 m³/h case the system consists of two columns with a height of 3.3 m and a diameter of 1.2 m. With a distance of 1 m between the two columns this results in a footprint of 17 m². For the 100 m³/h case the system consists of two columns with a height of 3.5 m and a diameter of 3.6 m, resulting in a footprint of 57 m².

The results for treatment cost calculations and space requirement calculations are given in table 7.3:

Table 7.3: treatment cost and space requirements for GAC

GAC	10 m³/h	100 m³/h
treatment cost (NLG/m³)	3.4	1.5
footprint (m²)	17	57
maximum height (m)	3.3	3.5

Packed tower aeration + gas-phase GAC (PTA+)

Air stripping is a commonly applied technique for VOC-removal, especially for large water flows (>10 m³/h) with medium to small concentrations (<500 wt.ppm). The usual construction is a packed tower with countercurrent operation using random packing in the 1-to-2-inch nominal size range (packed tower aeration). A common choice for the treatment of the VOC-containing air from the stripper is gas-phase GAC treatment with on-site steam regeneration of the carbon. Compared to liquid-phase GAC, packed tower aeration plus gas-phase GAC can be more cost-efficient (depending on the specific case) because the adsorption capacities of carbon for a number of organic compounds are higher in the vapour phase than in the liquid phase [13,14], especially when the relative humidity of the tower off-gas is reduced, thus minimising the effects of humidity on the carbon's adsorption capacity.

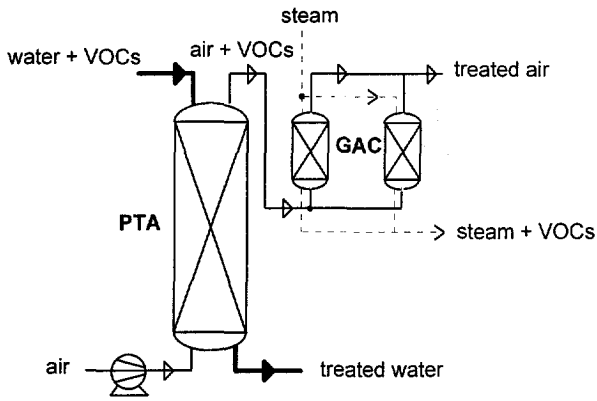

Figure 7.2: Packed tower aeration + gas-phase GAC

The effectiveness of stripping an organic pollutant from water is mainly determined by its hydrophobicity, indicated by its low aqueous solubility, rather than by its pure-component volatility. An important parameter determining the stripper effectiveness is the Henry coefficient H_e of the compound to be removed. Both Henry's coefficient and the required removal efficiency have a significant impact on the cost-effective design of a PTA system.
For low concentrations, the proportionality factor between the partial pressure and the concentration of the component in question is H_e:

$$P_i = H_e \cdot x_i (\approx \gamma_{ix}^{\infty} \cdot x_i \cdot P_{vap}) \qquad (7.3A)$$

P_i:	partial pressure of component "i" in the gas phase	[bar]
H_e:	Henry coefficient of component "i"	[bar]
x_i:	mole fraction of component "i" in water	[mole/mole]

For a satured solution the relation reads:

$$P_{vap} = H_e \cdot x_{sol} \qquad (7.3\ B)$$

According to equation (7.3 B), H_e can be determined using the vapour pressure and the solubility in water of the component:

$$H_e = \frac{P_{vap}}{x_{sol}} \qquad (7.4)$$

P_{vap}:	vapour pressure	[bar]
x_{sol}:	maximum solubility in water	[mole/mole]

H_e can also be determined using the activity coefficient. For gas-liquid equilibrium, the activity coefficient at infinite dilution is given by:

$$\gamma_{ix}^{\infty} = \frac{H_e}{P_{vap}} \rightarrow H_e = \gamma_{ix}^{\infty} \cdot P_{vap} \qquad (7.5)$$

γ_{ix}^{∞}: activity coefficient of comp. "i" in water at infinite dilution [-]

The mole fraction based distribution coefficient K is:

$$\frac{y_i}{x_i} = K = \gamma_{ix}^{\infty} \cdot \frac{P_{vap}}{P_{sys}} = \frac{H_e}{P_{sys}} \qquad (7.6)$$

y_i:	mole fraction of component "i" in the gas phase	[mole/mole]
K:	mole fraction based distribution coefficient	[-]
P_{sys}:	system pressure	[bar]

Values for H_e reported in literature for a specific component vary rather much. H_e is especially a strong function of temperature. Depending on the component, a 10°C temperature increase may double or even triple the value of H_e and vice versa [15]. For this reason, values for H_e should be looked at critically. According to Nyer [16], H_e for toluene as a function of temperature is given by:

$$\log(H_e)_{toluene} = 1.013 \cdot (7.427 - \frac{1492}{T}) \qquad (7.7)$$

T: temperature [K]

According to this equation, H_e for 12°C is 158 bar. Ram et. al. [10] have published a value for H_e (at 12°C) for toluene of 162 bar {160 atm·kmole(water)·kmole^{-1}(air)}, which gave the best fit between predicted and observed performance of air strippers in operation. This value {160(atm·kmole(water)·kmole^{-1}(air) or 0.13 atm·m^3(water)·m^{-3}(air)} will be used in our calculations, based on a program for drinking water and ground water remedation cost evaluation made by the U.S. EPA [17].

The calculation of the adsorption system, together with all assumed parameters, is given in Appendix E.2. For a range of air-to-water ratio's and pressure drops, the total cost for tower aeration + gas-phase carbon adsorption together with the tower bed height and tower diameter has been calculated (program "pta2"). For tower aeration, variations in the air-to-water ratio and pressure drop result in cost trade-offs between capital and electric power requirements. When gas-phase GAC treatment is included, a lower air-to-water ratio and a higher stripping tower may be more economical. For the optimal combination, an air-to-water ratio of 25 (m³ air)/(m³ water) and a pressure drop of 50 Pa/m, the fixed annual charge (20% of fixed capital investment) and the operation & maintenance cost for both the tower and the two GAC-columns are calculated (program "pta"). Cost for heating the tower off-gas from 12°C to 24°C are included to reduce the relative humidity to under 40%, thus minimising the effects of humidity on the carbon's adsorption capacity.

For 100 m^3/h feed rate, the gas-phase GAC treatment cost are 0.28 $/m^3$ (the total treatment cost for PTA+ are 0.36 $/m^3$, see Appendix E.2). These calculated gas-phase GAC treatment cost are in agreement with published off-gas treatment cost. Our case is represented by annual off-gas treatment cost of 152 $/(ft^3/min) at a flow rate of 1,472 ft^3/min air containing 1,038 ppmv toluene. According to [18], for a flow rate of 1,000 ft^3/min air containing 1,500 ppmv VOCs the annual treatment cost are 126 $/(ft^3/min), estimated with partly similar economic parameters.

Cost and size estimates are based on calculations accounted for in Appendix E.2.
The treatment cost for PTA+ are derived as follows:

	10 m^3/h	100 m^3/h
fixed capital investment "I" (NLG):	180,000	500,000
fixed annual charge at 20% of I:	36,000	100,000
packed tower:		
operation and maintenance:	15,000	21,000
electric power:	2,000	22,000
gas-phase GAC-treatment:		
operation and maintenance:	22,000	30,000
electric power:	3,000	25,000
on-site steam regeneration:	29,000	289,000
	---------- +	---------- +
annual treatment cost (NLG/y):	107,000	487,000
volume of treated water (m^3/y)	80,000	800,000
treatment cost (NLG/m^3):	1.3	0.6

The footprint of the system is determined by the diameters of the packed tower and of the gas-phase GAC-columns. For the 10 m^3/h case the packed tower has a diameter of 0.4 m and a height of 15 m, the two GAC-columns have a diameter of 0.6 m and a stacked height of 6 m. With a distance of 1 m between the packed tower and the GAC-columns this results in a total footprint of 10 m^2. For the 100 m^3/h case the packed tower has a diameter of 1.3 m and a height of 16 m, the two GAC-columns have a diameter of 1.9 m and a stacked height of 6 m. This results in a total footprint of 24 m^2. The maximum height of the system is determined by the packed tower in both cases.

Table 7.4: treatment cost and space requirements for PTA+

PTA+	10 m^3/h	100 m^3/h
treatment cost (NLG/m^3)	1.3	0.6
footprint (m^2)	10	24
maximum height (m)	15	16

Vacuum steam stripping (VSS)

Steam stripping can be competitive to air stripping if the organic compounds are nearly insoluble in water, because in that case a simple phase separation of the organic components is possible whereas air stripping needs an after-treatment (for instance gas-

phase GAC). The system basically consists of a column packed with stainless steel Pall rings, a reboiler, a feed preheater, a condenser, a decanter and a vacuum pump (see figure 7.3). For large feed rates steam stripping can only be competitive when operated under reduced pressure (lower boiling point) to minimise the required heat exchange surface area needed for feed preheating (see Appendix E.3).The column is operated at 0.073 bar with a boiling point of 40°C, high enough to use ambient cooling water for the condenser. A plate heat exchanger with an approach of 4°C is applied for feed preheating. The energy required for the reboiler is provided by low pressure steam already available at the site.

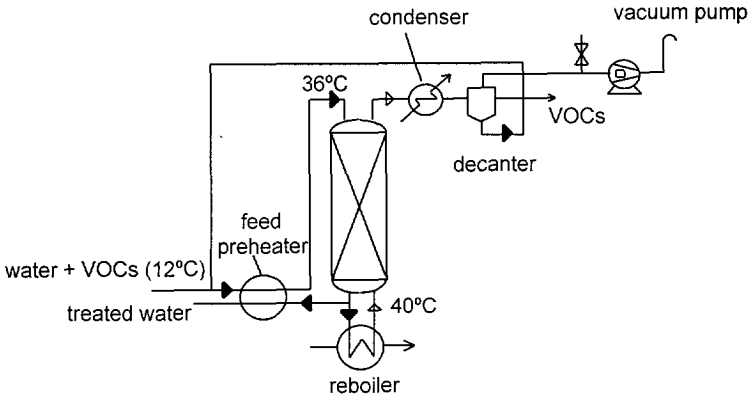

Figure 7.3: Vacuum steam stripping

The total amount of steam to be supplied is the sum of the steam needed for the reboiler (determined by the approach in the feed preheater) and the steam needed to transport the toluene to the condenser. The latter steam flow is determined by the partial pressure of toluene at the top of the column. From equations (7.3) and (7.4):

$$P_i = \frac{P_{vap} \cdot x_i}{x_{sol}} \tag{7.8}$$

The solubility of toluene in water as a function of temperature can be calculated using correlations from experimental data [19], P_{vap} for toluene as a function of temperature is given by Timmermans [20]. At 36°C, P_{vap} = 0.012 bar at equilibrium. If P_i is assumed to be 0.01 bar and the system pressure at the top is 0.073 bar, the partial pressure of water is 0.063 bar. So, for each kmole of toluene 6.3 kmole of steam are required to transport the toluene to the condenser. Or, for each m³ feed water (100 wt.ppm toluene) 0.123 kg steam is required. To heat the water from 36°C to 40°C using the heat of vaporisation of steam (reboiler), 6.97 kg steam is required for each m³ feed water (see Appendix E.3). So, the total amount of steam to be supplied (approximately 7.1 kg steam per m³ feed water) is determined by the temperature approach in the preheater.

The mole fraction based distribution coefficient K follows from equation (7.4) and (7.6):

$$K = \frac{P_{vap}}{x_{sol} \cdot P_{sys}} \tag{7.9}$$

For our system, K has a high value (approximately 8,340, see Appendix E.3). This means that the mass transfer resistance in the gas-phase is negligible. In this case, the number of overall liquid-phase transfer units is given by:

$$N_{oL} = \ln \frac{x_{in}}{x_{out}} \tag{7.10}$$

N_{oL}:	number of overall liquid-phase transfer units	[-]
x_{in}:	mole fraction at the top of the column	[mole/mole]
x_{out}:	mole fraction at the bottom of the column	[mole/mole]

The stripping factor S is given by:

$$S = \frac{K \cdot V}{L} \tag{7.11}$$

S:	stripping factor	[-]
V:	steam flow rate	[kmole/s]
L:	feed water flow rate	[kmole/s]

For our system S is 59, so a large excess of steam is available to strip the toluene from the water. In that case, the overall height of a transfer unit is approximately equal to the height H_L of a liquid-phase transfer unit. H_L can be estimated using Cornell's method [21] (see equation 7.12). For design purposes the height correction is omitted [22].

$$H_L = \frac{\Phi \cdot C}{3.28} \cdot \left(\frac{\eta_L}{\rho_L \cdot D_L}\right)^{0.5} \tag{7.12}$$

H_L:	height of a liquid-phase transfer unit	[m]
Φ:	correlation parameter for Pall rings [21]	[m]
C:	flooding correction factor	[-]
η_L:	liquid viscosity	[Pa·s]
ρ_L:	liquid density	[kg/m³]
D_L:	liquid diffusion coefficient	[m²/s]

In our case the height of a transfer unit is 0.23 m for 10 m³/h and 0.59 m for 100 m³/h. The packed bed height follows from the product of N_{oL} and H_L. The fixed capital investment "I" of the system is obtained by multiplying the estimated uninstalled or purchased equipment cost with a Lang factor of 3 (see Appendix E.3).

		10 m³/h	100 m³/h
fixed capital investment "I" (NLG):		320,000	870,000
fixed annual charge at 20% of I:		64,000	174,000
maintenance & repair at 3% of I		10,000	26,000
operating labour:		35,000	35,000
utilities:	steam:	17,000	170,000
	electric power:	1,000	10,000
		---------- +	---------- +
annual treatment cost (NLG/y):		127,000	415,000
volume of treated water (m³/y)		80,000	800,000
treatment cost (NLG/m³):		1.6	0.5

The footprint of the system is determined by the diameter of the column and the surface area of the feed preheater. For the 10 m³/h case the column has a diameter of 0.5 m and a height of 6 m, the feed preheater has a horizontal cross-section of 1.2 x 1.2 m² and a height of 1 m. With a distance of 1 m between the column and the feed preheater this results in a total footprint of 13 m². For the 100 m³/h case the column has a diameter of 1.1 m and a height of 8 m, the feed preheater has a horizontal cross-section of 1.4 x 1.4 m² and a height of 2 m. This results in a total footprint of 18 m². The maximum height of the system is determined by the column in both cases.

The results for treatment cost calculations and space requirement calculations are given in table 7.5:

Table 7.5: treatment cost and space requirements for VSS

VSS	10 m³/h	100 m³/h
treatment cost (NLG/m³)	1.6	0.5
footprint (m²)	13	18
maximum height (m)	6	8

7.4.4 Countercurrent foam absorption (CFA)

CFA uses cellular silicone (open-cell silicone rubber foam) with a large specific surface area and high packed bed porosity. The VOCs are absorbed in the bulk of this organophilic sorbent material. The foam bed is regenerated using steam. Countercurrent operation is enforced by segmenting the foam bed by check valves. The bed is transported mechanically and continuously through a sorption and regeneration section. See Chapter 6 for more details.

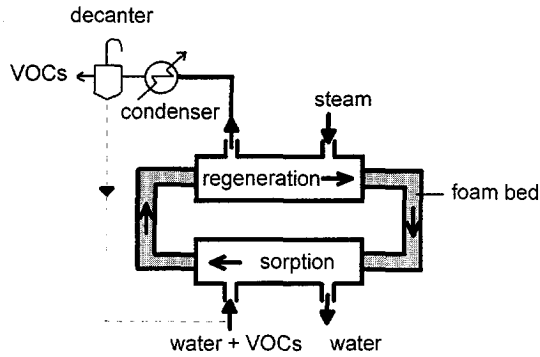

Figure 7.4: Countercurrent foam absorption

The system consists of units treating 10 m³/h water each. The preassembled/skid-mounted equipment cost was estimated as follows. The main parts of the actual separation equipment are the static cylinder and the slowly rotating housing (see Chapter 6 and Appendix D). The cost of these parts were estimated on the basis of a small series of CFA units and allocation of most of these parts to specialised workshops. Production and assembly of these parts cost approximately NLG 340,000, including small material and seals. Together with the other parts like the non-return valves, the planetary gear, the motorreductor, the frame, the condenser and the decanter, the total cost of one CFA unit is estimated at NLG 460,000, including assembly, interconnecting piping, cabling and instrumentation.

The calculated separation performance of a CFA unit is based on the application of cellular silicone with the following properties:
- porosity 90%
- mean pore diameter 700 μm
- pressure drop approximately 2.3E4 Pa/m at the allowable maximum liquid velocity of around 1 cm/s.

The liquid velocity is restricted to approximately 1 cm/s to avoid compression of the bed and to avoid unfavourable values of axial dispersion and pressure drop (Chapter 6).

Due to the relatively high steam velocity through the foam (0.3 m/s) and the wide dimensional margins of the design (in theory, for the given case CFA can achieve a removal efficiency of 99.9%, see Chapter 6), the same unit can remove higher concentrations or achieve lower effluent concentrations without significant increase in steam supply.

The fixed capital investment "I" for a system with one unit (10 m³/h) is obtained by multiplying the estimated preassembled/skid-mounted equipment cost with an installation factor of 1.5 (see Appendix E.4). As mentioned in §7.4.2, the fixed capital investment "I" for the 100 m³/h case is taken as seven times "I" for the 10 m³/h case and the operating labour for the 100 m³/h case is taken as three times the operating labour for the 10 m³/h case.
The treatment cost for CFA are derived as follows:

	10 m³/h:	100 m³/h:
fixed capital investment "I" (NLG):	690,000	4,830,000
fixed annual charge at 20% of I:	138,000	966,000
maintenance & repair at 8% of I:	55,000	386,000
operating labour:	35,000	105,000
steam:	54,000	540,000
sorbent material:	6,000	60,000
	---------- +	---------- +
treatment cost per year (NLG/y):	288,000	2,057,000
volume of treated water (m³/y):	80,000	800,000
treatment cost (NLG/m³):	3.6	2.6

The horizontally mounted drum with a capacity of 10 m³/h (packed bed width 1 meter, diameter 1 m, see Chapter 6) has a total width (front view, see figure 5.1) of approximately 1.5 m including water and steam supply and drain, and a total length (side view, see figure 5.2) of approximately 1.8 m including frame, drive and condenser/decanter. The resulting footprint for a system with one unit and an additional 1 m length in front of the system to enable exchange of sorbent material is about 17 m². The height is about 2.5 m, including 1 m between the floor and the bottom of the equipment. When stacked 2 high with a distance of 0.5 m in width and a distance of 2 m in length between the units to enable exchange of sorbent material, the footprint of the system for a feed rate of 100 m³/h is approximately 57 m² and the maximum height is approximately 5 m.
The results for cost and size estimates are given in table 7.6:

Table 7.6: treatment cost and space requirements for CFA

CFA	10 m³/h	100 m³/h
treatment cost (NLG/m³)	3.6	2.6
footprint (m²)	17	57
maximum height (m)	2.5	5

The fixed capital investment of the CFA units will decrease proportional with an increase of the allowable liquid velocity, resulting in a large decrease of treatment cost and space requirements. For this reason, the single best way to improve the competitiveness of CFA is the application of cellular silicone with an improved structure, allowing higher liquid velocities (see §7.4.6).

7.4.5 New and emerging techniques

The following cost and size estimates are based on information supplied by commercial organisations. The supplied data have been critically analysed in order to ensure that the methods used to derive cost and size estimates for these techniques are comparable to the methods used for the other techniques.

Macro-porous polymer extraction (MPPE)

MPPE stands for macro-porous polymer extraction. The extraction liquid, which is not soluble in water, is immobilised in the pores of the polymer and the dissolved VOCs are extracted from the water and concentrated in the polymer particles. The VOCs are evaporated out of the non-volatile extraction liquid using steam.

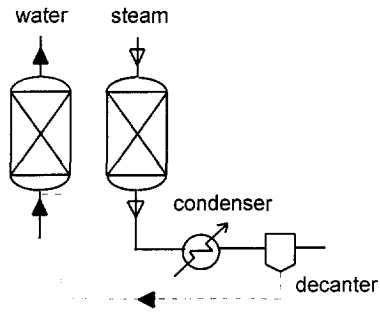

Figure 7.5: MPPE-system

MPPE can also remove less volatile components, but for these compounds regeneration takes place with fresh extraction liquid, which is stripped later on from the extracted hydrocarbons by distillation.

Cost and size estimates have been made by Akzo Nobel (Arnhem, The Netherlands), supplier of the MPPE system.

The fixed capital investment "I" of the MPPE system is estimated at 1.5 times the cost estimate for the preassembled MPPE system including ancillary equipment (NLG 325,000 for 10 m³/h feed rate, NLG 500,000 for 100 m³/h feed rate). The treatment cost for MPPE are derived as follows:

		10 m³/h	100 m³/h
fixed capital investment "I" (NLG):		490,000	750,000
fixed annual charge at 20% of I:		98,000	150,000
maintenance & repair at 4% of I		20,000	30,000
operating labour:		35,000	35,000
utilities:	steam:	3,000	31,000
	electric power:	2,000	10,000
performance guarantee / service contract, including replacement of MPPE granules:		35,000	70,000
		---------- +	---------- +
annual treatment cost (NLG/y):		193,000	326,000
volume of treated water (m³/y)		80,000	800,000
treatment cost (NLG/m³):		2.4	0.4

The footprint of the system is determined by the diameter of the two columns. These columns have a mutual distance of 0.5 m. For the 10 m^3/h case the column has a diameter of 0.7 m, resulting in a footprint of around 11 m^2. For the 100 m^3/h case the column has a diameter of 1.5 m, resulting in a footprint of around 19 m^2. The maximum height of the system is estimated by adding 1 m both to the bottom and to the top of the column. The height of the 10 m^3/h system is 3 m and the height of the 100 m^3/h system is 4.2 m.

Table 7.7: treatment cost and space requirements for MPPE

MPPE	10 m^3/h	100 m^3/h
treatment cost (NLG/m^3)	2.4	0.4
footprint (m^2)	11	19
maximum height (m)	3	4.2

Akzo Nobel considers an installation factor of 1.25 instead of 1.5 more appropriate for their MPPE-system. Akzo Nobel also comments that the cost estimate for the preassembled MPPE system includes automatic and remote control, resulting in overestimation of fixed capital investment and operating labour cost relative to the other techniques.

Aerobic biological treatment: biorotor (BIO)

Micro-organisms are able to reduce organic micro pollutants to harmless compounds. The water-solved organic molecule passes the cellular membrane and enters the cell metabolism (using oxygen), where intracellular enzymes facilitate the conversion into biomass, CO_2 en H_2O.

The biorotor, in fact a biofilmreactor, contains large Rashig-ring-like random packing material. On this packing a very thin and stable film will be established. The packing is rotated alternately through waste water and through air. The biorotor consists of a number of packed chambers in series, through which the waste water is pumped (see figure 7.6).

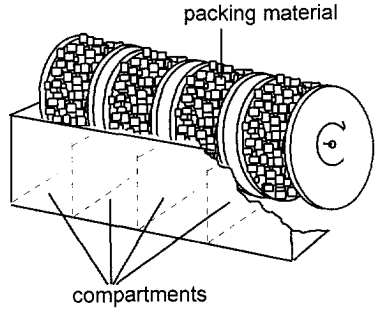

Figure 7.6: Biorotor

Cost and size estimates have been made by Tauw Milieu (Deventer, The Netherlands).

The fixed capital investment "I" for the biorotor system is estimated at 1.5 times the cost estimate for the biorotor modules (NLG 300,000 for 10 m³/h feed rate, NLG 1,000,000 for 100 m³/h feed rate). The operating labour cost is estimated at 1.5 times the operating labour cost for the 10 m³/h case (see §7.4.2).

The treatment cost for BIO are derived as follows:

	10 m³/h	100 m³/h
fixed capital investment "I" (NLG):	450,000	1,500,000
fixed annual charge at 20% of I:	90,000	300,000
maintenance & repair at 6% of I:	27,000	90,000
operating labour:	35,000	53,000
electric power:	10,000	16,000
	---------- +	---------- +
annual treatment cost (NLG/y):	162,000	459,000
volume of treated water (m³/y):	80,000	800,000
treatment cost (NLG/m³):	2.0	0.6

The maximum height of the modules is approximately 2 m. The footprint for the 10 m³/h case (2 modules) is about 35 m². The footprint for the 100 m³/h case (4 larger modules) is about 150 m².

Table 7.8: treatment cost and space requirements for BIO

BIO	10 m³/h	100 m³/h
treatment cost (NLG/m³)	2.0	0.6
footprint (m²)	35	150
maximum height (m)	2	2

Pertraction (PTAC)

This is in fact extraction in which the phases are separated by a non-selective membrane. The membranes are formed by porous polypropylene hollow fibers. For VOC-removal a kerosene-like extractant is applied. The extractant is regenerated using vacuum distillation. In principle, pertraction can be used for removal of both volatile and less volatile organic compounds in one step, however this will give cause to a complex regeneration system. Figure 7.7 shows the principle of pertraction [23]:

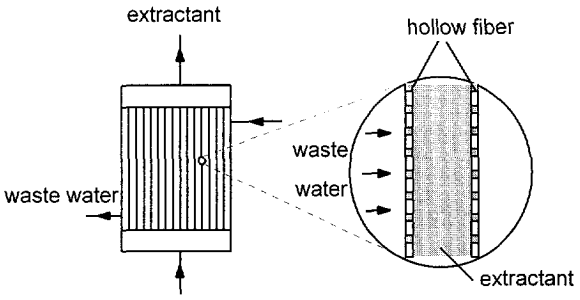

Figure 7.7: Pertraction

Cost and size estimates have been made by Tauw Milieu (Deventer, The Netherlands). The fixed capital investment "I" for the pertraction system is estimated at 1.5 times the cost estimate for the preassembled skid-mounted pertraction modules plus regeneration equipment (NLG 265,000 for 10 m³/h feed rate, NLG 1,525,000 for 100 m³/h feed rate). The treatment cost for PTAC are derived as follows:

	10 m³/h	100 m³/h
fixed capital investment "I" (NLG):	400,000	2,300,000
fixed annual charge at 20% of I:	80,000	460,000
maintenance & repair at 6% of I:	24,000	138,000
operating labour:	35,000	105,000
electric power:	8,000	35,000
membrane replacements:	30,000	187,000
regeneration extractant:	15,000	90,000
	---------- +	---------- +
annual treatment cost (NLG/y):	192,000	1,015,000
volume of treated water (m³/y):	80,000	800,000
treatment cost (NLG/m³):	2.4	1.3

The height of the pertraction modules is approximately 1 m. The maximum height of the system is determined by the vacuum distillation column for regeneration, which has a height of around 4.5 m. Each module has a footprint of 0.2 m² square including a distance of 0.1 m between the modules. A free space of 1 m around the near-square array of modules and the adjacent distillation column is incorporated in the footprint of the system. With a distance of 1 m between the pertraction modules and the distillation column the footprint for the 10 m³/h case is around 13 m² (22 modules and a distillation column diameter of 0.5 m). The footprint for the 100 m³/h case is around 26 m² (220 modules stacked 2 high and a distillation column diameter of 1.6 m).

Table 7.9 summarises the results for pertraction:

Table 7.9: treatment cost and space requirements for PTAC

PTAC	10 m³/h	100 m³/h
treatment cost (NLG/m³)	2.4	1.3
footprint (m²)	13	26
maximum height (m)	4.5	4.5

Pervaporation (PVAP)

Pervaporation is short for permeation and evaporation. In contrast to other membrane separation techniques, with pervaporation a phase change takes place across the membrane. Pervaporation uses a non-porous membrane through which components selectively diffuse, then evaporate on the other side. The selectivity is determined by the solubility of the component in the membrane. The driving force for this process is the difference between the transported component's partial pressure - high on the feed side, low on the permeate side. A vacuum pump is usually installed to maintain this differential, while a temperature gradient can also be used. The organophilic membranes contain silicone rubber or polyether-polyamide copolymers. Generally, the most volatile organics are easiest to recover.

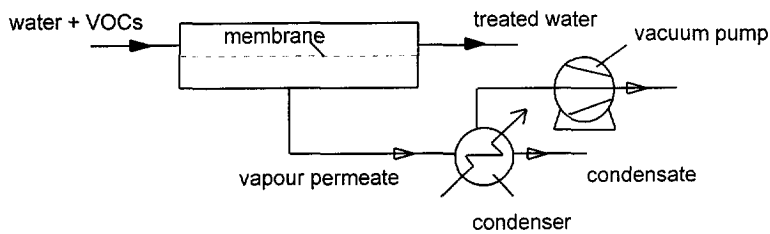

Figure 7.8: Pervaporation

Cost and size estimates have been made by SETEC (Voorschoten, The Netherlands). The fixed capital investment "I" for the pervaporation system is estimated at 1.5 times the cost estimate for the preassembled skid-mounted pervaporation system (NLG 500,000 for 10 m³/h feed rate, NLG 4,000,000 for 100 m³/h feed rate). The treatment cost for PVAP are derived as follows:

		10 m³/h	100 m³/h
fixed capital investment "I" (NLG):		750,000	6,000,000
fixed annual charge at 20% of I:		150,000	1,200,000
maintenance & repair at 6% of I:		45,000	360,000
operating labour:		35,000	105,000
utilities:	steam:	19,000	190,000
	electric power:	4,000	40,000
membrane replacements:		5,000	50,000
		--------- +	---------- +

annual treatment cost (NLG/y):	258,000	1,945,000
volume of treated water (m^3/y):	80,000	800,000
treatment cost (NLG/m^3):	3.2	2.4

The height of the pervaporation system is approximately 4 m. The 10 m^3/h system has a footprint of approximately 18 m^2 including a free space of 1 m around the system, the footprint of the 100 m^3/h system is approximately 40 m^2.

Table 7.10 summarises the results for the pervaporation system:

Table 7.10: treatment cost and space requirements for PVAP

PVAP	10 m^3/h	100 m^3/h
treatment cost (NLG/m^3)	3.2	2.4
footprint (m^2)	18	40
maximum height (m)	4	4

Thick film absorption (TFA)

TFA is a patented polymeric absorption process using flat, curved or tubular sheets of silicone rubber to absorb the VOCs, leaving a purified stream of water [24,25]. Figure 7.9 shows the principle of TFA. The silicone absorbent is regenerated using a combination of hot water and vacuum, delivering the VOCs as a purified organic stream. TFA is a modular process. Half of the modules is absorbing, the other half is regenerating. One module can remove 90% of the VOCs from water, so for 99% removal and regeneration at least 4 modules are required.

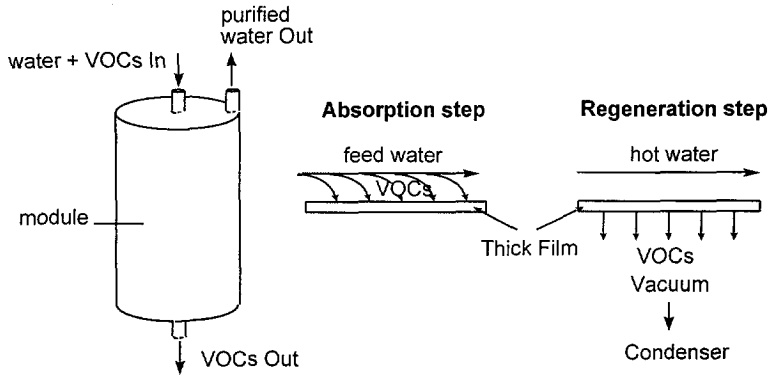

Figure 7.9: Thick film absorption

Cost and size estimates have been made by EnviroSep (Corvallis, Oregon, USA), supplier of the TFA system. The fixed capital investment "I" of the TFA system is estimated at 1.5 times the cost estimate for the preassembled skid-mounted TFA system including ancillary equipment ($119,000 for 10 m^3/h feed rate, $610,000 for 100 m^3/h feed rate). The treatment cost for TFA are derived as follows:

		10 m³/h	100 m³/h
fixed capital investment "I" (NLG):		305,000	1,555,000
fixed annual charge at 20% of I:		61,000	311,000
maintenance & repair at 8% of I:		24,000	124,000
operating labour:		35,000	105,000
utilities:	steam:	17,000	170,000
	electric power:	9,000	85,000
module element replacements:		82,000	816,000
annual treatment cost (NLG/y):		228,000	1,611,000
volume of treated water (m³/y):		80,000	800,000
treatment cost (NLG/m³):		2.9	2.0

The TFA modules are about 2 m high. To diminish the foot print of the system the modules can be stacked, for instance 2 high with an estimated total height of 4.5 m. For the 10 m³/h case, the footprint of the system including ancillary equipment is approximately 20 m². For the 100 m³/h case, the total footprint of the system is approximately 50 m².

Table 7.11 summarises the results for TFA:

Table 7.11: treatment cost and space requirements for TFA

TFA	10 m³/h	100 m³/h
treatment cost (NLG/m³)	2.9	2.0
footprint (m²)	20	50
maximum height (m)	4.5	4.5

Chemical oxidation: H_2O_2 + UV (H_2O_2+)

Hydrogen peroxide (H_2O_2) is considered an "all purpose" oxidant for a variety of systems, and can be applied directly or in conjunction with a catalyst. When H_2O_2 is activated using iron catalyst, ultraviolet light (UV) or ozone, hydroxyl free radicals are formed. Hydroxyl radicals are one of the most reactive intermediate chemical species known and have a high reactivity towards a wide variety of organics. H_2O_2 + UV can destroy many of the more "difficult" organic pollutants, such as chlorinated solvents and benzene, and is well suited for waste water treatment situations where low discharge limits must be met. In addition to generating hydroxyl radicals from H_2O_2, UV light activates many organic molecules, which makes them more amenable to destruction by the hydroxyl radical.

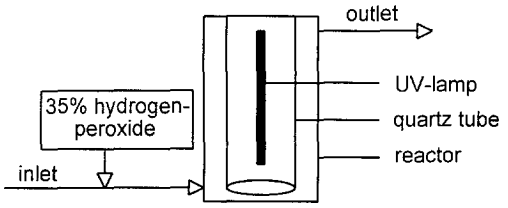

Figure 7.10: H_2O_2+ system

KEMIRA Chemicals B.V. (Rozenburg, The Netherlands) has made cost and size estimates for a H_2O_2+ system (see figure 7.10). The fixed capital investment "I" of the H_2O_2+ system is estimated at 1.5 times the cost estimate for the preassembled H_2O_2+ system including ancillary equipment (NLG 300,000 for 10 m³/h feed rate, NLG 2,100,000 for 100 m³/h feed rate). As mentioned in §7.4.2, the fixed capital investment "I" for the 100 m³/h case (10 times as many units) is estimated at seven times "I" for the 10 m³/h case. The treatment cost for H_2O_2+ are derived as follows:

		10 m³/h	100 m³/h
fixed capital investment "I" (NLG):		450,000	3,150,000
fixed annual charge at 20% of I:		90,000	630,000
maintenance & repair at 8% of I:		36,000	252,000
operating labour:		35,000	105,000
utilities:	hydrogen peroxide:	120,000	1,200,000
	electric power:	72,000	720,000
UV-lights replacements:		5,000	50,000
		---------- +	---------- +
annual treatment cost (NLG/y):		358,000	2,957,000
volume of treated water (m³/y):		80,000	800,000
treatment cost (NLG/m³):		4.5	3.7

The H_2O_2+ equipment for the 10 m³/h case consists of a 20 ft container (6m x 2.5m x 2.5m) and an outside 10 m³ buffer tank for pre-treatment of the waste water with H_2O_2 (without pre-treatment twice as much UV power has to be installed). The buffer tank is assumed to have a diameter of 2.3 m and a height of 2.5 m. For the 10 m³/h case the footprint of the system is approximately 30 m², assuming that the outside buffer tank is put directly against the 20 ft container. For the 100 m³/h case the containers and buffer tanks are stacked 2 high with an extra height of 1 m for stacking of the units. The maximum height is 6 m, the footprint is approximately 150 m².

Table 7.12: treatment cost and space requirements for H_2O_2+

H_2O_2+	10 m³/h	100 m³/h
treatment cost (NLG/m³)	4.5	3.7
footprint (m²)	30	150
maximum height (m)	2.5	6

7.4.6 Cost and size evaluation

Table 7.13 summarises the results of the cost and size estimates for all considered techniques. These values are particularly meant for mutual comparison of the considered techniques for comparable conditions. They are not intended nor suitable for financial calculations. Absolute values are dependent on specific actual conditions.

Table 7.13: summary of cost and size estimates

	10 m³/h			100 m³/h		
	treatment cost (NLG/m³)	footprint (m²)	maximum height (m)	treatment cost (NLG/m³)	footprint (m²)	maximum height (m)
GAC	3.4 (3.7)	17	3.3	1.5 (1.6)	57	3.5
PTA+	1.3 (1.4)	10	15	0.6 (0.6)	24	16
VSS	1.6	13	6	0.5	18	8
CFA	3.6 ↓	17	2.5	2.6 ↓	57	5
MPPE	2.4	11	3	0.4	19	4.2
BIO	2.0	35	2	0.6	150	2
PTAC	2.4	13	4.5	1.3	26	4.5
PVAP	3.2	18	4	2.4	40	4
TFA	2.9 (3.0)	20	4.5	2.0 (2.1)	50	4.5
H_2O_2+	4.5 ↓	30	2.5	3.7 ↓	150	6

Although much effort has been made to make reliable estimates for the given case, some comments could be made:

- For GAC, a clear cost driver for the 100 m³/h case is the replacement of carbon. The cost of granular activated carbon depends on the geographic location. Dutch prices are currently higher than US prices: liquid-phase carbon around 1.6 $/lb (gas-phase carbon around 2.4 $/lb), with a tendency of decreasing prices. Since the price for liquid-phase carbon can be 80% higher than used in the preliminary design calculations, the estimated treatment cost for GAC for the 100 m³/h case can be some 60% higher due to GAC replacement cost alone. GAC will probably have an accuracy between -20% and +80%. For PTA+, a clear cost driver for the 100 m³/h case is the operation and maintenance of GAC-treatment including on-site steam regeneration. These cost are relatively well known, and the calculated cost for this gas-phase GAC-treatment according to EPA's cost evaluation program is in reasonable agreement with cost estimates according to another practice related investigation for similar conditions (see §7.4.3). PTA+ will probably have an accuracy between -15% and +30%. The cost drivers for VSS and CFA are capital cost and steam consumption. These items are estimated with reasonable reliability, so the accuracy will lie between -15% and +30% as well.
- The accuracy of the other methods, based on information supplied by commercial organisations, is estimated at -20% to +60%.
- The figures in table 7.13 for CFA and H_2O_2+ are provided with a "↓"-sign to indicate that these figures will significantly decrease as the technology matures.

Treatment cost of other techniques like PVAP and TFA will also tend to decrease, but the potential margins are smaller than with CFA and H_2O_2+. For CFA cost (and size) figures can decrease substantially with the availability of more permeable silicone rubber foam resulting in a higher design velocity per unit, and with larger manufacturing tolerances resulting in lower cost of the main equipment (see later in this paragraph).

- Fixed capital investments for European conditions can be 10 to 15% higher than for United States conditions due to more sophisticated designs and higher labour cost [4]. The cost estimates for GAC, PTA+ and TFA for a fixed capital investment of 115% instead of 100% are given between brackets in table 7.13.
- The carbon use rate, especially for GAC, may be much higher in actual performance due to a reduction in bed life as a result of competing organics in the water and preadsorption of background organic matter onto the carbon, leading to higher treatment cost for practical conditions.
- For some of the separation techniques, depending on site-specific conditions recovered toluene may have to be disposed of as a toxic waste at a cost of approximately 0.5 NLG/kg. For each m^3 feed water, some 0.1 kg toluene concentrate is separated, possibly leading to an increase in treatment cost of 0.05 NLG/m^3. For other separation techniques recovered toluene may yield revenues of approximately 1 NLG/kg, resulting in a decrease in treatment cost of 0.1 NLG/m^3.
- For other VOCs than toluene or for cocktails of VOCs, cost and size estimates will have other results. When multiple contaminants must be removed, a number of performance calculations must point out which contaminant determines the equipment design.
- The assumed feed water temperature of 12°C is a good approximation for ground water treatment, but industrial waste water streams may have higher temperatures up to around 30°C before discharge. A higher feed water temperature can have both negative and positive effects on treatment cost for the various techniques.

Considering the above, it is obvious that for more accurate estimates the systems must be designed and analysed on a case-by-case basis, taking into account site-specific conditions.

The results from Van Zee's study on cost effectiveness for countercurrent fiber sorption for 100 m^3/h [26] cannot be compared to the results according to table 7.13. Van Zee uses silicone rubber fibers instead of foam and he uses a feed concentration of 530 wt.ppm instead of 100 wt.ppm toluene, resulting in quite different equipment dimensions and process conditions.

Continuous discharge of waste water containing 100 wt.ppm toluene (this is "doing nothing") would cost less than any of the considered separation techniques: approximately 0.25 NLG/m^3 will be charged by public authorities (The Netherlands), based on 2,500 inhabitant equivalents (IE) at 90 NLG/IE in case of 2,400 m^3/day. However, discharge of this waste water is not allowed, except for some companies under the supervision of the government.

For the 10 m³/h case, PTA+ has the lowest treatment cost (1.3 NLG/m³), but compared with all the other techniques this is accompanied by a large height. The cheapest techniques besides PTA+ have treatment cost between 1.6 and 2.4 NLG/m³. CFA stands out neither on cost nor on size. A number of other techniques are cheaper without large differences in size compared with CFA. All three traditional techniques have lower treatment cost than CFA.
However, for CFA a reduction in fixed capital investment by a factor 3 can be realised by doubling the liquid velocity (approximately 2 cm/s instead of approximately 1 cm/s) and by increasing the manufacturing tolerances of the static cylinder and rotating housing resulting in lower cost per kilogram of main equipment (approximately 150 NLG/kg instead of approximately 300 NLG/kg). A maximum liquid velocity of 2 cm/s is expected to be feasible when cellular silicone is optimised (research effort) for CFA application. The high cost of 300 NLG/kg for the main equipment according to the design of Chapter 6 can be largely attributed to the grinding tolerances prescribed by the supplier of the teflon seals to ensure correct sealing and low wear rates. As a consequence, the large static cylinder (Ø1 m x 1 m) alone requires 3 to 4 weeks of machining in a specialised workshop. Since the prescribed tolerances are probably well on the safe side and small leakage can be allowed without compromising the required removal efficiency (see Chapter 6), it is probably much better to assume a more realistic cost per kilogram of main equipment of 150 NLG/kg for further developed equipment. As a result, the treatment cost for CFA for the 10 m^3/h case can be reduced to approximately 2.0 NLG/m^3, positioning CFA in the top three separation techniques for the regarding case.

For the 100 m³/h case PTA+, VSS, MPPE and BIO have the lowest cost (0.4 to 0.6 NLG/m³). However, PTA+ is accompanied by a large height and for BIO the footprint of the system is quite large. MPPE is most attractive on both cost and size. Again, CFA stands out neither on cost nor on size for this case. All traditional techniques have lower treatment cost than CFA, VSS has also a smaller footprint than CFA without the large height of the PTA+ system.
The treatment cost for CFA have to be reduced to around 0.5 NLG/m^3 to be competitive, but due to the high cost of steam regeneration alone (see §7.4.4) this can never be achieved.

Although GAC (together with PTA+) is "Best Available Technology" for treatment of VOCs in water according to the U.S. EPA, GAC is less attractive than the traditional VSS technique with respect to cost and size for both the 10 m³/h case and the 100 m³/h case. This can be attributed to the relatively high feed concentration of 100 wt.ppm toluene, causing a relatively high liquid-phase carbon usage rate.

7.5 Other selection criteria

Besides cost and size, some other quantifiable criteria can be valid, for instance fixed capital investment and weight. For techniques with not too different treatment cost, a lower capital investment can be more attractive than lower treatment cost. The weight of

a system can be important for example for offshore applications and is roughly related to the size of the system.

Besides quantifiable criteria like cost and size, other criteria that are more difficult to quantify are also important to evaluate the attractiveness of a separation technique for VOC-removal from waste water. The most important of these criteria are evaluated in table 7.14:

Table 7.14: other selection criteria

	reliability	removing higher concentrations	higher removal efficiency	smaller flow rate	range of contaminants to be handled
GAC	+	-	+	-	+
PTA+	+	-	+	-	-
VSS	+	+	+	-	-
CFA	-	+	0	+	-
MPPE	+	+	+	-	+
BIO	-	-	-	-	+
PTAC	0	+	+	-	+
PVAP	0	+	0	+	-
TFA	0	+	-	+	-
H_2O_2+	0	-	+	+	+

+: more competitive
0: neutral
-: less competitive

As mentioned before in section 7.2, reliability of the separation system (including the response to sudden disturbances in flow rate or inlet concentration) is extremely important. For this reason, for a new technique using relatively complex equipment it is difficult to be accepted. The market is sceptic about the use of moving parts as with CFA (check valves, transported sorbent material, moving seals) compared with simple static packed beds as with GAC.
For higher feed concentrations (for instance 1000 wt.ppm instead of 100 wt.ppm), higher removal efficiencies (for instance 99.9% instead of 99%) and smaller flow rates (for instance 1 m^3/h instead of 10 or 100 m^3/h), the attractiveness of the various techniques relative to one another will be significantly different as can be seen from table 7.14. The change in competitiveness for smaller flow rates can be derived as a matter of fact from the change in cost and size estimates from 100 to 10 m^3/h flow rate (see table 7.13).
Some techniques will be relatively more competitive than other techniques when more contaminants, for instance a mixture of volatile and less volatile organic compounds, have to be removed. H_2O_2+ can remove both volatile and less volatile organic compounds in one single step. Depending on the application, this can be a decisive advantage. GAC, MPPE and PTAC can remove various contaminants as well, but they have to take into account possible implications for the regeneration section of the

system. When reticulated polyurethane foam is used as supporting packing material (BIOPUR®), both water and air can be purified in one step with the biorotor [27].

The reliability of CFA, which is relatively low compared to the other techniques as can be seen from table 7.14, will improve with field testing and subsequent improvements. According to table 7.14, the competitive potential of CFA lies more within applications with higher concentrations and smaller flow rates. The main competitors from the techniques considered in this evaluation will then be PVAP and TFA.

The restriction of the liquid velocity through the cellular silicone is one of the main reasons why the expected competitiveness of CFA with larger flow rates (section 7.2) has not been demonstrated. Accordingly, an important advance in competitiveness of CFA can be achieved by a higher allowable liquid velocity through the foam. However, the appropriate cellular silicone is not yet available.

Besides the criteria discussed so far, sometimes other criteria have to be taken into consideration as well. For instance, the modular systems (CFA, BIO, PTAC, PVAP, TFA and H_2O_2+) can easily be adapted to long lasting or permanent changes in feed water flow rate, feed water concentrations or removal efficiency as opposed to the systems using cylindrical columns (GAC, PTA+, VSS and MPPE). The extent to which a separation technique can be fitted into an existing process can be a criterion as well. For projects of short duration, start-up time is a valid criterion.

Sometimes, a number of otherwise important criteria are no longer important. For instance, for projects outdoors the relatively large footprint of biorotor systems is no longer significant and treatment cost can be the decisive criterion.

As already mentioned in §7.4.6, again it is obvious that in practice alternative systems must be evaluated on a case-by-case basis, taking into account site-specific conditions.

7.6 Alternative applications

It is useful to investigate the possibilities of using CFA for other applications or to even use the developed countercurrent equipment with a different process scheme (and with other packing materials if necessary) to be able to access other and potentially more important or more attractive markets. Besides the competition on cost and size and on other criteria such as reliability (simplicity) by other techniques (see sections 7.4 and 7.5), penetration of the market for VOC-removal is even more difficult because the market for these end-of-pipe techniques is reaching saturation. The future is to in-process-recycling rather than to end-of-pipe techniques. It is appropriate to try to cover other potential applications besides VOC-removal from water. Some suggestions are:

- removal of VOCs from air (bigger market)
- dewatering of solvents using hydrophilic absorption material
- heavy metal extraction from waste water using ion-exchange material

- protein recovery and antibiotics recovery from dedicated streams using highly selective sorption materials (accustomed to more sophisticated equipment)

Especially application of high selectivity sorption materials offers good perspectives to utilise the advantages of CFA at the most, since major challenges are often the removal of small quantities of material from large streams and the increase of volumetric productivity of separation equipment. Substantial improvements in these parameters may be obtained by combining CFA with more than one separation principle in a new process. The food industry shows an increasing demand to separate very specific components at low concentrations. The chemical, pharmaceutical and food- and beverage-industries consider high-selective sorption (together with membrane technology) essential to many future applications.

7.7 Conclusions

For our target application, removing dissolved toluene from water at flow rates of 10 m^3/h or 100 m^3/h, a concentration of 100 wt.ppm and a removal efficiency of 99%, cost and size estimates for Countercurrent Foam Absorption (CFA) lie within the margins set by the other applicable techniques, but CFA stands out neither on cost nor on space requirements. The economic attractiveness of CFA for VOC-removal from waste water will depend on site-specific conditions.
CFA can become more attractive if the allowable water velocity in the packed bed increases and the manufacturing cost of the main equipment decreases. A higher water velocity will require sorbent material with an optimised cellular structure (research effort). Also, CFA will be more competitive for higher concentrations and smaller flow rates. For a flow rate of 10 m^3/h, CFA will be competitive with the other techniques for the regarding application assuming a water velocity of approximately 2 cm/s (cellular silicone optimised for CFA application) and assuming a cost per kilogram of main equipment of approximately 150 NLG/kg (increased manufacturing tolerances).
Economically more attractive applications for countercurrent sorption equipment may be found in high selective sorption.

References

[1] Smallwood, I., *Solvent recovery handbook*, Arnold, London, 1993, ISBN 0-340-57467-4

[2] *Milieukosten van bedrijven 1993*, Centraal Bureau voor de Statistiek, Voorburg / Heerlen, 1996

[3] Based on discussions with several experienced people, 1996

[4] Communication with D.Th. Meijer, Akzo Nobel Nederland / MPP Systems, 1996

[5] Communication with J.M. van der Worp, TNO-MEP, 1996

[6] Graveland, A., *Biologisch actieve koolfiltratie in Weesperkarspel in gebruik*, H_2O, **26** (1993). pp. 312-315

[7] Communication with D. Bijstra, RIZA, 1996

[8] Roques, H. (Ed.), *Chemical water treatment; principles and practice*, VCH Publishers Inc., New York, 1996, ISBN 1-56081-518-3

[9] *DACE-prijzenboekje; kostengegevens t.b.v. ramingen (18th ed.)*, Dutch Association of Cost Engineers, Leidschendam, 1995

[10] Ram, N.M., Christman, R.F., Cantor, K.P., *Significance and treatment of volatile organic compounds in water*, Lewis, Chelsea, 1990, ISBN 0-87371-123-8

[11] Stenzel, M.H., *Remove organics by activated carbon adsorption*, Chem.Eng.Progr., April 1993, pp. 36-43

[12] Clark, R.M., Adams, J.Q., *EPA's drinking water and groundwater remediation evaluation; granular activated carbon*, Lewis, Chelsea, 1991, ISBN 0-87371-353-2

[13] Stenzel, M.H., Gupta, U.S., *Treatment of contaminated groundwaters with granular activated carbon and air stripping*, JAPCA, **35** (1985), pp. 1304-1309

[14] Adams, J.Q., Clark, R.M., *Evaluating the costs of packed-tower aeration and GAC for controlling selected organics*, JAWWA, **83** (1991), pp. 49-57

[15] Chidgopkar, V.R., *Applying Henry's law to groundwater treatment*, Pollution Engineering, March 1996, pp. 48-51

[16] Nyer, E.K., *Groundwater treatment technology (2nd ed.)*, Van Nostrand Reinhold, New York, 1992, ISBN 0-442-00562-8

[17] Clark, R.M., Adams, J.Q., *EPA's drinking water and groundwater remediation cost evaluation; air stripping*, Lewis, Chelsea, 1991, ISBN 0-87371-352-4

[18] Mukhopadhyay, N., Moretti, E.C., *Current and potential future industrial practices for reducing and controlling volatile organic compounds*, AIChE, New York, 1993, ISBN 0-8169-0615-7

[19] Yaws, C.L., Biu, L., Nijhawan, S., *Calculate the solubility of aromatics*, Chemical Engineering, February 1995, pp. 113-115

[20] Timmermans, J., *Physico-chemical constants of pure organic compounds*, Elsevier Publishing Company, Amsterdam, 1950

[21] Perry, R.H., Green, D.W., Maloney, J.O., *Perry's Chemical Engineers' Handbook (6th ed.)*, McGraw-Hill Book Co, Singapore, 1984, ISBN 0-07-066482-X

[22] Sinnot, R.K., *Coulson & Richardson's Chemical Engineering, Volume 6 (2nd ed.)*, Pergamon Press, Oxford, 1993, ISBN 0-08-041866x

[23] Klaassen, R., Jansen, A.E., Oesterholt, F.I.H.M., Bult, B.A., *Pertraction of hydrocarbons from waste water streams - final report*, Novem B.V., Utrecht, 1994, 94-039/112329-23127

[24] EnviroSep Inc., *Thick film equilibrium process and device*, International Patent WO 94/23814, 1994

[25] EnviroSep Inc., *Removing volatile and non-volatile organic in a thick film equilibrium process and device*, United States Patent 5,472,613, 1995

[26] Zee, G. van, *Counter current sorption using fiber sorbents (Ph.D.-thesis)*, Delft University Press, 1996, ISBN 90-407-1328-6

[27] Marsman, E.H., Appelman, J.J.M., Bult, B.A., Urlings, L.G.C.M., *Praktijkervaring met biofilmreactoren voor zuivering van grondwater verontreinigd met organische microverontreinigingen*, H_2O, **28** (1995), pp. 258-261

8

Conclusions

This research demonstrates the technical feasibility of continuous countercurrent sorption equipment using mechanical transport of the sorbent bed. The removal of low concentrations of VOCs dissolved in water was used as a model system. Silicone rubber proved to be the choice sorbent material, combining resistance to steam regeneration and availability of fiber and foam structures with a high diffusion coefficient for VOCs. A pilot unit was constructed which proved the correct functioning of continuous countercurrent equipment using mechanical transport of the sorbent bed. A design study showed that the pilot unit can be scaled up. The sorbent is packed in a rotating annulus and divided into a number of segments. Countercurrent operation is achieved by self-sealing non-return valves integrated in the sorbent between the different bed segments. This principle has been patented. The intended reduction in equipment size relative to traditional techniques has not been achieved yet due to limitations of the allowable liquid velocity for available silicone rubber fiber or foam beds. The economic feasibility of the process is limited by the allowable liquid velocity as well. The liquid velocity is limited by compressibility, pressure drop and dispersion of the packed bed. The economic feasibility will be higher for more homogeneous and more permeable fiber or foam bed structures, higher concentrations and smaller flow rates. For VOC-removal from water the process will be competitive for smaller flow rates with sorbent material optimised for the application and using further developed equipment with lower manufacturing cost.

Appendices

A.1 Linear elastic material behaviour

Linear elastic transversal isotropic material behaviour:

$$\begin{bmatrix} e_1 \\ e_2 \\ e_3 \\ e_4 \\ e_5 \\ e_6 \end{bmatrix} = \begin{bmatrix} \frac{1}{E_L} & -\frac{\nu_{TL}}{E_T} & -\frac{\nu_{TL}}{E_T} & 0 & 0 & 0 \\ -\frac{\nu_{TL}}{E_T} & \frac{1}{E_T} & -\frac{\nu_{TT}}{E_T} & 0 & 0 & 0 \\ -\frac{\nu_{TL}}{E_T} & -\frac{\nu_{TT}}{E_T} & \frac{1}{E_T} & 0 & 0 & 0 \\ 0 & 0 & 0 & \frac{1+\nu_{TT}}{E_T} & 0 & 0 \\ 0 & 0 & 0 & 0 & \frac{1}{G_{LT}} & 0 \\ 0 & 0 & 0 & 0 & 0 & \frac{1}{G_{LT}} \end{bmatrix} \cdot \begin{bmatrix} \sigma_1 \\ \sigma_2 \\ \sigma_3 \\ \sigma_4 \\ \sigma_5 \\ \sigma_6 \end{bmatrix}$$

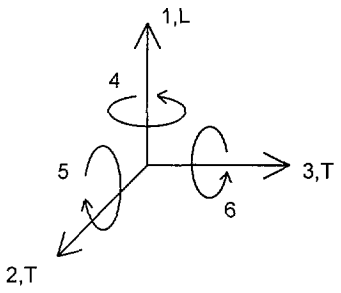

$$\begin{bmatrix} \sigma_1 \\ \sigma_2 \\ \sigma_3 \\ \sigma_4 \\ \sigma_5 \\ \sigma_6 \end{bmatrix} = \begin{bmatrix} E_L E_T \frac{(\nu_{TT}-1)}{(E_T \nu_{TT} - E_T + 2\nu_{TL}^2 E_L)} & -E_L E_T \frac{\nu_{TL}}{(E_T \nu_{TT} - E_T + 2\nu_{TL}^2 E_L)} & -E_L E_T \frac{\nu_{TL}}{(E_T \nu_{TT} - E_T + 2\nu_{TL}^2 E_L)} & 0 & 0 & 0 \\ E_L E_T \frac{\nu_{TL}}{(E_T \nu_{TT} - E_T + 2\nu_{TL}^2 E_L)} & E_T \frac{(E_T + \nu_{TL}^2 E_L)}{[(1+\nu_{TT})(E_T \nu_{TT} - E_T + 2\nu_{TL}^2 E_L)]} & -E_T \frac{(E_T \nu_{TT} + \nu_{TL}^2 E_L)}{[(1-\nu_{TT})(E_T \nu_{TT} - E_T + 2\nu_{TL}^2 E_L)]} & 0 & 0 & 0 \\ -E_L E_T \frac{\nu_{TL}}{(E_T \nu_{TT} - E_T - 2\nu_{TL}^2 E_L)} & -E_T \frac{(E_T \nu_{TT} + \nu_{TL}^2 E_L)}{[(1+\nu_{TT})(E_T \nu_{TT} - E_T + 2\nu_{TL}^2 E_L)]} & E_T \frac{(E_T - \nu_{TL}^2 E_L)}{[(1+\nu_{TT})(E_T \nu_{TT} - E_T + 2\nu_{TL}^2 E_L)]} & 0 & 0 & 0 \\ 0 & 0 & 0 & \frac{E_T}{(1+\nu_{TT})} & 0 & 0 \\ 0 & 0 & 0 & 0 & G_{LT} & 0 \\ 0 & 0 & 0 & 0 & 0 & G_{LT} \end{bmatrix} \cdot \begin{bmatrix} e_1 \\ e_2 \\ e_3 \\ e_4 \\ e_5 \\ e_6 \end{bmatrix}$$

G_{LT} is the shear factor [N/m^2].

Linear elastic isotropic material behaviour:

$$\begin{bmatrix} e_1 \\ e_2 \\ e_3 \\ e_4 \\ e_5 \\ e_6 \end{bmatrix} = \frac{1}{E} \begin{bmatrix} 1 & -\nu & -\nu & 0 & 0 & 0 \\ -\nu & 1 & -\nu & 0 & 0 & 0 \\ -\nu & -\nu & 1 & 0 & 0 & 0 \\ 0 & 0 & 0 & 1+\nu & 0 & 0 \\ 0 & 0 & 0 & 0 & 1+\nu & 0 \\ 0 & 0 & 0 & 0 & 0 & 1-\nu \end{bmatrix} \begin{bmatrix} \sigma_1 \\ \sigma_2 \\ \sigma_3 \\ \sigma_4 \\ \sigma_5 \\ \sigma_6 \end{bmatrix}$$

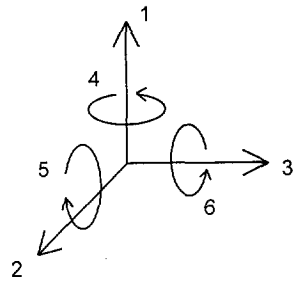

$$\begin{bmatrix} \sigma_1 \\ \sigma_2 \\ \sigma_3 \\ \sigma_4 \\ \sigma_5 \\ \sigma_6 \end{bmatrix} = \frac{E}{(1+\nu)\cdot(1-2\cdot\nu)} \begin{bmatrix} 1-\nu & \nu & \nu & 0 & 0 & 0 \\ \nu & 1-\nu & \nu & 0 & 0 & 0 \\ \nu & \nu & 1-\nu & 0 & 0 & 0 \\ 0 & 0 & 0 & 1-2\cdot\nu & 0 & 0 \\ 0 & 0 & 0 & 0 & 1-2\cdot\nu & 0 \\ 0 & 0 & 0 & 0 & 0 & 1-2\cdot\nu \end{bmatrix} \begin{bmatrix} e_1 \\ e_2 \\ e_3 \\ e_4 \\ e_5 \\ e_6 \end{bmatrix}$$

A.2 Friction coefficients

The friction coefficient between wet fiber or foam material and perspex, used in the modelling of the validating flow tests of §2.3.3, was determined using the equipment shown in figure A.1:

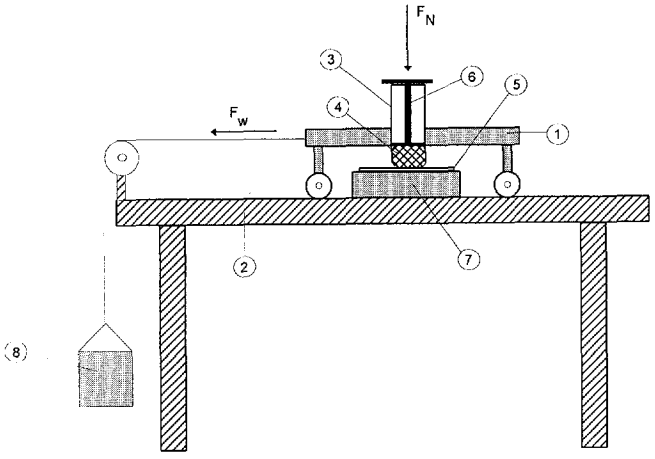

1	Lorry
2	Frame
3	Tube
4	Fibers or foam
5	Perspex plate
6	Stamp
7	Balance
8	Weight

Figure A.1: Equipment for friction tests

The equipment consists of a lorry that can roll over a polished stiff frame, levelled by adjustable table legs. A tube with square cross-section (50 mm x 50 mm) is fixed to the lorry. The tube is filled with a certain amount of fiber or foam material which is then enclosed between a perspex plate beneath the tube and a stamp which compresses the enclosed material. The stamp consists of a bottom plate 48 mm square and a top plate which touches the topside of the tube after compression of the enclosed material. This compression is achieved by additional steel plates covering the top plate of the stamp. The porosity of the enclosed material and consequently the normal force F_N (derived from the weight acting on the balance) required to compress it to its fixed volume between the bottom plate of the stamp and the perspex plate, is varied by the amount of fiber or foam material. The perspex plate under the tube is attached to a balance, which is fixed to the frame. The gap between the bottom of the tube and the perspex plate is approximately 1 mm.
A force F_W normal to F_N is applied at the centre of gravity of the lorry by a bucket filled with water. F_W is gradually increased by pouring water into the bucket until the lorry starts moving. At this point, the static friction coefficient μ is determined as the ratio between F_W and F_N. The friction force F_W is corrected for the rolling resistance of the lorry, which was determined separately for different weights of the lorry (different amounts of steel plates covering the top plate of the stamp). For friction between perspex and the used fiber and foam materials, wetted by pouring water into the tube, the friction coefficient μ appears to be constant over the range of applied porosities and accompanying values of F_N. The results are given in table A.1:

Table A.1: static friction coefficient μ on perspex, wet:

material	supplier	μ
PP-100 fibers	Polyost, Belgium	0.14
PP-65 fibers	"	0.2
PET fibers	"	0.19
PUR foam	Recticel, Belgium	0.65
cellular silicone	Dow Corning, Germany	0.65

A.3 Modelling of validating flow tests

PP-100 FIBERS

$L := 0.735$ initial packed bed length [m]

$i := 25$ number of bed segments [-]

$\varepsilon_0 := 0.965$ uncompressed porosity [-]

$\varepsilon := 0.85, 0.851 .. \varepsilon_0$ packed bed porosity [-]

$e_1 := 0.65$ precompressive strain [-]

$\varepsilon_1 := \frac{\varepsilon_0 - e_1}{1 - e_1}$ precompressed porosity [-]

$1000 \cdot \varepsilon_1 = 900$

$\sigma_1 := 120 \cdot \left[\left(\frac{1}{1 - e_1} \right)^3 - 1 \right]$ precompressive stress [N/m^2]

$\sigma_1 = 2.679 \cdot 10^3$

$L(\varepsilon) := \frac{L}{i} \cdot \frac{1 - \varepsilon_1}{1 - \varepsilon}$ bed segment length as a function of porosity [m]

$u := 0.12$ superficial liquid velocity [m/s]

$d := 100 \cdot 10^{-6}$ equivalent fiber diameter for foam [m]

$\eta := 10^{-3}$ dynamic viscosity of water [N.s/m^2]

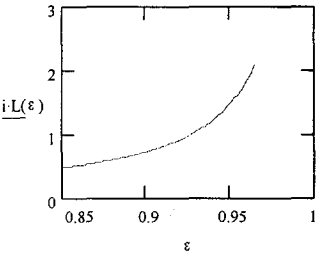

$$S(\varepsilon) := \frac{80}{3} \cdot \eta \cdot u \cdot \frac{1 - \varepsilon}{(-\ln(1 - \varepsilon) - 0.931) \cdot d^2} \cdot L(\varepsilon)$$

pressure drop [N/m^2]

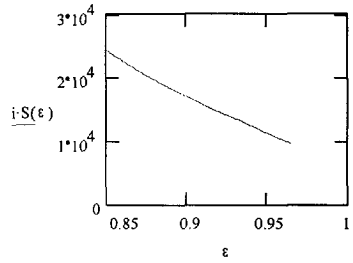

$$\varepsilon(P) := (P \geq 2687) \cdot \left[1 - (1 - \varepsilon_0) \cdot \left(1 + \frac{P}{120} \right)^{0.333} \right] + (P < 2687) \cdot \varepsilon_1$$

porosity as a function of pressure [-]

$1000 \cdot \varepsilon(2687) = 900.008$

PP-100 FIBERS (continued)

$P := 0, 100 .. 6000$ pressure acting on a bed segment [N/m ^{2}]

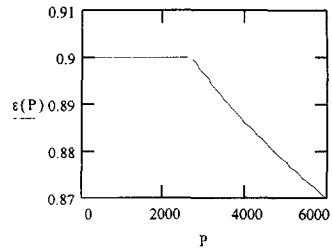

$D := 0.06$ tube diameter [m]

$\mu := 0.14$ friction coefficient [-]

$\nu := 0.31$ Poisson's constant [-]

$W(P) := \frac{4}{D} \cdot \mu \cdot \frac{\nu}{1 - \nu} \cdot \left[\sigma_1 + (P \geq 0) \cdot P \right] \cdot L(\varepsilon(P))$ wall friction term [N/m ^{2}]

$P := 0, 100 .. 3000$

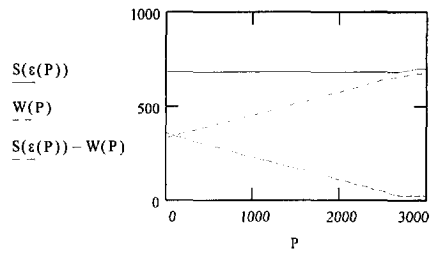

$j := 1 .. i$

$P_0 := 0$

$P_j := \left[\sum_{f=1}^{j} \left(S\left(\varepsilon\left(P_f\right)\right) - W\left(P_f\right) \right) \right]$ pressure acting on a bed segment [N/m ^{2}]

$\Delta P_j := \sum_{f=1}^{j} S\left(\varepsilon\left(P_f\right)\right)$

$\Delta P_i = 1.717 \cdot 10^4$ pressure drop of the test tube [N/m ^{2}]

$\varepsilon\left(P_i\right) = 0.899$ porosity of the bed segment nearest to the sieve plate [-]

$Z_j := \sum_{f=j}^{i} L\left(\varepsilon\left(P_f\right)\right)$

$Z_1 = 0.734$

total length of the packed bed subject to liquid flow [m]

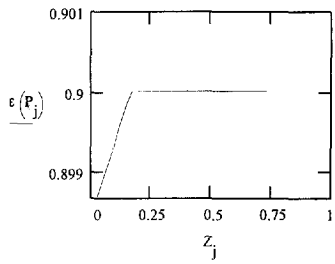

PP-100 FIBERS
(continued)

$S_j := S(\varepsilon(P_j))$ $W_j := W(P_j)$

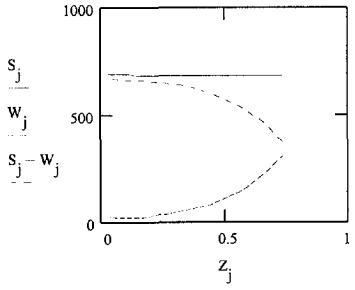

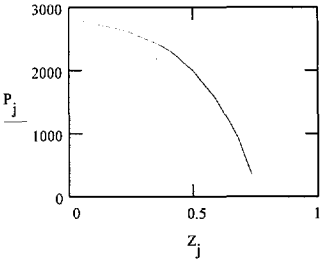

PP-65 FIBERS

$L := 0.56$ initial packed bed length [m]

$i := 25$ number of bed segments [-]

$\varepsilon_0 := 0.965$ uncompressed porosity [-]

$\varepsilon := 0.85, 0.851 .. \varepsilon_0$ packed bed porosity [-]

$e_1 := 0.65$ precompressive strain [-]

$\varepsilon_1 := \frac{\varepsilon_0 - e_1}{1 - e_1}$ precompressed porosity [-]

$1000 \cdot \varepsilon_1 = 900$

$\sigma_1 := 100.7 \cdot \left[\left(\frac{1}{1 - e_1}\right)^3 - 1\right]$ precompressive stress [N/m^2]

$\sigma_1 = 2.248 \cdot 10^3$

$L(\varepsilon) := \frac{L}{i} \cdot \frac{1 - \varepsilon_1}{1 - \varepsilon}$ bed segment length as a function of porosity [m]

$u := 0.07$ superficial liquid velocity [m/s]

$d := 65 \cdot 10^{-6}$ equivalent fiber diameter for foam [m]

$\eta := 10^{-3}$ dynamic viscosity of water [N.s/m^2]

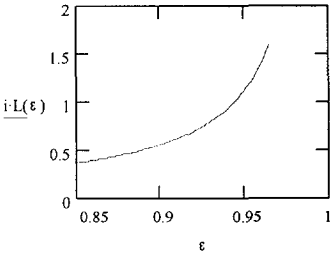

PP-65 FIBERS
(continued)

$$S(\varepsilon) := \frac{80}{3}\cdot\eta\cdot u\cdot\frac{1-\varepsilon}{(-\ln(1-\varepsilon)-0.931)\cdot d^2}\cdot L(\varepsilon)$$

pressure drop [N/m^2]

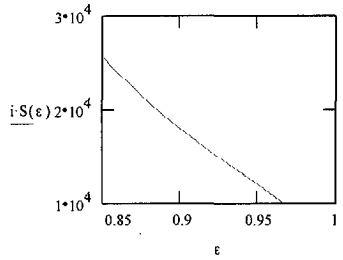

$$\varepsilon(P) := (P\geq 2255)\cdot\left[1-(1-\varepsilon_0)\cdot\left(1+\frac{P}{100.7}\right)^{0.333}\right]+(P<2255)\cdot\varepsilon_1$$ porosity as a function of pressure [-]

$1000\,\varepsilon(2255) = 900.006$

$P := 0, 100..4000$ pressure acting on a bed segment [N/m^2]

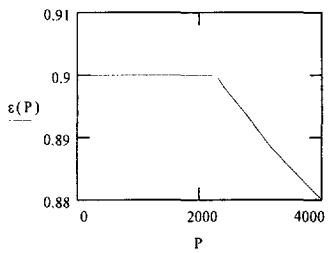

$D := 0.06$ tube diameter [m]

$\mu := 0.2$ friction coefficient [-]

$\nu := 0.34$ Poisson's constant [-]

$$W(P) := \frac{4}{D}\cdot\mu\cdot\frac{\nu}{1-\nu}\cdot\left[\sigma_1+(P\geq 0)\cdot P\right]\cdot L(\varepsilon(P))$$ wall friction term [N/m^2]

$P := 0, 100..3000$

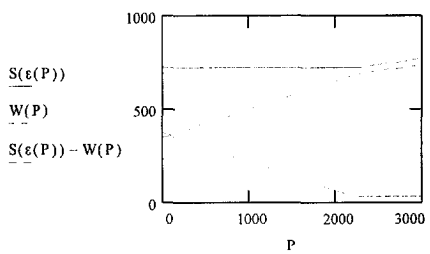

$j := 1..i$

$P_0 := 0$

$$P_j := \left[\sum_{f=1}^{j}\left(S\left(\varepsilon\left(P_f\right)\right)-W\left(P_f\right)\right)\right]$$ pressure acting on a bed segment [N/m^2]

PP-65 FIBERS
(continued)

$$\Delta P_j := \sum_{f=1}^{j} S\left(\varepsilon\left(P_f\right)\right)$$

$$Z_j := \sum_{f=j}^{i} L\left(\varepsilon\left(P_f\right)\right)$$

$\Delta P_i = 1.815 \cdot 10^4$ pressure drop of the test tube [N/m^2]

$\varepsilon\left(P_i\right) = 0.896$ porosity of the bed segment nearest to the sieve plate [-]

$Z_1 = 0.555$

total length of the packed bed subject to liquid flow [m]

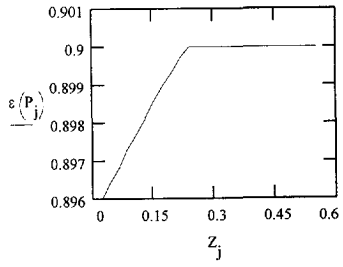

$S_j := S\left(\varepsilon\left(P_j\right)\right)$ $W_j := W\left(P_j\right)$

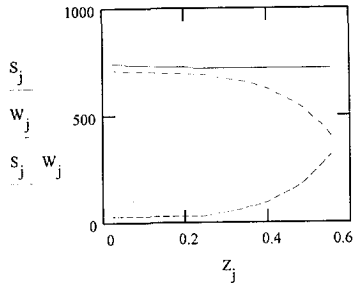

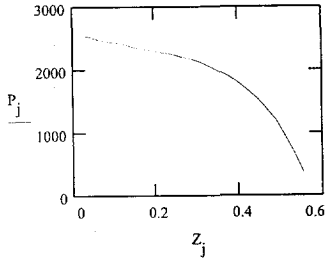

PET FIBERS

$L := 0.375$ initial packed bed length [m]

$i := 25$ number of bed segments [-]

$\varepsilon_0 := 0.98$ uncompressed porosity [-]

$\varepsilon := 0.85, 0.851 .. \varepsilon_0$ packed bed porosity [-]

$e_1 := 0.8$ precompressive strain [-]

$$\varepsilon_1 := \frac{\varepsilon_0 - e_1}{1 - e_1}$$ precompressed porosity [-]

$$1000 \cdot \varepsilon_1 = 900$$

$$\sigma_1 := 68 \cdot \left[\left(\frac{1}{1 - e_1} \right)^3 - 1 \right]$$ precompressive stress [N/m^2]

$$\sigma_1 = 8.432 \cdot 10^3$$

$$L(\varepsilon) := \frac{L}{i} \cdot \frac{1 - \varepsilon_1}{1 - \varepsilon}$$ *bed segment length as a function of porosity* [m]

$u := 0.012$ superficial liquid velocity [m/s]

$d := 15 \cdot 10^{-6}$ equivalent fiber diameter for foam [m]

$\eta := 10^{-3}$ dynamic viscosity of water [N.s/m^2]

$$S(\varepsilon) := \frac{80}{3} \cdot \eta \cdot u \cdot \frac{1 - \varepsilon}{(-\ln(1 - \varepsilon) - 0.931) \cdot d^2} \cdot L(\varepsilon)$$

pressure drop [N/m^2]

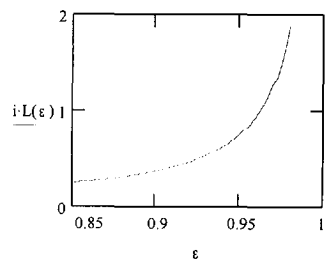

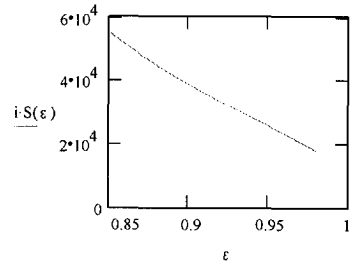

PET FIBERS
(continued)

$\varepsilon(P) := (P \geq 8476)\cdot\left[1 - \left(1 - \varepsilon_0\right)\cdot\left(1 + \frac{P}{68}\right)^{0.333}\right] + (P < 8476)\cdot\varepsilon_1$ porosity as a function of pressure [-]

$1000\,\varepsilon(8476) = 899.989$

$P := 0, 100 .. 150000$ pressure acting on a bed segment [N/m^2]

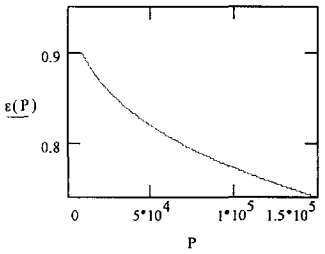

$D := 0.06$ tube diameter [m]

$\mu := 0.19$ friction coefficient [-]

$\nu := 0.3$ Poisson's constant [-]

$W(P) := \frac{4}{D}\cdot\mu\cdot\frac{\nu}{1-\nu}\cdot\left[\sigma_1 + (P \geq 0)\cdot P\right]\cdot L(\varepsilon(P))$ wall friction term [N/m^2]

$P := 0, 100 .. 10000$

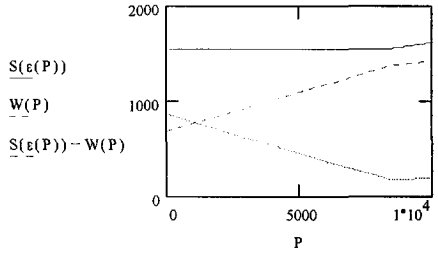

$j := 1 .. i$

$P_0 := 0$

$P_j := \left[\sum_{f=1}^{j}\left(S\left(\varepsilon\left(P_f\right)\right) - W\left(P_f\right)\right)\right]$ pressure acting on a bed segment [N/m^2]

$\Delta P_j := \sum_{f=1}^{j} S\left(\varepsilon\left(P_f\right)\right)$

$\Delta P_i = 3.907\cdot 10^4$ pressure drop of the test tube [N/m^2]

$\varepsilon\left(P_i\right) = 0.896$ porosity of the bed segment nearest to the sieve plate [-]

PET FIBERS
(continued)

$$Z_j := \sum_{f=j}^{i} L\left(\varepsilon\left(P_f\right)\right)$$

$Z_1 = 0.373$

total length of the packed bed subject to liquid flow [m]

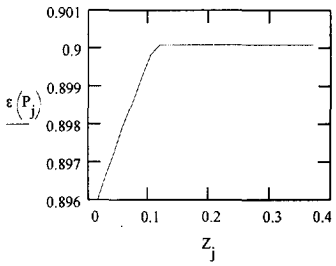

$S_j := S\left(\varepsilon\left(P_j\right)\right) \qquad W_j := W\left(P_j\right)$

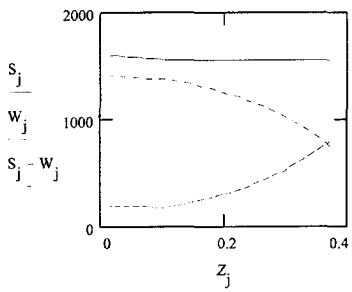

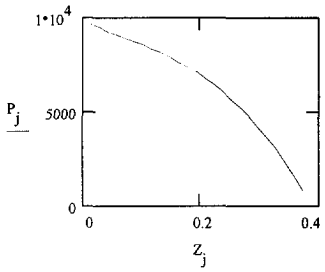

PUR FOAM

$L := 0.27$	initial packed bed length [m]	$\varepsilon_0 := 0.972$	uncompressed porosity [-]
$i := 25$	number of bed segments [-]	$\varepsilon := 0.9, 0.901 .. \varepsilon_0$	packed bed porosity [-]
		$e_1 := 0.34884$	precompressive strain [-]
		$\varepsilon_1 := \frac{\varepsilon_0 - e_1}{1 - e_1}$	precompressed porosity [-]

$$1000 \cdot \varepsilon_1 = 957$$

$\sigma_1 := 2.71 \cdot 10^4 \cdot \left[0.1 \cdot \left(e_1\right)^{-1.03} + 4.07 \cdot \left(e_1\right)^{10.93}\right] \cdot e_1$ precompressive stress [N/m^2]

$$\sigma_1 = 2.797 \cdot 10^3$$

PUR FOAM
(continued)

$L(\varepsilon) := \frac{L}{i} \cdot \frac{1 - \varepsilon_1}{1 - \varepsilon}$ bed segment length as a function of porosity [m]

$u := 0.018$ superficial liquid velocity [m/s]

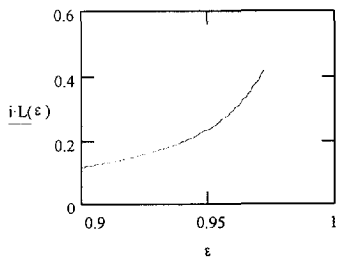

$d_{eq} := 8.5 \cdot 10^{-6}$ equivalent fiber diameter for foam [m]

$\eta := 10^{-3}$ dynamic viscosity of water [N.s/m^2]

$C_1 := 29.6$ structural parameter [-]

$S(\varepsilon) := C_1 \cdot \frac{\eta \cdot u \cdot (1 - \varepsilon)^2}{\varepsilon^3 \cdot d_{eq}^2} \cdot L(\varepsilon)$ pressure drop [N/m^2]

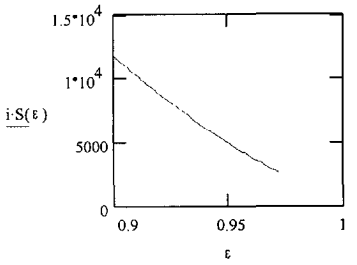

$\varepsilon(P) := (P > 3656) \cdot \left[0.93924 + \frac{28941 \cdot (\ln(P))}{P^2} \right] + (P \leq 3656) \cdot 0.957$ porosity as a function of pressure [-]

$1000 \cdot \varepsilon(3656) = 957$

$P := 0, 100 .. 5000$ pressure acting on a bed segment [N/m^2]

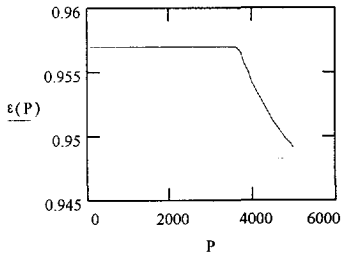

$D := 0.06$ tube diameter [m]

$\mu := 0.65$ friction coefficient [-]

$\nu(\varepsilon) := 0$ Poisson's constant [-]

$W(P) := \frac{4}{D} \cdot \mu \cdot \frac{\nu(\varepsilon(P))}{1 - \nu(\varepsilon(P))} \cdot \left[\sigma_1 + (P \geq 0) \cdot P \right] \cdot L(\varepsilon(P))$ wall friction term [N/m^2]

PUR FOAM
(continued)

$P := 0, 100 .. 4000$

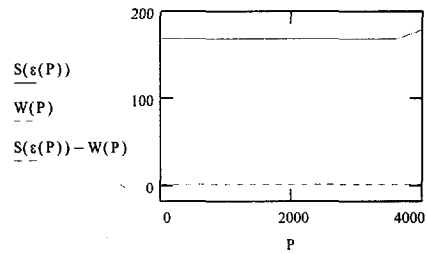

$j := 1 .. i$

$P_0 := 0$

$$P_j := \left[\sum_{f=1}^{j} \left(S\left(\varepsilon\left(P_f\right)\right) - W\left(P_f\right) \right) \right]$$

pressure acting on a bed segment [N/m^2]

$$\Delta P_j := \sum_{f=1}^{j} S\left(\varepsilon\left(P_f\right)\right)$$

$\Delta P_i = 4.242 \cdot 10^3$ pressure drop of the test tube [N/m^2]

$\varepsilon\left(P_i\right) = 0.953$ porosity of the bed segment nearest to the sieve plate [-]

$$Z_j := \sum_{f=j}^{i} L\left(\varepsilon\left(P_f\right)\right)$$

$Z_1 = 0.268$

total length of the packed bed subject to liquid flow [m]

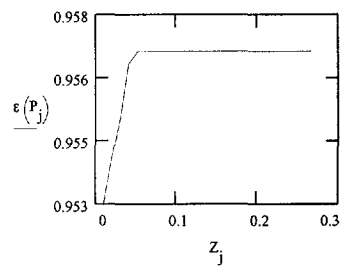

$S_j := S\left(\varepsilon\left(P_j\right)\right)$ $W_j := W\left(P_j\right)$

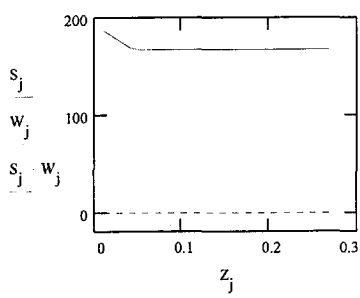

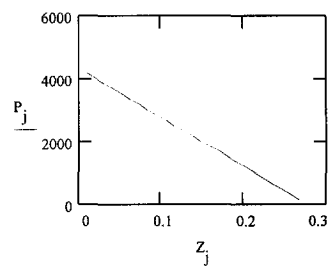

CELLULAR SILICONE

$L := 0.135$ initial packed bed length [m]

$i := 25$ number of bed segments [-]

$\varepsilon_0 := 0.87$ uncompressed porosity [-]

$\varepsilon := 0.76, 0.761 .. \varepsilon_0$ packed bed porosity [-]

$e_1 := 0.2353$ precompressive strain [-]

$\varepsilon_1 := \frac{\varepsilon_0 - e_1}{1 - e_1}$ precompressed porosity [-]

$1000\varepsilon_1 = 829.999$

$\sigma_1 := 9.26 \cdot 10^3 \cdot e_1^{0.467}$ precompressive stress [N/m^2]

$\sigma_1 = 4.711 \cdot 10^3$

$L(\varepsilon) := \frac{L}{i} \cdot \frac{1 - \varepsilon_1}{1 - \varepsilon}$ bed segment length as a function of porosity [m]

$u := 0.0046$ superficial liquid velocity [m/s]

$d_{eq} := 104.6 \cdot 10^{-6}$ equivalent fiber diameter for foam [m]

$\eta := 10^{-3}$ dynamic viscosity of water [N.s/m^2]

$C_1 := 3.88 \cdot 10^3$ structural parameter [-]

$S(\varepsilon) := C_1 \cdot \frac{\eta \cdot u \cdot (1 - \varepsilon)^2}{\varepsilon^3 \cdot d_{eq}^2} \cdot L(\varepsilon)$ pressure drop [N/m^2]

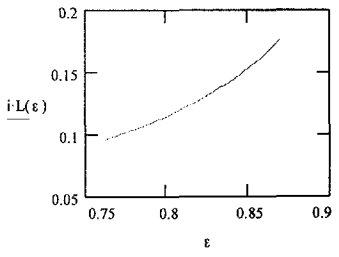

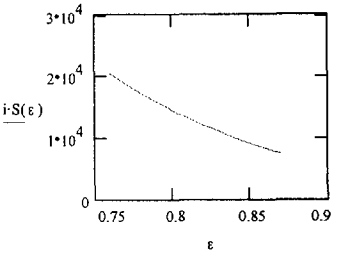

$\varepsilon(P) := (P \geq 4764.5) \cdot \left[(P \leq 6057) \cdot \left(0.87 - 1.602 \cdot 10^{-8} \cdot P^2 + 4.594 \cdot 10^{-10} \cdot P^{2.5} - 3.663 \cdot 10^{-12} \cdot P^3 \right) + (P > 6057) \cdot 0.78 \right] \ldots$
$+ (P < 4764.5) \cdot \varepsilon_1$

porosity as a function of pressure [-]

$1000\varepsilon(4764.5) = 829.999$

$1000\varepsilon(6057) = 779.999$

CELLULAR SILICONE (continued)

$P := 0, 100 .. 8000$ pressure acting on a bed segment [N/m^2]

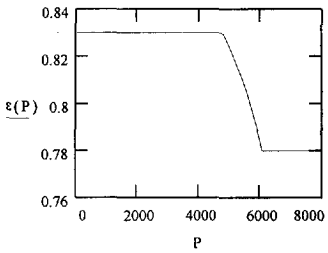

$D := 0.06$ tube diameter [m]

$\mu := 0.65$ friction coefficient [-]

$\nu(\varepsilon) := 0.067 + 0.195 \frac{\varepsilon_0 - \varepsilon}{1 - \varepsilon}$ Poisson's constant [-]

$W(P) := \frac{4}{D} \cdot \mu \cdot \frac{\nu(\varepsilon(P))}{1 - \nu(\varepsilon(P))} \cdot \left[\sigma_1 + (P \geq 0) \cdot P\right] \cdot L(\varepsilon(P))$ wall friction term [N/m^2]

$P := 0, 100 .. 6000$

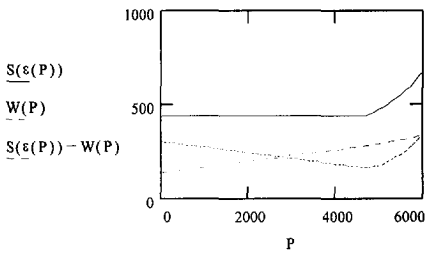

$j := 1 .. i$

$P_0 := 0$

$P_j := \left[\sum_{f=1}^{j} \left(S\left(\varepsilon\left(P_f\right)\right) - W\left(P_f\right)\right)\right]$ *pressure acting on a bed segment* [N/m^2]

$\Delta P_j := \sum_{f=1}^{j} S\left(\varepsilon\left(P_f\right)\right)$

$\Delta P_i = 1.141 \cdot 10^4$ pressure drop of the test tube [N/m^2]

$\varepsilon\left(P_i\right) = 0.804$ porosity of the bed segment nearest to the sieve plate [-]

$Z_j := \sum_{f=j}^{i} L\left(\varepsilon\left(P_f\right)\right)$

$Z_1 = 0.133$

total length of the packed bed subject to liquid flow [m]

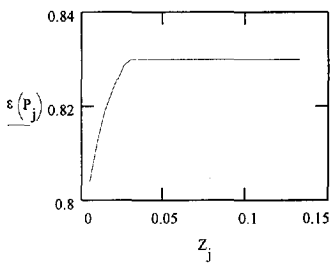

CELLULAR SILICONE
(continued)

$S_j := S(\varepsilon(P_j))$ $W_j := W(P_j)$

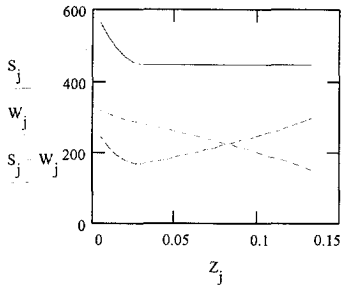

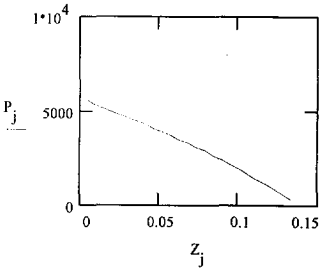

B.1 Fixed bed outlet concentration profiles / PUR foam

In the following graphs, the experimentally determined outlet concentration profile is represented by a dashed line and the calculated (modelled) outlet concentration profile (C(t)) is represented by a solid line.

PUR1 (fit parameters: $m_{SL} = 500$, $k_S = 3 \cdot 10^{-8}$):

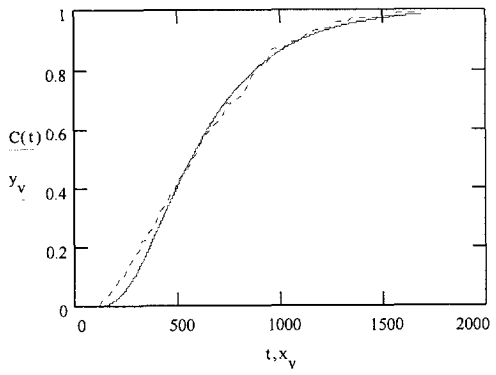

PUR2 (fit parameters: $m_{SL} = 500$, $k_S = 3 \cdot 10^{-8}$):

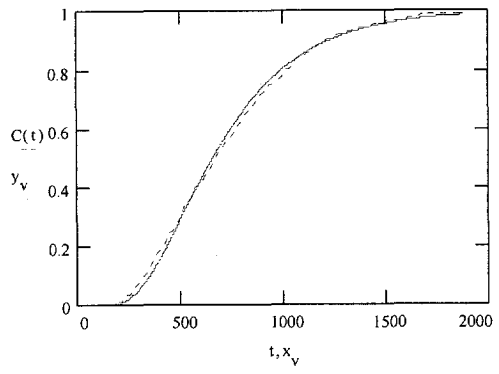

PUR3 (fit parameters: $m_{SL} = 470$, $k_S = 2.5 \cdot 10^{-8}$):

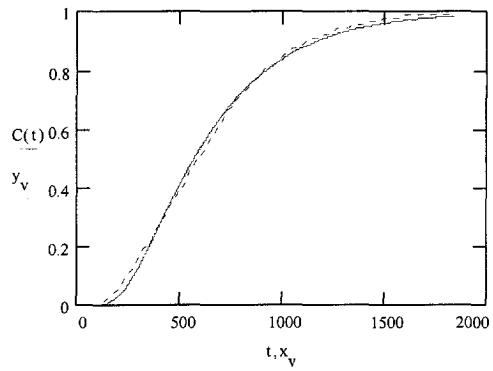

PUR4 (fit parameters: $m_{SL} = 430$, $k_S = 2.5 \cdot 10^{-8}$):

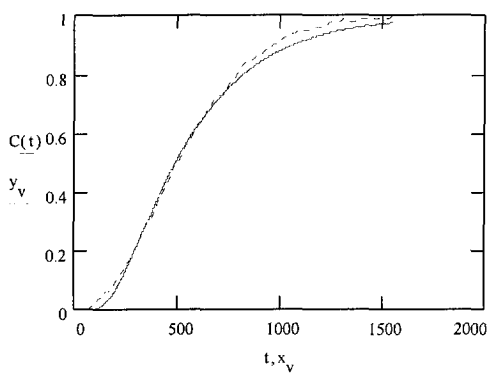

PUR5 (fit parameters: $m_{SL} = 400$, $k_S = 1.5 \cdot 10^{-8}$):

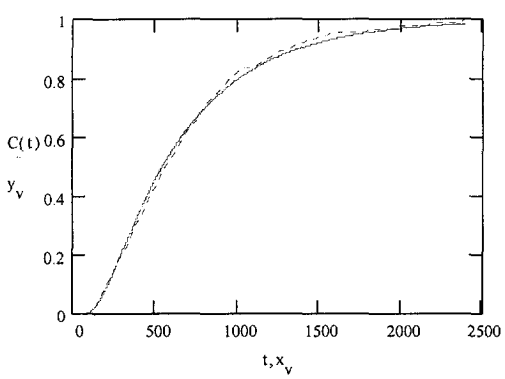

PUR6 (fit parameters: $m_{SL} = 500$, $k_S = 1.5 \cdot 10^{-8}$):

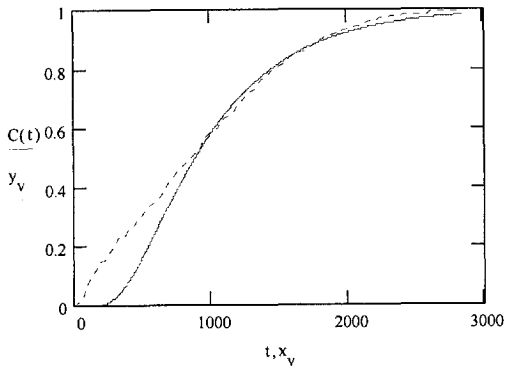

PUR7 (fit parameters: $m_{SL} = 440$, $k_S = 1.5 \cdot 10^{-8}$):

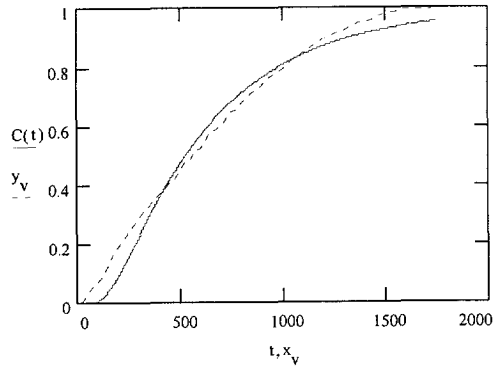

B.2 Fixed bed outlet concentration profiles / cellular silicone

In the following graphs, the experimentally determined outlet concentration profile is represented by a dashed line and the calculated (modelled) outlet concentration profile (C(t)) is represented by a solid line.

SIL1 (fit parameters: $m_{SL} = 260$, $k_S = 1 \cdot 10^{-6}$):

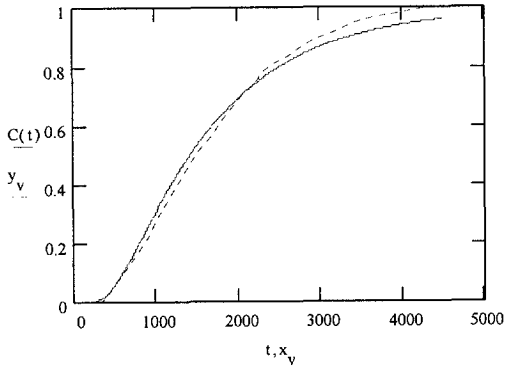

SIL2 (fit parameters: $m_{SL} = 260$, $k_S = 1 \cdot 10^{-6}$):

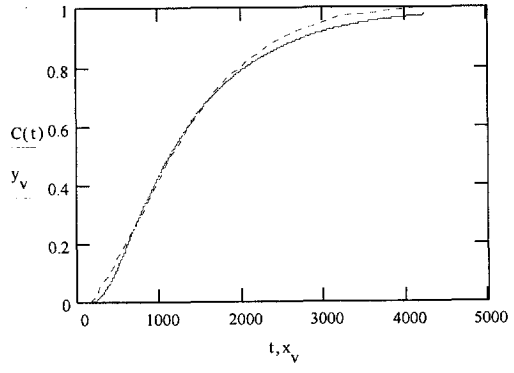

SIL3 (fit parameters: $m_{SL} = 260$, $k_S = 1 \cdot 10^{-6}$):

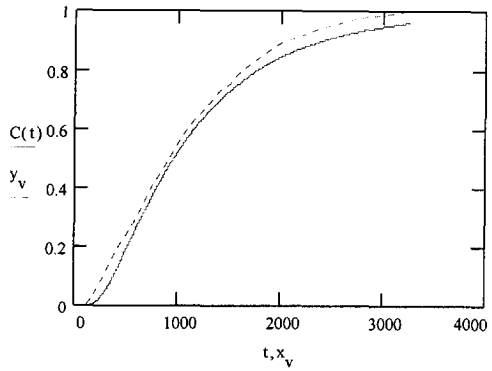

C.1 Calculation of the sorption section

PDMS fibers
SORPTION SECTION

Parameters:

$H := 0.45$ total packed bed length (m)

$u := 0.0443$ superficial flow velocity (m/s) relative to fixed co-ordinates

$v := 2.14 \cdot 10^{-4}$ sorbent velocity (m/s)

$\varepsilon := 0.77$ packed bed porosity (-)

$d := 200 \cdot 10^{-6}$ fiber diameter (m)

$a_s := \frac{4 \cdot (1 - \varepsilon)}{d}$ specific surface area of the fiber bed (m2/m3)

$a_s = 4.6 \cdot 10^{3}$

$k_S := 8.8 \cdot 10^{-7}$ sorbent side mass transfer coefficient (m/s)

$k_L := 2.37 \cdot 10^{-4} \cdot u^{0.4}$ liquid side mass transfer coefficient (m/s)

$k_L = 6.813 \cdot 10^{-5}$

$m_{sL} := 1300$ sorbent/water distribution coefficient [(kg/m3)/(kg/m3)]

$D_{ax} := 0.05 \cdot u$ axial dispersion coefficient (m2/s)

$D_{ax} = 0.002$

$C_{L0} := 1.65 \cdot 10^{-2}$ water input concentration (kg/m3)

$C_{S0} := 10^{-2}$ sorbent input concentration (kg/m3 solid based)

Mass transfer model (see Chapter 4)

$Pe := \frac{u \cdot H}{\varepsilon \cdot D_{ax}}$ $Pe = 11.688$ Peclet number (-)

$k_{oL} := \left(\frac{1}{k_L} + \frac{1}{m_{sL} \cdot k_S} \right)^{-1}$ $k_{oL} = 6.43 \cdot 10^{-5}$ liquid phase based overall mass transfer coefficient (m/s)

$N_{oL} := \frac{k_{oL} \cdot a_s \cdot H}{u}$ liquid phase based number of transfer units (-)

$S := \frac{m_{sL} \cdot (1 - \varepsilon) \cdot v}{u}$ $S = 1.444$ sorption factor (-)

$\Lambda := \frac{1}{S}$

$a := Pe + \Lambda \cdot N_{oL}$

$b := (1 - \Lambda) \cdot N_{oL} \cdot Pe$

$\lambda_1 := 0$

$\lambda_2 := \frac{a}{2} + \sqrt{\left(\frac{a}{2}\right)^2 + b}$

$\lambda_3 := \frac{a}{2} - \sqrt{\left(\frac{a}{2}\right)^2 + b}$

$$D_0 := \Lambda \cdot \left(\lambda_2 - \lambda_3\right) \cdot e^{a} + \lambda_3 \cdot \left(1 - \frac{\lambda_2}{Pe}\right) \cdot e^{\lambda_3} - \lambda_2 \cdot \left(1 - \frac{\lambda_3}{Pe}\right) \cdot e^{\lambda_2}$$

$$D_1 := \Lambda \cdot \left(\lambda_2 - \lambda_3\right) \cdot e^{a}$$

$$D_2 := \lambda_3 \cdot e^{\lambda_3}$$

$$D_3 := -\lambda_2 \cdot e^{\lambda_2}$$

$$Z := 0, 0.01 .. 1$$

$$i := 1, 2 .. 3$$

$$f_i := 1 + \frac{\lambda_i}{N_{oL}} - \frac{\left(\lambda_i\right)^2}{N_{oL} \cdot Pe}$$

$$X(Z) := \sum_i \frac{D_i}{D_0} \cdot e^{\lambda_i \cdot Z}$$

$$Y(Z) := \sum_i f_i \cdot \frac{D_i}{D_0} \cdot e^{\lambda_i \cdot Z}$$

$$C_L(Z) := X(Z) \cdot \left(C_{L0} - \frac{C_{S0}}{m_{sL}}\right) + \frac{C_{S0}}{m_{sL}}$$ liquid concentration (entering at Z=0)

$$C_S(Z) := Y(Z) \cdot \left(m_{sL} \cdot C_{L0} - C_{S0}\right) + C_{S0}$$ sorbent concentration (entering at Z=1)

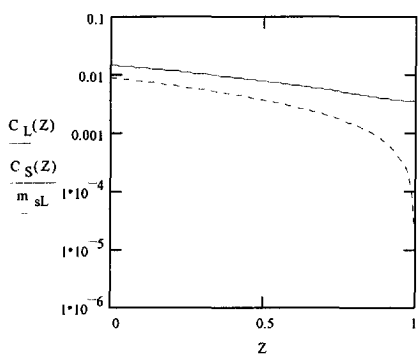

$C_{L0} = 0.017$ water input concentration (kg/m3)

$C_L(1) = 0.004$ water output concentration (kg/m3)

$C_{S0} = 0.01$ sorbent input concentration (kg/m3 solid based)

$C_S(0) = 11.677$ sorbent output concentration (kg/m3 solid based)

$100\left(1 - \frac{C_L(1)}{C_{L0}}\right) = 78.564$ **removal efficiency (%)**

PUR foam
SORPTION SECTION

Parameters:

$H := 0.45$ total packed bed length (m)

$u := 0.0326$ superficial flow velocity (m/s) relative to fixed co-ordinates

$v := 2.27 \cdot 10^{-3}$ sorbent velocity (m/s)

$\varepsilon := 0.963$ packed bed porosity (-)

$d_{eq} := 8.5 \cdot 10^{-6}$ equivalent fiber diameter (m)

$a_s := \frac{4 \cdot (1 - \varepsilon)}{d_{eq}}$ specific surface area (m2/m3)

$a_s = 1.741 \cdot 10^{4}$

$k_S := 2.2 \cdot 10^{-8}$ sorbent side mass transfer coefficient (m/s)

$k_L := 1.58 \cdot 10^{-3} \cdot u^{0.4}$ liquid side mass transfer coefficient (m/s)

$k_L = 4.017 \cdot 10^{-4}$

$m_{sL} := 465$ sorbent/water distribution coefficient [(kg/m3)/(kg/m3)]

$D_{ax} := 8.8 \cdot 10^{-3} \cdot u$ axial dispersion coefficient (m2/s)

$D_{ax} = 2.869 \cdot 10^{-4}$

$C_{L0} := 1.09 \cdot 10^{-1}$ water input concentration (kg/m3)

$C_{S0} := 10^{-2}$ sorbent input concentration (kg/m3 solid based)

Mass transfer model (see Chapter 4)

$Pe := \frac{u \cdot H}{\varepsilon \cdot D_{ax}}$ $Pe = 53.101$ Peclet number (-)

$k_{oL} := \left(\frac{1}{k_L} + \frac{1}{m_{sL} \cdot k_S} \right)^{-1}$ $k_{oL} = 9.976 \cdot 10^{-6}$ liquid phase based overall mass transfer coefficient (m/s)

$N_{oL} := \frac{k_{oL} \cdot a_s \cdot H}{u}$ liquid phase based number of transfer units (-)

$S := \frac{m_{sL} \cdot (1 - \varepsilon) \cdot v}{u}$ $S = 1.198$ sorption factor (-)

$\Lambda := \frac{1}{S}$

$a := Pe - \Lambda \cdot N_{oL}$

$b := (1 - \Lambda) \cdot N_{oL} \cdot Pe$

$\lambda_1 := 0$

$\lambda_2 := \frac{a}{2} + \sqrt{\left(\frac{a}{2}\right)^2 + b}$

$\lambda_3 := \frac{a}{2} - \sqrt{\left(\frac{a}{2}\right)^2 + b}$

$$D_0 := \Lambda \cdot \left(\lambda_2 - \lambda_3\right) \cdot e^{a} + \lambda_3 \cdot \left(1 - \frac{\lambda_2}{Pe}\right) \cdot e^{\lambda_3} - \lambda_2 \cdot \left(1 - \frac{\lambda_3}{Pe}\right) \cdot e^{\lambda_2}$$

$$D_1 := \Lambda \cdot \left(\lambda_2 - \lambda_3\right) \cdot e^{a}$$

$$D_2 := \lambda_3 \cdot e^{\lambda_3}$$

$$D_3 := -\lambda_2 \cdot e^{\lambda_2}$$

$$Z := 0, 0.01 .. 1$$

$$i := 1, 2 .. 3$$

$$f_i := 1 + \frac{\lambda_i}{N_{oL}} - \frac{\left(\lambda_i\right)^2}{N_{oL} \cdot Pe}$$

$$X(Z) := \sum_i \frac{D_i}{D_0} \cdot e^{\lambda_i \cdot Z}$$

$$Y(Z) := \sum_i f_i \cdot \frac{D_i}{D_0} \cdot e^{\lambda_i \cdot Z}$$

$$C_L(Z) := X(Z) \cdot \left(C_{L0} - \frac{C_{S0}}{m_{sL}}\right) + \frac{C_{S0}}{m_{sL}}$$ liquid concentration (entering at Z=0)

$$C_S(Z) := Y(Z) \cdot \left(m_{sL} \cdot C_{L0} - C_{S0}\right) + C_{S0}$$ sorbent concentration (entering at Z=1)

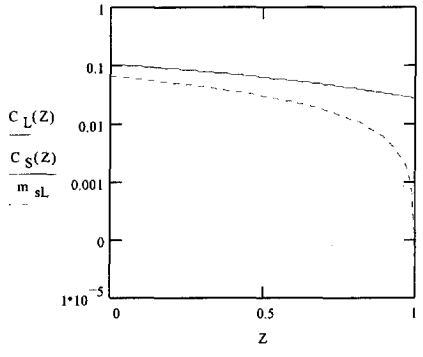

$C_{L0} = 0.109$ water input concentration (kg/m3)

$C_L(1) = 0.029$ water output concentration (kg/m3)

$C_{S0} = 0.01$ sorbent input concentration (kg/m3 solid based)

$C_S(0) = 31.158$ sorbent output concentration (kg/m3 solid based)

$$100 \left(1 - \frac{C_L(1)}{C_{L0}}\right) = 73.624$$ **removal efficiency (%)**

D.1 Calculation of required packed bed length

SORPTION SECTION

Parameters:

$H := 0.24$ total packed bed length (m)

$u := 0.01$ superficial liquid velocity (m/s) relative to fioxed co-ordinates

$v := 0.001$ transport velocity of sorbent (m/s)

$\varepsilon := 0.9$ packed bed porosity (-)

$k_L := 10^{-4}$ fluid side mass transfer coefficient (m/s)

$k_S := 10^{-6}$ sorbent side mass transfer coefficient (m/s)

$m_{sL} := 260$ sorbent/water distribution coefficient [(kg/m3)/(kg/m3)]

$D_{ax} := 10^{-4}$ axial dispersion coefficient (m2/s)

$d_{eq} := 77.8 \cdot 10^{-6}$ equivalent fiber diameter of the foam (m)

$a_s := \frac{4 \cdot (1 - \varepsilon)}{d_{eq}}$ specific surface area of the foam (m2/m3)

$a_s = 5.141 \cdot 10^3$

$C_{L0} := 10^{-1}$ water input concentration (kg/m3)

$C_{S0} := 10^{-2}$ sorbent input concentration (kg/m3)

Mass transfer model (see Chapter 4)

$Pe := \frac{u \cdot H}{\varepsilon \cdot D_{ax}}$ $Pe = 26.667$ Peclet number (-)

$k_{oL} := \left(\frac{1}{k_L} + \frac{1}{m_{sL} \cdot k_S} \right)^{-1}$ $k_{oL} = 7.222 \cdot 10^{-5}$ liquid phase based overall mass transfer coefficient (m/s)

$N_{oL} := \frac{k_{oL} \cdot a_s \cdot H}{u}$ liquid phase based number of transfer units (-)

$S := \frac{m_{sL} \cdot (1 - \varepsilon) \cdot v}{u}$ $S = 2.6$ sorption factor (-)

$\Lambda := \frac{1}{S}$

$a := Pe + \Lambda \cdot N_{oL}$

$b := (1 - \Lambda) \cdot N_{oL} \cdot Pe$

$\lambda_1 := 0$

$\lambda_2 := \frac{a}{2} - \sqrt{\left(\frac{a}{2}\right)^2 + b}$

$\lambda_3 := \frac{a}{2} - \sqrt{\left(\frac{a}{2}\right)^2 + b}$

$$D_0 := \Lambda \cdot \left(\lambda_2 - \lambda_3\right) \cdot e^{a} + \lambda_3 \cdot \left(1 - \frac{\lambda_2}{Pe}\right) \cdot e^{\lambda_3} - \lambda_2 \cdot \left(1 - \frac{\lambda_3}{Pe}\right) \cdot e^{\lambda_2}$$

$$D_1 := \Lambda \cdot \left(\lambda_2 - \lambda_3\right) \cdot e^{a}$$

$$D_2 := \lambda_3 \cdot e^{\lambda_3}$$

$$D_3 := -\lambda_2 \cdot e^{\lambda_2}$$

$$Z := 0, 0.01 .. 1$$

$$i := 1, 2 .. 3$$

$$f_i := 1 + \frac{\lambda_i}{N_{oL}} - \frac{\left(\lambda_i\right)^2}{N_{oL} \cdot Pe}$$

$$X(Z) := \sum_i \frac{D_i}{D_0} \cdot e^{\lambda_i \cdot Z}$$

$$Y(Z) := \sum_i f_i \cdot \frac{D_i}{D_0} \cdot e^{\lambda_i \cdot Z}$$

$$C_L(Z) := X(Z) \cdot \left(C_{L0} - \frac{C_{S0}}{m_{sL}}\right) + \frac{C_{S0}}{m_{sL}}$$ fluid concentration (entering at Z=0)

$$C_S(Z) := Y(Z) \cdot \left(m_{sL} \cdot C_{L0} - C_{S0}\right) + C_{S0}$$ *sorbent concentration (entering at Z=1)*

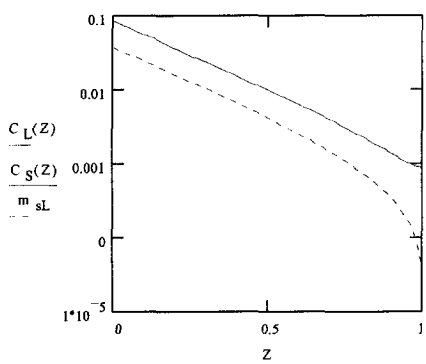

$C_{L0} = 0.1$ water input concentration (kg/m3)

$C_L(1) = 8.872\,10^{-4}$ water output concentration (kg/m3)

$C_{S0} = 0.01$ sorbent input concentration (kg/m3

$C_S(0) = 9.921$ *sorbent output concentration* (kg/m3)

$100 \cdot \left(1 - \frac{C_L(1)}{C_{L0}}\right) = 99.113$ **removal efficiency (%)**

REGENERATION SECTION

Parameters:

$H := 0.14$ total packed bed length (m)

$u := 0.3$ superficial gas flow velocity (m/s) relative to fioxed co-ordinates

$v := 0.001$ transport velocity of sorbent (m/s)

$\varepsilon := 0.9$ packed bed porosity (-)

$k_G := 10^{-2}$ gas side mass transfer coefficient (m/s)

$k_S := 10^{-6}$ sorbent side mass transfer coefficient (m/s

$m_{GS} := 0.02$ steam/sorbent distribution coefficient [(kg/m3)/(kg/m3)]

$D_{ax} := 10^{-3}$ axial dispersion coefficient (m2/s)

$d_{eq} := 77.8 \cdot 10^{-6}$ equivalent fiberdiameter of the foam (m)

$a_s := \frac{4 \cdot (1 - \varepsilon)}{d_{eq}}$ specific surface area of the foam (m2/m3)

$a_s = 5.141 \cdot 10^3$

$C_{S0} := 9.921$ sorbent input concentration (kg/m3)

$C_{G0} := 10^{-6}$ steam input concentration (kg/m3)

Mass transfer model (see Chapter 4)

$Pe := \frac{u \cdot H}{\varepsilon \cdot D_{ax}}$ $\quad Pe = 46.667$ Peclet number (-)

$k_{oS} := \left(\frac{1}{k_S} + \frac{1}{m_{GS} \cdot k_G} \right)^{-1}$ $\quad k_{oS} = 9.95 \cdot 10^{-7}$ sorbent phase based overall mass transfer coefficient (m/s)

$N_{oS} := \frac{k_{oS} \cdot a_s \cdot H}{(1 - \varepsilon) \cdot v}$ $\quad N_{oS} = 7.162$ sorbent phase based number of transfer units (-)

$S := \frac{m_{GS} \cdot u}{(1 - \varepsilon) \cdot v}$ $\quad S = 60$ stripping factor (-)

$\Lambda := \frac{1}{S}$

$a := Pe - N_{oS}$

$b := (\Lambda - 1) \cdot N_{oS} \cdot Pe$

$\lambda_1 := 0$

$\lambda_2 := \frac{a}{2} + \sqrt{\left(\frac{a}{2}\right)^2 + b}$

$\lambda_3 := \frac{a}{2} - \sqrt{\left(\frac{a}{2}\right)^2 - b}$

$D_0 := \frac{1}{\Lambda} \cdot \left(\lambda_2 - \lambda_3\right) \cdot e^a - \lambda_3 \cdot \left(1 - \frac{\lambda_2}{Pe}\right) \cdot e^{\lambda_3} - \lambda_2 \cdot \left(1 - \frac{\lambda_3}{Pe}\right) \cdot e^{\lambda_2}$

$$D_1 := \frac{1}{\Lambda}\cdot\left(\lambda_2 - \lambda_3\right)\cdot e^{a}$$

$$D_2 := \lambda_3 \cdot e^{\lambda_3}$$

$$D_3 := -\lambda_2 \cdot e^{\lambda_2}$$

$$Z := 0, 0.01 .. 1$$

$$i := 1, 2 .. 3$$

$$f_i := 1 + \frac{\lambda_i}{\Lambda \cdot N_{oS}} - \frac{\left(\lambda_i\right)^2}{\Lambda \cdot N_{oS} \cdot Pe}$$

$$X(Z) := 1 - \sum_i f_i \cdot \frac{D_i}{D_0} \cdot e^{\lambda_i \cdot (1-Z)}$$

$$Y(Z) := 1 - \sum_i \frac{D_i}{D_0} \cdot e^{\lambda_i \cdot (1-Z)}$$

$$C_S(Z) := X(Z)\cdot\left(C_{S0} - \frac{C_{G0}}{m_{GS}}\right) + \frac{C_{G0}}{m_{GS}}$$ sorbent concentration (entering at Z=0)

$$C_G(Z) := Y(Z)\cdot\left(m_{GS} C_{S0} - C_{G0}\right) + C_{G0}$$ steam concentration (entering at Z=1)

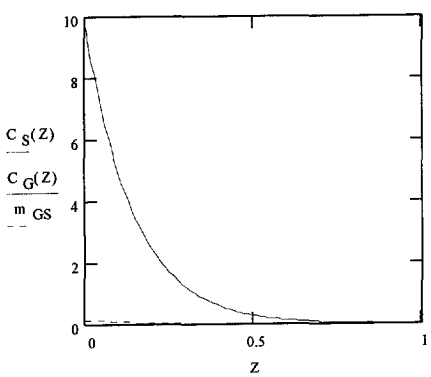

$C_S(0) = 9.921$ sorbent input concentration (kg/m3)

$C_S(1) = 0.009$ sorbent output concentration (kg/m3)
target: 0.01 kg/m3

$C_{G0} = 1 \cdot 10^{-6}$ steam input concentration (kg/m3) (clean steam)

$C_G(0) = 0.003$ steam output concentration (kg/m3)

D.2 Calculation of curved bed segments

Sorption section

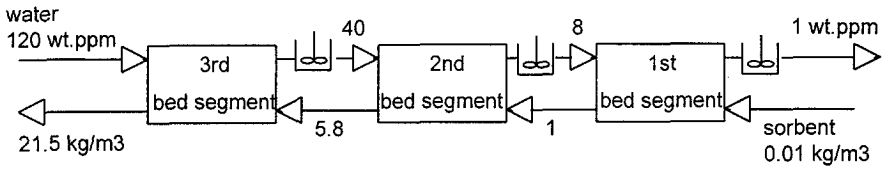

First bed segment:

water input concentration: 8 wt.ppm
sorbent input concentration: 0.01 kg/m^3

layer number	mean radius (m)	curved length (m)	flow velocity (m/s)	transport velocity (m/s)	water output concentration (wt.ppm)	flow rate (fraction)	flow rate x output concentration	
1	0.489	0.147	0.007	0.0013	0.13	0.06364	0.00827	outer layer
2	0.466	0.14	0.0076	0.00124	0.19	0.06909	0.01313	
3	0.443	0.133	0.0082	0.00118	0.27	0.07455	0.02013	
4	0.42	0.126	0.0088	0.00112	0.39	0.08	0.0312	
5	0.398	0.119	0.0094	0.00106	0.54	0.08545	0.04614	
6	0.375	0.113	0.01	0.001	**0.71**	0.09091	0.06455	straight bed
7	0.352	0.106	0.0106	0.00094	0.94	0.09636	0.09058	
8	0.33	0.099	0.0112	0.00088	1.22	0.10182	0.12422	
9	0.307	0.092	0.0118	0.00082	1.54	0.10727	0.1652	
10	0.284	0.085	0.0124	0.00076	1.9	0.11273	0.21419	
11	0.261	0.078	0.013	0.0007	2.3	0.11818	0.27181	inner layer
SUM:						1	**1.05 wt.ppm**	

Second bed segment:

water input concentration: 40 wt.ppm
sorbent input concentration: 1 kg/m^3

layer number	mean radius (m)	curved length (m)	flow velocity (m/s)	transport velocity (m/s)	water output concentration (wt.ppm)	flow rate (fraction)	flow rate x output concentration	
1	0.489	0.147	0.007	0.0013	4.27	0.06364	0.27174	outer layer
2	0.466	0.14	0.0076	0.00124	4.53	0.06909	0.31298	
3	0.443	0.133	0.0082	0.00118	4.91	0.07455	0.36604	
4	0.42	0.126	0.0088	0.00112	5.42	0.08	0.4336	
5	0.398	0.119	0.0094	0.00106	6.1	0.08545	0.52125	
6	0.375	0.113	0.01	0.001	**6.9**	0.09091	0.62728	straight bed
7	0.352	0.106	0.0106	0.00094	7.95	0.09636	0.76606	
8	0.33	0.099	0.0112	0.00088	9.2	0.10182	0.93674	
9	0.307	0.092	0.0118	0.00082	10.65	0.10727	1.14243	
10	0.284	0.085	0.0124	0.00076	12.29	0.11273	1.38545	
11	0.261	0.078	0.013	0.0007	14.11	0.11818	1.66752	inner layer
SUM:						1	**8.43 wt.ppm**	

Third bed segment:

water input concentration: 120 wt.ppm
sorbent input concentration: 5.8 kg/m^3

layer number	mean radius (m)	curved length (m)	flow velocity (m/s)	transport velocity (m/s)	water output concentration (wt.ppm)	flow rate (fraction)	flow rate x output concentration	
1	0.489	0.147	0.007	0.0013	23.7	0.06364	1.50827	outer layer
2	0.466	0.14	0.0076	0.00124	24.55	0.06909	1.69616	
3	0.443	0.133	0.0082	0.00118	25.77	0.07455	1.92115	
4	0.42	0.126	0.0088	0.00112	27.44	0.08	2.1952	
5	0.398	0.119	0.0094	0.00106	29.65	0.08545	2.53359	
6	0.375	0.113	0.01	0.001	**32.26**	0.09091	2.93276	straight bed
7	0.352	0.106	0.0106	0.00094	35.66	0.09636	3.4362	
8	0.33	0.099	0.0112	0.00088	39.73	0.10182	4.04531	
9	0.307	0.092	0.0118	0.00082	44.45	0.10727	4.76815	
10	0.284	0.085	0.0124	0.00076	49.79	0.11273	5.61283	
11	0.261	0.078	0.013	0.0007	60.2	0.11818	7.11444	inner layer
SUM:						1	**37.76 wt.ppm**	

Regeneration section

First bed segment:

sorbent input concentration: 21.5 kg/m^3
steam input concentration: 10^{-6} kg/m^3 (clean steam)

layer number	mean radius (m)	curved length (m)	flow velocity (m/s)	transport velocity (m/s)	steam output concentration (kg/m^3)	flow rate (fraction)	flow rate x output concentration	sorbent output concentration (kg/m^3)	
1	0.489	0.147	0.209	0.0013	0.0133	0.06333	0.00084	0.079	outer layer
2	0.466	0.14	0.227	0.00124	0.0117	0.06879	0.0008	0.078	
3	0.443	0.133	0.246	0.00118	0.0103	0.07455	0.00077	0.077	
4	0.42	0.126	0.264	0.00112	0.0091	0.08	0.00073	0.077	
5	0.398	0.119	0.282	0.00106	0.0081	0.08545	0.00069	0.077	
6	0.375	0.113	0.3	0.001	**0.0071**	0.09091	0.00065	0.073	straight bed
7	0.352	0.106	0.318	0.00094	0.0063	0.09636	0.00061	0.073	
8	0.33	0.099	0.336	0.00088	0.0056	0.10182	0.00057	0.073	
9	0.307	0.092	0.354	0.00082	0.005	0.10727	0.00054	0.074	
10	0.284	0.085	0.373	0.00076	0.0044	0.11303	0.0005	0.075	
11	0.261	0.078	0.391	0.0007	0.0038	0.11848	0.00045	0.076	inner layer
SUM:						1	***0.0072 kg/m^3***		

D.3 Drawings of static cylinder and rotating drum

Drawing number:	Description:
1A:	rear part of static cylinder
1B:	pattern of openings for inlet and outlet ports in **1**
2:	front part of static cylinder, bolted to **1**
3:	housing inner face
4A:	housing side face (rear), bolted to **3**
4B:	housing side face (front), bolted to **3**
5:	check valve plate (14 x), bolted between **3** and **4**
6:	sieve plate (28 x), fits into slots between **3** and **4**, fixed to **4A** and **4B** with brackets

Appendix D

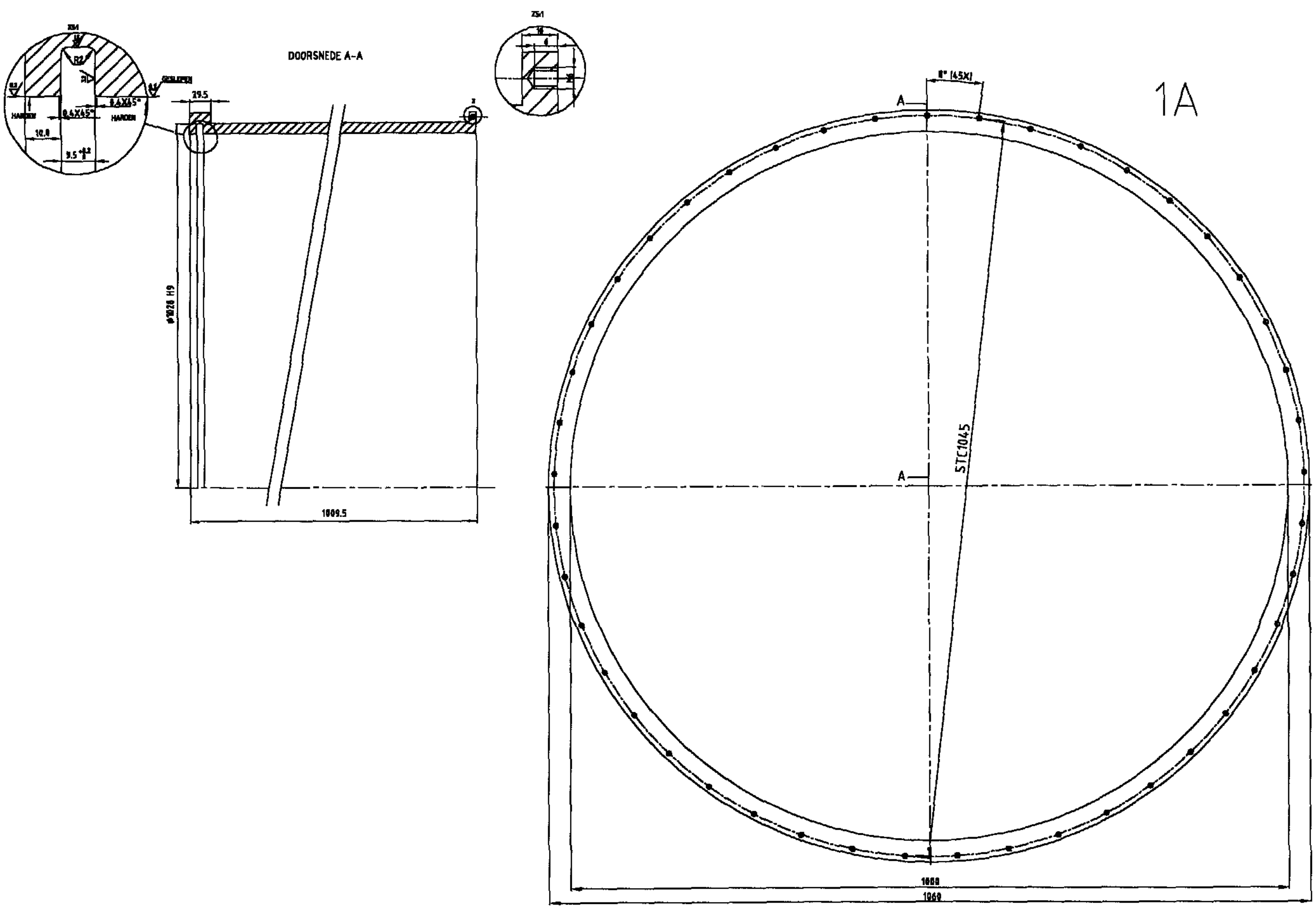

1A
DOORSNEDE A-A
29.5
1009.5
ø1028 H9
HARDEN
GESLEPEN
0.4X45°
10.8
9.5
Z5:1
A
A
8° (45X)
STC1045
1060
1069

Appendix D

1B

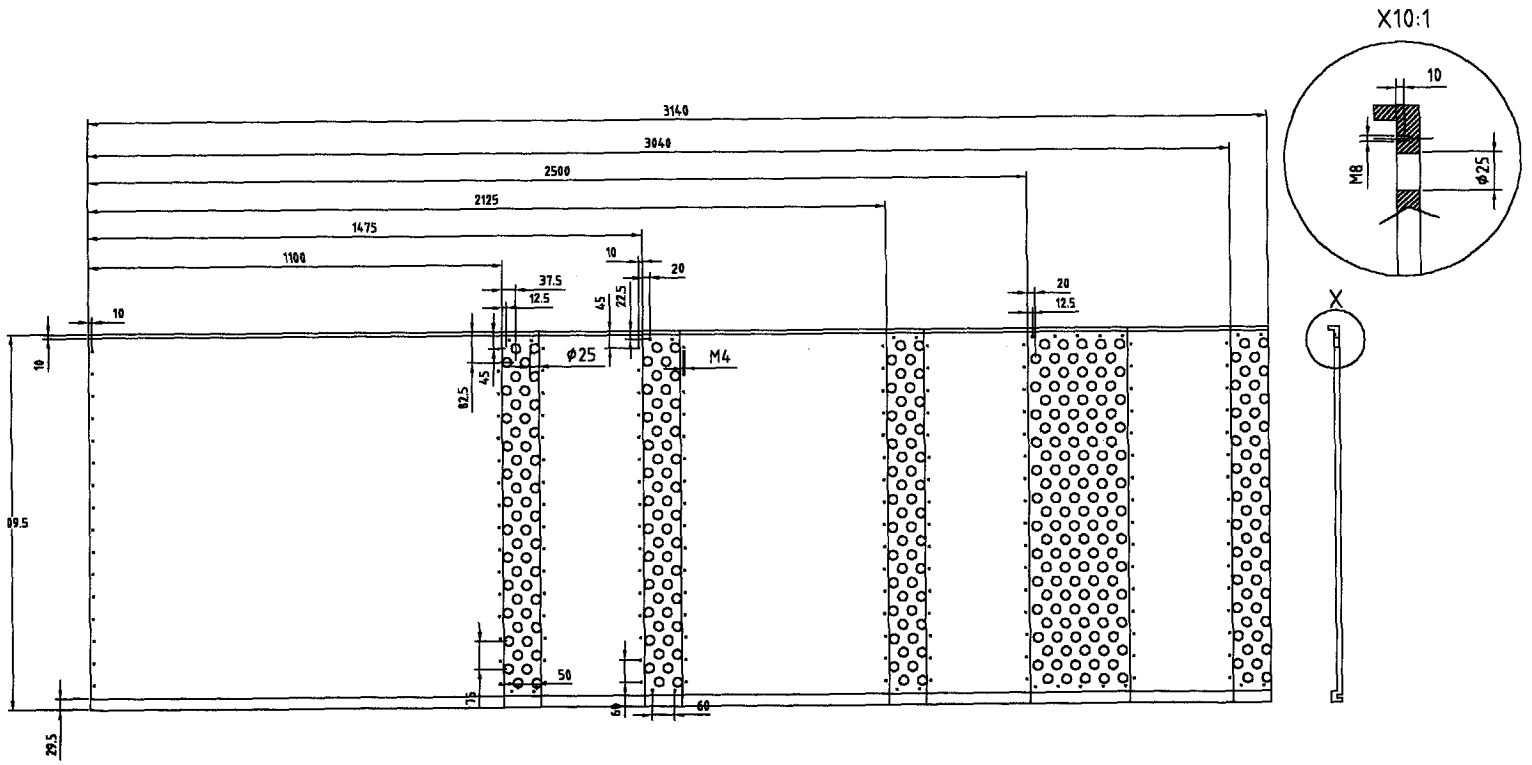
X10:1
10
M8
ϕ25
X
3140
3040
2500
2125
1475
1100
10
37.5
12.5
20
45
22.5
ϕ25
M4
82.5
20
12.5
10
10
095
29.5
50
60

Appendix D

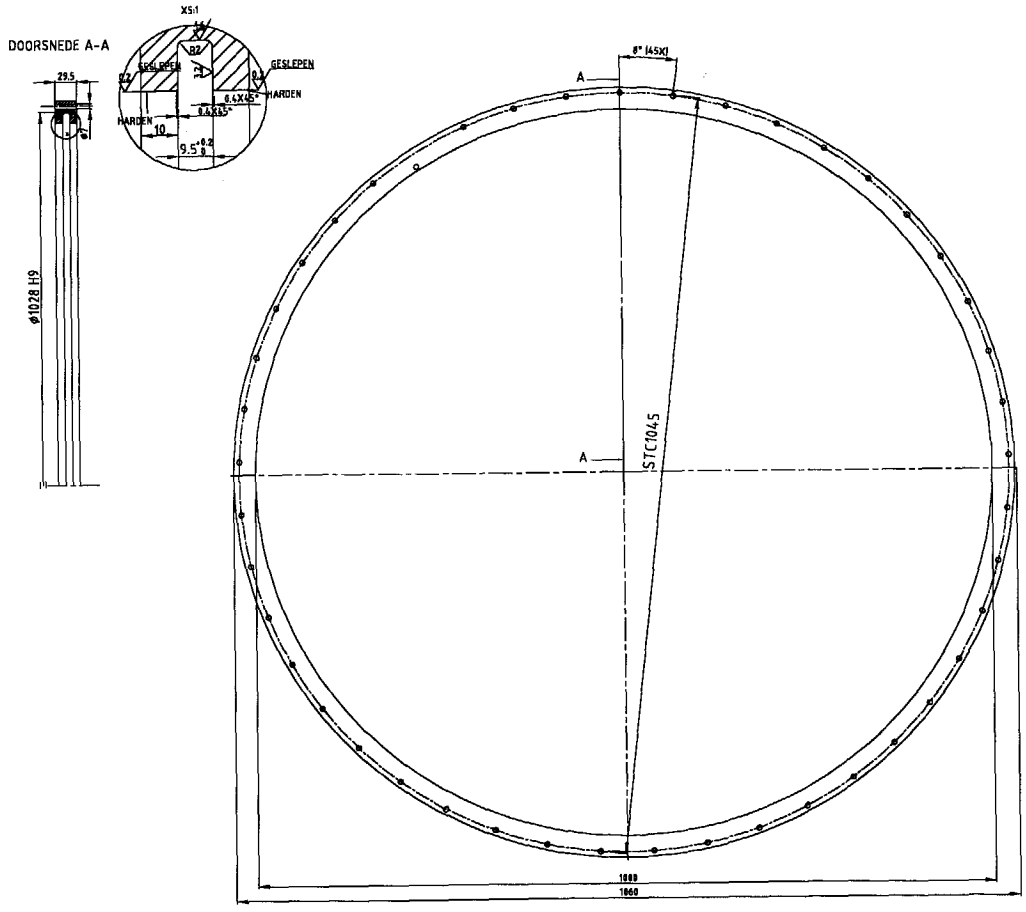
DOORSNEDE A-A
X5:1
29.5
ø10Z8 H9
GESLEPEN
HARDEN
10
9.5
8* (45X)
A
A
STC1045
1888
1860

2

Appendix D

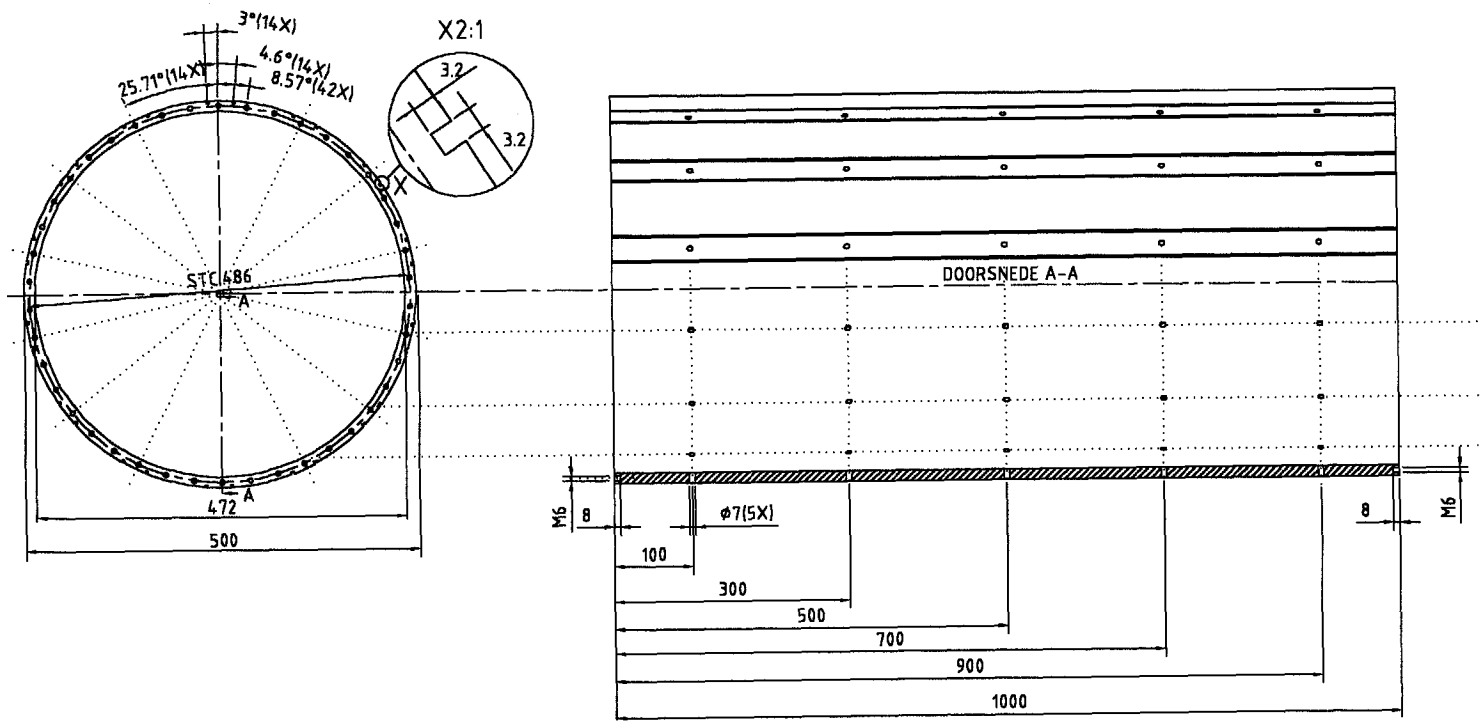
3°(14X)
4.6°(14X)
8.57°(42X)
25.71°(14X)
X2:1
3.2
3.2
X
STC486
A
A
472
500
DOORSNEDE A-A
M6
8
ø7(5X)
100
300
500
700
900
1000
8
M6

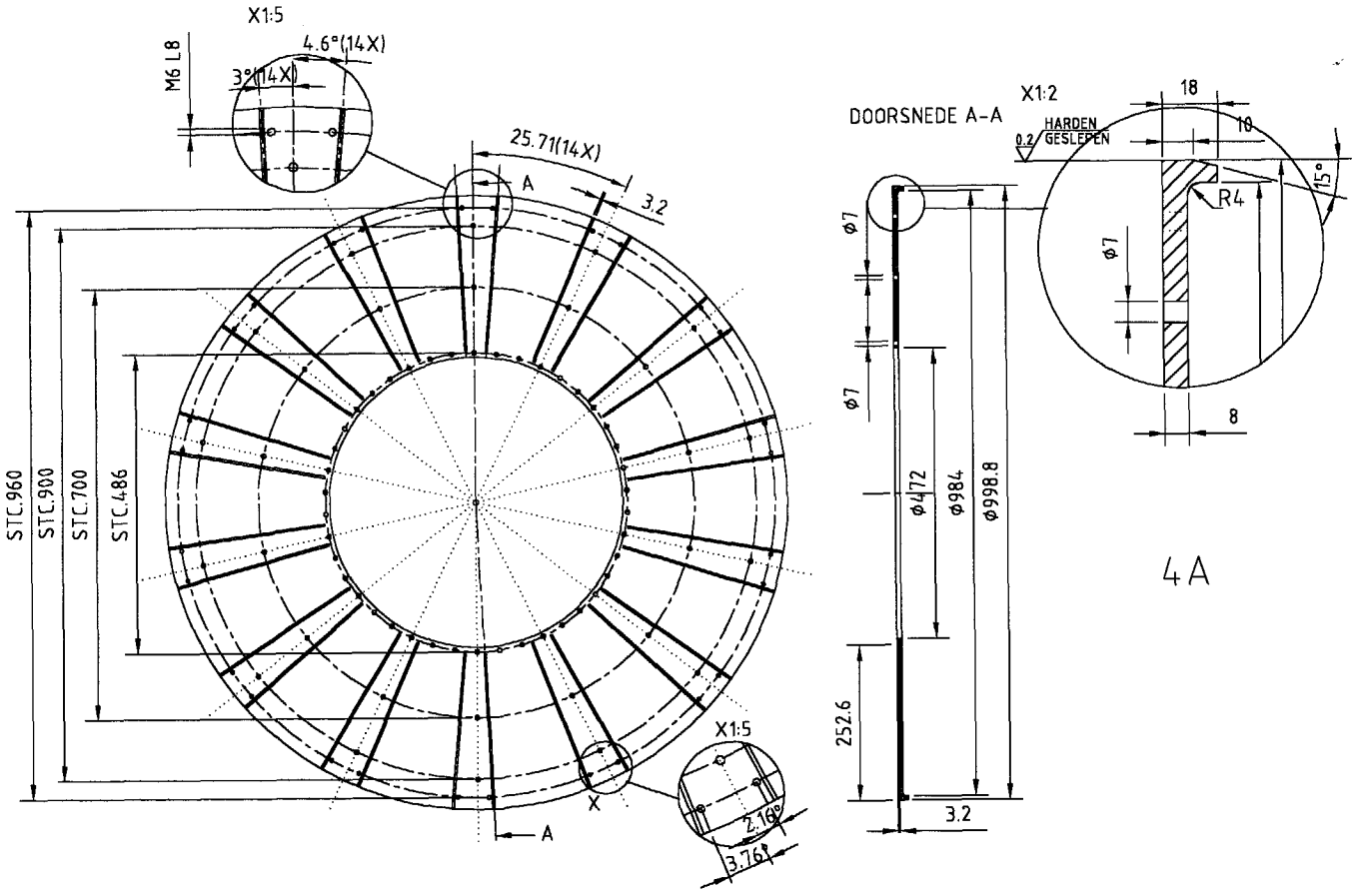
X1:5
M6 L8
4.6°(14X)
3°(14X)
25.71(14X)
3.2
A
STC.960
STC.900
STC.700
STC.486
X1:5
2.16°
3.76°
X
A
DOORSNEDE A-A
X1:2
18
10
HARDEN
GESLEPEN
0.2
15°
R4
ø7
ø7
ø7
8
ø472
ø984
ø998.8
252.6
3.2
4A

Appendix D

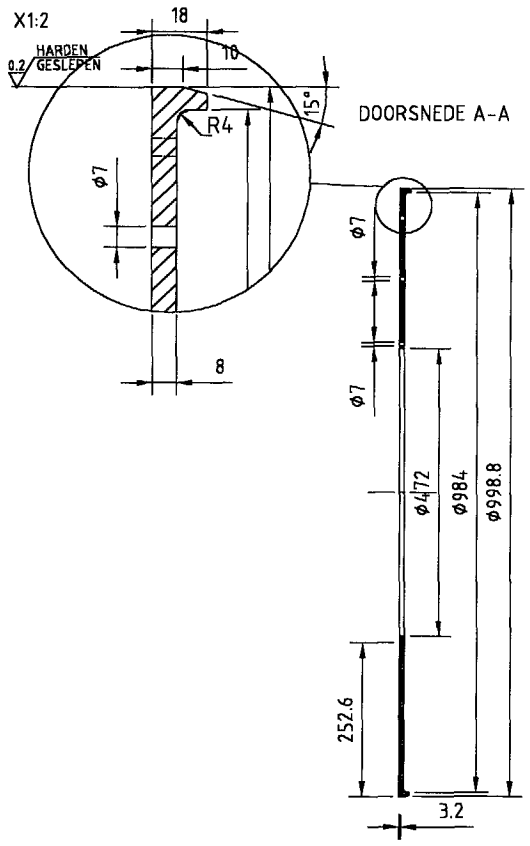
X1:2
18
10
HARDEN
0.2 GESLEPEN
15°
R4
ø7
8
DOORSNEDE A-A
ø7
ø7
ø472
ø984
ø998.8
252.6
3.2

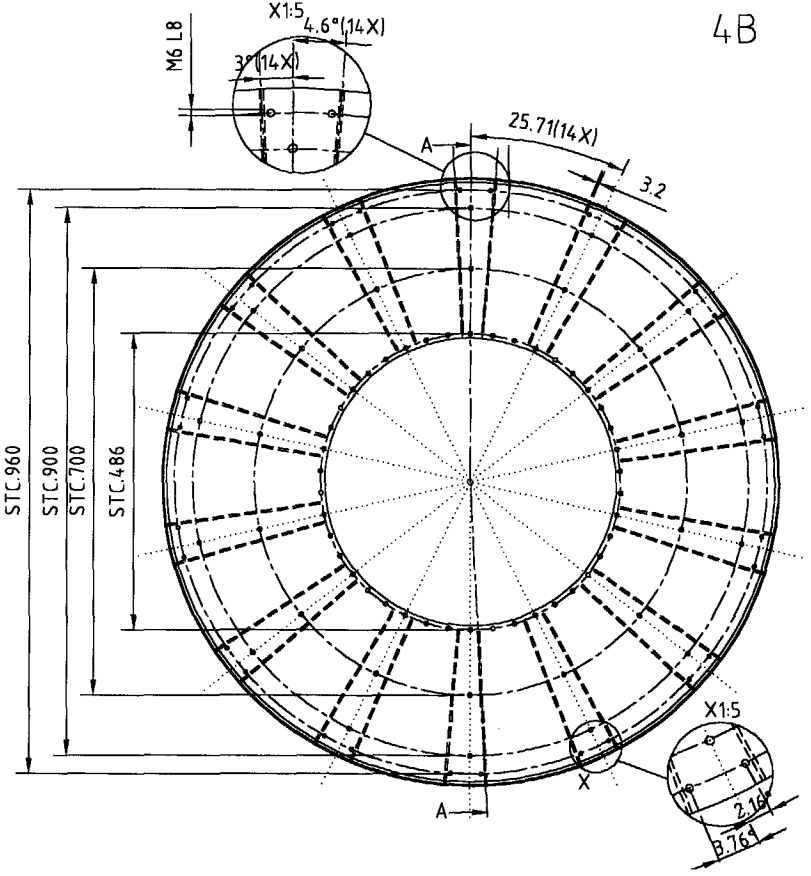
4B
X1:5
4.6°(14X)
M6 L8
3°(14X)
A
25.71(14X)
3.2
STC.960
STC.900
STC.700
STC.486
X
A
X1:5
2.16
B.76

Appendix D

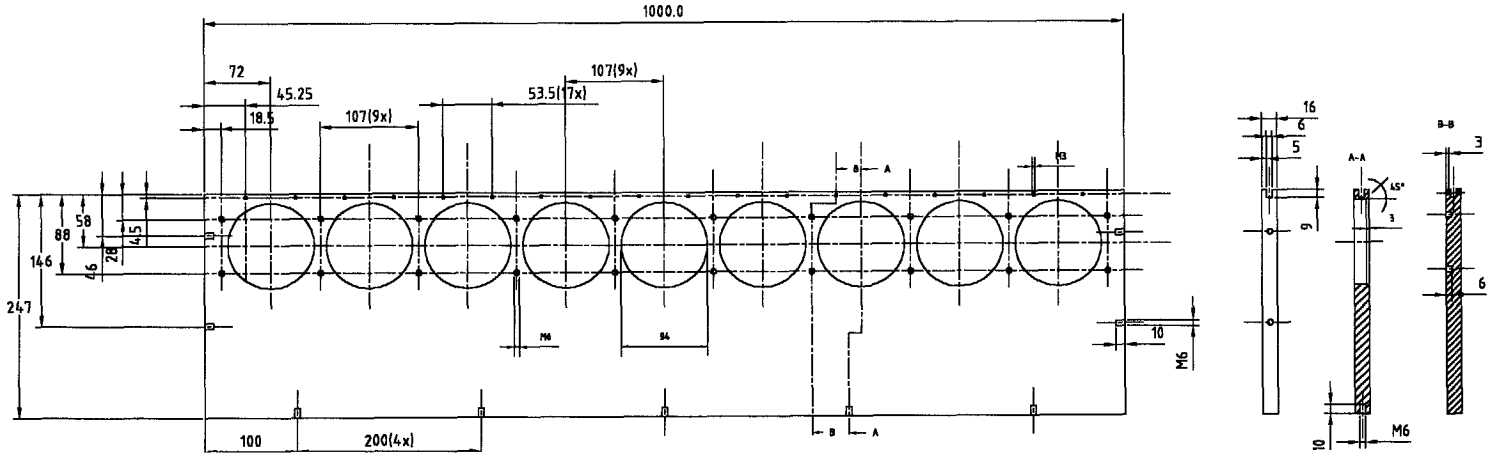
1000.0
72
45.25
18.5
107(9x)
53.5(17x)
107(9x)
58
88
146
247
45
28
46
M6
94
10
M6
100
200(4x)
A
B
16
6
5
9
A-A
45°
3
B-B
3
6
10
M6

Appendix D

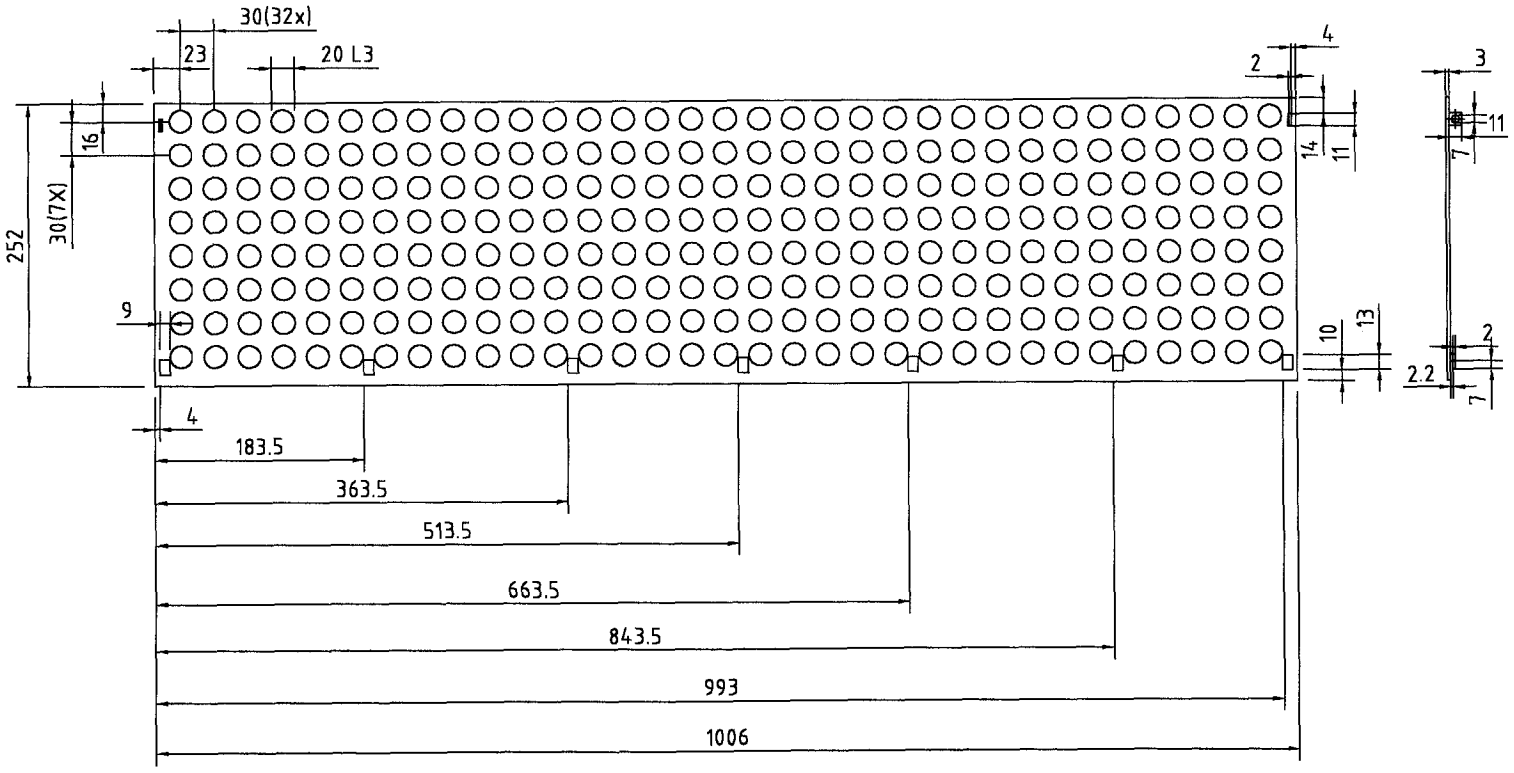
30(32x)
23
20 L3
4
2
3
11
7
14
11
16
30(7X)
252
9
10
13
2
2.2
7
4
183.5
363.5
513.5
663.5
843.5
993
1006

Appendix D

E.1 Granular Activated Carbon adsorption (GAC)

EPA program for cost evaluation

The parameters used for EPA's cost evaluation program [1] according to the file "param.dat" are as follows:

.90 100000.	= ($/LB) GAC COST AT (LBS) QUANTITY
15	= (%) CAPITAL RECOVERY INTEREST RATE
10.	= (YEARS) CAPITAL RECOVERY PERIOD
5.	= (% OF CONSTRUCTION COST) OVERHEAD & PROFIT FACTOR
5.	= (% OF CONSTRUCTION COST) SPECIAL SITEWORK FACTOR
10.	= (% OF CONSTRUCTION COST) CONSTRUCTION CONTINGENCIES
10.	= (% OF CONSTRUCTION COST) ENGINEERING FEE FACTOR
5708. Oct 1996	= (CCI BASE YEAR 1913) ENR CONSTRUCTION COST INDEX
394. Sep 1996	= (PPI BASE YEAR 1967=100) PRODUCERS PRICE INDEX
40.	= ($/MANHOUR) LABOR RATE + FRINGE
10.	= (% OF LABOR) LABOR OVERHEAD FACTOR
.11	= ($/KWH) ELECTRIC RATE
0.95	= ($/GALLON) FUEL OIL RATE
.0055	= ($/CU.FT.) NATURAL GAS RATE
0.35	= ($/1000 GAL) PROCESS WATER RATE
30.	= (LBS/CU.FT.) GAC BULK DENSITY
12.	= (% BY VOLUME) GAC LOSS RATE FROM REACTIVATION / TRANSPORT
50.	= (LBS/SQ.FT./DAY) MULTIHEARTH LOADING RATE
O	= (O or G) TYPE OF FUEL: O for fuel oil, G for natural gas

Parameters used in the program "cphsdm" (see [1]):

bulk bed density:	0.487	[g/cm³]
carbon particle diameter:	0.105	[cm]
apparent particle density:	0.825	[g/cm³]
superficial fluid velocity:	0.272	[cm/s]
Freundlich K:	474	[(μmole/g)(L/μmole)$^{1/n}$]
Freundlich 1/n:	0.33	[-]
initial concentration of compound:	100,000	[μg/L]
degree of overshoot as percent:	0	[-]
molecular weight of the compound:	92.15	[g/mole]
molal volume of the compound:	118.2	[cm³/mole]
operating temperature:	12	[°C]
surface/pore diffusion flux ratio:	3.72	[-]
points on the breakthrough curve:	100	[-]

Print-out for "cphsdm" for an empty bed contact time of 5 minutes:

CONSTANT PATTERN RESULTS FOR - toluene
PHYSICAL PARAMETERS:

EMPTY BED CONTACT TIME, EBCT, (MIN.)	= 5.0000000
BULK DENSITY OF THE BED, RHOB (g/cm^3)....	= 0.48699999
RADIUS OF ADSORBENT PARTICLE, RAD (cm)....	= 0.52499998E-01
APPARENT PARTICLE DENSITY, RHOP (g/cm^3)..	= 0.82499999
VOID FRACTION OF THE PARTICLE, EPOR.....	= 0.64099997
VOID FRACTION OF BED, EBED (DIM.).....	= 0.40969697
SUPERFICIAL FLUID VELOCITY (cm/sec).....	= 0.27200001
SURFACE LOADING, SF (gpm/ft^2).....	= 4.0049281
REYNOLDS NUMBER, RE, (DIM.)	= 5.6236157
TEMPERATURE OF WATER, TEMP, (DEG C.)	= 12.000000
DENSITY OF WATER, DW, (g/cm^3)	= 0.99952000
VISCOSITY OF WATER, VW, (g/cm-sec)	= 0.12390000E-01
SURFACE/PORE DIFFUSION FLUX RATIO, PSDFR .	= 3.7200000

PARAMETERS FOR COMPOUND: toluene

INITIAL BULK LIQUID-PHASE CONC., (ug/L).....	= 99999.992
FREUNDLICH ISO. CAP., K (umol/g)/(umol/L)^1/N	= 474.00000
FREUNDLICH ISOTHERM EXPONENT, N (DIM.)	= 0.33000001
MOLAL VOLUME AT THE BOILING PT. (cm^3/g-mol)	= 118.20000
MOLECULAR WEIGHT OF COMPOUND, MW	= 92.150002
LIQUID DIFFUSIVITY, DIFL, (cm^2/sec)	= 0.62469871E-05
FILM TRANSFER COEFFICIENT, KF, (cm/sec)	= 0.25536215E-02
SURFACE DIFFUSION COEFFICIENT, DS, (cm^2/sec).	= 0.41174406E-08
SOLUTE DISTRIBUTION PARAMETER, DG, (DIM.)	= 5212.6250
BIOT NUMBER, BI (DIM.).....	= 9.0000362
SCHMIDT NUMBER, SC, (DIM.)	= 1984.3086

CONSTANT PATTERN PARAMETERS FOR COMPOUND: toluene

THE MINIMUM STANTON NUMBER, STM	= 3.8768475
THE MINIMUM EBCT, ETMIN, (minutes)	= 2.2503767
THE MINIMUM EBCT, EMLEN, (cm)	= 36.726147
THROUGHPUT AT 95% OF THE MTZ, T95, ...	= 1.7665764
THROUGHPUT AT 5% OF THE MTZ, T05, ...	= 0.57082784
THE EBCT OF THE MTZ, ETMTZ, (minutes).....	= 2.6908846
THE LENGTH OF THE MTZ, EMTZL, (cm)	= 43.915241

CONSTANT PATTERN SOLUTION
FOR AN EBCT OF 5.00 MINUTES

Ce/Co	Ce (ug/L)	BED VOL. FED	GAC BED LIFE (DAYS)	GAC USE RATE LBS/K-gal	FIELD ADJUSTED BED LIFE (DAYS)	FIELD ADJUSTED USE RATE LBS/K-gal
0.010	1000.00	1593.0	5.5	2.55106	12.4	1.14064

PARAMETERS USED FOR EMPIRICAL EQUATION THAT DESCRIBE
SOLUTIONS TO HSDM FOR FIXED BED REACTOR

A0	A1	A2	A3	A4
-0.1733580	1.0000000	0.1203110	0.0159400	0.1339730

Parameters used in the program "gac-cost" (see [1]):

- overall system design capacity: 0.6341 (for 100 m^3/h) [mgd]
  0.06341(for 10 m^3/h) [mgd]
- average system production: 0.6341 (for 100 m^3/h) [mgd]
  0.06341 (for 10 m^3/h) [mgd]
- number of GAC contactors: 1 [-]
- hydraulic loading: 4 [gpm/sqft]
- steel pressure contactor
- bed life in days according to the result of the program "cphsdm"
- no reactivation on-site

Print-out for "gac-cost" for a 10 m^3/h feed rate and an empty bed contact time of 5 minutes:

COST ESTIMATION PROGRAM FOR GAC TREATMENT SYSTEMS

PROBLEM ID = toluene removal at 10 m3/h

UGAC=0.90 AT 100000. LBS CRI=15.0 CRP=10.0 COH= 5.0
CCI=5708.0 PPI=394.0 ULAB=40.00 LOH= 10.0 UPOW=0.11
UFUEL=0.95 UNGAS=0.0055 UH2O= 0.35 BDEN=30.0 LOSS=12.0
MLR=50.0 FTYPE=O
CSITE= 5.0 CINTR=10.0 CENG=10.0

TOTAL SYSTEM DESIGN CAPACITY (MGD)	= 0.06
AVG SYSTEM PRODUCTION (MGD)	= 0.06
NUMBER OF GAC CONTACTORS	= 1.
DESIGN CAPACITY PER CONTACTOR (MGD)	= 0.06
CROSS-SECTIONAL AREA OF EACH CONTACTOR (SQ. FT)	= 11.01
EBCT (MINUTES)	= 5.00
HYDRAULIC LOADING (GPM/SQ. FT)	= 4.00
GAC BED DEPTH (FT)	= 2.67
VOLUME PER EACH CONTACTOR (CU. FT)	= 29.4
TOTAL GAC VOLUME OF SYSTEM (CU.FT)	= 29.43
TOTAL GAC MASS OF SYSTEM (LBS)	= 883.05

ADSORBER TYPE IS STEEL PRESSURE CONTACTORS
(GAC PACKAGE PLANT)

GAC BED SERVICE LIFE (DAYS)	= 5.5
GAC USE RATE (GALLONS/LB)	= 394.9
SPENT CARBON (LBS/YEAR)	= 58602.

SPENT CARBON IS REPLACED WITH VIRGIN GAC

CONSTRUCTION COSTS	($)
----------	---
ADSORPTION SYSTEM	112669.
REACTIVATION SYSTEM	0.
TOTAL =	112669.

ADSORPTION SYSTEM	($/YEAR)	
ELECTRIC POWER	1070.	
MAINT & PROCESS LABOR	28552.	
MAINT & PROCESS MATERIALS	496.	
TOTAL O&M COST	30118.	130.1 (CENTS/1000 GAL)
TOTAL CAPITAL COST	22450.	97.0 (CENTS/1000 GAL)
TOTAL ADSORPTION COST	52567.	227.1 (CENTS/1000 GAL)

SPENT GAC REPLACEMENT	
VIRGIN GAC ($/YEAR) =	54901.
VIRGIN GAC (CENTS/LB) =	93.7
VIRGIN GAC (CENTS/1000 GAL) =	237.2

OVERALL SYSTEM TOTALS	($/YEAR)	(CENTS/1000 GAL)
SYSTEMS CAPITAL	22450.	97.0
SYSTEMS O&M	85019.	367.3
SYSTEMS TOTAL	107468.	464.3

Treatment cost

According to Stenzel [2], for liquid-phase carbon adsorption in most cases an on-site thermal reactivation facility is not cost-effective until more than 10,000 lb/d of carbon are required. For our case less than 10,000 lb/d of carbon are required (both for 10 m^3/h and 100 m^3/h) and, as expected, according to EPA's program [1] it is more cost-effective to replace spent carbon with fresh carbon.

With increasing empty bed contact time (EBCT), the replacement frequency and hence the cost of spent carbon will decrease but the construction cost will increase. The optimal EBCT has been determined by calculating the treatment cost per m^3 feed water for a range of EBCT's, see table E.1 for a feed rate of 10 m^3/h and table E.2 for a feed rate of 100 m^3/h. EPA's program yields the construction cost and annual operation & maintenance cost ("O&M") for one contactor. The treatment cost in $/$m^3$ feed water are obtained by dividing the sum of 20% of the construction cost for two contactors (0.20 x 2 contactor) plus annual O&M cost for two contactors (2 x O&M) plus annual carbon replacement cost (1 x GAC) by the annual feed water volume (8,000 hours multiplied with a feed rate of 10 m^3/h or a feed rate of 100 m^3/h).

Table E.1: treatment cost for a range of empty bed contact times for 10 m^3/h

EBCT [min]	bed height [ft]	bed life (days)	contactor ($)	O&M ($)	GAC ($)	$/m^3
2	1.07	1.1	81134	29944	106856	2.49
3	1.6	2.6	93250	30009	69033	2.08
4	2.14	4	103545	30065	60166	2.02
5	**2.67**	**5.5**	**112669**	**30118**	**54901**	**2**
6	3.21	7	120956	30166	51884	2.01
7	3.74	8.5	128606	30212	49928	2.02
8	4.28	10	135750	30256	48556	2.04

Table E.2: treatment cost for a range of empty bed contact times for 100 m³/h

EBCT [min]	bed height [ft]	bed life (days)	contactor ($)	O&M ($)	GAC ($)	$/m³
4	2.14	4	275590	47689	549707	0.94
5	2.67	5.5	306010	47940	501603	0.9
6	**3.21**	**7**	**333640**	**48177**	**474032**	**0.88**
7	3.74	8.5	392736	48403	456157	0.89
8	4.28	10	418986	48620	443628	0.89
9	4.81	11.5	443711	48831	434358	0.89
10	5.35	12.9	467157	49035	430403	0.89

For 10 m³/h the optimal EBCT is 5 minutes, for 100 m³/h the optimal EBCT is 6 minutes. Using an exchange rate of 1.7 NLG/$, the treatment cost for 10 m³/h are approximately 3.4 NLG/m³ and the treatment cost for 100 m³/h are approximately 1.5 NLG/m³.

Space requirements

10 m³/h:

column area: 1.02 m² → column diameter D = 1.2 m
height of packing = 0.8 m
height of bottom section = 2 m
height of top section = 0.5 m
total column height ≈ 3.3 m
distance "d" between columns = 1 m
footprint of columns = (1+D+d+D+1) x (1+D+1) ≈ 17 m²

100 m³/h:

column area: 10.2 m² → column diameter D = 3.6 m
height of packing = 1.0 m
height of bottom section = 2 m
height of top section = 0.5 m
total column height ≈ 3.5 m
distance "d" between columns = 1 m
footprint of columns = (1+D+d+D+1) x (1+D+1) ≈ 57 m²

Summary

	10 m³/h:	100 m³/h:
treatment cost [NLG/m³]:	3.4	1.5
footprint [m²]:	17	57
maximum height [m]:	3.3	3.5

References

[1] Clark, R.M., Adams, J.Q., *EPA's drinking water and groundwater remediation evaluation; granular activated carbon*, Lewis, Chelsea, 1991, ISBN 0-87371-353-2

[2] Stenzel, M.H., *Remove organics by activated carbon adsorption*, Chem.Eng.Progr., April 1993, pp. 36-43

E.2 Packed Tower Aeration + gas-phase GAC (PTA+)

EPA program for cost evaluation

The parameters used for EPA's cost evaluation program [1] according to the files "parm.dat", "pta.in" and "pta.gas" are as follows:

File "parm.dat":

```
15.              = (%) CAPITAL RECOVERY INTEREST RATE
10.              = (YEARS) CAPITAL RECOVERY PERIOD
5.               = (% OF CONSTRUCTION COST) OVERHEAD & PROFIT FACTOR
5.               = (% OF CONSTRUCTION COST) SPECIAL SITEWORK FACTOR
10.              = (% OF CONSTRUCTION COST) CONSTRUCTION CONTINGENCIES
10.              = (% OF CONSTRUCTION COST) ENGINEERING FEE FACTOR
5708.  OCT 1996          = (CCI BASE YEAR 1913) ENR CONSTRUCTION COST INDEX
394.   SEP 1996          = (PPI BASE YEAR 1967=100) PRODUCERS PRICE INDEX
40.              = ($/MANHOUR) LABOR RATE + FRINGE
10.              = (% OF LABOR) LABOR OVERHEAD FACTOR
.11              = ($/KWH) ELECTRIC RATE
```

File "pta.in":

```
TOLUENE                  NAME OF COMPOUND
92.15                    MOLECULAR WEIGHT
118.2                    MOLAL VOLUME, CU.CM/G-MOLE
14.    at 12-deg C       VAPOR PRESSURE, MM HG
571.                     SOLUBILITY, MG/L
110.6                    BOILING POINT OF COMPOUND, DEG-C
0.13   CUMMINS(PILOT)    HENRY'S COEF., M3 WATER / M3 AIR, CALC IF 0
1.1                      KLa SAFETY FACTOR
1.1                      HENRY'S COEF. SAFETY FACTOR, USED IF CALC
12.                      WATER TEMPERATURE, DEG-C
999.52                   WATER DENSITY, KG/CU.M
1.                       ATM PRESSURE, ATM
2 INCH-SADDLES           PACKING MEDIA DESCRIPTION
.0508                    NOMINAL DIAMETER OF PACKING MEDIA, M
20.                      PACKING FACTOR
110.                     SPECIFIC SURFACE AREA OF PACKING, M2/M3
.033                     SURFACE TENSION OF PACKING MEDIA, N/M
35.                      NET EFFICIENCY OF BLOWER/MOTOR, %
80.                      NET EFFICIENCY OF PUMP/MOTOR, %
```

File "pta.gas":

```
33.              = GAC BULK DENSITY, LBS/CU.FT.
2.0  20000.  BPL = GAC PRICE ($/LB) AT GIVEN QTY (LBS)
0.95  10000.     = OFF-SITE GAC REGENERATION PRICE, $/LB
2                1=OFF-SITE REGEN  2=ONSITE STEAM  3=VIRGIN GAC
12.              = % GAC LOSSES FROM REGEN + TRANSPORT
50.              = GAS VELOCITY, FT/MIN
24.              = GAS PHASE TEMPERATURE. deg-C  POST-HEATER
27.              = SOLUBILITY VAPOR PRESSURE AT OFF-GAS TEMP
0.867            = LIQUID DENSITY OF COMPOUND, g/ml
1.4773           = REFRACTIVE INDEX OF COMPOUND
```

Parameters used in the program "pta2" (see [1]):

total design flow:	440.33 (for 100 m^3/h)	[gpm]
	44.033 (for 10 m^3/h)	[gpm]
total average operating flow:	440.33 (for 100 m^3/h)	[gpm]
	44.033 (for 10 m^3/h)	[gpm]
influent concentration:	100,000	[µg/L]
effluent concentration:	1,000	[µg/L]
air pressure drop start / end / incr.:	50 85 5	[N/m^3]
air-to-water ratio start / end / incr.:	10 45 5	[-]
GAC bed depth:	1	[ft]

Print-out for "pta2" for a 10 m^3/h feed rate:

THE COMPOUND IS TOLUENE
HENRY"S COEF., CU.M WATER/CU.M AIR = 0.13000

TOTAL DESIGN FLOW, GPM = 44.03 (0.00278 CU.M/SEC)
TOTAL AVG FLOW, GPM = 44.03 (0.00278 CU.M/SEC)
INFLUENT CONC., ug/L = 100000.000
EFFLUENT CONC., ug/L = 1000.000

WATER TEMPERATURE, deg-K = 285.0
ATMOSPHERIC PRESSURE, ATM = 1.00

TYPE OF PACKING MEDIA: = 2 INCH-SADDLES

REMOVAL EFFICIENCY, % = 99.00

TOTAL PTA COST (CENTS/1000 GAL):

	PRESSURE DROP THRU MEDIA (N/SQ.M/M)							
(SF) (A/W)	50.0	55.0	60.0	65.0	70.0	75.0	80.0	85.0
(1.30) (10.0)	122.8	122.8	122.9	122.9	123.0	123.1	123.1	123.2
(1.95) (15.0)	105.6	105.6	105.7	105.7	105.8	105.8	105.9	105.9
(2.60) (20.0)	100.7	100.8	100.8	100.9	100.9	101.0	101.0	101.1
(3.25) (25.0)	98.5	98.5	98.5	98.6	98.6	98.7	98.8	98.8
(3.90) (30.0)	99.1	98.4	97.8	97.3	97.4	97.4	97.5	97.6
(4.55) (35.0)	99.5	98.8	98.2	97.7	97.2	96.9	96.8	96.8
(5.20) (40.0)	99.9	99.2	98.6	98.0	97.6	97.2	96.8	96.5
(5.85) (45.0)	100.3	99.5	98.9	98.3	97.9	97.5	97.1	96.8

TOWER PACKING HEIGHT (FEET):

	PRESSURE DROP THRU MEDIA (N/SQ.M/M)							
(SF) (A/W)	50.0	55.0	60.0	65.0	70.0	75.0	80.0	85.0
(1.30) (10.0)	95.2	95.2	95.2	95.2	95.2	95.2	95.2	95.2
(1.95) (15.0)	52.3	52.3	52.3	52.3	52.3	52.3	52.3	52.3
(2.60) (20.0)	42.3	42.3	42.3	42.3	42.3	42.3	42.3	42.3
(3.25) (25.0)	37.8	37.8	37.8	37.8	37.8	37.8	37.8	37.8
(3.90) (30.0)	34.1	34.5	34.9	35.2	35.2	35.2	35.2	35.2
(4.55) (35.0)	31.8	32.2	32.5	32.9	33.1	33.4	33.5	33.5
(5.20) (40.0)	30.2	30.6	30.9	31.2	31.5	31.8	32.0	32.2
(5.85) (45.0)	29.0	29.4	29.7	30.0	30.3	30.6	30.8	31.0

TOWER DIAMETER (FEET):

	PRESSURE DROP THRU MEDIA (N/SQ.M/M)							
(SF) (A/W)	50.0	55.0	60.0	65.0	70.0	75.0	80.0	85.0
(1.30) (10.0)	1.4	1.4	1.4	1.4	1.4	1.4	1.4	1.4
(1.95) (15.0)	1.4	1.4	1.4	1.4	1.4	1.4	1.4	1.4
(2.60) (20.0)	1.4	1.4	1.4	1.4	1.4	1.4	1.4	1.4
(3.25) (25.0)	1.4	1.4	1.4	1.4	1.4	1.4	1.4	1.4
(3.90) (30.0)	1.5	1.4	1.4	1.4	1.4	1.4	1.4	1.4
(4.55) (35.0)	1.5	1.5	1.5	1.4	1.4	1.4	1.4	1.4
(5.20) (40.0)	1.6	1.5	1.5	1.5	1.4	1.4	1.4	1.4
(5.85) (45.0)	1.6	1.6	1.5	1.5	1.5	1.4	1.4	1.4

TOTAL SYSTEM COST: PTA + OFF-GAS CONTROL (CENTS/1000 GAL):

	PRESSURE DROP THRU MEDIA (N/SQ.M/M)							
(SF) (A/W)	50.0	55.0	60.0	65.0	70.0	75.0	80.0	85.0
(1.30) (10.0)	272.0	272.0	272.1	272.1	272.2	272.3	272.3	272.4
(1.95) (15.0)	262.6	262.7	262.7	262.8	262.8	262.9	262.9	263.0
(2.60) (20.0)	264.4	264.5	264.5	264.6	264.6	264.7	264.7	264.8
(3.25) (25.0)	268.1	268.0	268.1	268.1	268.2	268.3	268.3	268.4
(3.90) (30.0)	273.9	273.2	272.7	272.2	272.3	272.3	272.4	272.5
(4.55) (35.0)	279.4	278.6	278.0	277.5	277.1	276.7	276.6	276.7
(5.20) (40.0)	284.4	283.7	283.0	282.5	282.0	281.6	281.3	281.0
(5.85) (45.0)	289.1	288.4	287.7	287.2	286.7	286.3	285.9	285.6

SUMMARY OF GAC GAS-ADSORPTION:

	UNIT COST	GAC VOL CU.FT	USE RATE mg/L-H2O	BED LIFE DAYS
(1.30) (10.0)	149.2	1.2	271.613	0.3
(1.95) (15.0)	157.1	1.8	279.649	0.4
(2.60) (20.0)	163.7	2.4	286.202	0.5
(3.25) (25.0)	169.6	2.9	291.804	0.6
(3.90) (30.0)	174.9	3.5	296.734	0.7
(4.55) (35.0)	179.8	4.1	301.161	0.9
(5.20) (40.0)	184.4	4.7	305.195	1.0
(5.85) (45.0)	188.8	5.3	308.912	1.1

Print-out for "pta2" for a 100 m³/h feed rate:

THE COMPOUND IS TOLUENE
HENRY"S COEF., CU.M WATER/CU.M AIR = 0.13000

TOTAL DESIGN FLOW, GPM = 440.33 (0.02778 CU.M/SEC)
TOTAL AVG FLOW, GPM = 440.33 (0.02778 CU.M/SEC)
INFLUENT CONC., ug/L = 100000.000
EFFLUENT CONC., ug/L = 1000.000

WATER TEMPERATURE, deg-K = 285.0
ATMOSPHERIC PRESSURE, ATM = 1.00
TYPE OF PACKING MEDIA: = 2 INCH-SADDLES
REMOVAL EFFICIENCY, % = 99.00

TOTAL PTA COST (CENTS/1000 GAL):

	PRESSURE DROP THRU MEDIA (N/SQ.M/M)							
(SF) (A/W)	50.0	55.0	60.0	65.0	70.0	75.0	80.0	85.0
(1.30) (10.0)	47.7	47.8	47.9	47.9	48.0	48.0	48.1	48.1
(1.95) (15.0)	33.9	34.0	34.0	34.1	34.1	34.2	34.2	34.3
(2.60) (20.0)	30.5	30.6	30.6	30.7	30.7	30.8	30.8	30.9
(3.25) (25.0)	29.0	29.0	29.1	29.2	29.2	29.3	29.3	29.4
(3.90) (30.0)	29.4	29.0	28.6	28.4	28.4	28.5	28.6	28.6
(4.55) (35.0)	29.7	29.3	28.9	28.7	28.4	28.2	28.2	28.3
(5.20) (40.0)	30.0	29.6	29.2	28.9	28.7	28.5	28.3	28.2
(5.85) (45.0)	30.3	29.9	29.5	29.2	28.9	28.7	28.6	28.4

TOWER PACKING HEIGHT (FEET):

	PRESSURE DROP THRU MEDIA (N/SQ.M/M)							
(SF) (A/W)	50.0	55.0	60.0	65.0	70.0	75.0	80.0	85.0
(1.30) (10.0)	95.2	95.2	95.2	95.2	95.2	95.2	95.2	95.2
(1.95) (15.0)	52.3	52.3	52.3	52.3	52.3	52.3	52.3	52.3
(2.60) (20.0)	42.3	42.3	42.3	42.3	42.3	42.3	42.3	42.3
(3.25) (25.0)	37.8	37.8	37.8	37.8	37.8	37.8	37.8	37.8
(3.90) (30.0)	34.1	34.5	34.9	35.2	35.2	35.2	35.2	35.2
(4.55) (35.0)	31.8	32.2	32.5	32.9	33.1	33.4	33.5	33.5
(5.20) (40.0)	30.2	30.6	30.9	31.2	31.5	31.8	32.0	32.2
(5.85) (45.0)	29.0	29.4	29.7	30.0	30.3	30.6	30.8	31.0

TOWER DIAMETER (FEET):

	PRESSURE DROP THRU MEDIA (N/SQ.M/M)							
(SF) (A/W)	50.0	55.0	60.0	65.0	70.0	75.0	80.0	85.0
(1.30) (10.0)	4.3	4.3	4.3	4.3	4.3	4.3	4.3	4.3
(1.95) (15.0)	4.3	4.3	4.3	4.3	4.3	4.3	4.3	4.3
(2.60) (20.0)	4.3	4.3	4.3	4.3	4.3	4.3	4.3	4.3
(3.25) (25.0)	4.3	4.3	4.3	4.3	4.3	4.3	4.3	4.3
(3.90) (30.0)	4.6	4.5	4.4	4.3	4.3	4.3	4.3	4.3
(4.55) (35.0)	4.8	4.7	4.6	4.5	4.4	4.3	4.3	4.3
(5.20) (40.0)	5.0	4.9	4.8	4.6	4.6	4.5	4.4	4.3
(5.85) (45.0)	5.1	5.0	4.9	4.8	4.7	4.6	4.5	4.4

TOTAL SYSTEM COST: PTA + OFF-GAS CONTROL (CENTS/1000 GAL):

	PRESSURE DROP THRU MEDIA (N/SQ.M/M)							
(SF) (A/W)	50.0	55.0	60.0	65.0	70.0	75.0	80.0	85.0
(1.30) (10.0)	130.5	130.6	130.6	130.7	130.7	130.8	130.9	130.9
(1.95) (15.0)	121.2	121.2	121.3	121.3	121.4	121.4	121.5	121.5
(2.60) (20.0)	121.7	121.7	121.8	121.8	121.9	121.9	122.0	122.0
(3.25) (25.0)	123.7	123.7	123.8	123.9	123.9	124.0	124.0	124.1
(3.90) (30.0)	127.4	127.0	126.6	126.4	126.4	126.5	126.6	126.6
(4.55) (35.0)	130.8	130.4	130.0	129.7	129.5	129.3	129.3	129.3
(5.20) (40.0)	134.1	133.6	133.3	133.0	132.7	132.5	132.3	132.2
(5.85) (45.0)	137.0	136.5	136.2	135.9	135.6	135.4	135.2	135.1

SUMMARY OF GAC GAS-ADSORPTION:

	UNIT COST	GAC VOL CU.FT	USE RATE mg/L-H2O	BED LIFE DAYS
(1.30) (10.0)	82.8	11.8	271.613	0.3
(1.95) (15.0)	87.3	17.7	279.649	0.4
(2.60) (20.0)	91.2	23.5	286.202	0.5
(3.25) (25.0)	94.7	29.4	291.804	0.6
(3.90) (30.0)	98.0	35.3	296.734	0.7
(4.55) (35.0)	101.1	41.2	301.161	0.9
(5.20) (40.0)	104.0	47.1	305.195	1.0
(5.85) (45.0)	106.7	53.0	308.912	1.1

Parameters used in the program "pta" (see [1]):

total design flow:	440.33 (for 100 m^3/h)	[gpm]
	44.033 (for 10 m^3/h)	[gpm]
total average operating flow:	440.33 (for 100 m^3/h)	[gpm]
	44.033 (for 10 m^3/h)	[gpm]
influent concentration:	100,000	[µg/L]
effluent concentration:	1,000	[µg/L]
air pressure drop:	50	[N/m^3]
air-to-water ratio:	25	[-]
GAC bed depth:	1	[ft]

Print-out for "pta" for a 10 m^3/h feed rate:

THE COMPOUND IS TOLUENE		
HENRY"S COEF., CU.M WATER/CU.M AIR	= 0.13000	
TOTAL DESIGN FLOW, GPM	= 44.03	(0.00278 CU.M/SEC)
TOTAL AVG FLOW, GPM	= 44.03	(0.00278 CU.M/SEC)
INFLUENT CONC., ug/L	= 100000.000	
EFFLUENT CONC., ug/L	= 1000.000	
EQUILIBRIUM CONC., ug/L	= 30461.538	
WATER TEMPERATURE, deg-K	= 285.0	
ATMOSPHERIC PRESSURE, ATM	= 1.00	
TYPE OF PACKING MEDIA:	= 2 INCH-SADDLES	
PRESS DROP: MEDIA, N/SQ.M/M	= 50.0	
AIR-TO-WATER RATIO	= 25.0	
MINIMUM A/W RATIO	= 7.62	
DESIGN AIRFLOW RATE, CFM	= 147.17	(0.07 CU.M/SEC)
STRIPPING FACTOR	= 3.25	
KLa MASS-TRANS COEFF, 1/SEC	= 0.010771	
LIQUID LOADING, GPM/SQ.FT	= 29.79	
TOWER DIAMETER, FT	= 1.37	(0.42 M)
TOTAL TOWER X-SECT AREA, SQ.FT	= 1.5	(0.1 SQ.M)
PACKING HEIGHT, FT	= 37.76	(11.51 M)
TOTAL PACKING VOLUME, CU.FT	= 55.8	(1.6 CU.M)
NUMBER OF TOWERS	= 1.0	
REMOVAL EFFICIENCY, %	= 99.00	
DESIGN POWER FOR BLOWERS, KW/HOUR	= 0.28	

DESIGN POWER FOR PUMPS, KW/HOUR	= 0.70	
PRELIMINARY COST ESTIMATES FOR SYSTEM:		
PTA CONSTRUCTION COST ($)	= 49984.	
INDIRECT CONSTRUCTION ($)	= 14995.	
TOTAL PTA CONSTRUCTION ($)	= 64979.	
PTA AMORTIZED CAPITAL ($/YR)	= 12947.	(55.9 CENTS/1000 GAL)
TOWER PUMPING POWER ($/YR)	= 677.	
BLOWER ELECTRIC ($/YR)	= 274.	
FIN-WATER PUMP POWER ($/YR)	= 349.	
MAINTENANCE MATERIAL ($/YR)	= 171.	
PTA O&M LABOR ($/YR)	= 8381.	
SUM PTA O&M COST ($/YR)	= 9852.	(42.6 CENTS/1000 GAL)
TOTAL PTA SYSTEM COST ($/YR)	= 22799.	(98.5 CENTS/1000 GAL)
DESIGN AND COSTS FOR TOWER OFF-GAS CONTROL BY GAC:		
GAC BED DEPTH, FT	= 1.00	
GAS VELOCITY, FT/MIN	= 50.0	
GAC EBCT FOR GAS-PHASE, SEC	= 1.20	
TOTAL GAC X-SECT AREA, SQ.FT	= 2.94	
TOTAL EFFECTIVE GAC VOLUME, CU.FT	= 2.94	
TOTAL GAC REQD FOR ADSORBERS, LBS	= 97.1	
GAS-PHASE CONCENTRATION, ug/L-AIR	= 3960.00	
PART PRESS/VAPOR PRESS RATIO	= 0.02710	
GAC GAS-PHASE CAPACITY, ug/g-GAC	= 339269.4	
GAC USE RATE-GAS ADSRP, mg/L-WATER	= 291.8035	
GAC USE RATE, LBS/1000 GAL-WATER	= 2.4352	
GAC USE RATE, mg-GAC/L-AIR	= 11.6709	
SPENT GAC QUANTITY, LBS/YEAR	= 56359.9	
GAC BED LIFE, DAYS	= 0.6	
OFF-GAS BLOWER, KW per HOUR	= 0.1	
OFF-GAS HEATER, KW per HOUR	= 1.5	
GAC CONSTRUCTION COST ($)	= 30743.	
INDIRECT CONSTR COST ($)	= 9223.	
TOTAL GAC CONSTR COST ($)	= 39966.	
GAC AMORTIZED CAPITAL ($/YR)	= 7963.	(34.4 CENTS/1000 GAL)
OFF-GAS BLOWER POWER ($/YR)	= 59.	
OFF-GAS HEATER POWER ($/YR)	= 1418.	
MAINT MATERIAL ($/YR)	= 227.	
O&M LABOR ($/YR)	= 12496.	
ON-SITE STEAM REGEN ($/YR)	= 17026.	
GAC REPLACE ($/YR)	= 51.	
SUM GAC O&M COST ($/YR)	= 31278.	(135.1 CENTS/1000 GAL)
TOTAL GAC GAS-ADSORP ($/YR)	= 39241.	(169.6 CENTS/1000 GAL)

OVERALL SYSTEM COSTS:

TOTAL SYSTEM CONSTR COST ($)	= 104945.	
TOTAL SYSTEM CAPITAL ($/YR)	= 20910.	(90.4 CENTS/1000 GAL)
TOTAL SYSTEM O&M COST ($/YR)	= 41130.	(177.7 CENTS/1000 GAL)
OVERALL SYSTEM COST ($/YR)	= 62041.	(268.1 CENTS/1000 GAL)

Print-out for "pta" for a 100 m³/h feed rate:

THE COMPOUND IS TOLUENE		
HENRY"S COEF., CU.M WATER/CU.M AIR	= 0.13000	
TOTAL DESIGN FLOW, GPM	= 440.33	(0.02778 CU.M/SEC)
TOTAL AVG FLOW, GPM	= 440.33	(0.02778 CU.M/SEC)
INFLUENT CONC., ug/L	= 100000.000	
EFFLUENT CONC., ug/L	= 1000.000	
EQUILIBRIUM CONC., ug/L	= 30461.538	
WATER TEMPERATURE, deg-K	= 285.0	
ATMOSPHERIC PRESSURE, ATM	= 1.00	
TYPE OF PACKING MEDIA:	= 2 INCH-SADDLES	
PRESS DROP: MEDIA, N/SQ.M/M	= 50.0	
AIR-TO-WATER RATIO	= 25.0	
MINIMUM A/W RATIO	= 7.62	
DESIGN AIRFLOW RATE, CFM	= 1471.69	(0.69 CU.M/SEC)
STRIPPING FACTOR	= 3.25	
KLa MASS-TRANS COEFF, 1/SEC	= 0.010771	
LIQUID LOADING, GPM/SQ.FT	= 29.79	
TOWER DIAMETER, FT	= 4.34	(1.32 M)
TOTAL TOWER X-SECT AREA, SQ.FT	= 14.8	(1.4 SQ.M)
PACKING HEIGHT, FT	= 37.76	(11.51 M)
TOTAL PACKING VOLUME, CU.FT	= 558.1	(15.8 CU.M)
NUMBER OF TOWERS	= 1.0	
REMOVAL EFFICIENCY, %	= 99.00	
DESIGN POWER FOR BLOWERS, KW/HOUR	= 2.85	
DESIGN POWER FOR PUMPS, KW/HOUR	= 7.03	

PRELIMINARY COST ESTIMATES FOR SYSTEM:

PTA CONSTRUCTION COST ($)	= 161529.	
INDIRECT CONSTRUCTION ($)	= 48459.	
TOTAL PTA CONSTRUCTION ($)	= 209988.	
PTA AMORTIZED CAPITAL ($/YR)	= 41841.	(18.1 CENTS/1000 GAL)
TOWER PUMPING POWER ($/YR)	= 6771.	
BLOWER ELECTRIC ($/YR)	= 2742.	
FIN-WATER PUMP POWER ($/YR)	= 3487.	
MAINTENANCE MATERIAL ($/YR)	= 320.	

PTA O&M LABOR ($/YR)	= 12045.	
SUM PTA O&M COST ($/YR)	= 25366.	(11.0 CENTS/1000 GAL)
TOTAL PTA SYSTEM COST ($/YR)	= 67206.	(29.0 CENTS/1000 GAL)

DESIGN AND COSTS FOR TOWER OFF-GAS CONTROL BY GAC:

GAC BED DEPTH, FT	= 1.00
GAS VELOCITY, FT/MIN	= 50.0
GAC EBCT FOR GAS-PHASE, SEC	= 1.20
TOTAL GAC X-SECT AREA, SQ.FT	= 29.43
TOTAL EFFECTIVE GAC VOLUME, CU.FT	= 29.43
TOTAL GAC REQD FOR ADSORBERS, LBS	= 971.3
GAS-PHASE CONCENTRATION, ug/L-AIR	= 3960.00
PART PRESS/VAPOR PRESS RATIO	= 0.02710
GAC GAS-PHASE CAPACITY, ug/g-GAC	= 339269.4
GAC USE RATE-GAS ADSRP, mg/L-WATER	= 291.8035
GAC USE RATE, LBS/1000 GAL-WATER	= 2.4352
GAC USE RATE, mg-GAC/L-AIR	= 11.6709
SPENT GAC QUANTITY, LBS/YEAR	= 563599.4
GAC BED LIFE, DAYS	= 0.6
OFF-GAS BLOWER, KW per HOUR	= 0.6
OFF-GAS HEATER, KW per HOUR	= 14.7
GAC CONSTRUCTION COST ($)	= 63342.
INDIRECT CONSTR COST ($)	= 19003.
TOTAL GAC CONSTR COST ($)	= 82345.

GAC AMORTIZED CAPITAL ($/YR)	= 16407.	(7.1 CENTS/1000 GAL)
OFF-GAS BLOWER POWER ($/YR)	= 594.	
OFF-GAS HEATER POWER ($/YR)	= 14181.	
MAINT MATERIAL ($/YR)	= 496.	
O&M LABOR ($/YR)	= 16774.	
ON-SITE STEAM REGEN ($/YR)	= 170263.	
GAC REPLACE ($/YR)	= 468.	
SUM GAC O&M COST ($/YR)	= 202776.	(87.6 CENTS/1000 GAL)
TOTAL GAC GAS-ADSORP ($/YR)	= 219183.	(94.7 CENTS/1000 GAL)

OVERALL SYSTEM COSTS:

TOTAL SYSTEM CONSTR COST ($)	= 292333.	
TOTAL SYSTEM CAPITAL ($/YR)	= 58248.	(25.2 CENTS/1000 GAL)
TOTAL SYSTEM O&M COST ($/YR)	= 228142.	(98.6 CENTS/1000 GAL)
OVERALL SYSTEM COST ($/YR)	= 286390.	(123.7 CENTS/1000 GAL)

Treatment cost

The program "pta2" gives treatment cost, tower packing height and tower diameter for a range of air-to-water ratio's and pressure drops (see print-out). The minimal treatment cost for both 10 m^3/h and 100 m^3/h feed rate are achieved at an air-to-water ratio of 15 (m^3 air)/(m^3 water). However, an air-to-water ratio of 25 (m^3 air)/(m^3 water) for both 10 m^3/h and 100 m^3/h has been chosen because the upper limit on practical packing height is about 40 ft [1]. The pressure drop has almost no influence on treatment cost, tower packing height or tower diameter at the chosen air-to-water ratio. Therefore, the minimum value of 50 Pa/m for pressure drop has been assumed.

The results of the subsequent program "pta" are as follows:

	10 m^3/h:	100 m^3/h:
construction of packed tower ($):	65,000	210,000
construction of GAC-treatment ($):	40,000	82,000
	---------- +	---------- +
fixed capital investment ($):	105,000	292,000
fixed annual charge at 20% ($/y):	21,000	58,000
operation and maintenance of packed tower ($/y):	10,000	25,000
operation and maintenance of GAC-treatment including on-site steam regeneration ($/y):	31,000	203,000
	---------- +	---------- +
annual treatment cost ($/y):	62,000	286,000
volume of treated water (m^3/y)	80,000	800,000
treatment cost ($/$m^3$):	0.78	0.36

Using an exchange rate of 1.7 NLG/$, the treatment cost for 10 m^3/h are approximately 1.3 NLG/m^3 and the treatment cost for 100 m^3/h are approximately 0.6 NLG/m^3.

Space requirements

10 m^3/h:

packed tower:

column diameter D_P= 0.4 m

height of packing = 11.5 m

height of bottom section = 2 + $D_P/2$ = 2.2 m

height of top section = 1 + $D_P/2$ = 1.2 m

column height ≈ 15 m

GAC-columns:

column area: 0.27 m^2 → column diameter D_G= 0.6 m

height of packing = 0.3 m

height of bottom section ≈ 1 m

height of top section ≈ 1 m

number of columns N = 2 (placed on top of each other)

height of columns ≈ (N x 2.3) + 1 ≈ 6 m

total system
distance "d" between packed tower and GAC-columns = 1 m
footprint of system ≈ $(1+D_P+d+D_G+1) \times (1+D_G+1) \approx 10$ m²
maximum height is 15 m

100 m³/h:
packed tower:
column diameter $D_P = 1.3$ m
height of packing = 11.5 m
height of bottom section = $2 + D_P/2 = 2.7$ m
height of top section = $1 + D_P/2 = 1.7$ m
column height ≈ 16 m
GAC-columns:
column area: 2.73 m² → column diameter $D_G = 1.9$ m
height of packing = 0.3 m
height of bottom section ≈ 1 m
height of top section ≈ 1 m
number of columns N = 2 (placed on top of each other)
height of columns ≈ (N x 2.3) + 1 ≈ 6 m
total system
distance "d" between packed tower and GAC-columns = 1 m
footprint of system ≈ $(1+D_P+d+D_G+1) \times (1+D_G+1) \approx 24$ m²
maximum height is 16 m

Summary

	10 m³/h:	100 m³/h:
treatment cost [NLG/m³]:	1.3	0.6
footprint [m²]:	10	24
maximum height [m]:	15	16

References

[1] Clark, R.M., Adams, J.Q., *EPA's drinking water and groundwater remediation cost evaluation; air stripping*, Lewis, Chelsea, 1991, ISBN 0-87371-352-4

E.3 Vacuum Steam Stripping (VSS)

Feed preheater
plate heat exchanger with $\Delta T = 4°C$ and $U = 1{,}000\ W/(m^2 \cdot °C)$
feed water temperature: 12°C

atmospheric stripper:
per m^3/h feed rate:

$$\text{power } P = \frac{1{,}000(kg)}{3{,}600(s)} \cdot 4.2 \cdot 10^3 \left(\frac{J}{kg \cdot °C}\right) \cdot (96-12)(°C) = 9.8 \cdot 10^4\ W$$

$$\text{area } A = \frac{P}{U \cdot \Delta T} = \frac{9.8 \cdot 10^4 (W)}{1{,}000\left(\frac{W}{m^2 \cdot °C}\right) \cdot 4(°C)} = 24.5\ m^2$$

equipment cost:
$10\ m^3/h \rightarrow A = 245\ m^2 \rightarrow$ NLG 57,000 [1]
$100\ m^3/h \rightarrow A = 2{,}450\ m^2 \rightarrow$ NLG 539,000 [1]

vacuum stripper:
choose the boiling point of water at 40°C (high enough to use ambient cooling water for the condenser) $\rightarrow$ system pressure is 0.073 bar

per m^3/h feed rate:

$$\text{power } P = \frac{1{,}000(kg)}{3{,}600(s)} \cdot 4.2 \cdot 10^3 \left(\frac{J}{kg°C}\right) \cdot (36-12)(°C) = 2.8 \cdot 10^4\ W$$

$$\text{area } A = \frac{P}{U \cdot \Delta T} = \frac{2.8 \cdot 10^4 (W)}{1{,}000\left(\frac{W}{m^2 \cdot C}\right) \cdot 4(°C)} = 7\ m^2$$

equipment cost:
$10\ m^3/h \rightarrow A = 70\ m^2 \rightarrow$ NLG 21,000 [1]
$100\ m^3/h \rightarrow A = 700\ m^2 \rightarrow$ NLG 154,000 [1]

$\Rightarrow$ operate column under vacuum (0.073 bar), at least for a feed rate of 100 m^3/h.

Reboiler
shell and tube heat exchanger, with $\Delta T \approx (100-50) \approx 50°C$ and $U = 1{,}000\ W/(m^2 \cdot °C)$

per m^3/h feed rate:

$$\text{power } P = \frac{1{,}000(kg)}{3{,}600(s)} \cdot 4.2 \cdot 10^3 \left(\frac{J}{kg \cdot °C}\right) \cdot (40-36)(°C) = 4.7 \cdot 10^3\ W$$

$$\text{area } A = \frac{P}{U \cdot \Delta T} = \frac{4.7 \cdot 10^3 (W)}{1{,}000(\frac{W}{m^2 \cdot °C}) \cdot 50(°C)} = 0.1 \text{ m}^2$$

equipment cost:
10 m³/h → A = 1 m² → NLG 16,000 [1]
100 m³/h → A = 10 m² → NLG 22,000 [1]

steam needed to raise the temperature of 1 m³ water from 36°C to 40°C:

$$\frac{1{,}000(kg) \cdot 4.2 \cdot 10^3(\frac{J}{kg \cdot °C}) \cdot (40 - 36)(°C)}{2.41 \cdot 10^6(\frac{J}{kg})} = 6.97 kg$$

To transport the toluene to the condenser, for each m³ feed water 0.123 kg steam is required (see §7.4.3). In total approximately 7.1 kg steam is needed for each m³ feed water.

Packed bed height
The mole fraction based distribution coefficient K can be calculated as follows (see §7.4.3):

$$K = \frac{P_{vap}}{x_{sol} \cdot P_{sys}}$$

P_{vap} at 36°C = 50 mmHg [2] = 0.067 bar
x_{sol} at 36°C = 563 wt.ppm [3] = $1.1 \cdot 10^{-4}$ mole/mole
P_{sys} = 0.073 bar

With these values, K is around 8,340. This means that the mass transfer resistance in the gas-phase is negligible, so the number of overall liquid-phase transfer units can be approximated by:

$$N_{oL} = \ln \frac{x_{in}}{x_{out}} = \ln \frac{100 \text{ wt.ppm}}{1 \text{ wt.ppm}} = 4.6$$

The overall height of a transfer unit is approximately equal to the height H_L of a liquid-phase transfer unit (large stripping factor, see §7.4.3). H_L can be estimated for design purposes using Cornell's method with omitted height correction (see §7.4.3):

$$H_L = \frac{\Phi \cdot C}{3.28} \cdot (\frac{\eta_L}{\rho_L \cdot D_L})^{0.5}$$

η_L at 40°C = $6.56 \cdot 10^{-4}$ Pa·s [4]
ρ_L at 40°C ≈ 1000 kg/m³
D_L at 40°C = $1.3 \cdot 10^{-9}$ [5]

10 m³/h:	***100 m³/h:***
$2.15 \cdot 10^3$ lb/(h·ft²)	$4.44 \cdot 10^3$ lb/(h·ft²)
1-inch Pall rings	2-inch Pall rings
$\Phi = 0.04$ m [6]	$\Phi = 0.09$ m [6]
50% flooding	60% flooding
C = 0.85 [6]	C = 0.95 [6]
$H_L = 0.23$	$H_L = 0.59$
packed bed height "Z":	
$Z = 4.6 \cdot H_L \approx 1.1$ m	$Z = 4.6 \cdot H_L \approx 2.7$ m

Column

The packing consists of AISI 304 Pall rings, 1-inch for a feed rate of 10 m³/h and 2-inch for a feed rate of 100 m³/h.
The column diameter for a desired pressure drop of 8 mm H_2O per meter can be calculated from the generalised pressure drop correlation for random packing [5]:

$$\text{flow factor } F_{Lv} = \frac{L_w}{V_w}\sqrt{\frac{\rho_v}{\rho_L}}$$

$$\frac{L_W}{V_W} = \frac{1{,}000(\text{kg})}{7.1(\text{kg})} \approx 14$$

$$\rho_v \text{ at } 40°C = \frac{0.073 \cdot 10^5(\frac{N}{m^2}) \cdot 0.018(\frac{kg}{mole})}{8.31(\frac{J}{mole \cdot K}) \cdot 313(K)} \approx 0.05 \frac{kg}{m^3}$$

$F_{Lv} \approx 1 \rightarrow K_4$ wanted is 0.2 (see [5] figure 11.44), at flooding $K_4 = 0.6$

$$\text{gas mass flow rate per unit column length } V_w = \sqrt{\frac{K_4 \cdot \rho_v(\rho_L - \rho_v)}{13.1 \cdot F_p \cdot (\frac{\eta_L}{\rho_L})^{0.1}}}$$

10 m³/h:	***100 m³/h:***
$F_p = 160$ m^{-1} (1-inch) [5]	$F_p = 66$ m^{-1} (2-inch) [5]
$V_w = 0.14$ kg/(m².s)	$V_w = 0.22$ kg/(m².s)
% flooding $= \sqrt{\frac{0.14}{0.6}} = 0.5$	% flooding $= \sqrt{\frac{0.22}{0.6}} = 0.6$

The wetting rate can be checked using the appropriate diagram (see [7] figure 4.23).

10 m³/h feed rate:

$$\text{column area } A = \frac{\frac{10 \cdot 7.1}{3{,}600} \cdot (\frac{kg}{s})}{0.14 \cdot (\frac{kg}{m^2 \cdot s})} = 0.14 \text{ m}^2 \rightarrow \text{column diameter } D = 0.42 \text{ m} \approx 0.5 \text{ m}$$

height of packing = 1.1 m
height of bottom section = 3 + D/2 ≈ 3.3 m
height of top section = 1 m
total column height H ≈ 6 m (≈ 3 m between tangent lines)

minimum required wall thickness "t", with external pressure $P = 10^5$ N/m² and Young's modulus $E = 2.1 \cdot 10^{11}$ N/m²:

$$t = D \cdot \sqrt[3]{\frac{P}{2.2 \cdot E}} = 0.003 \text{ m}$$

cost of column: NLG 34,000 for H II steel, t = 8 mm, 5 m between tangent lines and D = 0.5 m [1]

cost of 1-inch
AISI 304 Pall rings: ≈ NLG 2,000 for a volume of $(\pi/4)(0.5)^2 * 1.1 \approx 0.2$ m³ [1]

100 m³/h feed rate:
A = 0.9 m² → column diameter D ≈ 1.1 m

height of packing = 2.7 m

$$\text{height of bottom section} = 3 + \sqrt{\frac{4 \cdot A_{inlet}}{\pi}} = 3.7 \text{ m}$$

$$\text{with } A_{inlet} = \frac{\frac{100 \cdot 7.1}{3{,}600} \cdot (\frac{kg}{s})}{0.05(\frac{kg}{m^3})} / 10(m/s) = 0.4 \text{ m}^2$$

height of top section = D = 1.1 m

total column height H ≈ 8 m (≈ 5 m between tangent lines)

$$t = D \cdot \sqrt[3]{\frac{P}{2.2 \cdot E}} = 0.007 \text{ m}$$

cost of column: NLG 57,000 for H II steel, t = 8 mm, 5 m between tangent lines and D = 1.1 m [1]

cost of 2-inch
AISI 304 Pall rings: ≈ NLG 13,000 for a volume of $(\pi/4)(1.1)^2 \times 2.7 \approx 2.6$ m³ [1]

Condenser
Shell and tube heat exchanger, with $\Delta T \approx (30 - 20) \approx 10°C$ and $U = 1{,}000$ W/(m²·°C), sized for 2 times the steam flow rate needed to transport the toluene to the condenser (2 x 0.123 ≈ 0.25 kg steam per m³ feed water).

per m³/h feed rate:

$$\text{power } P = \frac{0.25(\text{kg})}{3{,}600(\text{s})} \cdot 2.41 \cdot 10^6 (\frac{\text{J}}{\text{kg}}) = 167\text{W}$$

$$\text{area } A = \frac{P}{U \cdot \Delta T} = \frac{167(\text{W})}{1{,}000(\frac{\text{W}}{\text{m}^2 \cdot {}^\circ\text{C}}) \cdot 10({}^\circ\text{C})} \approx 0.02 \text{ m}^2$$

equipment cost:
10 m³/h → A = 0.2 m² → NLG 16,000 (2 m²) [1]
100 m³/h → A = 2 m² → NLG 16,000 [1]

$$(\text{cooling water flow} = \frac{167(\text{W})}{4.2 \cdot 10^3 (\frac{\text{J}}{\text{kg} \cdot {}^\circ\text{C}}) \cdot 10({}^\circ\text{C})} = 4 \cdot 10^{-3} \frac{\text{kg}}{\text{s}} \quad \text{(very low)})$$

Vacuum pump
sized to evacuate the column from 1 bar to 0.073 bar in 1 hour

volume of gas to be evacuated per hour: $V = \frac{\frac{\pi}{4} \cdot D^2 \cdot (H - 2)}{P_{sys}}$

10 m³/h feed rate:
V ≈ 11 m³ per hour → power of vacuum pump is approximately 0.5 kW
equipment cost ≈ NLG 1,000

100 m³/h feed rate:
V ≈ 78 m³ per hour → power of vacuum pump is approximately 3 kW
equipment cost ≈ NLG 5,000

Water pumps
pump efficiency: 0.7

10 m³/h feed rate:
total water flow rate ≈ feed rate (cooling water flow rate is very low) ≈ 10 m³/h
water head ≈ 6 m

$$\text{power } P = \frac{10(\text{m}^3)}{3{,}600(\text{s})} \cdot 6 \cdot 10^4 (\frac{\text{N}}{\text{m}^2}) \cdot \frac{1}{0.7} \approx 0.3\text{kW}$$

equipment cost ≈ NLG 1,000

100 m³/h feed rate:
total water flow rate ≈ 100 m³/h
water head ≈ 8 m

$$\text{power } P = \frac{100(m^3)}{3{,}600(s)} \cdot 8 \cdot 10^4 (\frac{N}{m^2}) \cdot \frac{1}{0.7} \approx 4\,kW$$

equipment cost ≈ NLG 7,000

Decanter
equipment cost: estimated at NLG 15,000

Space requirements

footprint
column:
free space around column (diameter D) is 1 m
footprint of column = $(D + 2)^2$ m²

feed preheater:
free space around feed preheater is 1 m
distance between plates is 0.5 cm
10 m³/h: plates 1 m high, square surface 1.2 x 1.2 m² (B = 1.2 m)
100 m³/h: plates 2 m high, square surface 1.4 x 1.4 m² (B = 1.4 m)

system:
distance "d" between column and condenser = 1 m
10 m³ feed rate: footprint ≈ $(D + 2)^2 + (B+2-d)(B+2)$ ≈ 13 m²
100 m³ feed rate: footprint ≈ $(D + 2)^2 + (B+2-d)(B+2)$ ≈ 18 m²

maximum height
10 m³ feed rate: column, 6 m
100 m³ feed rate: column, 8 m

Fixed capital investment
purchased equipment cost:

	10 m³/h:	100 m³/h:
feed preheater:	21,000	154,000
reboiler:	16,000	22,000
column:	34,000	57,000
Pall rings:	2,000	13,000
condenser:	16,000	16,000
pumps:	2,000	12,000
decanter:	15,000	15,000
total:	NLG 106,000	NLG 289,000

The fixed capital investment is estimated at 3 times the purchased equipment cost.

Fixed capital investment:
10 $m^3/h \rightarrow I = 3 \times 106{,}000 \approx$ NLG 320,000
100 $m^3/h \rightarrow I = 3 \times 289{,}000 \approx$ NLG 870,000

Treatment cost

	10 m^3/h:	100 m^3/h:
fixed annual charge at 20% of I:	64,000	174,000
maintenance & repair at 3% of I:	10,000	26,000
operating labour:	35,000	35,000
utilities:		
steam:	17,000	170,000
electric power	1,000	10,000
treatment cost per year:	127,000	415,000
annual volume of treated water:	80,000 m^3	800,000 m^3
treatment cost per m^3 water:	± NLG 1.6	± NLG 0.5

Summary

	10 m^3/h:	100 m^3/h:
treatment cost (NLG/m^3)	1.6	0.5
footprint (m^2)	13	18
maximum height (m)	6	8

References

[1] *DACE-prijzenboekje; kostengegevens t.b.v. ramingen (18th ed.)*, Dutch Association of Cost Engineers, Leidschendam, 1995

[2] Timmermans, J., *Physico-chemical constants of pure organic compounds*, Elsevier Publishing Company, Amsterdam, 1950

[3] Yaws, C.L., Biu, L., Nijhawan, S., *Calculate the solubility of aromatics*, Chemical Engineering, February 1995, pp. 113-115

[4] Coulson, J.M., Richardson, J.F., Backhurst, J.R., Harker, J.H., *Chemical engineering, Volume 1 (5th ed.)*, Butterworth-Heinemann, Oxford, 1996, ISBN 0 7506 2557 0

[5] Sinnot, R.K., *Coulson & Richardson's Chemical Engineering, Volume 6 (2nd ed.)*, Pergamon Press, Oxford, 1993, ISBN 0-08-041866x

[6] Perry, R.H., Green, D.W., Maloney, J.O., *Perry's Chemical Engineers' Handbook (6th ed.)*, McGraw-Hill Book Co, Singapore, 1984, ISBN 0-07-066482-X

[7] Coulson, J.M., Richardson, J.F., Backhurst, J.R., Harker, J.H., *Chemical engineering, Volume 2 (4th ed.)*, Butterworth-Heinemann, Oxford, 1996, ISBN 0 7506 2942 8

E.4 Countercurrent Foam Absorption (CFA)

Required steam flow rate for one unit treating 10 m³/h

stripping of the absorbed toluene from the cellular silicone:
(see Chapter 6)

steam flow rate = $0.3(\frac{m}{s})\cdot 1(m)\cdot 0.25(m)\cdot 0.6(\frac{kg}{m^3}) = 4.5\cdot 10^{-2}(\frac{kg}{s})$

heating of water:
sorption section temperature: 12°C
regeneration section temperature: 100°C
volume of bed segments: 0.4 m³
percentage undrained water entering the regeneration section: 30% of the volume of bed segments

rotational speed of the drum: $4.24\cdot 10^{-4}(\frac{rev}{s})$

undrained water flow rate $= 4.24\cdot 10^{-4}(\frac{rev}{s})\cdot 0.4\cdot 0.3(\frac{m^3}{rev})\cdot 10^3(\frac{kg}{m^3}) = 5.1\cdot 10^{-2}(\frac{kg}{s})$

steam flow rate for heating water =

$$\frac{5.1\cdot 10^{-2}(\frac{kg}{s})\cdot 4.2\cdot 10^3(\frac{J}{kg\cdot °C})\cdot (100-12)(°C)}{2.26\cdot 10^6(\frac{J}{kg})} = 8.3\cdot 10^{-3}(\frac{kg}{s})$$

heating of foam:
volume of bed segments: 0.4 m³
porosity of foam: 90%

foam flow rate $= 4.24\cdot 10^{-4}(\frac{rev}{s})\cdot 0.4\cdot 0.1(\frac{m^3}{rev})\cdot 1.03\cdot 10^3(\frac{kg}{m^3}) = 1.7\cdot 10^{-2}(\frac{kg}{s})$

steam flow rate for heating foam =

$$\frac{1.7\cdot 10^{-2}(\frac{kg}{s})\cdot 2\cdot 10^3(\frac{J}{kg\cdot °C})\cdot (100-12)(°C)}{2.26\cdot 10^6(\frac{J}{kg})} = 1.3\cdot 10^{-3}(\frac{kg}{s})$$ (relatively negligible)

heating of stainless steel:
stainless steel mean cross section surface area =
$1\cdot 0.015 + 2\cdot 0.25\cdot 0.01 + 13\%\cdot 1\cdot 0.25 = 5.3\cdot 10^{-2}$ m²

speed at mean diameter is 1 mm/s

stainless steel flow rate = $10^{-3}(\frac{m}{s}) \cdot 5.3 \cdot 10^{-2}(m^2) \cdot 7.8 \cdot 10^{3}(\frac{kg}{m^3}) = 0.4$ (kg/s)

steam flow rate for heating stainless steel =

$$\frac{0.4(\frac{kg}{s}) \cdot 4.6 \cdot 10^{2}(\frac{J}{kg \cdot °C}) \cdot (100-12)(°C)}{2.26 \cdot 10^{6}(\frac{J}{kg})} = 7.2 \cdot 10^{-3}(\frac{kg}{s})$$

total steam flow rate for one unit treating 10 m³/h:

$$4.5 \cdot 10^{-2} + 8.3 \cdot 10^{-3} + 1.3 \cdot 10^{-3} + 7.2 \cdot 10^{-3} = 6.2 \cdot 10^{-2}(\frac{kg}{s})$$

Main equipment ("drum")

The main equipment (the "drum") consists of a static cylinder, a slowly rotating housing composed of a housing inner face, two housing side faces, check valve plates and sieve plates, R-omni-rings, teflon strips and check valves (see Chapter 6 for details). The R-omni-rings and the check valves (non-return valves) can be supplied by Eriks (Alkmaar, The Netherlands).

The Central Workshop of Delft University of Technology has made a cost estimate for all main parts (see detailed drawings in Appendix D.3). The cost of these parts are estimated on the basis of a small series of CFA units and allocation of most of these parts to specialised workshops. The main equipment will cost approximately NLG 340,000 including seals and assembly, but excluding the check valves. These valves cost approximately NLG 35,000 per CFA unit (including assembly).

Drive

The planetary gear (see Chapter 6) and the motorreductor (≈ 0.12 kW, see Chapter 6) cost around NLG 35,000 including assembly.

Frame

Estimated at NLG 20,000 including assembly.

Condenser (10 m³/h) and decanter

Condenser: shell and tube heat exchanger. The cost of the cooling water flow is negligibly small. The cost for the condenser and decanter are estimated at NLG 30,000 including assembly.

Water pumps (10 m³/h)

pump efficiency: 0.7

total water flow rate ≈ feed rate (cooling water flow rate is very low, drain water flow rate is low relative to feed rate) ≈ 10 m³/h

total pressure drop ≈ $3 \cdot 10^{4}$ Pa

$$\text{power } P = \frac{10(m^3)}{3{,}600(s)} \cdot 3 \cdot 10^4 (\frac{N}{m^2}) \cdot \frac{1}{0.7} \approx 0.1 kW$$

equipment cost will be negligible relative to the main equipment

Sorbent material
When commercially available, the bulk price for cellular silicone with the properties assumed in the design (see Chapter 6) and in this techno-economic evaluation will be approximately 15,000 NLG/m³ in foamed condition, according to Dow Corning (Wiesbaden, Germany). For one CFA unit (treating 10 m³ water per hour), 0.4 m³ foam is required, at a cost of about NLG 6,000 (one exchange per year).

Fixed capital investment

preassembled/skid-mounted equipment (10 m³/h), including interconnecting piping, cabling and instrumentation:

main equipment (drum):	340,000
non-return valves:	35,000
drive:	35,000
frame:	20,000
condenser + decanter	30,000
	---------- +
total:	NLG 460,000

The fixed capital investment is estimated at 1.5 times the preassembled/skid-mounted equipment cost.

Fixed capital investment:
10 m³/h → I = 1.5 x 460,000 = NLG 690,000
100 m³/h → I = 7 x 690,000 = NLG 4,830,000

Treatment cost

	10 m³/h:	100 m³/h:
fixed annual charge at 20% of I:	138,000	966,000
maintenance & repair at 8% of I:	55,000	386,000
operating labour:	35,000	105,000
steam:	54,000	540,000
sorbent material:	6,000	60,000
	---------- +	---------- +
treatment cost per year (NLG/y):	288,000	2,057,000
volume of treated water (m³/y):	80,000	800,000
treatment cost (NLG/m³):	± NLG 3.6	± NLG 2.6
	=========	=========

Remark: the total electric power demand (electro motor plus feed pump for one unit) is approximately 0.2 kW, so the cost of electric power is negligibly small.

Space requirements
(see Chapter 6)
The free space around the system is 1 m around, but in front of the drum an additional 1 m has to be free to enable exchange of sorbent material (translation of the drum outside the static cylinder).

10 m³/h:
system length in direction of rotation axis: L = 1.8 m
system width : W = 1.5 m
footprint = (1+L+2)(1+W+1) ≈ 17 m²
maximum height: 2.5 m (including 1 m between the CFA unit and the ground)

100 m³/h:
system consists of 2 x 5 units stacked 2 high
distance between two units in direction of rotation axis (length): 2 m
distance between two units in width: 0.5 m
footprint = (1+L+2)(1+W+0.5+W+0.5+W+1) + (L+2)(1+W+0.5+W+1) ≈ 57 m²
maximum height is 5 m (including 1 m in height between the CFA units)

Summary

	10 m³/h:	100 m³/h:
treatment cost (NLG/m³)	3.6	2.6
footprint (m²)	17	57
maximum height (m)	2.5	5

Notation

indices

subscript:

$_0$:	in uncompressed condition / initial value
$_1$:	in direction 1 (see figure 2.1)
$_2$:	in direction 2 (see figure 2.1)
$_3$:	in direction 3 (see figure 2.1)
$_C$:	cross-sectional
$_G$:	gas phase
$_i$:	property of component "i"
$_L$:	in longitudinal direction (see figure 2.1)
	or: liquid phase
$_N$:	in normal direction
$_S$:	sorbent phase
$_T$:	in transversal direction (see figure 2.1)
$_W$:	frictional

superscript:

^{0}:	outside the column at the inlet side

symbols

A:	surface area	[m^2]
	or: phase boundary surface area (equations 4.1 and 4.2)	[m^2]
a_S:	specific sorbent surface area (equation 4.29)	[m^2/m^3]
C:	tracer concentration	[kg/m^3]
C_1:	structural parameter for laminar flow pressure drop (equation 3.6)	[-]
C_2:	structural parameter for turbulent flow pressure drop (equation 3.6)	[-]
C_{IN}:	water input concentration (also symbolised by C_{LO})	[kg/m^3]
C_{LO}:	water input concentration (also symbolised by C_{IN})	[kg/m^3]
C_{OUT}:	water output concentration	[kg/m^3]
C_{SO}:	sorbent input concentration	[kg/m^3 solid based]
c:	constant for compressibility of fiber masses (equation 2.13)	[-]
	or: concentration	[kg/m^3]
D:	diameter	[m]
	or: diffusion coefficient	[m^2/s]
D_{ax}:	axial dispersion coefficient	[m^2/s]
D_G:	mean diameter of annular packed bed	[m]
d:	fiber diameter	[m]
d_{eq}:	uncompressed equivalent fiber diameter (equation 3.9)	[m]
d_p:	uncompressed mean pore diameter (empty space based)	[m]
d'_p:	compressed mean pore diameter	[m]
E:	Young's modulus	[N/m^2]
	or: removal efficiency (= 1 - C_{OUT}/C_{IN})	[-]
E_F:	elastic foam modulus	[N/m^2]

E_P:	Young's modulus of polymer	[N/m^2]
e:	strain (equation 2.1)	[-]
F:	force	[N]
$f(e_l)$:	strain function (equation 2.12)	[-]
H:	packed bed height (also symbolised by L)	[m]
H_e:	Henry coefficient	[bar]
H_L:	height of a liquid-phase transfer unit	[m]
I:	fixed capital investment	[NLG]
K:	permeability coefficient	[m^2]
	or: mole fraction based distribution coefficient	[-]
k:	Kozeny's constant	[-]
	or: permeability of a packed fiber bed (equation 3.27)	[m^2]
	or: mass transfer coefficient	[m/s]
k_{oL}:	liquid side overall mass transfer coefficient	[m/s]
k_{oS}:	sorbent side overall mass transfer coefficient	[m/s]
L:	packed bed length (also symbolised by H)	[m]
	or: feed water flow rate	[kmole/s]
M:	molecular weight	[kg/kmole]
m:	mass	[kg]
m_{GL}:	distribution coefficient (= (c_G/c_L) at equilibrium)	[(kg/m^3)/(kg/m^3)]
m_{GS}:	distribution coefficient (=(c_G/c_S) at equilibrium)	[(kg/m^3)/(kg/m^3)]
m_{LS}:	reciprocal value of m_{SL}	[(kg/m^3)/(kg/m^3)]
m_{SL}:	distribution coefficient (=(c_S/c_L) at equilibrium)	[(kg/m^3)/(kg/m^3)]
N:	number of revolutions per hour	[1/hr]
N_{oL}:	liquid side number of overall mass transfer units	[-]
P:	pressure applied in one direction	[N/m^2]
P_i:	partial pressure of component "i" in the gas phase	[bar]
P_{sys}:	system pressure	[bar]
P_{vap}:	vapour pressure	[bar]
ΔP:	pressure drop (also symbolised by S)	[N/m^2]
R:	shape-anisotropy ratio	[-]
S:	pressure drop (also symbolised by ΔP)	[N/m^2]
	or: specific surface area of fibers	[m^2/m^3]
	or: stripping factor	[-]
	or: sorption factor	[-]
s:	stress relaxation factor	[-]
T:	temperature	[K]
t:	time	[s]
UV_0:	UV-signal at the start of the experiment	[-]
UV_e:	UV-signal at the end of the experiment	[-]
u:	superficial fluid velocity (relative to fixed co-ordinates)	[m/s]
u_G:	fluid velocity at D_G	[m/s]
u_{max} :	maximum allowable superficial liquid velocity	[m/s]
V:	volume	[m^3]
	or: steam flow rate	[kmole/s]
v:	sorbent transport velocity	[m/s]
W_L:	mass of the liquid phase	[kg]

W_S:	mass of the sorbent phase	[kg]
x:	co-ordinate along packed bed (Chapter 2)	[m]
x_i:	mole fraction of component "i" in water	[mole/mole]
x_{in}:	mole fraction at the top of the column	[mole/mole]
x_{out}:	mole fraction at the bottom of the column	[mole/mole]
x_{sol}:	maximum solubility in water	[mole/mole]
Y:	Young's modulus of a single fiber	[N/m²]
y_i:	mole fraction of component "i" in the gas phase	[mole/mole]
z:	co-ordinate along packed bed	[m]

Greek symbols

ε:	packed bed porosity (equation 2.14)	[-]
γ:	component's activity coefficient in the liquid phase	[-]
γ':	component's activity coefficient in the sorbent phase	[-]
γ_{ix}^{∞}:	activity coefficient of component "i" in water at infinite dilution	[-]
η:	dynamic viscosity	[N·s/m²]
Λ:	capacity ratio (inverse value of sorption or stripping factor S)	[-]
μ:	friction coefficient	[-]
ν:	Poisson's ratio	[-]
	or: kinematic viscosity	[m²/s]
ν_{TL}:	transversal-longitudinal Poisson's ratio	[-]
ν_{TT}:	transversal Poisson's ratio	[-]
ρ:	density	[kg/m³]
σ:	stress	[N/m²]

dimensionless numbers

Péclet number $Pe = \frac{u \cdot H}{\varepsilon \cdot D_{ax}}$

Reynolds number $Re = \frac{\rho \cdot u \cdot d}{(1-\varepsilon) \cdot \eta}$

Schmidt number $Sc = \frac{\nu}{D}$

Sherwood number $Sh = \frac{k \cdot d}{D}$

Acknowledgement

This research was sponsored by **SENTER**, The Hague, The Netherlands, within the framework of the Innovative Research Program "IOP Preventie" and was designated Project IMP91504.

Most of the cellular silicone used in this research was kindly put at our disposal by **DOW CORNING EUROPE**.

Dankwoord

Op deze plaats wil ik een ieder bedanken die een positieve bijdrage heeft geleverd aan dit projekt. Dit is op de eerste plaats mijn vroegere collega Gerard van Zee (inmiddels gepromoveerd), die het onderzoek destijds heeft opgestart en van wiens samenwerking ik nog geruime tijd de vruchten heb kunnen plukken. Daarnaast wil ik Prof. Veenman en Prof. de Graauw bedanken voor hun betrokkenheid en inzet bij dit onderzoek.

Een speciaal woord van dank ben ik verschuldigd aan de vaste medewerkers van het Laboratorium Apparatenbouw voor de Procesindustrie, niet in de laatste plaats de mechanische en electronische werkplaats. Zonder hun inzet is het uitvoeren van praktisch onderzoek immers praktisch onmogelijk. Hetzelfde geldt voor de Centrale Werkplaats, die de aanloopproblemen met het experimentele scheidingsapparaat goed wist op te lossen en bij storingen altijd snel hulp bood. Ook André van den Bosch van de tekenkamer wil ik speciaal bedanken voor zijn ondersteuning gedurende dit projekt.

Tenslotte wil ik alle afstudeerders en stagiaires bedanken alsmede de leden van de SENTER-begeleidingscommissie.

Aan dit projekt hebben vanaf 1 maart 1993 als afstudeerder en stagiair meegewerkt (inclusief Gerard van Zee's promotie-onderzoek):

M. Bisschops
H.E. Standhardt
A.J.H. Visschedijk
A. de la Rie
H.-J.J.B. Verweyen
P.C. Verheul
W. Smit
H.A. Jaddoe
S.A. Beers
M. van Gestel
O.J.D. van Doeland
A.C. Dirks
D.W.O d'Engelbronner
M.D. Lock
R.J. Jansen
R.J. Bot
J. Boesten
M.J.B. van der Kamp.

Curriculum Vitae

André Diederen
geboren op 26 april 1964 in Den Haag
getrouwd met Anja Lenselink en vader van Thomas

1976 - 1982:	Gymnasium B, Bernardinuscollege, Heerlen.
1982 - 1987:	Studie Werktuigbouwkunde aan de TU Eindhoven.
1988 - 1989:	Dienstplichtig onderofficier, 59 TKBAT, 't Harde.
1989 - 1993:	Hoofdconstructeur bij Ontwikkeling & Beproeving / afdeling Basisassen van Van Doorne's Bedrijfswagenfabriek DAF B.V. te Eindhoven.
1993 - 1997:	Promotie-onderzoek aan de TU Delft, faculteit Werktuigbouwkunde, vakgroep Apparatenbouw voor de Procesindustrie.
per 1 maart 1997:	Wetenschappelijk medewerker van de researchgroep Munitie uitwerking en Ballistische bescherming van het TNO Prins Maurits Laboratorium te Rijswijk.

Publikaties

Diederen, A.M., Zee, G. van, Veenman, A.W., Graauw, J. de, *A novel apparatus for countercurrent sorption separation processes using fibrous sorbents*, te publiceren in Chem.Engng.Processing.

Diederen, A.M., *Evaluatie VOC-verwijdering uit afvalwater*, te publiceren in NPT Procestechnologie.

Octrooi

Diederen, A.M., Zee, G. van, *Apparatus for separating a fluidum in at least two components*, international patent application PCT/NL97/00189, Delft University of Technology, 1997.